

2014

A Data-Driven Storm Surge Analysis for the U.S. Gulf Coast

Harold Francis Needham

Louisiana State University and Agricultural and Mechanical College, hal@srcc.lsu.edu

Follow this and additional works at: https://digitalcommons.lsu.edu/gradschool_dissertations



Part of the [Social and Behavioral Sciences Commons](#)

Recommended Citation

Needham, Harold Francis, "A Data-Driven Storm Surge Analysis for the U.S. Gulf Coast" (2014). *LSU Doctoral Dissertations*. 3250.
https://digitalcommons.lsu.edu/gradschool_dissertations/3250

This Dissertation is brought to you for free and open access by the Graduate School at LSU Digital Commons. It has been accepted for inclusion in LSU Doctoral Dissertations by an authorized graduate school editor of LSU Digital Commons. For more information, please contact gradetd@lsu.edu.

A DATA-DRIVEN STORM SURGE ANALYSIS FOR THE U.S. GULF COAST

A Dissertation

Submitted to the Graduate Faculty of the
Louisiana State University and
Agricultural and Mechanical College
in partial fulfillment of the
requirements for the degree of
Doctor of Philosophy

in

The Department of Geography and Anthropology

by

Hal F. Needham

B.S., Pennsylvania State University, 1997

M.S., Louisiana State University, 2010

August 2014

*For Della, Luke and our Unborn Baby-
Keep Exploring*

ACKNOWLEDGEMENTS

I thank God for the opportunity to work and study at LSU over the past six years. I am thankful for my wife, Kari, and my children, Luke, Della, and an unborn baby, for their sacrifice and support through this time. This has been a long road for us, as I took my first graduate class 11 years ago in Upstate New York, and continued pursuing graduate studies in Alaska, Colorado and Louisiana. My parents, Harold and Nancy Needham, of Pike County, Pennsylvania, have been extremely supportive of me throughout this entire process. Through the years, my mom continually gave me her age-old advice, “Just do your best,” while my dad influenced me in many ways to do empirical research. When he helped me with my math homework in grade school, he would constantly remind me that I wasn’t done with a problem until I went back, checked my work, and asked myself if the final answer made sense. I would also like to thank my sister, Abigail, for her support and encouragement through the years. Finally, my “Louisiana Family,” particularly Robert and Cheryl Hebert, of Brusly, helped us in so many practical ways through the years that it is hard to imagine how we would have survived without their help.

At LSU, I am especially appreciative of Dr. Barry Keim, who extended himself many times to give me opportunities. I have observed Dr. Keim continuously give time to his students in an effort to shape them into qualified scientists. In empirical research, he taught me to “let the data speak for themselves.” My committee, Barry Keim, Carol Friedland and Jill Trepanier, provided critical insights into this research, and provided much encouragement. They pushed me in my research, but were not interested to make me jump through hoops. I am grateful for all of them. Many faculty, staff and students at LSU have encouraged me and helped with this research. I would like to thank David Sathiaraj for his friendship and the IT support he provided, such as web-based mapping and tools. Amanda Billiot provided assistance with statistical research that helped me analyze storm surge return levels. Finally, many people helped build SURGEDAT, as I could not have built such an extensive database on my own. Those that contributed are Kyle Brehe, a staff member at SRCC, and many students, including Steve Beckage, Jonathan Lambert, Jesse Clifton, Christina Touzet, and Bryant Garcin. The faculty, staff and students that I worked with at LSU pushed themselves far beyond the minimum requirements, which explains how we were able to accomplish so much as a team. Finally, I would like to acknowledge the National Oceanic and Atmospheric Administration for providing grants NA080AR4320886 and EA133E-07-CN-0084, which provided financial support for this research.

TABLE OF CONTENTS

| | |
|--|------|
| ACKNOWLEDGEMENTS | iii |
| LIST OF TABLES | viii |
| LIST OF FIGURES | xii |
| ABSTRACT..... | xv |
| CHAPTER 1. INTRODUCTION | 1 |
| 1.1 Background | 1 |
| 1.2 Objective | 7 |
| 1.3 Organization..... | 7 |
| 1.4 References..... | 9 |
| CHAPTER 2. A REVIEW OF TROPICAL-CYCLONE GENERATED STORM SURGES: GLOBAL DATA SOURCES, OBSERVATIONS AND IMPACTS | 12 |
| 2.1 Introduction..... | 12 |
| 2.2 Western North Pacific (East Asia)..... | 17 |
| 2.2.1 Storm Surge Literature..... | 17 |
| 2.2.2 Storm Surge Observations | 19 |
| 2.2.2.1 The Philippines | 20 |
| 2.2.2.2 China..... | 24 |
| 2.2.2.3 Japan | 25 |
| 2.2.2.4 Vietnam and Thailand..... | 27 |
| 2.2.2.5 South Korea | 28 |
| 2.2.3 Storm Surge Impacts..... | 29 |
| 2.2.3.1 The Philippines | 29 |
| 2.2.3.2. China..... | 31 |
| 2.2.3.3 Japan | 33 |
| 2.2.3.4 Vietnam and Thailand..... | 34 |
| 2.2.3.5 South Korea | 35 |
| 2.3 Northern Indian Ocean..... | 36 |
| 2.3.1 Storm Surge Literature..... | 36 |
| 2.3.2 Storm Surge Observations | 38 |
| 2.3.2.1 Bay of Bengal | 39 |
| 2.3.2.2 Arabian Sea..... | 41 |
| 2.3.3 Storm Surge Impacts..... | 42 |
| 2.3.3.1 Bay of Bengal | 42 |
| 2.3.3.2 Arabian Sea..... | 44 |
| 2.4 Western North Atlantic | 45 |
| 2.4.1 Storm Surge Literature..... | 45 |
| 2.4.2 Storm Surge Observations | 48 |
| 2.4.2.1 U.S. Gulf Coast | 50 |
| 2.4.2.2 U.S. Atlantic Coast | 51 |

| | |
|---|-----|
| 2.4.2.3 The Caribbean, Mexico and Central America | 52 |
| 2.4.2.4 Canada..... | 52 |
| 2.4.3 Storm Surge Impacts..... | 53 |
| 2.5 Eastern North Pacific | 58 |
| 2.5.1 Storm Surge Literature..... | 58 |
| 2.5.1.1 Mexico | 58 |
| 2.5.1.2 Hawaii | 60 |
| 2.5.2 Storm Surge Observations | 61 |
| 2.5.2.1 Mexico | 61 |
| 2.5.2.2 Hawaii | 62 |
| 2.5.3 Storm Surge Impacts..... | 63 |
| 2.5.3.1 Mexico | 63 |
| 2.5.3.2 Hawaii | 64 |
| 2.6 Australia, New Zealand and Oceania..... | 65 |
| 2.6.1 Storm Surge Literature..... | 65 |
| 2.6.2 Storm Surge Observations | 67 |
| 2.6.3 Storm Surge Impacts..... | 73 |
| 2.7 Southwest Indian Ocean | 76 |
| 2.7.1 Storm Surge Literature..... | 76 |
| 2.7.2 Storm Surge Observations | 77 |
| 2.7.3 Storm Surge Impacts..... | 79 |
| 2.8 Global Comparison | 80 |
| 2.8.1 Comparing Global Surge Literature..... | 81 |
| 2.8.2 Comparing Global Surge Observations | 82 |
| 2.8.3 Comparing Global Surge Impacts..... | 93 |
| 2.9 Discussion | 96 |
| 2.10 Summary and Conclusion | 101 |
| 2.11 References..... | 104 |

| | |
|--|------------|
| CHAPTER 3. CORRELATING STORM SURGE HEIGHTS WITH TROPICAL CYCLONE WINDS AT AND BEFORE LANDFALL | 126 |
| 3.1 Introduction..... | 126 |
| 3.2 Data | 129 |
| 3.3 Methods..... | 130 |
| 3.3.1 Landfall/ surge classification system..... | 135 |
| 3.3.2 Building a 3-hour incremental wind speed dataset | 142 |
| 3.4 Results..... | 144 |
| 3.4.1 LOESS and linear regression models | 144 |
| 3.4.2 Non-linear wind/ surge relationship..... | 149 |
| 3.5 Discussion | 152 |
| 3.6 Summary and Conclusion | 162 |
| 3.7 References..... | 166 |

| | |
|---|------------|
| CHAPTER 4. AN EMPIRICAL ANALYSIS ON THE RELATIONSHIP BETWEEN TROPICAL CYCLONE SIZE AND STORM SURGE HEIGHTS ALONG THE U.S. GULF COAST | 171 |
|---|------------|

| | |
|--|-----|
| 4.1 Introduction..... | 171 |
| 4.2 Data..... | 174 |
| 4.2.1 Storm Surge Data..... | 174 |
| 4.2.2 Tropical Cyclone Wind and Position Data | 174 |
| 4.2.3 Tropical Cyclone Size Data | 174 |
| 4.3 Methods..... | 176 |
| 4.4 Results..... | 180 |
| 4.4.1 Analysis of Rmax Size for Storm Surge Generation | 180 |
| 4.4.2 Analysis of Wind Swath Size for Storm Surge Generation..... | 185 |
| 4.5 Discussion | 189 |
| 4.6 Summary and Conclusion | 191 |
| 4.7 References..... | 193 |
| | |
| CHAPTER 5. STORM SURGE RETURN PERIODS FOR THE U.S. GULF COAST.. | 197 |
| 5.1 Introduction..... | 197 |
| 5.2 Data..... | 201 |
| 5.3 Methods..... | 203 |
| 5.3.1 Data Selection | 203 |
| 5.3.2 Adjusting for Geodetic and Tidal Datums | 214 |
| 5.3.2.1 Adjusting Geodetic Datum References..... | 214 |
| 5.3.2.2 Adjusting Tidal Datum References..... | 222 |
| 5.3.3 Statistical Analysis..... | 226 |
| 5.3.3.1 Extreme Value Theory..... | 226 |
| 5.3.3.2 Point Process Model for Extreme Values | 227 |
| 5.3.3.3 Logarithmic Plotting | 235 |
| 5.4 Results..... | 237 |
| 5.4.1 Comparing Estimates from the PP and LP Methods | 237 |
| 5.4.2 Evaluating the PP and LP Methods | 241 |
| 5.5 Discussion | 248 |
| 5.6 Summary and Conclusion | 257 |
| 5.7 References..... | 261 |
| | |
| CHAPTER 6. THE VULNERABILITY OF OIL REFINERIES AND POWER PLANTS TO STORM SURGE ALONG THE U.S. GULF COAST..... | 270 |
| 6.1 Introduction..... | 270 |
| 6.2 Data..... | 276 |
| 6.2.1 Storm Surge Data..... | 276 |
| 6.2.2 Energy Facility Data | 279 |
| 6.3 Methods..... | 280 |
| 6.4 Results..... | 286 |
| 6.5 Discussion | 292 |
| 6.6 Summary and Conclusion | 300 |
| 6.7 References..... | 304 |
| | |
| CHAPTER 7. CONCLUSION..... | 311 |
| 7.1 Justification for Research..... | 311 |

| | |
|---|-----|
| 7.2 Summary of Results | 312 |
| 7.3 Benefits of this Research | 315 |
| 7.4 Limitations | 317 |
| 7.5 Suggestions for Future Research | 318 |
| 7.6 References | 320 |
| VITA..... | 323 |

LIST OF TABLES

| | |
|---|----|
| Table 2.1. Average annual number of tropical cyclones that develop in selected ocean basins, based on data from 1981-2010. Taken from Landsea and Delgado (2013)..... | 14 |
| Table 2.2. Ocean basins, sub-basins and countries represented in the global literature review of observed storm surge information..... | 15 |
| Table 2.3. Top 10 tropical cyclone-induced surge levels in the Western North Pacific from 1880-2013. Compiled from the following sources: Arafiles and Alcances (1978), PAGASA (1987), Henderson (1988), Bankoff (2003), Mai et al. 2006; Neumann et al. 2012; Needham (2013)..... | 23 |
| Table 2.4. The top 10 highest Northern Indian Ocean tropical cyclone-induced storm surge levels, from Dube et al. (1997)..... | 39 |
| Table 2.5. The top 10 highest Northern Indian Ocean fatality total from tropical cyclones, from Dube et al. (2008); and Fritz et al. (2009)..... | 43 |
| Table 2.6. Top 10 Western North Atlantic tropical cyclone-induced surge levels, from 1880-2012. Multiple events tied for ninth-place, so this list contains 13 events. Compiled from the following sources: Garriott (1898); U.S. Corps of Engineers (1935); U.S. Army Engineer District (1962); Sugg and Pelissier (1968); Simpson et al. (1970); Hebert (1976); Schuck-Kolben (1990); Pielke et al. (2003); Landsea et al. (2004); Anonymous (2007); Drye (2007); Mandia (2010); and Knabb et al. (2011)..... | 49 |
| Table 2.7. Atlantic Basin tropical cyclone fatalities by region, from Rappaport and Fernandez-Partagas (1995)..... | 54 |
| Table 2.8. Population statistics for the U.S. coastal counties and parishes along the Gulf of Mexico in 1900, 1950, and 2000, from Keim and Muller (2009)..... | 54 |
| Table 2.9. Top 10 tropical cyclone-induced surge levels in Australia, New Zealand and Oceania, from 1880-2013. Compiled from the following sources: Whittingham (1958); Nelson (1975); Harper (1998); Australia Bureau of Meteorology (2000); Emergency Management Australia (2006); Australia Bureau of Meteorology (2006); Anonymous (2010); and Australia Bureau of Meteorology (2014a)..... | 69 |
| Table 2.10. Numeric counts of storm surge and storm tide observations by basin. Taken from SURGEDAT database..... | 82 |

| | |
|---|-----|
| Table 2.11. Summary statistics for storm surge observations in selected basins. Surge counts indicate the number of surge events that have exceeded the threshold. Counts of 1, 2, and 3 m surges in China provided by Tang et al. (2011). All other data provided by SURGEDAT database..... | 87 |
| Table 2.12. The number of storm surge/ storm tide events per decade exceeding various threshold levels. Rates of 1, 2, and 3 m storm surges in China derived from Tang et al. (2011). All other values derived from SURGEDAT database..... | 88 |
| Table 2.13. Deaths in tropical cyclones since 1700-1997, from Dube et al. (1997)..... | 94 |
| Table 3.1. Frequency of the 14 landfall classes, with a determination of inclusion/exclusion in this study..... | 134 |
| Table 3.2. Residual Standard Error (RSE) between surge heights and wind speeds at landfall and 18 hours before landfall. Lower values indicate better correlation..... | 144 |
| Table 3.3. Multiple R-Squared values correlating storm surge heights vs. winds at 3-hour increments preceding landfall. Correlation tests were run on data from 1880-2011 (117 events) and 1960-2011 (63 events). These values are plotted in Figure 3.7a..... | 147 |
| Table 3.4. Multiple R-Squared values of surge vs. actual and exponential wind speeds for data from 1960-2011 (63 events). The exponential power that produced optimal fit is also listed..... | 149 |
| Table 4.1. Landfall/ surge event types that were removed from analysis in Chapter 3. A total of 72 events were removed from the analysis..... | 177 |
| Table 4.2. Comparison of storm surge heights, hurricane size and maximum sustained wind speed at 18 hours before landfall for the 13 Florida Keys surge events analyzed in this study. Data compiled from Ho et al. (1975), Landsea et al. (2003), Demuth et al. (2006), Landsea et al. (2007), Landsea et al. (2011), and Hagen et al. (2012)..... | 184 |
| Table 4.3. Spearman rank order correlations measuring the relationship between storm surge heights and radius of 63 km/hr (34-kt), 93 km/hr (50-kt), and 119 km/hr (64-kt) winds..... | 186 |
| Table 4.4. Correlation between Rmax sizes and the radius of 63 km/hr (34-kt), 93 km/hr (50-kt) and 119 km/hr (64-kt) winds. All of these correlations are inverse, meaning there is a negative relationship between the variables..... | 189 |

| | |
|---|-----|
| Table 5.1 The number of observations provided by circles with 8-km (5-mile), 16-km (10-mile), and 40-km (25-mile) radii at 26 locations along the U.S. Gulf Coast. The latitude and longitude values depict the coordinates of circle centers..... | 208 |
| Table 5.2. Physical Homogeneity Index (PHI) classification provided by circles with 8-km (5-mile), 16-km (10-mile), and 40-km (25-mile) radii..... | 210 |
| Table 5.3. Comparison of water levels at Galveston and interior portions of Galveston Bay, from tropical cyclones that made landfall between Corpus Christi and Galveston, Texas, and produced at least 2 m storm surge/ storm tide in Galveston Bay. Adapted from Zoch (1949); U.S. Weather Bureau (1959); U.S. Army Corps of Engineers (1962); Harris (1963); National Hurricane Center (1983); National Hurricane Center (1989); Federal Emergency Management Agency (2009)..... | 214 |
| Table 5.4. Sea-level trends for 26 locations along the U.S. Gulf Coast. Data provided by Penland and Ramsey (1990); Galloway et al. (1999); National Oceanic and Atmospheric Administration (2013); and U.S. Department of Transportation (2013)..... | 216 |
| Table 5.5. Subsidence rates near Baytown, Texas, from 1906-2013..... | 221 |
| Table 5.6. The height of MSL, MLW and MLLW at locations along the U.S. Gulf Coast. The difference between MSL and MLW or MSL and MLLW were used for tidal datum adjustments. Data provided by National Oceanic and Atmospheric Administration (2014)..... | 224 |
| Table 5.7. Comparison of observed storm surge/ storm tide events at each location and the number of events \geq than the 0.91 m threshold used in the Point Process method.... | 230 |
| Table 5.8. Storm surge return levels (m) for 26 locations along the U.S. Gulf Coast, using the Point Process Model..... | 234 |
| Table 5.9. Storm surge return levels (m) for 26 locations along the U.S. Gulf Coast, using Logarithmic Plotting..... | 236 |
| Table 5.10. Return periods of the maximum water level at each site using the Point Process Model and Logarithmic Plot..... | 242 |
| Table 5.11. Expected water level exceedences above specific return periods..... | 244 |
| Table 5.12. Actual exceedences above return levels using the PP method..... | 245 |
| Table 5.13. Actual exceedences above return levels using the LP method..... | 246 |

| | |
|--|-----|
| Table 5.14. Two-tailed KS Statistic. Lower values indicate a better fit between observed and expected values..... | 247 |
| Table 5.15. Comparison of 100-yr water levels at Galveston. Adapted from Stoeten (2013), page 55. Original table included first three studies, and results referenced to Needham and Keim (2012), from presentation at Galveston in Oct. 2012. These results were for entire Upper Texas Coast, and have therefore been removed from this table..... | 249 |
| Table 5.16. Tidal errors as percentage of the 100-year water level. Tidal data provided by NOAA Tides and Currents..... | 253 |
| Table 6.1. Storm surge return levels (m) for 26 locations along the U.S. Gulf Coast, using Logarithmic Plotting..... | 277 |
| Table 6.2. The number of oil refineries and electric power plants assigned to each of the 26 cities with adequate storm surge data..... | 285 |
| Table 6.3. Number of facilities and proportion of facilities flooded by each storm surge return level along U.S. Gulf Coast. Return levels are localized but these data are compiled from a basin-wide count..... | 286 |
| Table 6.4. The number of power plants flooded by various storm surge return levels at 26 locations along the U.S. Gulf Coast. 100-yr refers to the height of the 100-year storm surge level..... | 289 |
| Table 6.5. The number of refineries flooded by various storm surge return levels at 26 locations along the U.S. Gulf Coast. 100-yr refers to the height of the 100-year storm surge level..... | 290 |

LIST OF FIGURES

Figure 1.1. The location and height of peak storm surge levels along the U.S. Gulf Coast since 1880. Each circle represents a unique surge event. Adapted from Needham and Keim (2012).....5

Figure 1.2. The location and height of more than 400 high-water marks produced by Hurricane Ike in 2008. Adapted from Doran et al. (2009); Federal Emergency Management Agency (2009); and Berg (2010).....6

Figure 2.1. Map of the regions included in the global literature review.....16

Figure 2.2. Global storm surge distribution graph.....83

Figure 2.3. Western North Pacific storm surge distribution graph.....84

Figure 2.4. Australia and Oceania storm surge distribution graph.....85

Figure 2.5. Northern Indian Ocean storm surge distribution graph.....85

Figure 2.6. Western North Atlantic storm surge distribution graph.....86

Figure 2.7. The number of storm surge events per decade exceeding various thresholds in selected regions/ ocean basins.....89

Figure 2.8. Count of storm surges per decade that equal or exceed 5m for selected regions/ ocean basins.....90

Figure 2.9. Time series of storm surge and storm tide observations for the four major basins that are impacted by tropical cyclone-generated storm surges.....91

Figure 3.1. Hourly storm position and observed high water marks for Hurricane Andrew. The storm passed closest to the location of peak surge more than five hours before the center of circulation actually crossed the coast.....133

Figure 3.2. The 14 landfall/surge classification types. An example storm is provided for each type.....136

Figure 3.3. Hurricane Humberto formed into a tropical storm 24 hours before the time of COO. Therefore, no observations are available for 27, 30, 33 and 36 hours before landfall.....142

Figure 3.4. Hurricane Charley was centered over the Gulf of Mexico for approximately 12 hours before COO in Southwest Florida. Therefore, no observations are included in the analysis from 15 through 36 hours before landfall, when the cyclone was centered over the Caribbean Sea.....143

Figure 3.5a (left) and 3.5b (right): LOESS (red line) and linear (black line) regression models for relationship between maximum sustained wind speeds and surge magnitudes. Orange circles depict observed events.....145

Figure 3.6. Residual Standard Error values from LOESS regression model investigating the relationship between maximum sustained winds and peak surge magnitudes at 3-hour increments before landfall. Values depicted for years 1880-2011 (blue) and 1960-2011 (red). Lower values indicate better correlation.....146

Figure 3.7a (Top): Correlation of surge height vs. wind speeds at 3-hour intervals for data from 1880-2011 (117 events) and 1960-2011 (63 events). Figure 3.7b (Bottom): Correlation of surge heights vs. actual and exponential wind speeds at 3-hour intervals for data from 1960-2011.....148

Figure 4.1. LOESS (black line) and linear (red line) regression models for the relationship between surge heights and the radius of maximum winds (nmi). Orange circles depict observed events.....182

Figure 4.2. LOESS (black line) and linear (red line) regression models for the relationship between surge heights and radius of 93 km/hr (50-kt) winds (nmi) at 18 hours before landfall. Orange circles depict observed events.....187

Figure 5.1. The NOS tide gauge at Calcasieu Pass, Louisiana, malfunctioned shortly after water levels exceeded 1.22 m (4 feet) on September 24, 2005, during Hurricane Rita’s storm surge.....205

Figure 5.2. The NOS tide gauge at Galveston Pier 21, Texas, malfunctioned after water levels exceeded 3.05 m (10 feet) on September 13, 2008, during Hurricane Ike’s storm surge. The gauge began recording water levels again once the peak surge passed.....205

Figure 5.3. The storm surge web tool enables users to select surge data for coastal communities. In this screen shot, a user has selected all observed storm surge and storm tide heights within 16 km (10 miles) of Corpus Christi, Texas.....207

Figure 5.4. A geodetic datum adjustment at Galveston, Texas, reduced the storm tide level for Hurricane Rita from 1.43 m above NGVD29 to 0.91 m above the “annual datum” of 2005. Rita’s storm surge impacted Texas and Louisiana on September 23-24, 2005. Data adapted from Knabb et al. (2006) and National Oceanic and Atmospheric Administration (2013).....222

Figure 5.5. Tidal datum adjustment at Key West reduced the storm tide for Hurricane Alma from 1.07 m above MLW to 0.87 m above MSL. Data adapted from Sugg (1967) and National Oceanic and Atmospheric Administration (2014).....223

Figure 5.6. Parameter estimates of location μ , scale σ , and shape ξ determined by fitting the point process model at various thresholds. Vertical bars show the standard error of each parameter estimate.....229

Figure 5.7. Logarithmic plot of storm surge return periods and storm surge magnitudes (m) for Morgan City, Louisiana.....236

Figure 5.8. Storm surge return levels and observed storm surges for the U.S. Gulf Coast produced by the Point Process Model.....238

Figure 5.9. Storm surge return levels and observed storm surges for the U.S. Gulf Coast produced by Logarithmic Plotting.....238

Figure 5.10. Return level plot using a probabilistic modeling approach on thousands of synthetic surge scenarios, provided by Stoeten (2013), page 56. The blue line estimates return levels at the Open Coast, which pertains to Galveston City, and the red line predicts storm surge levels closest to Baytown, Texas. These water levels are considerably lower than my data-driven estimates.....241

Figure 5.11. Water level heights generated by Hurricane Ike in 2008. This image shows that proximity to landfall is not the only important factor that influences storm surge heights. Note that Shell Beach (city 11) observed higher water levels than Morgan City (city 9) and Grand Isle (city 10), even though Ike made landfall at Galveston (city 5). Adapted from Doran et al. (2009); Federal Emergency Management Agency (2009); Berg (2010).....250

Figure 6.1. Storm surge return levels and observed surge events for 26 cities along the U.S. Gulf Coast. This graphic was produced in Chapter 5.....278

Figure 6.2. The location of oil refineries, power plants, and cities with surge data.....283

Figure 6.3. Surge return levels and power plant elevations for the U.S. Gulf Coast.....287

Figure 6.4. Surge return levels and refinery elevations for the U.S. Gulf Coast.....288

Figure 6.5. Number of flooded and non-flooded power plants in the 100-yr surge.....288

Figure 6.6. Number of flooded and non-flooded refineries in the 100-yr surge.....292

ABSTRACT

This dissertation provides the first empirical storm surge analysis for the U.S. Gulf Coast. Data are provided by SURGEDAT, a comprehensive storm surge database. A global storm surge literature review provided more than 700 observations in six ocean basins. The most severe storm surges have occurred in the Bay of Bengal, and the most frequent low-magnitude surges have occurred in East Asia. The U.S. Gulf Coast experiences the second highest frequency of low- and high- magnitude storm surges. Two Gulf Coast studies revealed that storm surge heights correlate better with pre-landfall tropical cyclone conditions, such as maximum wind speed and size, than cyclonic conditions at landfall. Surges correlated best with maximum wind speeds and storm size 18 hours before landfall. Logarithmic plotting provided the best statistical method for estimating storm surge return levels in the region. These levels showed considerable geographic variability, as the highest 100-yr level was 7.95 m at Bay St. Louis/ Pass Christian, Mississippi, and the lowest 100-yr level was 2.53 m at Cedar Key, Florida. Along the Northern Gulf Coast, surge levels were relatively low near Morgan City, however rapid sea-level rise threatens this area. The 100-year storm surge along the Gulf Coast would inundate 72% of the oil refineries and 63% of the power plants in the coastal zone, if not for local flood protection. Southeast Texas contains a dense network of vulnerable energy infrastructure, as the 100-year flood threatens to inundate 92% (12 of 13) of the refineries in the Galveston-Baytown-Sabine Pass region, and 18 power plants near Baytown. These results will be valuable to planners, emergency management personnel, professionals in the energy and insurance industry, as well as coastal scientists and storm surge modelers.

CHAPTER 1. INTRODUCTION

1.1 Background

Through the ages, people have used observed facts to validate and test scientific theories. In the 4th Century B.C., Greek philosopher Aristotle supported a method of logic called inductive reasoning, whereby scientific theories are built on observed facts. He applied this methodology in many ways; for example, he theorized that the world was round based on observations, such as the curvature of Earth's shadow on the moon during a lunar eclipse (Martin 2005). In our modern world, the fruits of inductive reasoning surround us. For example, the development of the electric motor, radio, television, computer and cell phone all rely on properties of electricity and magnetism that were discovered by British scientist Michael Faraday in the 19th century. Although Faraday made discoveries through meticulous experiments and careful observations, much of his work was not readily accepted, as it contradicted the most advanced theories of his day (Hirshfeld 2006).

In the past decade, tropical cyclone-generated storm surges have emerged as a major scientific problem that we do not understand very well. Hurricane Katrina's devastating storm surge in 2005 was a turning point in this field, as this massive dome of water defied the best scientific theories of the time. For example, when Katrina struck, the National Oceanic and Atmospheric Administration generalized that a category-3 hurricane would likely generate a storm surge ranging from 2.7-3.7 m (Irish et al. 2008). However, Katrina generated an 8.47-m storm surge (Knabb et al. 2011), which was the highest surge level ever recorded in the United States (Needham and Keim 2012). This massive storm surge surprised the public and scientists alike. What was most surprising

about this massive dome of water is that it was noticeably higher than the devastating storm surge generated in 1969 by Hurricane Camille along the same coastline, even though Camille made landfall as a category-5 hurricane (Simpson et al. 1970) and Katrina as a category-3 hurricane (Knabb et al. 2011).

Following Katrina, many papers investigated the mechanisms by which tropical cyclones generate storm surge. These papers found that in addition to maximum sustained winds, other tropical cyclone parameters influence storm surge heights, including cyclone size (Irish et al. 2008; Nielsen 2009; Dietrich et al. 2011), cyclone forward speed (Rego and Li 2009), as well as coastline shape and offshore bathymetry (Weisberg and Zheng 2006; Resio and Westerink 2008; Westerink et al. 2008; Chen et al. 2008).

As if on cue, several hurricanes after Katrina demonstrated the importance of hurricane size for generating storm surge. In 2008, Hurricane Ike generated a 5.33-m storm surge along the Texas Coast, even though the storm made landfall as a category-2 hurricane (Berg 2010). At that time, the National Oceanic and Atmospheric Administration (NOAA) generalized category-2 hurricanes as having the potential to generate surge levels from 1.8 – 2.4 m (Irish et al. 2008). Soon after this event, NOAA removed storm surge height estimates from the Saffir-Simpson Scale. In 2012, Hurricane Isaac generated a storm tide exceeding 4.3 m in Southeast Louisiana (McCallum et al. 2012), even though the storm strengthened to a category-1 hurricane just hours before landfall. Isaac's large size likely contributed to this large storm tide, as the storm produced tropical storm force winds extending 333 km (180 nmi) from the center of circulation for several days before making landfall (Demuth et al. 2006). Later in 2012,

Hurricane Sandy produced a devastating storm surge that killed 147 people and inflicted approximately \$50 billion in damage along the U.S. Mid-Atlantic Coast (Blake et al. 2012). Although Sandy tracked towards the New Jersey coast as a category-1 hurricane (Blake et al. 2012), the storm generated a broad wind field, as tropical storm force winds extended 778 km (420 nmi) and hurricane force winds extended 333 km (180 nmi) from the center of circulation (Demuth et al. 2006). These destructive storm surges confirmed that the category of a hurricane at landfall, which is based upon the maximum sustained wind speed, does not always correlate well with surge heights, as even category-1 and -2 hurricanes sometimes generate massive storm surges.

Another area of research that has received much attention involves improving our understanding of storm surge vulnerability at specific locations. This topic became especially important after Hurricane Katrina inflicted more than \$100 billion in losses (Blake et al. 2011), and insurance premiums increased dramatically in many coastal areas (Green et al. 2007; Mowbray 2007; Warner 2007). The Federal Emergency Management Agency (FEMA) has addressed this topic by reevaluating storm surge risk along the U.S. Atlantic and Gulf Coasts, as the agency has collaborated with the National Hurricane Center to determine storm surge potential for specific areas. FEMA is using this updated information to create new Flood Insurance Rate Maps (FIRM), which consider the risk of both freshwater and saltwater flooding.

While these studies have advanced our understanding of coastal flooding, they have relied on modeling, and therefore contain a limited amount of observed data to validate the results. For example, the National Hurricane Center relied on the Sea, Lake and Overland Surges from Hurricanes (SLOSH) model to predict maximum potential

surge heights in coastal areas (Jennings 2013). Weisberg and Zheng (2006) used a high-resolution finite volume coastal ocean model to simulate storm surge potential in Tampa Bay. Other efforts utilized the ADvanced CIRCulation model (ADCIRC) to investigate storm surge processes and potential (Westerink et al. 2008; Dietrich et al. 2011; Kerr et al. 2013).

In May 2010, I completed a master's thesis that utilized observed data to analyze storm surge along the U.S. Gulf Coast. This thesis, titled, *Identifying Historic Storm Surges and Calculating Storm Surge Return Periods for the Gulf of Mexico Coast*, was submitted to the Graduate School at Louisiana State University (LSU) in partial fulfillment of the requirements for a master's degree (Needham 2010). In this thesis, I developed the first storm surge database for the U.S. Gulf Coast. This dataset identified the location and height of peak storm surge for 193 unique surge events in the region from 1880-2009, compiling data from federal government sources, academic literature and newspaper archives.

Portions of this thesis were published as a peer-reviewed journal article that documented the steps for creating the database, while providing an updated list of surge events in the region since 1880 (Needham and Keim 2012). This article provided a map of historic storm surge activity in the region (Figure 1.1), which revealed that the northern and western Gulf Coast, as well as the Florida Keys, have observed many high-magnitude storm surges since 1880, while the West Coast of Florida has observed less storm surge activity. This article also provided a name for the database, which we called The Storm Surge Database, using the abbreviation SURGEDAT.

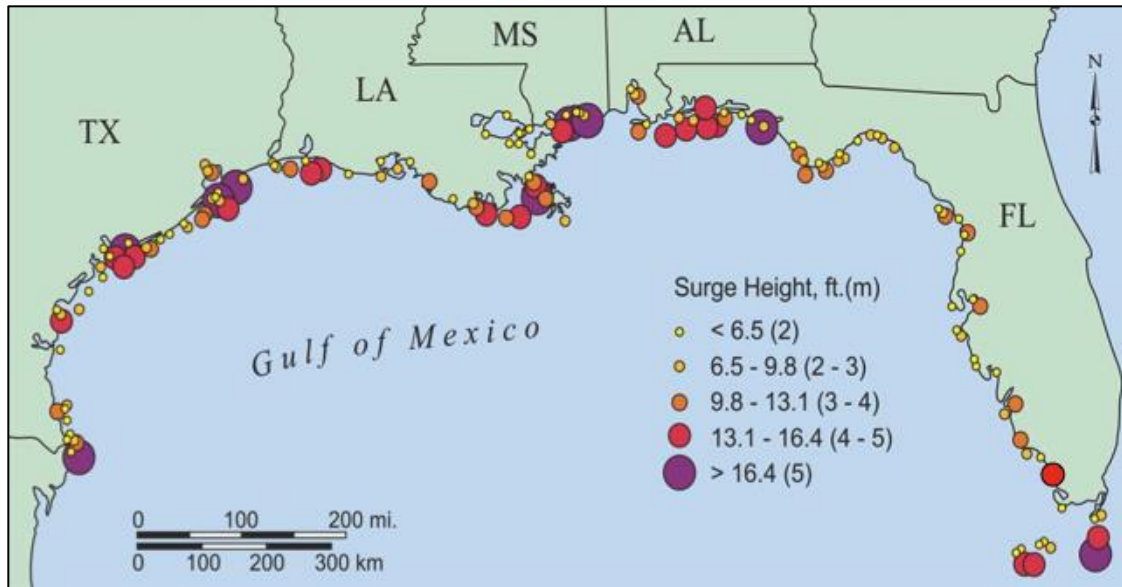


Figure 1.1. The location and height of peak storm surge levels along the U.S. Gulf Coast since 1880. Each circle represents a unique surge event. Adapted from Needham and Keim (2012).

Although SURGEDAT provided new insights into storm surge climatology, a major limitation of this dataset was that it only identified the location and height of the peak storm surge. However, large hurricanes often generate extensive storm surges that inundate hundreds of kilometers of coastline. To make SURGEDAT more useful, I led a research team to develop the dataset more extensively. In this process, we identified all high water marks for all tropical cyclones along the U.S. Gulf Coast since 1880, separated storm surge from storm tide observations, and referenced datums, or vertical lines from which high water observations are measured. This expansion generated considerably more data than the first version of SURGEDAT; for example, a map of Hurricane Ike’s storm surge and storm tide observations now contained more than 400 high-water marks, instead of just the peak water level (Figure 1.2).

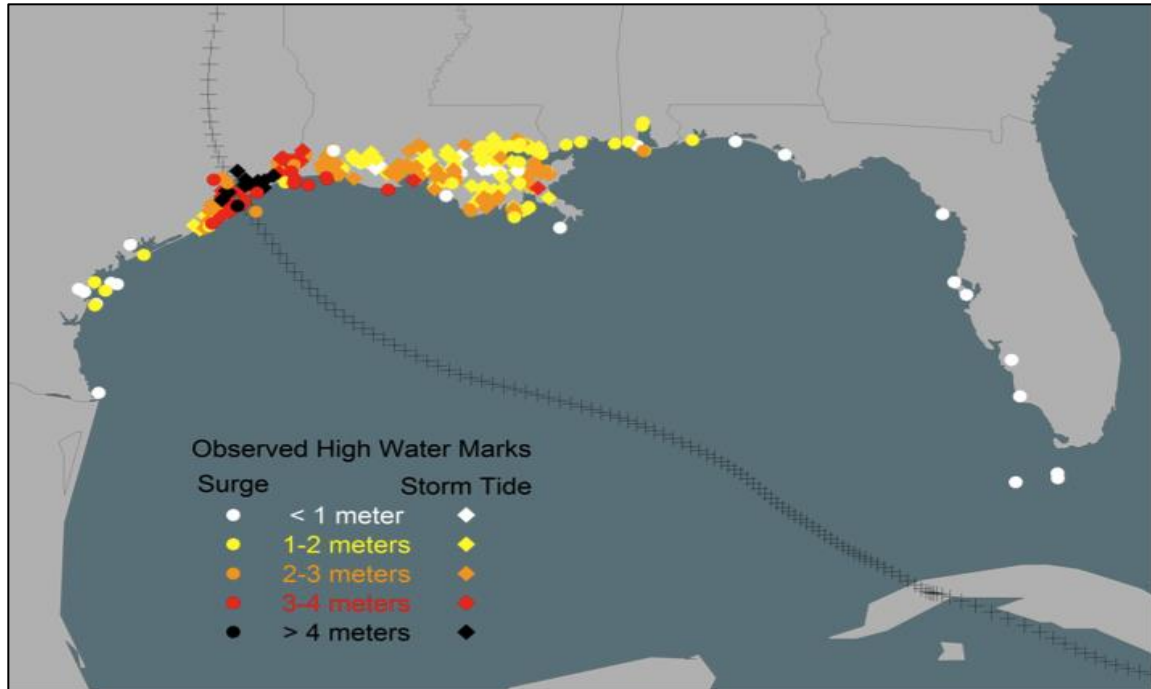


Figure 1.2. The location and height of more than 400 high-water marks produced by Hurricane Ike in 2008. Adapted from Doran et al. (2009); Federal Emergency Management Agency (2009); and Berg (2010).

We also expanded coverage to include the U.S. Atlantic Coast, following Beckage (2012), who developed the first peak storm surge database for this region. As of June, 2013, we had identified more than 7,600 high-water marks in the United States, including 5,200 along the Gulf Coast, and the updated SURGEDAT database was featured on the front page of *Eos Transactions* (Needham et al. 2013).

This updated version of SURGEDAT provided the first credible database for empirical storm surge analysis. This was timely, as destructive storm surges have inflicted damage from Texas to New York during the past decade, and scientific research published on this topic until this time took a modeling approach.

1.2 Objective

This dissertation builds on the momentum created by SURGEDAT to analyze surge data and build an even more extensive global database. This effort seeks to answer the following six research questions (or categories of questions):

- 1) How many storm surge observations are available globally, and for which ocean basins are these records provided?
- 2) How does storm surge along the U.S. Gulf Coast fit into a global context? How frequently does this basin experience high and low storm surges, and how do those levels of activity compare to other basins?
- 3) How well do storm surge heights along the U.S. Gulf Coast correlate with tropical cyclone wind speeds at and before landfall?
- 4) How important is tropical cyclone size for generating storm surge along the U.S. Gulf Coast?
- 5) How vulnerable are specific cities along the U.S. Gulf Coast to storm surge? For example, what is the 100-year storm surge level for various locations, and which statistical method(s) produce the best analysis?
- 6) How vulnerable is energy infrastructure to storm surge inundation along the U.S. Gulf Coast?

1.3 Organization

The dissertation is divided into seven chapters. The first chapter provides an introduction, the last chapter a conclusion, and the five chapters in between provide analysis of storm surge data. Four of the five analysis chapters investigate storm surge

along the U.S. Gulf Coast, while the other provides a global literature review of observed storm surge data. Specifically, the chapter titles are as follows:

Chapter 1) Introduction

Chapter 2) A Review of Tropical-Cyclone Generated Storm Surges: Global Data Sources, Observations and Impacts

Chapter 3) Correlating Storm Surge Heights with Tropical Cyclone Winds at and before Landfall

Chapter 4) An Empirical Analysis on the Relationship between Tropical Cyclone Size and Storm Surge Heights along the U.S. Gulf Coast

Chapter 5) Storm Surge Return Periods for the U.S. Gulf Coast

Chapter 6) The Vulnerability of Oil Refineries and Power Plants to Storm Surge along the U.S. Gulf Coast

Chapter 7) Conclusion

I conducted the global literature review in Chapter 2, and then investigated the processes by which tropical cyclones generate storm surge in Chapters 3 and 4. These two chapters have already been adapted into peer-reviewed journal articles that have been accepted for publication by *Earth Interactions*. I investigated the vulnerability of specific locations to storm surge in Chapter 5, and then applied these results to a study on the vulnerability of energy infrastructure to storm surge in Chapter 6. I intend to submit Chapters 2, 5, and 6 for publication after I defend my dissertation and apply minor alterations.

While the chapters of this dissertation answer many questions about storm surge, they also are bound by limitations in data availability and analytical methodology. After

questions are answered in each chapter, new questions are posed and future avenues for scientific research are presented. However, this work provides a pioneering step towards building a credible, global storm surge database, as well as several studies that demonstrate the usefulness of observed data for scientific analysis in the field of storm surge research.

1.4 References

Beckage, S., 2012: *An analysis of tropical storm surge trends for the Atlantic coast of the United States*. Master's thesis defended May, 2012. Louisiana State University.

Berg, R., 2010: Tropical Cyclone Report, Hurricane Ike. The National Hurricane Center, Miami, Florida, United States. Report made available on the Web at: www.nhc.noaa.gov/pdf/TCR-AL092008_Ike_3May10.pdf.

Blake, E.S., C.W. Landsea, and E.J. Gibney, 2011: The Deadliest, Costliest, and Most Intense United States Tropical Cyclones from 1851 to 2010 (And Other Frequently Requested Hurricane Facts). *NOAA Technical Memorandum NWS NHC-6*. This publication is available on the Web at: <http://www.nhc.noaa.gov/pdf/nws-nhc-6.pdf>.

Blake, E.S., T.B. Kimberlain, R.J. Berg, J.P. Cangialosi and J.L. Beven II, 2012: Tropical Cyclone Report, Hurricane Sandy, (AL182012), 22-29 October 2012. National Hurricane Center, Miami, Florida. Report available on the Web at: http://www.nhc.noaa.gov/data/tcr/AL182012_Sandy.pdf.

Chen, Q., L. Wang, and R. Tawes, 2008: Hydrodynamic response of northeastern Gulf of Mexico to hurricanes. *Estuaries and Coasts*, 31, 1098-1116.

Demuth, J., M. Demaria, and J.A. Knaff, 2006: Improvement of advanced microwave sounder unit tropical cyclone intensity and size estimation algorithms. *Journal of Applied Meteorology*, 45, 1573-1581.

Dietrich, J.C., M. Zijlema, J.J. Westerink, L.H. Holthuijsen, C. Dawson, R. A. Luettich, Jr., R. Jensen, J.M. Smith, G.S. Stelling, and G.W. Stone, 2011: Modeling Hurricane Waves and Storm Surge using Integrally-Coupled, Scalable Computations. *Coastal Engineering*, 58, 45-65.

Doran, K.S., N.G. Plant, H.F. Stockdon, A.H. Sallenger, and K.A. Serafin, 2009: Hurricane Ike: Observations and Analysis of Coastal Change. . Open-File Report 2009-1061. United States Geological Survey (USGS), Reston, Virginia Available on the Web at: <http://pubs.usgs.gov/of/2009/1061/pdf/ofr2009-1061.pdf>.

Federal Emergency Management Agency, 2009: Mitigation Assessment Team Report: *Hurricane Ike in Texas and Louisiana – Building Performance Observations, Recommendations and Technical Guidance*. Publication ID: FEMA P-757. Available on the Web at: <http://www.fema.gov/media-library/assets/documents/15498>.

Green, R., L.K. Bates, and A. Smyth, 2007: Impediments to recovery in New Orleans' Upper and Lower Ninth Ward: one year after Hurricane Katrina. *Disasters*, 31, 4, 311-335.

Hirshfeld, A.W., 2006: *The Electric Life of Michael Faraday*. Published by Walker & Company, New York. 256 pp.

Irish, J.L., D.T. Resio, and J.J. Ratcliff, 2008: The Influence of Storm Size on Hurricane Surge. *Journal of Physical Oceanography*, 38, 2003-2013.

Jennings, R., 2013: Personal correspondence with R. Jennings, Hurricane Program Specialist with FEMA Region 4. Communication through e-mail, November 2013.

Kerr, P.C., J.J. Westerink, J.C. Dietrich, R.C. Martyr, S. Tanaka, D.T. Resio, J.M. Smith, H.J. Westerink, L.G. Westerink, T. Wamsley, M. van Ledden, W. de Jong, 2013: Surge Generation Mechanisms in the Lower Mississippi River and Discharge Dependency. *Journal of Waterway, Port, Coastal, and Ocean Engineering*, 139, 326-335.

Knabb, R.D., J.R. Rhome, D.P. Brown, 2011: National Hurricane Center Tropical Cyclone Report on Hurricane Katrina. Published on the Web at: http://www.nhc.noaa.gov/pdf/TCR-AL122005_Katrina.pdf.

Martin, G.J., 2005: *All Possible Worlds- A History of Geographical Ideas*. 4th Edition. Oxford University Press, Oxford, United Kingdom. 605 pp.

McCallum, B.E., B.D. McGee, D.R. Kimbrow, M.S. Runner, J.A. Painter, E.R. Frantz, and A.J. Gotvald, 2012: Monitoring Storm Tide Flooding from Hurricane Isaac along the Gulf Coast of the United States, August 2012. Open-File Report 2012-1263. Available on the Web at: <http://pubs.usgs.gov/of/2012/1263/>.

Mowbray, R., 2007: Insurance panel locked in struggle to survive; rate-control strategy ineffective, some say. *Times-Picayune*. February 5.

Needham, H., 2010: *Identifying historic storm surges and calculating storm surge return periods for the Gulf of Mexico coast*. Master's thesis submitted May, 2010. Louisiana State University.

Needham, H.F., and B.D. Keim, 2012: A Storm Surge Database for the U.S. Gulf Coast. *International Journal of Climatology*, 32, 14, 2108-2123. DOI: 10.1002/joc.2425.

Needham, H.F., B.D. Keim, D. Sathiaraj, and M. Shafer, 2013: A Global Database of Tropical Storm Surges. *EOS, Transactions American Geophysical Union*, 94, 24, 213-214.

Nielsen, P., 2009: How storm size matters for surge height. *Coastal Engineering*, 56, 1002-1004.

Rego, J.L., and C. Li, 2009: On the importance of the forward speed of hurricanes in storm surge forecasting: A numerical study. *Geophysical Research Letters*, 36, 7.

Resio, D.T., and J.J. Westerink, 2008: Modeling the physics of storm surges. *Physics Today*, 61, 33-38.

Simpson, R. H., A.L. Sugg, and Staff at National Hurricane Center, 1970: The Atlantic hurricane season of 1969. *Monthly Weather Review*, 98, 293-306.

Warner, C., 2007: Insurance rate increases ok'd: Coastal parishes to bear bulk of higher changes. *Times-Picayune*. May 1.

Weisberg, R.H., and L. Zheng, 2006: Hurricane Storm Surge Simulations for Tampa Bay. *Estuaries and Coasts*, 29, 899-913.

Westerink, J.J., R.A. Luetich, J.C. Feyen, J.H. Atkinson, C. Dawson, H.J. Roberts, M.D. Powell, J.P. Dunion, E.J. Kubatko, and H. Pourtaheri, 2008: A Basin- to Channel-Scale Unstructured Grid Hurricane Storm Surge Model Applied to Southern Louisiana. *Monthly Weather Review*, 136, 833-864.

CHAPTER 2. A REVIEW OF TROPICAL-CYCLONE GENERATED STORM SURGES: GLOBAL DATA SOURCES, OBSERVATIONS AND IMPACTS

2.1 Introduction

Tropical cyclone-generated storm surges are among the most deadly and costly global catastrophes. The most severe storm surge events have killed hundreds of thousands of people and inflicted extraordinary economic losses. For example, the 1970 Bhola Cyclone generated a 9.1-m storm surge in Bangladesh that killed approximately 300,000 people (Frank and Husain 1971; Dube et al. 1997), while the 1900 Galveston Hurricane produced a 6.1-m storm surge (Garriott 1900) that killed at least 8,000 people (Blake et al. 2011) in the deadliest natural disaster in U.S. history (Emanuel 2005). More recently, Hurricane Katrina inflicted the most costly natural disaster in the history of the United States, as losses from this storm exceeded \$100 billion (Blake et al. 2011).

From a broader perspective, storm surge may have killed as many as 2.6 million people during the past 200 years (Nicholls 2003), or an average of 13,000 people annually. This rate fits well with the estimate of 10,000 to 15,000 annual storm surge deaths since 1850, provided by Nicholls (2006), and an annual rate of 15,000 surge deaths provided by Smith (1989). Most years observe less than this number of surge deaths, as several mega-catastrophes in the historical record, like the 1970 Bhola Cyclone, substantially increase the annual fatality average. Nonetheless, as many as 250 million people who live lower than the maximum storm surge level (Intergovernmental Panel on Climate Change 1994) are vulnerable to inundations from storm surge every year.

Unfortunately, a thorough literature review reveals an absence of review papers that summarize available information related to global storm surge observations. In

addition, the absence of a credible, global storm surge database leaves coastal populations and stakeholders unaware of coastal flooding events that have already impacted vulnerable areas. Such information would be valuable to people living in high-risk areas, as well as professionals in the fields of emergency management and law enforcement, insurance, construction, urban planning, health care, science and engineering.

This chapter addresses this void in the literature by providing a global review of tropical cyclone-generated storm surge data sources, observations and societal impacts. Surge impacts are not intended to provide a comprehensive overview of all impacts experienced by this hazard, but rather a general overview of the effects of storm surge inundation on various regions. A summary of surge impacts by basin also demonstrates that certain regions are severely impacted by storm surge inundations even though the magnitude or frequency of surges may be relatively modest compared to other regions.

Historical impacts do not necessarily depict the current vulnerability of these basins and sub-basins to storm surge. The development of technological innovations in the 20th and 21st centuries, such as wireless communications, radio, television, telephones, meteorological satellites, and, more recently, millions of personal computers networked through the World Wide Web, have worked together to inform vulnerable coastal populations of impending disasters. However, in certain regions, the coastal population has dramatically increased during the past several decades, placing millions of additional lives at risk, and perhaps countering the benefits of technological innovations. Storm surge observations found in this literature review are added to SURGEDAT, a global storm surge database (Needham et al. 2013). This archive provides the location

and height of peak storm surge observations around the world since 1880. An interactive Web map of these data is available at <http://surge.srcc.lsu.edu>.

The geographic scope of this chapter focuses primarily on the ocean basins that are most vulnerable to tropical cyclone-generated storm surges. Landsea and Delgado (2013) provide a list the following seven ocean basins as the most active to tropical cyclone (TC) activity: 1) Atlantic, 2) Northeast/ Central Pacific, 3) Northwest Pacific, 4) Northern Indian, 5) Southwest Indian, 6) Southeast Indian, and 7) Southwest Pacific. They also list the average annual number of TCs exceeding 17 m s^{-1} per basin (Table 2.1), which varies from 26 TCs/ year in the active Northwest Pacific, to a minimum of 4.8 TCs per year in the Northern Indian Ocean.

Table 2.1. Average annual number of tropical cyclones that develop in selected ocean basins, based on data from 1981-2010. Taken from Landsea and Delgado (2013).

| Basin | Tropical storm occurrences (sustained winds $> 17 \text{ m s}^{-1}$) | | Hurricane/ Typhoon occurrences (sustained winds $> 33 \text{ m s}^{-1}$) | |
|-----------------|--|------------|--|------------|
| | Average | Percentage | Average | Percentage |
| Atlantic | 12.1 | 14.1 | 6.4 | 13.6 |
| NE Pacific | 16.6 | 19.3 | 8.9 | 19.0 |
| NW Pacific | 26.0 | 30.2 | 16.5 | 35.2 |
| N Indian | 4.8 | 5.6 | 1.5 | 3.2 |
| SW Indian | 9.3 | 10.8 | 5.0 | 10.7 |
| Aus, SE Indian | 7.5 | 8.7 | 3.6 | 7.7 |
| Aus, SW Pacific | 9.9 | 11.5 | 5.2 | 11.1 |
| Global Total | 86 | 100 | 46.9 | 100 |

I have organized this chapter by the same regions, however, I combined the Southeast Indian and Southwest Pacific basins because most of the storm surge activity in these regions occurs in Australia. Combining these areas into one larger basin made it possible to keep all of the Australia storm surge literature within the same area of organization. As such, I have conducted a thorough literature for the following basins and sub-basins:

1) Western North Pacific, including East Asia; 2) Northern Indian Ocean, including the Bay of Bengal and Arabian Sea; 3) Western North Atlantic, including the Caribbean Sea, Gulf of Mexico and Atlantic Coast; 4) Eastern North Pacific, including Mexico and Hawaii; 5) Southeast Indian Ocean and Southwest Pacific Ocean, including Australia, New Zealand and Oceania; and 6) Southwest Indian Ocean. Table 2.2 provides a list of these regions as well as the major countries included in this chapter, while Figure 2.1 provides a world map depicting these regions.

Table 2.2. Ocean basins, sub-basins and countries represented in the global literature review of observed storm surge information.

| Ocean Basin | Sub-basins | Countries |
|---------------------------------|---|---|
| Western North Pacific | S. China Sea, E. China Sea, Yellow Sea | The Philippines, China, Japan, S. Korea, Vietnam, Thailand |
| Northern Indian Ocean | Bay of Bengal, Arabian Sea | India, Bangladesh, Myanmar, Pakistan, Oman |
| Western North Atlantic | Gulf of Mexico, Atlantic Ocean, Caribbean Sea | United States, Mexico, Belize, Honduras, Nicaragua, Caribbean Islands, Canada |
| Eastern North Pacific | Pacific Ocean | Mexico, Hawaii (U.S.) |
| Australia, New Zealand, Oceania | Pacific Ocean, Indian Ocean, Gulf of Carpentaria, Timor Sea | Australia, New Zealand, Island Nations in Oceania |
| Southwest Indian Ocean | Indian Ocean, Mozambique Channel | Madagascar, Reunion, Mozambique |

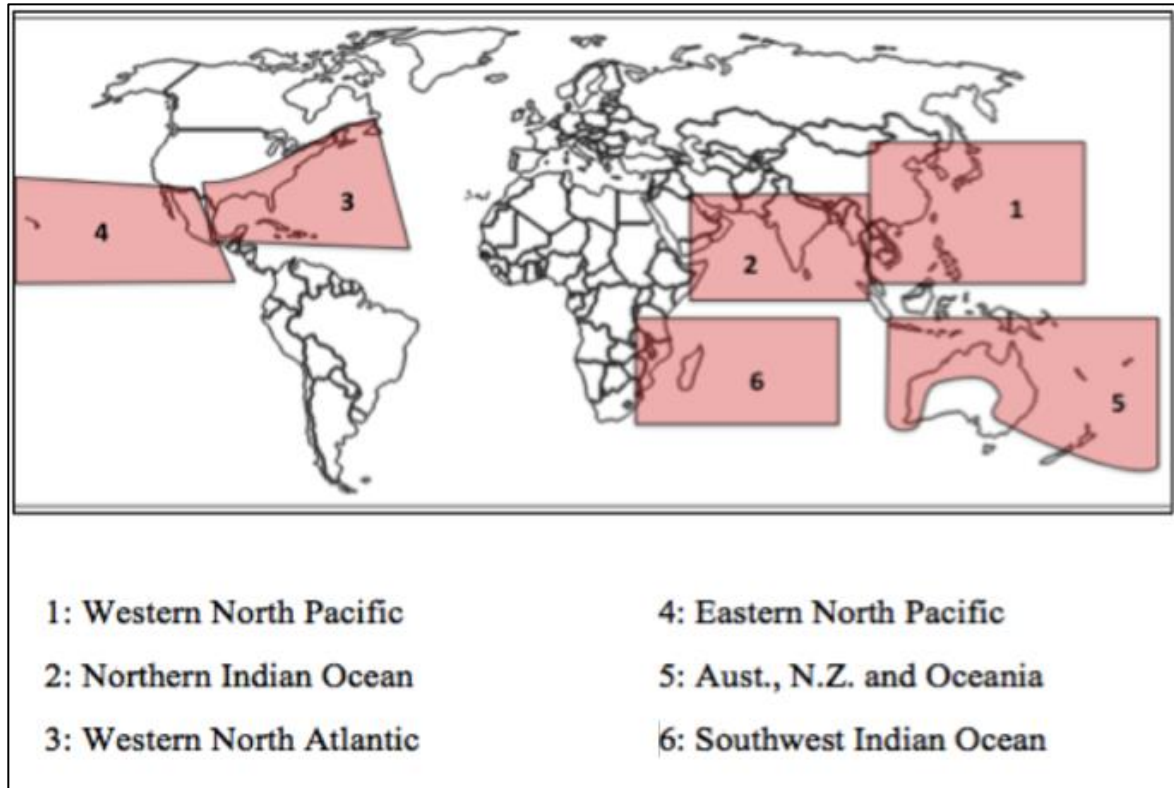


Figure 2.1. Map of the regions included in global literature review.

This literature review was conducted primarily in English, Spanish, French and Portuguese. English literature was found for every basin, but the highest volume of English literature was found for the Western North Atlantic and the Australia, New Zealand and Oceania basins. Spanish documentation was found for the Western North Atlantic, particularly Mexico, the Caribbean and Central America. French resources were found primarily for the Southwest Indian Ocean, especially for Madagascar and Réunion, although a few French documents were available for the Caribbean Sea. Portuguese resources were limited to Mozambique, as this was the only Portuguese speaking country that is frequently threatened by TCs. I also obtained Chinese literature that contained English titles or abstracts. In many of these cases, the body of the article was in Chinese, which was then translated into English for this literature review.

This review focuses on tropical-cyclone generated storm surges, although extra-tropical cyclones and strong frontal passages sometimes cause severe coastal flooding events, particularly in higher latitudes outside the subtropics. For example, Northern Europe has experienced many coastal flood events in its history, particularly in Germany, the Netherlands, the United Kingdom, and France. Extra-tropical storm surges have also impacted North America, especially along the U.S. Mid-Atlantic and New England coasts, in Eastern Canada, the Mackenzie Delta of Northwest Canada, and portions of western and northern Alaska. Although this chapter does not review the storm surge literature Europe, Northwest Canada or Alaska, I provide some observations from well-known extra-tropical surge events that occurred within basins that also observe TC strikes. Most of these events have occurred in Japan, Eastern Canada, the West Coast of Florida, or along the U.S. Mid-Atlantic and New England Coasts.

2.2 Western North Pacific (East Asia)

2.2.1 Storm Surge Literature

The Philippine Atmospheric, Geophysical and Astronomical Services Administration (PAGASA), provides scientific literature on a variety of geophysical hazards that impact the Philippines, including typhoons and storm surge (PAGASA 2014). Mr. C.P. Arafles, former deputy director of PAGASA, is recognized as the pioneer of storm surge research in the Philippines (Soriano 2003), and several articles he authored have become foundational for developing storm surge climatology in the region (Arafles and Alcances 1978; Arafles et al. 1984). Bankoff (2003) provides a comprehensive overview of natural hazards in the Philippines, including typhoons, storm surges and tsunamis.

The China Meteorological Administration (2014) maintains the CMA Tropical Cyclone Data Center, which provides best-track typhoon data, satellite reanalysis data, and information related to landfalling typhoons, observed wind and rainfall. Various re-analysis projects highlighted on this website provide typhoon data as far back as 1893. However, the site does not provide observed storm surge data. China's National Maritime Bureau has produced storm surge statistics in Chinese (Tang et al. 2011).

Most storm surge observations for China from English literature or Chinese literature with English abstracts or titles are made available through peer-reviewed journal articles. Various authors have provided summaries of the highest surge observations by time period or geographic region, which provides insight into the maximum surge potential along the coast of China. For example, Le (2002) provides the peak storm surge and storm tide heights for 18 typhoons that struck China from 1949-1997. Other sources provide the maximum water levels for 18 locations in Guangdong Province (Ma 2003; Zhang 2009). Most of these locations include at least 40 years of observations, and some records extend more than 50 years. Liu (2002) provides a similar list of peak storm surge levels for 25 cities in southeast China, for data ranging from 1949-1990. These sources summarize the highest water levels in the most surge-prone locations.

The Tokyo Typhoon Center, a Regional Specialized Meteorology Center (RSMC), affiliated with the Japanese Meteorological Agency (JMA), provides TC best track data for Japan from 1951-2013, as well as a summary of TC strikes per month for this same time period. However, the typhoon center and JMA have not provided historical storm surge records in English. Gilmore et al. (1995) have provided

climatological summaries for various ports in Japan, including high-water marks and storm surge history for some locations. For example, they provide a list of storm surge heights for Tokyo, Japan, during six typhoons that struck from 1911-1959. Also, Kawai (1999) and Kawai et al. (2009) provide storm surge observations from various typhoons to strike Japan.

The Joint Typhoon Warning Center (JTWC), a task force of the U.S. Navy and Air Force, provides TC reports for the Western North Pacific from 1959 - 2012 (Joint Typhoon Warning Center 2014). Although these reports contain detailed information about TC tracks and intensities, as well as rain and wind observations, they generally do not provide storm surge observations. However, in some cases, these reports provide flood depths over small islands or atolls, which are essentially storm surge observations, because most of the water in these floods comes from the sea. For example, a JTWC report states that Typhoon Ophelia in 1960 put 0.61 m of water over Ulithi Atoll, a small island in the present-day Federated States of Micronesia (Joint Typhoon Warning Center 1960). As the elevation of this island is approximately 1.22 m, the maximum surge level in this storm was approximately 1.83 m.

2.2.2 Storm Surge Observations

Approximately one-third of the world's TCs develop in the Western North Pacific basin (Elsner and Liu 2003), making this region the most active area on Earth for TCs. An annual average of 26.6 TCs formed in this basin during the 57-year period of 1951-2007 (Japan Meteorological Agency 2009). In this basin, TCs are called typhoons.

Storm surges in the Western North Pacific are observed in mainland East Asia in the countries of China, Vietnam, Thailand and South Korea, as well as island nations,

such as the Philippines, Japan, The Federated States of Micronesia, the republic of Palau, and the U.S. Territory of Guam. Available literature provides 119 coastal flooding events in the region, including 76 events in China, 28 in the Philippines, 11 in Japan, two in South Korea and one event in both Vietnam and the Federated States of Micronesia. These coastal flooding events were comprised of 73 storm-surge observations, 45 storm-tide observations, plus the high-water mark from Super Typhoon Haiyan in 2013, which combines storm tide plus waves. As field teams record high-water marks from this event, more accurate storm surge and storm tide observations that eliminate the effects of waves should become available.

Throughout much of East Asia, typhoons often generate enormous waves that rise well above observed storm surge levels, because relatively deep bathymetry near the coastline enables wave energy to approach close to the coast before dissipating. For example, Typhoon Doug in 1994 generated a storm surge level from 1.5 – 3 m near Lungtung Harbor, Taiwan, however, the storm generated destructive waves that reached a height of 20 m (Wang et al. 2005).

2.2.2.1 The Philippines

The archipelago of the Philippines may be affected by TCs more than any nation on Earth. From 1948-1990, 850 typhoons entered the Philippines Area of Responsibility (PAR), which means this region observes approximately 20 typhoons per year (Soriano 1992; Bankoff 2003). During that period, 384 typhoons made landfall in the Philippines, or about nine typhoons per year on average (Arafiles et al. 1984; Soriano 1992). The country observes storm surges approximately four to six times per year (Arafiles et al. 1984).

The most intense TC s ever recorded have been observed near the Philippines. Typhoon Tip in 1979 tracked through the eastern section of the PAR, but remained off shore and eventually tracked north, making landfall in Japan (Dunnavan and Diercks 1980). While east of the Philippines, this typhoon became the most intense TC in world history, registering a minimum central pressure of 870 mb (Dunnavan and Diercks 1980; Cerveny et al. 2007). Typhoon Haiyan in 2013 made landfall in Samar and Leyte, while maintaining maximum sustained winds of 87 m s^{-1} , which was the strongest sustained wind at landfall for any TC in world history (Masters 2013).

Due in part to the high number of super typhoons that have struck the Philippines, this nation has recorded the highest storm surge levels in East Asia. The four highest storm surges in East Asia exceeded 6.5 m and all occurred in the Philippines (Table 2.3). Typhoon Didang generated a 9.14-m storm surge in 1968 at Narvacan, Illocos Sur, in the northwestern portion of Luzon (Arafiles and Alcances 1978; Henderson 1988). Further research should be conducted on the accuracy of this surge level because it is substantially higher than other surges in western Luzon, and was presumably caused by wrap-around winds on the back side of a typhoon that clipped the northern tip of the island, while tracking towards the northwest. Although the strong typhoons strike northern Luzon more than any other area of the Philippines (Bankoff 2003), the islands of Samar and Leyte, including portions of the Eastern Visayas region of the Philippines, have more frequently observed high-magnitude storm surges. The Typhoon of Samar and Leyte generated a 7.3-m storm tide in 1897 (Bankoff 2003), followed by a 7.0-m storm surge from the Typhoon of Leyte and Cebu in 1912 (Arafiles and Alcances 1978; PAGASA 1987). In 2013, Typhoon Haiyan generated a destructive coastal flooding event

at Tacloban, on the island of Leyte. The water level reached approximately 6.50 m at the Tacloban Airport, however, such measurements are preliminary and include a combination of storm tide and waves (Needham 2013).

Various sources provide insight into the timing of storm surges in the Philippines. For example, historical records indicate that the 7.3-m storm tide persisted for at least three hours in southern Leyte during the 1897 typhoon (Bankoff 2003). Typhoon literature also reveals that storm surges sometimes rapidly strike the Philippines. For example, a storm surge struck the community of Tarol so suddenly in 1908 that many people did not have time to flee to safety. According to Arafiles and Alcances (1978, pg. 366),

“It was about 4 A.M. of the 13th, when we observed that the water was rising and beginning to flood the lowland of the town, but no one gave this fact any importance as it is usual, when a typhoon passes, that the water of the river rises about a meter. But at about 6 A.M. almost suddenly the waves of the sea like mountains of water precipitated themselves upon the barrio of Tarol destroying houses and whatever they met in their way. The level of the sea rose so rapidly that only some of the inhabitants had time to escape and save their lives.”

More recently, Typhoon Haiyan's storm surge struck the city of Tacloban nearly instantaneously, as a wall of water more typical of a tsunami than a storm surge destroyed much of the city in a matter of minutes (Weber 2014). Strong offshore winds blowing from north to south over San Pedro and San Pablo Bay initially impeded the rising storm surge while Haiyan's center was positioned east of Tacloban, but as the eye of the typhoon approached the city, sustained winds at approximately 87 m s^{-1} suddenly blew in from the southeast and pushed a massive wall of water towards the city (NOVA 2014). This sudden storm surge inflicted catastrophic flooding in the city of Tacloban and surrounding areas.

Table 2.3. Top 10 tropical cyclone-induced surge levels in the Western North Pacific from 1880-2013. Compiled from the following sources: Arafiles and Alcances (1978), PAGASA (1987), Henderson (1988), Bankoff (2003), Mai et al. (2006); Neumann et al. (2012); Needham (2013).

| Rank | Height (m) | Year | Storm Name | Maximum Surge Location |
|------|------------|------|-------------------------|-----------------------------------|
| 1 | 9.14 | 1968 | Didang | Narvacan Ilocos Sur, Philippines |
| 2 | 7.30 | 1897 | Typhoon of Samar/ Leyte | Samar and Leyte, Philippines |
| 3 | 7.00 | 1912 | Typhoon of Leyte/ Cebu | Leyte and Cebu, Philippines |
| 4 | 6.50 | 2013 | Haiyan | Tacloban, E. Visayas, Philippines |
| 5 | 5.94 | 1980 | China Typhoon No. 8007 | Nandu, Guangdong, China |
| 6 | 5.02 | 1956 | China Typhoon No. 5612 | Hanpu, China |
| 7 | 4.60 | 1984 | Unnamed | Sarangani Island, Philippines |
| 8 | 4.50 | 1983 | Unnamed | Near Infanta, Philippines |
| 9 | 4.50 | 1981 | Rosita | South of Tinambac, Philippines |
| 10 | 4.00 | 2005 | Damrey | Vietnam |

Water Height: a = Storm Surge; b = Storm Tide; c= Storm Tide + Waves

The coastal configuration of the Philippines, including the shape, orientation and position of its many islands, bays and gulfs, has a strong influence on storm surge characteristics in the Philippines (Arafiles and Alcances 1978; Soriano 1992). This ingredient likely explains why storm surges can suddenly inundate coastal communities in this nation. In contrast to broad, open coastlines that often experience gradual water level rises as TCs approach, the Philippines sometimes experiences rapid water level rises when intense winds in the eyewall of a typhoon suddenly blow massive amounts of water into bays or narrow inlets of water. The complex coastal configuration of the Philippines also produces very localized surge levels (Soriano 1992) that can vary substantially over the distance of just several km.

The Philippines is also vulnerable to tsunami inundations, as the archipelago experiences earthquakes and volcanoes that sometimes generate seismically-induced

water-level rises. At least 27 tsunamis have been reported since 1603, with waves crests exceeding 25 m in the most severe events (Bankoff 2003). Unfortunately, a severe tsunami occurred in 1897, the same year that the Typhoon of Samar and Leyte produced a destructive storm surge. During the tsunami, the ocean rose 6 m above its bed along the Philippine coast (Bankoff 2003).

2.2.2.2 China

China's extensive coastline exposes the country to frequent typhoon strikes and inundations from storm surges. This irregular coastline is one of the longest in the world, measuring a distance of greater than 18,000 km on the mainland and more than 32,000 km when including the coastline of numerous islands (Han et al. 1995). During the 50-year period from 1952-2001, China observed an average of seven typhoon strikes per year and a maximum of 12 typhoon strikes in the most active years (Xuejie et al. 2002).

China's National Maritime Bureau has provided statistics on the frequency of storm surge events along the coast of China. During the 50-year period from 1949-1998, storm surges exceeding 1m were observed 270 times, surges exceeding 2m were experienced 48 times, while surges greater than 3 m occurred 15 times (Tang et al. 2011). These statistics reveal that surges frequently strike China, with an annual rate of 5.4 surges exceeding 1m, 0.96 surges greater than 2m, and 0.3 surges exceeding 3m.

Scientific literature in English or in Chinese with English abstracts or titles provided coastal flooding observations for 76 historical typhoons that have struck China. These records are comprised of both storm surge and storm tide observations. The body of many articles was written in Chinese, which was translated to English. Fortunately, the terms "storm surge" and "tide" often translated directly from Chinese to English,

however, a common term for storm surge is translated directly into English as “highest water rising.”

The highest storm surge level observed in China occurred in July, 1980, as Typhoon No. 8007 generated a storm surge of 5.94 m at Nandu Tide Gauge in the city of Leizhou, Guangdong Province (Liu and Wang 1989; Ma 2003, Zhang 2009). This tide gauge has consistently observed high storm surge levels, as four of the six highest water levels observed in coastal flooding events in China were recorded at this location, according to available scientific literature. These storm surge observations include a 3.52-m surge produced by Typhoon No. 8616 in 1986 (Le 2002), a 3.84-m surge produced by Typhoon No. 9111 in 1991 (Le 2002), and a 3.66-m surge generated by Typhoon No. 0312 in 2003 (Ma 2004). A devastating storm surge that did not peak at Nandu Tide Gauge occurred in 1956, when Typhoon No. 5612 generated a storm surge that exceeded 5 m along the shore of Hangzhou Bay, east of Hangzhou, Zhejiang Province (Wang et al. 1991; Le 2002).

Although an English literature review does not capture data for the majority of the storm surge events that have struck China, various peer-reviewed journal articles summarize the highest observed water levels by location or the peak water level produced by different typhoons (Le 2002; Lui 2002; Ma 2003; Zhang 2009). These summaries ensure that the largest storm surges in the history of China are documented in the scientific literature.

2.2.2.3 Japan

From 1951-2007, an average of 5.6 typhoons per year came within 300 km of the four main Japanese islands (Japan Meteorological Agency 2008), while the number of

typhoon landfalls in these islands averaged 2.9 per year (Grossman and Zaiki 2009). Many of these typhoons generated low-magnitude storm surges, however, at least two typhoons in modern-day Japan have generated substantial surges that have exceeded 3 m.

In 1959, Super Typhoon Vera generated a storm surge between 3 and 4 m along the northern coastline of Ise Bay, near the city of Nagoya (Kawai 1999; Donovan and Grossi 2009). Due to the severe inundation around Ise Bay, the Japan Meteorological Agency called the storm “Isewan.” The storm inundated over 310 km² of land (Donovan and Grossi 2009).

Typhoon Bart generated a storm surge with a similar magnitude in 1999, producing a surge of approximately 3.5 m in Yatsushiro Bay (Kawai et al. 2009). The timing of this surge event was unfortunate, as it occurred near the time of spring tide, enabling water to reach the roofs of single-story houses (Kawai et al. 2009).

As Japan is positioned off the coast of East Asia, it is also vulnerable to coastal flooding produced by non-tropical systems, such as extratropical storms and frontal passages. Most of Japan is far enough north to observe strong cold front passages, and strong winds behind such fronts sometimes produce minor coastal flooding along west- or north-facing shores, as strong winds push water from the Sea of Japan onshore. For example, the port of Otaru, which is situated on north-facing Ishikari Bay, observed a 1.7-m surge in 1951 that was produced by a non-tropical system (Gilmore et al. 1995).

Historically, tsunamis have generated higher-magnitude coastal flooding events than storm surges in Japan. The most severe tsunami in Japan’s history occurred in March, 2011, when a 9.0-magnitude earthquake off the east coast of Japan generated a tsunami as high as 19.5 m on the Sendai Plain of Tohoku (Mori et al. 2011). Wave runup

from this tsunami reached a height of 38.9 m in Iwate Prefecture (National Geophysical Data Center 2012). In 1946, an 8.1-magnitude earthquake produced a 5-6 m tsunami on the east and south coasts of Shikoku, as well as along the east coast of the Kii Peninsula on Honshu (MCEER 2014). The Great Tokyo Earthquake of 1923 generated waves as high as 6 m on the Boso and Izu Peninsulas (MCEER 2014).

2.2.2.4 Vietnam and Thailand

Destructive storm surges are less common in the history of Vietnam and Thailand than countries to the north and east, like China and the Philippines. Vietnam and Thailand are located near the southern edge of the active typhoon belt in the Western North Pacific, and typhoons that approach these countries will often weaken after encountering land, such as the archipelago of the Philippines. However, both of these countries have experienced some strong typhoons. Vietnam is impacted by four to six typhoons per year on average (Mai et al. 2008), while an average of three typhoons per year have tracked near Thailand from 1951-2006 (Vongvisessomjai 2009).

TCs and associated storm surges that impact Vietnam are the greatest threat along the northern and central coastline of the country. Storm surges along Vietnam's Gulf of Tonkin have historically ranged from 0.5 – 3.0 m high (Hanh and Furukawa 2007). Typhoons Linda in 1997 and Damrey in 2005 were the two most severe storm surges to strike Vietnam in recent decades. Damrey produced a storm surge of 3-4 m and pushed salt water 3-4 km inland (Mai et al. 2006; Neumann et al. 2012). Typhoon Linda in 1997 was a rare, destructive typhoon that struck southern Vietnam (Thuy 2003). Linda's surge produced the highest water levels in a 20-year period in the Mekong River Delta, as the storm unfortunately struck at high tide (Le et al. 2007). The funnel-like shape of the

Mekong River estuarine area generates a high tidal range, with an average tide of 2.2 m and a maximum range of 3.2 m (Wolanski et al. 1996).

After generating a destructive storm surge in Vietnam, Typhoon Linda inundated Thailand. Although observed surge data are not available for this surge event in Thailand, numerical modeling indicates that surge heights may have reached approximately 70 cm in the northwestern Gulf of Thailand (Ascharyaphotha et al. 2011). The northern portion of the Gulf of Thailand is relatively protected from storm surge because this relatively small basin has a fetch of only approximately 100 km, which may also explain why the storm surge from Typhoon Vae in 1952 barely exceeded 1 m (Vongvisessomjai 2007). Typhoons Harriet in 1962 and Gay in 1989 struck farther south in Thailand and generated higher surge and waves because they had longer fetches for displacing water (Vongvisessomjai 2007).

Sea-level rise may exacerbate storm surge inundations in Vietnam, as the elevation of the majority of the Mekong Delta is less than 2 m above sea level (Wassmann et al. 2004) and the Delta is experiencing considerable subsidence (Syvitski et al. 2009). A relative sea-level rise of 20 or 45 cm would move elevation contours by 25 or 50 km, respectively (Wassmann et al. 2004), which means that future storm surges would push inland considerably farther.

2.2.2.5 South Korea

South Korea is less vulnerable to storm surge than nearby countries like China and Japan, because the country has a smaller coastline and is less exposed to TC tracks than its neighbors. On average, two or three TCs pass near the Korean Peninsula each year (Moon et al. 2003). However, the country has experienced several severe storm

surge inundations from TCs. Typhoon Sarah in 1959 generated a destructive storm surge in the southern part of the peninsula, and coastal flooding was also experienced in August, 1971, and July, 1987 (Moon et al. 2003). More recently, Typhoon Maemi generated a destructive storm surge in 2003, as storm surge at Masan Port reached a level of 2.30 m (Kang et al. 2009).

Large tidal variations along the Korean Peninsula threaten to elevate water levels well beyond the height of storm surge. Unfortunately, the storm surge from Typhoon Maemi coincided with spring high tide, nearly doubling water levels to a maximum water height of 4.3 m above the local datum at Masan Port (Kang et al. 2009). The 9-m tidal range at the port of Inchon, South Korea, threatens to generate very high water levels if a storm surge inundation coincides with high tide (Gilmore et al. 1995).

South Korea is also vulnerable to coastal flooding from TCs that strike China, as high water levels sometimes extend across the Yellow Sea. For example, Typhoon Winnie in 1997 generated water levels that broke 36-year records at the Korean ports of Kunsan and Mokpo (Moon et al. 2003), even though these cities did not experience strong winds, as the typhoon tracked more than 800 km south of the Korean Peninsula and struck China.

2.2.3. Storm Surge Impacts

2.2.3.1 The Philippines

Storm surges have killed more people in the Philippines than other typhoon hazards, such as heavy rain or strong wind (Soriano 1992). For example, storm surge was responsible for 1,923 of the 2,074 typhoon-related fatalities in 1984 (Soriano 1992).

Storm surge also likely killed the majority of the 14,159 people Philipinos who died from typhoons from 1948-1990 (Soriano 1992).

Super Typhoon Haiyan's storm surge was likely the deadliest in the history of the Philippines. The storm killed approximately 8,000 people (Aon Benfield 2014), most of whom died in storm surge on the islands of Leyte and Samar, including the city of Tacloban. The storm inflicted 13 billion U.S. dollars in economic losses (Aon Benfield 2014). Approximately 1,300 deaths from the Typhoon of Samar and Leyte in 1897 were directly caused by the devastating storm surge (Arafiles and Alcances 1978). Typhoon Irma's storm surge in 1981 drowned at least 100 people, storm surge caused many of the deaths in Typhoon Nitang in 1984, and surge caused 200 of the 882 fatalities in the Bicol region during Typhoon Nina in 1987 (Henderson 1988).

Less deadly and lower-magnitude storm surge events have sometimes inundated the region around Manila Bay. Water levels in these events have reached as high as 2 m (Perez et al. 1999). However, this is the most densely populated region in the archipelago, and even modest water-level rises cause extensive damage and displace large numbers of people. Densely populated areas around Manila Bay, such as Navotas and Malabon, may adapt to gradual sea level increases associated with climate change, but will not likely survive storm surge events (Perez et al. 1999).

Storm surge also impacts the agricultural sector in the Philippines. Such impacts may be especially pronounced in areas where coastal mangroves have been converted to agriculture or aquaculture, such as fish-breeding ponds (Primavera 2000). Storm surge inflicted an annual average of \$968,000 in losses from 1970-1986 in the Philippines (Henderson 1988).

2.2.3.2 China

The most deadly typhoons to impact coastal East Asia during the twentieth century both struck China, killing 50,000 people in 1912 and 60,000 people in 1922 (National Oceanic and Atmospheric Administration 1999). Although the number of deaths caused by storm surge in these events is not available, several sources provide evidence that the 1922 typhoon generated a storm surge that devastated the region around the city of Swatow, China. A *New York Times* article (Anonymous 1922a) reports that the typhoon generated a destructive storm surge in this region, while the *Monthly Weather Review* (Anonymous 1922b, pg. 435) recounts that a storm surge accompanied the storm, and that, “houses that escaped being blown down were washed away by the waters which spread over the whole country side, and the loss of life was enormous.”

Since 1950, the most deadly storm surge events in China have killed between 1,000 and 2,000 people. Typhoon 6903 was the deadliest recent surge event in Guangdong Province, killing 1,554 people in 1969 (Zhang 2009). Typhoon Fred (Typhoon 9417) generated the most fatal surge in Zhejiang Province, killing 1,216 people in 1994 (Le 2000).

Some sources indicate that typhoons killed 300,000 people in China in the 1880s (Frank and Husain 1971; Dube et al. 1997), however, considerable uncertainty remains regarding the timing of this event and magnitude of fatalities. Frank and Husain (1971) state that the Chinese typhoon occurred in 1881, Dube et al. (1997) provides the year as 1886, and Gunn (2008) reports that an intense typhoon struck Vietnam in 1881. Bankoff (2003) indicates that a major typhoon struck Indo-China in 1881, but provides a total of 20,000 fatalities. While these sources suggest a catastrophic typhoon struck Southeast

Asia sometime in the 1880s, these conflicting accounts cast doubt upon the details, specifically, the extraordinary number of deaths- five times the next highest fatality total in this region.

Storm surges cause more economic loss than any other marine hazard in China (Le 2000). The surge generated by Typhoon 9615 in 1996 inflicted the most severe economic loss of any storm surge in Guangdong Province, totaling approximately 129 billion Yuan, or 20 billion U.S. dollars (Zhang 2009). Typhoon Winnie in 1997 caused 33.7 billion Yuan or approximately 5.5 billion U.S. dollars in economic loss (Le 2000), while Typhoon Fred in 1994 inflicted damage totaling 17.8 billion Yuan or nearly 3 billion U.S. dollars in Zhejiang Province (Le 2000).

The high population density along the coast of China increases the destructive potential for storm surges, as the 1-m coastal flood plain contains approximately 73 million people (Han et al. 1995). Past storm surge events in China have therefore caused considerable damage. For example, Typhoon Fred ruined 520 km of seawalls, flooded 189 towns and inundated more than 22 million people (Le 2000), even though the maximum surge level in this event was only 2.69 m (Le 2002).

Storm surges in China also inflict severe damage on several economic sectors, including agriculture and the energy industry. Typhoon No. 9615 in 1996, for example, flooded 44,400 km² of farmland in Guangdong Province, the most of any surge event in the history of that province (Zhang 2009). Storm surges also threaten the onshore and offshore energy industry, including coastal nuclear and thermal power plants (Fengshu and Xinian 1989). Typhoon No. 9711 in 1997 shut down the tidal power station at Beishakou and damaged infrastructure on the Shengil oil field (Le 2000).

2.2.3.3 Japan

Typhoon Vera inflicted the greatest losses of any Japanese storm surge. The storm killed 4,687 people (Kawai 1999), and most of these fatalities were caused by the severe storm surge (Donovan and Grossi 2009). The storm surge inflicted heavy losses on the city of Nagoya, turning the harbor into a “sea of dead” (Joint Typhoon Warning Center 1959, pg. 189), while enormous waves killed 300 people and destroyed 250 homes in the town of Handa, southeast of Nagoya (Joint Typhoon Warning Center 1959).

Wind and surge damage from this event totaled \$260 million in 1959 dollars (Joint Typhoon Warning Center 1959). The storm damaged 834,000 buildings, nearly half of which were damaged by flooding (AXCO 2009). Industrial losses near the harbor of Nagoya were also severe (Donovan and Grossi 2009). More recently, in 2004, Typhoon Chaba generated record-high storm tides at the ports of Takamatsu and Uno, Japan, flooding 16,799 houses above floor level in Japan (Kohno et al. 2009).

Tsunamis in Japan have caused even greater losses of life and property. As of March, 2012, The National Police Agency of Japan reported 15,854 deaths and more than 3,000 people missing from the March 2011 tsunami (National Geophysical Data Center 2012). This tsunami also caused a serious accident at the Fukushima Nuclear Power Plant, damaged nearly 250,000 homes, and may carry a price tag as high as 25 trillion yen or more than 24 billion U.S. dollars (Mimura et al. 2011). Earthquake-generated tsunamis in Japan also killed 31,000 people in 1498 and 13,000 people in 1771 (National Geophysical Data Center 2012).

Some sources indicate that a typhoon in Japan killed 250,000 people in 1923 (Frank and Husain 1971; Dube et al. 1997). Such a catastrophe would rank among the

most deadly typhoons in global history and make this event more than 50 times as deadly as any other typhoon in Japan's history. Investigation into this event reveals that an intense earthquake struck near Tokyo in 1923, and catastrophic fires resulting from the quake killed more than 100,000 people (Himoto 2007; Schencking 2008). The unfortunate timing of a passing typhoon fanned the flames into a raging inferno that was responsible for more than 90% of the deaths (Himoto 2007). While this nearby typhoon may have exacerbated the tragedy, it was not the initial cause of this disaster, and no sources indicate that storm surge contributed to this catastrophe.

2.2.3.4 Vietnam and Thailand

Typhoon Linda in 1997 inflicted severe damage in southern Vietnam. Fatality reports vary, as at least one source reported nearly 4,000 people killed or missing because of the storm surge (Le et al. 2007), while other sources indicated that the fatality total was closer to 600 (Ascharyaphotha et al. 2011; Vongvisessomjai 2009). Approximately 30,000 people were displaced in Vietnam, where the storm caused 472 million U.S. dollars in losses (Vongvisessomjai 2009). The wind and surge impacts of this storm were less severe in Thailand and Cambodia, but more than 30 deaths were still reported and 200 fishermen were missing due to this storm (Ascharyaphotha et al. 2011). Typhoon Damrey in 2005 killed at least 68 people in Vietnam, forced the evacuation of 150,000 and either destroyed or severely damaged schools and hospitals (LeDang 2013). Damrey's storm surge caused sea-dike breaches along more than 8km of the Nam Dinh coastline, which resulted in direct losses of more than 500 million U.S. dollars (Disaster Management Working Group 2005; Mai et al. 2008).

Coastal flooding has also inflicted severe agricultural impacts in the low-lying Mekong River Delta of Vietnam, as surges have inundated croplands with salt water. For example, Typhoon Damrey flooded more than 1300 km² of rice fields, while also damaging irrigation systems (Mai et al. 2006). The impact of extensive storm surges could have severe economic repercussions in the region, as rice production makes up 78% of land use in the Vietnamese Mekong Delta, and Vietnam has become the third largest rice exporter in the world (Sanh et al. 1998; Wasserman et al. 2004).

Sea-level rise threatens to exacerbate the impacts of storm surges in Vietnam in the future. The country ranks among the top-five developing countries that would be most impacted by 1m of sea-level rise, considering factors such as land use, economics, the extent of urban and agricultural lands, as well as population distribution (Dasgupta et al. 2009). The World Bank considers Vietnam among the top 12 countries at risk from rising seas (World Bank 2009; Neumann et al. 2012).

2.2.3.5 South Korea

Although storm surges in South Korea are generally smaller and less frequent than those that strike China and Japan, the most severe events have killed hundreds of people, produced millions of dollars in damage, and affected the national economy. Super Typhoon Sarah in 1959 was the worst typhoon to hit South Korea in 50 years, left 849 people dead and inflicted \$200 million in damage (Oh et al. 1993; Moon et al. 2003). The storm generated a storm surge that inundated the areas near Pusan. Damage to the port of Pusan exceeded \$100,000, 28,834 people were left homeless, and 15,379 homes were destroyed or damaged (Joint Typhoon Warning Center 1959). More recently, Typhoon Maemi in 2003 inflicted the most severe coastal disaster in the history of South Korea

(Lee et al. 2009). This storm killed more than 117 people, left more than 25,000 people homeless, and destroyed or marooned 465 vessels (Ye 2004). Maemi inflicted 5.52 trillion KRW, or 4.8 billion U.S. dollars, in economic losses on the country (Ye 2004). Maemi's storm surge also impacted the national economy, as this surge destroyed critical infrastructure in the port of Pusan, the country's largest port, which handles approximately 80 percent of South Korea's container shipping (Ye 2004). The combined effects of wind and storm surge pushed over 11 enormous container-lifting cranes, which each weighed 900 tons (Ye 2004). Economic losses from slowed exports impacted companies such as Samsung, LG Electronics and Hyundai Heavy Industries (Chinapost 2003; Ye 2004). Although Typhoon Winnie struck China in 1997, it still generated a coastal flooding event along the Korean Peninsula that damaged more than 18 million dollars in property (Moon et al. 2003).

2.3 Northern Indian Ocean

2.3.1 Storm Surge Literature

The India Meteorological Department (2013) has recently begun posting annual TC reviews on its website. Annual reviews are available for 2010 and 2011, while preliminary reports of specific TCs are available for the 2011 and 2012 seasons. These reports provide observed data for various natural hazards associated with TCs, including storm surge.

The Bangladesh Meteorology Department (2013) provides a TC webpage, however, the content on this site is devoted to TC tracks and wind fields, as well as sea surface temperature maps and satellite imagery. The site provides no observed storm surge or coastal flooding data.

The Myanmar Department of Meteorology and Hydrology (2011) provides a webpage with an overview of TC disasters in this country. This site provides a list of cyclone damage and socioeconomic impacts from TCs since 1884. This list mostly provides the number of human fatalities, agricultural losses, such as number of cattle fatalities, the economic losses in the currency of Myanmar Kyats, as well as the percent of structures damaged in selected cities. This site also provides at least one storm surge height observation, from cyclone Mala, which struck near Gwa, in 2006.

The Joint Typhoon Warning Center (2014) is the U.S. Department of Defense agency responsible for issuing TC warnings for the Pacific and Indian Oceans. This agency provides an archive of Annual TC Reports from 1959-2011. Unfortunately, the links to these reports were broken as of 2013.

Peer-reviewed journal articles provided the majority of storm surge observations for this region. Dube et al. (1997) provide the Basin's most comprehensive storm surge data. They provide a list maximum storm tide levels from 29 unique TCs that struck Bangladesh, peak storm surge levels from eight separate cyclones that affected India, surge impacts from cyclones that have struck the region since the 1970s, and a ranked list of deaths in the 22 of the most deadly TC events worldwide over the past 300 years. Dube et al. (2008) and Dube et al. (2009) provide some updated storm surge observations, and use observed surge data to validate surge modeling analyses. Das (1994) provides a short list of fatalities from some TCs in this region, while providing storm tide observations for some TCs from 1970-1990. Fritz et al. (2009) provide observed storm surge levels and impacts from field work following Cyclone Nargis in

Myanmar, while Fritz et al. (2010) provide similar observations and impacts from Oman, following TC Gonu, which struck the Sultanate in 2007.

Although some of these sources separate storm surge from storm tide, none of these sources provide specific datum from which storm tide heights are measured. For example, Das (1994) provides a list of six high-water elevations, which are listed as the observed value of storm surge plus tide levels. I concluded that these water heights refer to storm tide elevations, but do not have a specific datum from which these heights are measured. In other cases, the distinction between storm surge and storm tide is a bit more ambiguous. For example, Dube et al. (1997) provides a list of maximum water elevations for India, listed as, “peak surge” (pg. 286), whereas the observations for Bangladesh are listed as, “observed maximum water levels” (pg. 285). Given the wording of these observations, it appears as though the Indian observations refer to storm surge, while the Bangladesh observations are storm tide, however, some ambiguity exists over such distinctions.

2.3.2. Storm Surge Observations

Scientific literature provides a total of 57 storm surge or storm tide observations for the Northern Indian Ocean. Fifty-three of these observations occurred in the Bay of Bengal, along the coastlines of eastern India, Bangladesh, Myanmar and Sri Lanka, while four observations are provided from the Arabian Sea, along the coast of Western India, Pakistan and Oman. The oldest record, a 12-m storm surge that struck India in 1737 (Dube et al. 1997), is one of the earliest surge observations in the world. Most observations in this basin are more recent; 54 of these records occurred since 1952. Most of these surge events occur before (April-May) or after (October-November) the summer

monsoon season (Ali 1996; Jakobsen et al. 2006; Fritz et al. 2010), although some cyclones occurred in June, September and December.

2.3.2.1 Bay of Bengal

Storm surges along the northern shores of the Bay of Bengal in Bangladesh and India have reached extraordinary heights. Surge levels in the most catastrophic events range from 12 to 14 m (Jakobsen et al. 2006). The 13.7-m storm tide observed in 1876 at the Meghna Estuary was the highest water level observed in this basin. A list of the 10 highest water levels in the Bay of Bengal (Table 2.4), constructed from observations provided by Dube et al. (1997), range from 8.8 to 13.7 m.

Table 2.4. The top 10 highest Northern Indian Ocean tropical cyclone-induced storm surge levels, from Dube et al. (1997).

| Rank | Height (m) | Year | Maximum Surge Location | Country |
|------|--------------------|------|---------------------------|------------|
| 1 | 13.70 ^a | 1876 | Precise Location Unknown | Bangladesh |
| 2 | 12.00 ^b | 1737 | Sunderbans | India |
| 2 | 12.00 ^b | 1864 | Calcutta and Surroundings | India |
| 4 | 9.60 ^a | 1966 | Precise Location Unknown | Bangladesh |
| 5 | 9.10 ^a | 1960 | Precise Location Unknown | Bangladesh |
| 5 | 9.10 ^a | 1963 | Precise Location Unknown | Bangladesh |
| 5 | 9.10 ^a | 1970 | North of Chittagong | Bangladesh |
| 8 | 8.80 ^a | 1961 | Precise Location Unknown | Bangladesh |
| 8 | 8.80 ^a | 1961 | Precise Location Unknown | Bangladesh |
| 8 | 8.80 ^a | 1967 | Precise Location Unknown | Bangladesh |

Water Height: a = Storm Tide; b = Storm Surge

Slightly higher greater water levels were observed in the Northern Indian Ocean during the 2004 Indian Ocean Tsunami. A field report of flood observations from the Andaman and Nicobar Islands in the Northern Indian Ocean reveals a maximum run-up level of 17.26 m at Little Andaman passenger jetty during this event (Cho et al. 2008). This water level is approximately 3.5 m higher than the catastrophic storm tide event at

Meghna Estuary in 1876, however the tsunami observation includes water run-up, while the storm tide observation refers to elevated sea levels, apart from run-up or waves.

TCs also generate storm surges along the eastern shores of the Bay of Bengal, although the heights of these surges are lower than surges in the northern portion of this Basin. Storm surges in the eastern Bay of Bengal sometimes strike Myanmar, most commonly during the month of May. Surge events during this month occurred in 1967, 1968, 1970, 1975, 1982, 1992, 1994, 2006 and 2008 (Dube et al. 2009). The Gwa Cyclone of 1982 and the Mala Cyclone of 2006 produced storm surges of approximately 4 m in magnitude along the Myanmar Coast (Dube et al. 2009), while Cyclone Nargis in 2008 produced a peak storm surge exceeding 5 m along Myanmar's Irrawaddy Delta (Fritz et al. 2009). It should be noted, as well, that surges propagate inland considerable distances into this Delta; the 1975 surge event inundated this low-lying region at least 100 km inland (Dube et al. 2008), while the surge from Cyclone Nargis propagated inland 50 km (Fritz et al. 2009).

Storm surges in the southwestern Bay of Bengal are observed in Sri Lanka and southeastern India. Single cyclones in this region sometimes generate storm surges in both locations. For example, the Rameswaram Cyclone of December 1964 generated a 5-m surge near Tondi, in Southeastern India, and likely produced a surge of more than 4 m along Sri Lanka's West Coast (Dube et al. 2009). The most severe surge events that have impacted Sri Lanka have occurred during the month of November, particularly during the years 1964, 1978 and 1992 (Dube et al. 2008).

2.3.2.2 Arabian Sea

Storm surges along the coast of the Arabian Sea are less frequent and have lower magnitudes than in the Bay of Bengal. The lower frequency can partly be attributed to climatology, as TCs in the Bay of Bengal occur four times more often than in the Arabian Sea (Singh et al. 2001). It is possible that the lower magnitudes can be explained, at least in part, by the fact that the northern Bay of Bengal is quite shallow and has a concave shape, which may enhance surge levels compared to the Arabian Sea.

Although TCs rarely strike coastlines along the Western Arabian Sea, several intense TCs in the past decade have produced severe flooding from both heavy rains and storm surge. TC Gonu struck the Sultanate of Oman in 2007, followed by TC Phet in 2010, which also struck Oman. TC Gonu produced the highest storm surge levels recorded along the Arabian Sea, as water levels near the eastern tip of the Arabian Peninsula, at Ras al-Hadd, reached approximately 5 m (Fritz et al. 2010). This was a storm tide observation and likely included waves because many observations used rafted debris or exterior mudlines as indicators of water-level heights (Fritz et al. 2010). Nonetheless, these coastal flooding observations are substantial and indicate that large-magnitude storm surge events threaten this region. This cyclone developed into a category-5 TC in this region with winds of 72 m s^{-1} (Unisys Corporation 2013), becoming the most intense TC on record in the Arabian Sea (Fritz et al. 2010). The cyclone weakened to a category-1 TC with winds of 41 m s^{-1} as it passed just offshore of the easternmost tip of the Arabian Peninsula.

In May/June of 2010, TC Phet formed in this region and quickly developed into a category-4 TC with winds of 64 m s^{-1} (Unisys Corporation 2013). The storm made

landfall in Oman as a category-2 cyclone, with winds of 46 m s^{-1} , and generated rainfall and storm surge flooding.

Storm surge observations in the eastern Arabian Sea region generally range from 1-3 m. Several modeling experiments have predicted higher storm surge heights, but observations have not been identified to validate these results. For example, models predicted a maximum sea surface height of approximately 4 m in the Porbandar Cyclone in 1975 along the Gujarat Coast (Dube et al. 1985; Dube et al. 1997), however, the maximum observed surge level available for this event was approximately 2.8 m (Dube et al. 1985; Dube et al. 1997). A model hindcasted maximum surge levels of approximately 5 m for the Kandla Cyclone in June 1998, however, the maximum observed surge level found in the literature was approximately 2.5 m at Kandla (Chittibabu et al. 2000; Dube et al. 2009). Finally, a surge model predicted a 4-m surge along Pakistan's Badin/ Keti Bandar Coast, near the Indian border, from a TC that struck in May 1999 (Siddiqui 2009). Unfortunately, no observations were provided for validation. The difference between observed and modeled surge heights in these cases may not be an indication of poor model performance, but rather sparse observations. Although the observational record does not provide a storm surge height greater than 3 m, precautions should be taken related to coastal planning in this sub-basin because modeling results consistently suggest higher storm surge levels are possible.

2.3.3 Storm Surge Impacts

2.3.3.1 Bay of Bengal

Storm surges in the Bay of Bengal have historically inflicted catastrophic devastation. The 1737 cyclone in India and the 1970 Bhola Cyclone in Bangladesh were

the most deadly TCs in this region. Both cyclones killed approximately 300,000 people (Dube et al. 2008). These events inflicted even more fatalities than the 2004 tsunami, which killed nearly 228,000 people (United States Geological Survey 2008). Table 2.5 lists the top 10 fatality totals for TCs that have struck this basin. Although it's not possible to separate deaths caused by storm surge from deaths caused by wind damage in these events, given the extraordinary storm surge heights that have occurred along the low-lying coasts of the Bay of Bengal, storm surge most likely accounts for the majority of these deaths. The fatality totals in these events are truly extraordinary; at least 138,000 people died in each of the six most deadly events. At least 15 cyclones in Bangladesh and India have killed 5,000 people (Dube et al. 2008).

Table 2.5. The top 10 highest Northern Indian Ocean fatality totals from tropical cyclones, from Dube et al. (2008); Fritz et al. (2009).

| Rank | Fatalities | Year | Location | Source |
|------|------------|------|------------|---------------------|
| 1 | 300,000 | 1737 | India | Dube et al. (2008) |
| 1 | 300,000 | 1970 | Bangladesh | Dube et al. (2008) |
| 3 | 200,000 | 1876 | Bangladesh | Dube et al. (2008) |
| 4 | 175,000 | 1897 | Bangladesh | Dube et al. (2008) |
| 5 | 140,000 | 1991 | Bangladesh | Dube et al. (2008) |
| 6 | 138,000 | 2008 | Myanmar | Fritz et al. (2009) |
| 7 | 50,000 | 1833 | India | Dube et al. (2008) |
| 7 | 50,000 | 1864 | India | Dube et al. (2008) |
| 9 | 40,000 | 1822 | Bangladesh | Dube et al. (2008) |
| 10 | 19,279 | 1965 | Bangladesh | Dube et al. (2008) |

Several factors lead to these catastrophes. In this region, large populations inhabit low-lying, water-bogged coastal zones, placing millions of people at risk. Bangladesh, for example, is the most densely populated mega-country in the world, with a population density of 2,600 per square mile (Streatfield and Karar 2008). By comparison, if the entire world's population were placed in the United States, the population density would only be 1,740 per square mile (Streatfield and Karar 2008). Unfortunately, 46 percent of

Bangladesh's population resides within 10 m of average sea level (Earth Institute Columbia University 2007), placing millions in danger of storm surge inundation. Also, because these people are among the world's poorest, many do not have the means to evacuate, and absence of technological infrastructure may keep storm warnings from reaching the masses.

Although the loss of life and magnitude of destruction is greatest along the shores of the Northern Bay of Bengal, storm surges have caused extensive losses in other portions of this sub-basin as well. Cyclone Nargis, for example, inflicted approximately 138,000 fatalities and more than \$10 billion in damage when it struck Myanmar, along the shores of the Eastern Bay of Bengal, in May, 2008 (Fritz et al. 2009). This was the eighth deadliest TC in world history and the most costly Indian Ocean cyclone (Fritz et al. 2009). Also, storm surges in November 1964, November 1978 and November 1992 inflicted fatalities and property loss in Sri Lanka (Dube et al. 2008); the 1978 cyclone killed 373 people (Murty 1988).

2.3.3.2 Arabian Sea

Storm surges inflict less damage and fatalities along the Arabian Sea Coast than along the shores of the Bay of Bengal, however, loss of life and economic damages are still substantial. The Kandla TC killed approximately 3,000 people, damaged 200,000 homes and generated \$700 million in economic losses in June, 1998, in the Gujarat region of India (Kalsi and Gupta 2003). Along the shores of the Western Arabian Sea, TC Gonu inflicted 49 fatalities and caused \$4 billion in damage in Oman in June 2007 (Joint Typhoon Warning Center 2007; Dube et al. 2009, Fritz et al. 2010), making this

cyclone the worst natural disaster in the Sultanate's history (Fritz et al. 2010), however, much of this destruction may have been caused by heavy rainfall runoff.

2.4 Western North Atlantic

2.4.1 Storm Surge Literature

The United States government provides the most comprehensive storm surge data in the world. These data are provided by several agencies and organizations, including the National Hurricane Center (NHC), U.S. Army Corps of Engineers, Federal Emergency Management Agency (FEMA), and U.S. Geological Survey (USGS).

The National Hurricane Center, based in Miami, Florida, provides TC reports for the Atlantic Ocean, Caribbean Sea, and the Gulf of Mexico from 1958- present (National Hurricane Center 2013). These reports provide extensive TC information, including TC tracking data and intensity, rainfall observations, as well as storm surge and storm tide levels.

The U.S. Army Corps of Engineers provides a rich history of storm surge and storm tide data for the U.S. Gulf and Atlantic Coasts. These data are often plotted as water height levels on maps. The time period covered by these data is longer than other government organizations, as maps exist for storm surge events as far back as 1909 (U.S. Army Corps of Engineers 1972). Some of these maps are displayed as figures in scientific literature, such as a storm tide level map for the 1935 Labor Day Hurricane, provided by Knowles (2009) and a map containing more than 150 high-water marks from the 1938 Great New England Hurricane, provided by Harris (1963).

FEMA provides extensive storm surge and storm tide data for several hurricanes that impacted the United States during the past decade. For example, the agency

contracted URS Group, Inc. (URS) to collect data in Louisiana, Mississippi and Alabama following Hurricane Katrina. URS prepared separate reports for each of these three states, containing geo-referenced storm surge and storm tide data that were collected by URS and USGS (URS 2006a; URS 2006b; URS 2006c). More than 400 observations are provided in each of the Louisiana and Mississippi reports, while the Alabama report contains more than 200 observations. These reports provide a combined total of more than 1,000 high-water marks, which is the most extensive archive of coastal flooding data for any TC in history. FEMA also provides nearly 400 observations along the Texas and Louisiana Coast following Hurricane Ike (Federal Emergency Management Agency 2008).

The USGS provides storm surge and storm tide data through the Inland Storm-Tide Monitoring Program (U.S. Geological Survey 2013). This program collects data by deploying mobile tide gauges prior to the landfall of TCs along the U.S. Gulf and Atlantic Coasts. The program began collecting data in Hurricane Rita in 2005.

Mexico's Servicio Meteorológico Nacional (2013) provides an archive of TC reports for the Atlantic Ocean, Gulf of Mexico and Caribbean Sea from 1997- present. These reports are in Spanish and are hosted on the website for the Comisión Nacional Del Agua, or Conagua. They contain detailed information related to TC development, tracking and intensity, while providing ground-based observations for maximum sustained winds, wind gusts, and rainfall totals. However, a thorough review of these documents revealed no observations related to coastal flooding.

The National Meteorological Service of Honduras provides a TC website in Spanish (Servicio Meteorologico Nacional de Honduras 2013). This site includes a list of

97 TCs that have affected Honduras since 1870, and the site provides hurricane-tracking maps from Unisys Corporation (2013). No TC wind or storm surge data are provided.

The Nicaraguan Institute of Territorial Studies (Instituto Nicaraguense de Estudios Territoriales 2013) provides the most comprehensive information related to earth, oceanic and atmospheric sciences in Nicaragua. The Spanish-language website provides no historical TC data, including any information on past storm surges.

The Belize National Meteorological Service (2013) provides a TC webpage, in English, which lists 59 storms that have affected the country since 1889. TC data are provided, including the name and date of storm, distance from Belize, hurricane category and intensity at landfall. No storm surge information is provided.

A literature review of meteorological resources from Caribbean islands or island groups reveals that Cuba provides the best information related to storm surge observations and impacts in the region. The Meteorological Institute of the Republic of Cuba provides seasonal TC summaries, in Spanish, from 2000 – 2013 (Instituto de Meteorologia de la Republica de Cuba 2014). These reports provide storm tide heights for TCs Michelle in 2001, Lili in 2002 and Emily in 2005 (Perez and Torres 2013a). The summaries also provide the inland extent of storm surge flooding for several surge events. For example, seawater came in 400 to 500 m from the coastline during Hurricane Michelle in 2001, and 200 m inland during Hurricane Isabel in 2003 (Perez and Torres 2013b).

The Canadian Hurricane Centre, supported by Environment Canada, provides maps of historical hurricane tracks since 1954, brief storm summaries since 2008 and feature articles on noteworthy hurricanes of the past. (Canadian Hurricane Centre 2014).

This website provides an overview of Canadian hurricane records, including the hurricanes with the strongest winds, most fatalities and highest wave heights. However, the site does not provide storm surge data for Canada.

Numerous academic publications also provide storm surge or storm tide levels within the Western North Atlantic basin. Fritz et al. (2007) provide 152 field observations along the U.S. Gulf Coast following Hurricane Katrina, as they surveyed high-water marks left by interior and exterior water marks, rafted debris, damaged trimlines and tree bark removal. These observations were crucial, due to the widespread failure of tide gauges in the region. Two American universities have also developed programs to archive and map historic storm surge and storm tide data. The Southern Regional Climate Center at Louisiana State University hosts SURGEDAT, an international storm surge database that provides peak surge levels for global surge events since 1880 (Needham and Keim 2012; Needham et al. 2013). SURGEDAT provides storm surge and storm tide data for more than 350 hurricanes and tropical storms along the U.S. Gulf and Atlantic Coasts, supported by more than 8,000 unique high-water marks since 1880 (Needham et al. 2013). The Program for the Study of Developed Shorelines at Western Carolina University has also developed a storm surge database for the U.S. Gulf and Atlantic Coasts. The archive contains 5800 storm surge data points from 42 hurricanes (Peek and Young 2013).

2.4.2 Storm Surge Observations

Storm surge inundation threatens much of the Western North Atlantic basin, including the U.S. Atlantic Coast, the U.S. and Mexican Gulf Coast, and the Caribbean Sea in Mexico, Central America, and on many islands. Historical literature provides

maximum water levels for 389 TCs in this region since 1880. Approximately 90% of these observations were recorded in the United States. A numeric breakdown by sub-basin includes 242 surge events along the U.S. Gulf Coast, 110 surge events along the U.S. Atlantic Coast, 14 events in Central American and Mexico’s Atlantic Basin, 17 events on Caribbean islands and five events in Canada’s maritime region. These observations were comprised of both storm surge and storm tide observations. For example, records along the U.S. Gulf Coast included 169 storm tide and 74 storm surge observations, while high-water marks along the U.S. Atlantic Coast were comprised of 63 storm surge and 46 storm tide observations. A list of the highest magnitude storm surge or storm tide levels in this basin provides 13 events that produced water levels of at least 5.49 m (Table 2.6).

Table 2.6. Top 10 Western North Atlantic tropical cyclone-induced surge levels, from 1880-2012. Multiple events tied for ninth-place, so this list contains 13 events. Compiled from the following sources: Garriott (1898); U.S. Corps of Engineers (1935); U.S. Army Engineer District (1962); Sugg and Pelissier (1968); Simpson et al. (1970); Hebert (1976); Schuck-Kolben (1990); Pielke et al. (2003); Landsea et al. (2004); Anonymous (2007); Drye (2007); Mandia (2010); Knabb et al. (2011).

| Rank | Height (m) | Year | Storm Name | Maximum Surge Location |
|------|-------------------|------|-------------------|---------------------------|
| 1 | 8.53 ^b | 2005 | Katrina | Mississippi, USA |
| 2 | 7.50 ^b | 1969 | Camille | Mississippi, USA |
| 3 | 6.71 ^b | 1961 | Carla | Texas, USA |
| 4 | 6.50 ^a | 1932 | Unnamed | Santa Cruz del Sur, Cuba |
| 5 | 6.49 ^a | 1938 | Great New England | Massachusetts, USA |
| 6 | 6.10 ^b | 1900 | Galveston | Texas, USA |
| 7 | 6.10 ^a | 1989 | Hugo | South Carolina, USA |
| 8 | 5.55 ^b | 1975 | Eloise | Florida Panhandle, USA |
| 9 | 5.49 ^b | 1935 | Labor Day | Florida Keys, USA |
| 9 | 5.49 ^a | 1967 | Beulah | Texas, USA |
| 9 | 5.49 ^a | 1898 | Unnamed | Georgia, USA |
| 9 | 5.49 ^a | 2007 | Dean | Yucatan Peninsula, Mexico |
| 9 | 5.49 ^b | 2007 | Felix | Northern Coast, Nicaragua |

Water Height: a = Storm Surge; b = Storm Tide

2.4.2.1 U.S. Gulf Coast

The highest magnitude storm surge events in the Western North Atlantic basin have occurred along the U.S. Gulf Coast, particularly along the northern and western shores of this basin (Needham and Keim 2012). The combination of relatively high TC frequency and shallow bathymetry in this Gulf provides an ideal setup for high storm surge magnitudes. The two highest storm surges in this sub-basin both occurred along the Mississippi Coast. Hurricane Katrina in 2005 generated an 8.53-m storm tide (Knabb et al. 2011) in Mississippi, with total water levels, including waves, exceeding 10 m in some locations (Fritz et al. 2007). Hurricane Camille in 1969 generated a 7.5-m storm tide in nearly the same location (Simpson et al. 1970). Records of many small and medium storm surges are also available for the U.S. Gulf Coast, which explains the abundance of observations for this sub-basin.

The Eastern Gulf of Mexico, particularly the West Coast of Florida, is also vulnerable to non-tropical storm surges, generated by passing cold fronts and extratropical storms. In some locations, non-tropical storm surge levels have exceeded water levels generated by TCs. For example, the “Storm of the Century,” or “Superstorm,” of March, 1993, generated record water levels in Western Florida, north of Tampa. Storm surge heights ranged from 2.74 – 3.66 m from Pasco to Taylor Counties (National Weather Service 2013). The storm surge during this event at Cedar Key, Florida, reached 2.9 m, surpassing the 2.59-m surge generated by Hurricane Alma in 1966 (Sugg 1967), which is the highest water level produced by a TC at this location.

2.4.2.2 U.S. Atlantic Coast

The U.S. Atlantic Coast has also observed some high-magnitude storm surge events. Storm surges of 6.5 m in Massachusetts during the 1938 Great New England Hurricane (Beckage 2012), and 6.1 m in Hurricane Hugo along the South Carolina Coast in 1989 (Schuck-Kolben 1990; Beckage 2012), have demonstrated the storm surge vulnerability of both the northeast and southeast sections of the U.S. Atlantic Coast. Hurricane Sandy in 2012 generated a destructive storm surge along the highly-populated mid-Atlantic coastline, including the New York metropolitan area. Storm tide levels at the Battery, on the southern tip of Manhattan, reached 4.29 m above the Mean Lower Low Water datum (Blake et al. 2013). The majority of observed storm surge events have occurred in the southeast portion of this sub-basin; approximately 78% of observed tropical surge events occurred from Florida to North Carolina, while only 22% of these events have occurred from Virginia to Maine.

Extratropical storms, called nor'easters along the U.S. Atlantic Coast, have also generated substantial storm surges in the region. The "Ash Wednesday Storm" of 1962 produced one of the most destructive non-tropical storm surges from North Carolina to New York. Water levels reached 2.74 m in Norfolk, Virginia, and 2.13 m in other locations of the Virginia coast (National Oceanic and Atmospheric Administration 2014). The "Perfect Storm" in November, 1991, caused coastal flooding unusually far north, as Boston observed a 1.52-m storm surge and storm tide levels exceeding 4.27 m (National Oceanic and Atmospheric Administration 2014). The highest waves from Boston to the coast of Maine reached 9.14 m, and storm surge in Maine exceeded 1 m (National Oceanic and Atmospheric Administration 2014). The "Great Nor'easter" of 1992

generated unusually high water levels in New York and New Jersey, where storm tides in New York City reached 3.66 m, and record water levels were recorded in New Jersey, where Sandy Hook observed a storm tide of 3.14 m and Atlantic City, New Jersey, observed a storm tide of 2.83 m (National Oceanic and Atmospheric Administration 2014). Other nor'easters that generated substantial storm surge along the U.S. Atlantic Coast included "No'Ida" in 2009, the 1993 "Superstorm," the "Blizzard of '78," and a nor'easter in 1956 (National Oceanic and Atmospheric Administration 2014).

2.4.2.3 The Caribbean, Mexico and Central America

The 6.5-m storm surge observed in 1932 at Santa Cruz del Sur in Camaguey, Cuba (Pielke et al. 2003), demonstrates that island locations in the Caribbean are also susceptible to major surge events. Various sources also provide evidence of major surge events in Mexico and Central America. A 5.25-m storm surge produced by Hurricane Gilbert in 1988 (National Hurricane Center 1988; Meyer-Arendt, K.J. 1991), as well as Hurricane Dean's 5.49-m storm surge in 2007 (Anonymous 2007), are examples of substantial storm surge events along Mexico's Yucatan Peninsula, while the 5.49-m surge generated by Hurricane Felix in Northern Nicaragua (Drye 2007) is the highest storm surge observation on record in Central America. A considerable amount of storm surge observations are missing from Mexico, Central America and the Caribbean Islands, which casts uncertainty about numerous high-magnitude surge events in these areas.

2.4.2.4 Canada

Although tropical storm surges have been observed in Canada, these events have generally been low-magnitude inundations. The five observations provided by the historical literature are remarkably similar, as all of these inundations range from 1.2 –

1.5 m. These levels fit well with the assessment that storms along the coasts of Canada can produce storm surges up to 2 m in height (Danard et al. 2003). These observations have occurred in New Brunswick, Nova Scotia and Prince Edward Island. Hurricane Juan generated what is considered to be the highest tropical storm surge in the region, when it generated a 1.5-m surge at Halifax, Nova Scotia, in September, 2003 (Bowyer 2003). The surge peaked as tides were high, producing a storm tide level of 2.9 m, which was a record for Halifax Harbour (Bowyer 2003). Significant wave heights along the Nova Scotia coast reached 9-13 m, and maximum wave heights reached 19-20 m (Bowyer 2003).

Extra-tropical storm surges in Atlantic Canada have sometimes produced storm surges that are slightly higher than tropical storm surges. For example, a storm surge of approximately 2 m was observed at Argentia, Newfoundland, in January, 1982 (Murty and Greenberg 1987). The following year, in October, 1983, a storm surge at Cape Breton Island, Nova Scotia, produced debris lines as high as 1.5 m above the normal high water mark (Danard et al. 2003).

2.4.3 Storm Surge Impacts

Although storm surge is the biggest killer in TCs globally, many of the highest fatality events in the Atlantic Basin are rain-induced disasters on steep terrain of the Caribbean and Central America. In 1998, for example, torrential rains from Hurricane Mitch killed more than 9,000 people in Honduras and Nicaragua (Guiney and Lawrence 1999). Hurricane Flora in killed more than 7,000 in the Caribbean in 1963, particularly in Haiti and Cuba. Flash flooding from torrential rains caused most of these deaths; in Cuba, rainfall amounts reached 229 cm at Velasco and 202 cm at Tacajo (Dunn et al. 1964). As

approximately 50 percent of Atlantic basin hurricane fatalities occur on the mountainous Greater and Lesser Antilles (Rappaport and Fernandez-Partagas 1995, see Table 2.7), surely rainfall causes high numbers of cyclone fatalities in this basin.

Table 2.7. Atlantic Basin tropical cyclone fatalities by region, from Rappaport and Fernandez-Partagas (1995).

| Location | Fatalities | % of basin-wide deaths |
|--|------------|------------------------|
| Greater Antilles | 45,000 | 29% |
| Offshore Losses | 35,000 | 22% |
| Lesser Antilles | 35,000 | 22% |
| United States Mainland (1900 Galveston Hurricane: 8,000) | 25,000 | 16% |
| Mexico and Central America | 20,000 | 12% |
| Elsewhere (Azores, Bahamas, Bermuda, Canada, Cape Verde Islands, South America, Ireland) | 1,000 | < 1% |

In the United States, however, storm surges cause a substantial portion of hurricane-related deaths. The American Meteorological Society (1973) reported that coastal inundations cause 90% of hurricane fatalities. It is unclear, however, how this figure might have changed in recent decades, as improved forecasting, which has mollified the number of coastal fatalities, counters the coastal population explosion, which has nearly quadrupled the inhabitants of coastal counties and parishes along the Gulf of Mexico from 1950 to 2000 (Keim and Muller 2009, see Table 2.8).

Table 2.8. Population statistics for the U.S. coastal counties and parishes along the Gulf of Mexico in 1900, 1950, and 2000, from Keim and Muller (2009).

| State | No. of Counties | 1900 | 1950 | 2000 |
|---------|-----------------|---------|---------|-----------|
| Florida | 23 | 175,000 | 841,000 | 4,916,000 |
| Alabama | 2 | 76,000 | 272,000 | 540,000 |

Table 2.8 (continued). Population statistics for the U.S. coastal counties and parishes along the Gulf of Mexico in 1900, 1950, and 2000, from Keim and Muller (2009).

| | | | | |
|-------------|----|---------|-----------|------------|
| Mississippi | 3 | 50,000 | 127,000 | 364,000 |
| Louisiana | 11 | 474,000 | 930,000 | 1,611,000 |
| Texas | 14 | 178,000 | 1,581,000 | 5,006,000 |
| Total | 53 | 953,000 | 3,751,000 | 12,437,000 |

The most disastrous surge events in the basin occur along the U.S. Gulf Coast. Some of the greatest fatality totals include the 1900 Galveston Hurricane, which killed at least 8,000 people (Blake et al. 2011); The “Cheniere Caminada” Hurricane of 1893, which killed around 2,000 people in coastal Louisiana (National Weather Service Lake Charles 2003a); and Hurricane Katrina, which caused 1833 fatalities (McTaggart-Cowan et al. 2008). The storm surge likely killed the majority of people in the 1893 Cheniere Caminada Hurricane and the 1900 Galveston Hurricane, however, storm surge was directly responsible for 600-700 fatalities in Hurricane Katrina (Boyd 2011), which is less than half of the total casualties.

Storm surge impacts in Mexico, Central America and Caribbean Islands are not as well known, as little has been published on this topic in English, Spanish or French. However, the destruction of the 1932 storm surge event in Sant Cruz del Sur, Cuba, is well-documented. This catastrophic storm surge swept the town away, causing 2,870 deaths in a town with a population of only 4,800 (Pielke et al. 2003).

In addition to human fatalities, storm surge in the Western North Atlantic inflicts substantial economic losses. Hurricane Katrina was the most costly natural disaster in U.S. history (Kessler et al. 2006; Baade et al. 2007), as damage from this storm exceeded

\$100 billion (Blake et al. 2011). Most of this damage was caused by the storm surge, which breached levees and flooded approximately 80% of the New Orleans metropolitan area (Kates et al. 2006).

Storm surge also impacts agriculture in low-lying coastal plains where saltwater can wash inland considerable distances. For example, hurricanes Rita in 2005 and Ike in 2008 generated extensive storm surges that destroyed crops in southwest Louisiana. Hurricane Rita generated a storm tide that exceeded 5.4 m in southwest Louisiana (URS 2006d), and washed inland more than 60 km (McGee et al. 2013). Although Hurricane Ike's storm surge peaked at 5.33 m in Chambers County, Texas (Berg 2009), storm tide heights exceeded 3.5 m in portions of southwest Louisiana and washed inland at least 55 km (Federal Emergency Management Agency 2008). Hurricane Rita's storm surge destroyed sugar cane and rice crops worth approximately \$50 million in this region (Kurth and Burckel 2006). Also, rice production fell dramatically Vermillion Parish in the years following Rita and Ike, as soils across the region remained salty after surge inundations. In 2005, 310 producers cultivated a rice crop on 76,000 acres, but following Rita, this number fell to 290 producers harvesting a crop on 34,000 acres in 2006 (Louisiana State University Ag Center 2014). Although cultivation rebounded several years after Rita, production was drastically reduced again following Ike. In 2008, 275 rice farmers cultivated a product on 62,000 acres, but this number fell to 200 producers cultivating 41,000 acres in 2009 (Louisiana State University Ag Center 2014).

Storm surges in Texas and Louisiana have also caused considerable loss of cattle. Hurricane Rita inflicted the greatest number of cattle losses in the literature, as the surge and strong winds killed approximately 9,500 cattle in Southwest Louisiana (Kurth and

Burckel 2006). A storm surge in Lake Pontchartrain drowned 100 cattle near Frenier, Louisiana, in 1931 (Anonymous 1931), a storm surge in 1943 drowned several hundred cattle along the Bolivar Peninsula of Texas (Sumner 1944), and Hurricane Juan in 1985 drowned two hundred cattle in Terrebonne Parish, Louisiana (National Weather Service Lake Charles 2003b).

Transportation infrastructure is also vulnerable to storm surge inundation along the U.S. Atlantic and Gulf Coasts. Coastal roads in these areas vulnerable to salt water inundations, as more than 60,000 miles of roads are located in the 100-year coastal floodplain (Chen et al. 2007). In 2012, Hurricane Sandy highlighted the vulnerability of public transportation infrastructure along the mid-Atlantic Coast, where the storm generated a destructive storm surge and inflicted \$50 billion in losses (Blake et al. 2013). In the New York City metropolitan area, Sandy's storm surge overtopped the flood protection barriers, flooding the subway system with sea water and causing billions of dollars in damage. The Federal Transit Administration provided \$5.7 billion in recovery assistance to transit agencies in New York and New Jersey following the storm (Bernstein 2013).

Although storm surge affects nearly every coastal industry in surge-prone areas, impacts to the energy industry are particularly noteworthy because of the high density of energy infrastructure in the coastal zone. This is particularly true along the U.S. Western and Central Gulf Coast, where 17 oil seaport and import sites represent the largest concentration in the nation (U.S. Energy Information Administration 2010). Also, the 27 oil refineries in Texas and 17 in Louisiana account for approximately 30% of the nation's 147 refineries (U.S. Energy Administration 2010). This high density of energy

infrastructure is vulnerable to impacts from storm surge inundations, as the greatest storm surge activity, in terms of both frequency and magnitude, occur along the Western and Central Gulf Coast (Needham and Keim 2012).

Storm surge impacts to the energy industry threaten to disrupt energy production and distribution, while triggering hazardous chemical releases. In 2005, hurricanes Katrina and Rita destroyed more than 110 offshore oil platforms (Minerals Management Service 2006), while damaging a combined total of 457 energy pipelines (Cruz and Krausmann 2008). Although these storms triggered hundreds of offshore hazardous-materials releases (Minerals Management Service 2006), the highest-impact releases occurred in the coastal zone, where the storm surge was particularly devastating. For example, approximately 10,500 gallons of the Shell Oil Spill reached the coastline, including several marshes, while the Murphy Oil Spill released approximately 820,000 gallons of oil into a densely populated area of St. Bernard Parish, Louisiana (Pine 2006). Such hazardous events threaten the livelihood of people in the coastal zone, while potentially inflicting long-term environmental impacts in the region.

2.5 Eastern North Pacific

2.5.1 Storm Surge Literature

2.5.1.1 Mexico

Mexico's Servicio Meteorológico Nacional (2013) provides TC reports from 1997- present, the same time period as reports for the Western North Atlantic Ocean. Like the Atlantic archives, the reports for the Eastern North Pacific are in Spanish and are hosted on the website for the Comisión Nacional Del Agua, or Conagua. These reports also provide information related to TC development and tracking, while providing

ground-based observations for maximum sustained winds, wind gusts, and rainfall totals. However, these reports do not provide coastal flooding observations.

The U.S. National Hurricane Center, based in Miami, Florida, provides TC reports for the Eastern North Pacific from 1988- present. The area covered by these reports extends from the coast of Central America and Western Mexico, west to 140 degrees longitude. This area does not cover TC observations for the Hawaiian Islands. These reports contain detailed information related to TC development, tracking and intensity, while providing ground-based observations for maximum sustained winds, wind gusts, and rainfall totals. Although these reports cover several dozen TCs that impacted Western Mexico, the only quantitative storm surge height provided is the 5-m storm surge produced by Hurricane Kenna in 2002 (Franklin 2002). Coastal flooding also occurred in Hurricane Marty in 2003 (Franklin 2004) and Hurricane Norbert in 2008 (Franklin 2009), however the TC reports provide no estimates of storm surge heights or damage estimates from coastal flooding.

The National Climatic Data Center prepared a comprehensive report of TC activity in the Eastern North Pacific Ocean, from 1949-2006 (Blake et al. 2009). Although this report provides an extensive history of TCs in the region, it contains no observations related to storm surge or coastal flooding. This report provides tables with chronological lists of hurricanes and hurricane statistics, as well as detailed maps of hurricane tracks and landfall points.

The *Monthly Weather Review* provides annual TC reports for the Eastern North Pacific, as well as a publication that provides an overview of TC history in this region from 1839- 1929 (Henry 1929). These publications provide a rich history of TC tracks

and intensity, as well as wind and rainfall observations. Although this literature does not provide quantitative storm surge heights, some accounts do mention storm surge inundations, such as the coastal flooding event that occurred in Acapulco from Hurricane Bridget in 1971 (Denny 1972). In other cases, damage descriptions include the loss of ships in harbors, such as the 12 lost ships in the harbor of Mazatlan in 1839, and three lost vessels at San Blas in 1840 (Henry 1929). Such descriptions may imply the presence of destructive storm surge and waves, although the literature for these events does not provide surge or wave heights.

2.5.1.2 Hawaii

The Central Pacific Hurricane Center, based in Honolulu, Hawaii, provides TC information for the Central Pacific, defined as the area from 140W to 180 degrees longitude. This area includes all of the Hawaiian Islands, as well as Johnson Atoll and the Midway Islands. TC reports are made available for every storm in this region since 1957 (Central Pacific Hurricane Center 2012). Summaries from 1980-present are taken from the annual Tropical Cyclone Reports, which are published as National Oceanic and Atmospheric Administration Technical Memorandums. Storm summaries are also available for more than 20 noteworthy TCs that have impacted the region between 1832-1956 (Central Pacific Hurricane Center 2012).

Additional resources are available to describe storm observations and impacts from Hurricane Iniki, which struck the island of Kauai in 1992, producing the most destructive hurricane impacts in Hawaii during the 20th Century (Post, Buckley, Schuh & Jernigan, Inc. 1993). A report developed by the U.S. Department of Commerce (1993), provides valuable storm surge and high-water mark information, as well as estimates of

wave heights produced by Iniki. Another report developed for several federal departments and agencies (Post, Buckley, Schuh & Jernigan 1993) provides an overview of the storm impacts and disaster response, but no direct coastal flooding observations.

2.5.2 Storm Surge Observations

2.5.2.1 Mexico

Although few storm surge observations exist for Western Mexico, the 5-m storm surge estimate at San Blas in 2002 during Hurricane Kenna (Franklin 2002) is valuable because this surge event may provide an indication of the maximum potential surge heights for this region. In Western Mexico, only an unnamed hurricane in 1959 and Hurricane Madeline in 1976 were more intense at landfall than Hurricane Kenna (Franklin 2002). Also, Kenna was even more powerful before landfall, generating winds of 75 m s^{-1} , which classified the storm as a category-5 hurricane on the Saffir-Simpson Scale, until shortly before landfall (Unisys Corporation 2013). This observation is important because pre-landfall winds correlate better with storm surge heights than wind speeds at landfall (Jordan and Clayson 2008; See Chapter 3). Therefore, given Kenna's intensity as it approached the coast, it may have produced the highest storm surge level in the modern history of Western Mexico, and may provide an approximation of the maximum potential storm surge levels in this region.

Although storm surge heights in other communities are not available for this event, surge inundation also impacted Puerto Vallarta. Unfortunately, surge heights were not measured in this location. However, at the bay near Puerto Vallarta, waves as high as 3.05 m (10 ft) were observed rushing inland from the bay (Franklin 2002).

2.5.2.2 Hawaii

The Hawaiian Islands observe modest storm surge heights when impacted by TCs, due, at least in part, to the steep slope of the terrain both offshore and onshore. Deep offshore bathymetry enables underwater currents to redistribute storm surge, moderating water level rises (Needham and Keim 2011). However, the steep offshore bathymetry also enables large waves to approach closely to the Hawaiian coast before breaking.

For this reason, most of the scientific literature uses the terms “heavy surf” or “high surf” to describe TC-induced coastal flood events. The literature usually provides surf heights instead of storm surge levels to describe high water events. Surf heights tend to represent a combination of wave heights and storm surge levels in most of the literature. The highest surf levels approach or exceed 10 m on the coast during TCs that impact Hawaii.

In 1957, Hurricane Nina produced the highest coastal surf levels found in the literature, as the storm pounded the South Kauai Coast with surf levels of 10.67 m (Blumenstock 1957). The literature provides many other events in which surf levels reached at least 3.05 m (10 ft). Observations from Hurricane Diana in 1972 and Iniki in 1992 are valuable because both surf and storm surge levels are available for these events. Diana produced 9.14-m surf along the Puna Coast of the Big Island, while storm surge levels at Hilo ranged from 1.22-1.52 m (Central Pacific Hurricane Center 1972). Iniki impacted the South Kauai Coast most severely, with high-water marks from storm surge and waves approaching 9.14 m, and storm surge ranging from 1.22-1.83 (U.S. Department of Commerce 1993), which is the highest water level not including waves found in the literature for Hawaii.

The heights of tsunami waves in Hawaii have equaled or exceeded the highest surf levels generated by TCs. The April 1, 1946, Aleutian Island Earthquake generated a massive Pacific-wide tsunami that produced wave run-up as high as 16 m in Hawaii (Lander and Lockridge 1989; Johnson and Satake 1997), while the May 23, 1960, Chilean earthquake generated a 10.67-m wave at Hilo (Eaton et al. 1961).

2.5.3 Storm Surge Impacts

2.5.3.1 Mexico

The archive of TC reports provided by the Servicio Meteorológico Nacional of Mexico and the U.S. National Hurricane Center provide little information on the impacts of storm surge flooding in Western Mexico. As a whole, these reports reveal that freshwater flooding and mudslides cause most of the TC deaths in Western Mexico, followed by fatalities from wind damage. These hazards also cause most of the economic damage from TCs.

However, some coastal flooding impacts are provided in the literature for several TCs in the past decade. Hurricane Kenna, in 2002, produced the most extensive damage. Damage estimates were made available for Puerto Vallarta, where storm damage totaled \$5 million U.S. Dollars, most of which was caused by the storm surge (Franklin 2002). Hotels along the coast observed most of the damage. Extensive surge damage also occurred in San Blas, where the media reported that 80 to 90% of the homes were damaged or destroyed (Franklin 2002). Storm surge and waves also impacted marinas and the fishing industry, as these forces combined to transport shrimp boats more than 300 m from their docks (Franklin 2002).

In June, 1971, Hurricane Bridget generated a storm surge and destructive waves that sank 20 boats in Acapulco Bay and damaged waterfront facilities (Denny 1972). At the time the storm struck, it was the most violent hurricane to hit Acapulco in more than 25 years. Damage in the Acapulco area was estimated at \$40 million U.S. dollars (Denny 1972), although it is not clear what proportion of this damage was caused by coastal flooding. Storm surge also inflicted damage to marine interests near the locations of La Paz and Puerto Escondido during Hurricane Marty in 2003 (Franklin 2004). The surge and waves in this storm also eroded beaches at San Felipe in the northern Gulf of California. Several years later, in 2008, storm surge generated by Hurricane Norbert flooded the fishing town of Puerto San Carlos, however, no damage estimates are available (Franklin 2009).

2.5.3.2 Hawaii

Scientific literature provides evidence of coastal flooding from at least 13 TCs in Hawaii since 1925. The most severe impacts are generally the flooding of coastal structures and roads. The literature provides no evidence of fatalities in Hawaii that were directly caused by tropical-cyclone generated storm surge, however, isolated drownings from high surf may not have been recorded in the literature.

Hurricane Iniki inflicted the most severe coastal flooding damage to Hawaii, as waves and storm surge destroyed 63 homes on Kauai's South Coast (Central Pacific Hurricane Center 1992). Storm surge inundated coastal structures, such as beachfront homes, during at least seven separate TCs: The Ramage Cyclone of 1925, Hurricane Nina in 1957, Hurricane Diana in 1972, Hurricane Fico in 1978, Hurricane Ignacio in 1985, Hurricane Estelle in 1986, and Hurricane Iniki in 1992 (Central Pacific Hurricane Center

2012). Five other TCs flooded roads, sometimes washing out entire sections of roadway or piling debris on the road surface. These storms were Hurricane Iwa in 1982, Hurricanes Nele and Pauline in 1985, Hurricane Fefa in 1991, and Hurricane Fernanda in 1993 (Central Pacific Hurricane Center 2012). Hurricane Uleki washed seawater onto the runway at Midway Island in 1988 (Central Pacific Hurricane Center 1988).

The highest magnitude tsunamis have more severely impacted Hawaii than coastal inundations from TCs. The 1946 Aleutian Island Earthquake produced a devastating Pacific-wide tsunami that killed 159 people in Hawaii (Lander and Lockridge 1989; Johnson and Satake 1997), in the most deadly coastal flood event in Hawaiian history. This event inflicted \$300 million in damage in Hilo (adjusted to 2011 U.S. dollars), and destroyed most of the waterfront buildings in that city (Western States Seismic Policy Council 2013). The 1960 Chilean earthquake killed 61 people in Hawaii and inflicted \$20 million in damage (Eaton et al. 1961).

2.6 Australia, New Zealand and Oceania

2.6.1 Storm Surge Literature

The Australia Bureau of Meteorology provides a webpage that contains an abundance of historical cyclone information (Australia Bureau of Meteorology 2013a). This site provides TC tracking maps from 1906-2007 for the Australia region, and from 1969- present for the Southern Hemisphere. This resource also provides more than 400 individual cyclone reports from 1970-present, as well as historical cyclone summaries for Queensland, Northern Territory, Western Australia and New South Wales.

The tracking maps do not provide storm surge information, but they do provide a best estimate of storm position, wind speed and central pressure, which may be useful for

constructing storm surge history. The individual cyclone reports provide a rich history of storm surge and storm tide observations for many storms, as well as data related to storm position, minimum central pressure, maximum wind speeds and rainfall totals. The historical cyclone summaries by state differ in organization and content. The summary for Western Australia provides a page of TC extremes in that region, including the highest storm surge observations (Australia Bureau of Meteorology 2013b).

The Meteorological Service of New Zealand houses a Tropical Cyclone Warning Center in Wellington, New Zealand (World Meteorological Organization 2013). This site hosts map-based severe weather warnings for a wide variety of hazards, including TCs, thunderstorms and heavy snow (MetService 2013). The site focuses on forecasting severe weather and does not provide a TC archive or any coastal flooding data.

The Fiji Meteorological Service in Nadi, Fiji, hosts the Regional Specialized Meteorological Centre (RSMC) for the South-West Pacific Ocean (Fiji Meteorological Service 2013). The RSMC's website provides a three day TC outlook, a seasonal TC forecast and the tracking map for the latest TC to impact the region. The site does not provide any historical TC reports or coastal flooding observations.

Several academic sources provide extensive storm surge data for Australia and Oceania. Nelson (1975) provides a list of 30 historical storm surge and storm tide elevations from 1880-1967 for Queensland, Northern Territory, Western Australia and New South Wales in Australia. Harper (1998) provides a list of storm surge and storm tide observations for approximately 70 TCs that have impacted Queensland from 1858-1996. This publication compiled these records from various sources, including Whittingham (1958), Holthouse (1971), Harvey (1974) and Nelson (1975). Terry (2007)

provides more than 10 storm surge and storm tide heights in Australia and Oceania since 1899, including a table with surge observations, a storm tide graph from a coastal flooding event in Samoa in 2004, and some inundation photos and TC tracking maps. Haigh et al. (2013) provide a list of the largest observed tropical cyclone-generated storm surges at 17 tide gauges in Australia, as well as the ranking of those surges at each site.

2.6.2 Storm Surge Observations

These sources provided 134 high-water observations for Australia and Oceania. Storm surge heights were provided by 105 of these observations, storm tide heights were given for 25 observations, and four data records provided the level of storm tide and waves. Observations that include waves are usually removed from storm surge/ storm tide datasets, however, in these four cases, the high-water marks that include waves are the only available observations and were therefore included in the data. These data are provided from tide gauges, debris lines, field surveys and estimation of storm surge/ storm tide levels based on water depth above ground level.

In some cases, storm tide observations include the datum from which they were measured. Such datum levels include mean sea level, high water springs, highest spring tide, high water, low water neaps, chart datum, and Australian Height Datum. In addition, various data sources indicate if maximum water levels exceeded the level of the Highest Astronomical Tide (HAT). For example, 13 of 21 notable storm surges in Queensland exceeded HAT, and nine events exceeded this level by at least 2 m (Harper 1998).

In other cases, high water levels are classified as storm tide observations even though no vertical datum is provided. This is common if a storm surge impacted a rural area with little development and no tide gauges. In such cases, field surveys may identify

high water marks, which are actually storm tide levels because it was not possible to remove predicted tide levels from the maximum water level, as would be done if a tide gauge provided the data. The maximum storm tide level for TC Barry in 1996, which occurred south of the Staaten River Mouth in Northern Queensland, provides an example of this type of observation. A helicopter field survey in this region found evidence of a storm tide level reaching at least 4 m (Australia Bureau of Meteorology 1996).

Unfortunately, storm surge or storm tide observations are unavailable for some severe TCs that have made landfall in rural areas of Australia. This is most common in portions of the Northern Territory, Western Australia and the Cape York Peninsula of Queensland. For example, storm surge data are unavailable for Severe TC George, which came ashore as a physically large and intense TC in Western Australia during March of 2007. This storm likely produced a substantial storm surge as it made landfall as a category 5 TC, east of Port Hedland (Australia Bureau of Meteorology 2007). While evidence suggests that Severe TC Dominic generated a substantial storm surge in the Cape Keerweer area of Queensland in 1982, quantitative data are completely missing from the area of peak storm surge (Australia Bureau of Meteorology 1982).

Most of the high-water marks in this basin were observed in Australia, where 117 observations were recorded, while 17 observations were identified in Oceania. Maximum surges in this region generally occur from January to March, a period of active tropical weather within the larger November- April Southern Hemisphere TC season (De Scally 2008). Observations in both Australia and Oceania are provided for a large swath of territory. Queensland's 69 observations provided more than half the total for Australia, while Western Australia contained 31 records, Northern Territory contained 15 and New

South Wales contained two records. Observations in Oceania are provided for French Polynesia, Fiji, Western Samoa, Tuvalu, Cook Islands, Tuamotu Archipelago, and the Solomon Islands.

Table 2.9 provides a list of the top 10 highest water levels in the region. The three highest magnitude events exceed 9 m; two of these events occurred in Queensland, Australia. Western Australia contains four observations ranked in the top 10 of this region, while three records in this list were located in Northern Territory. All of the water levels in the top-10 list are ≥ 6 m. These data suggest that storm surge is a hazard that seriously threatens at least three states and thousands of kilometers of coastline in Australia.

Table 2.9. Top 10 tropical cyclone-induced surge levels in Australia, New Zealand and Oceania, from 1880-2013. Compiled from the following sources: Whittingham (1958); Nelson (1975); Harper (1998); Australia Bureau of Meteorology (2000); Emergency Management Australia (2006); Australia Bureau of Meteorology (2006); Anonymous (2010); and Australia Bureau of Meteorology (2014).

| Rank | Height (m) | Year | Storm Name | Maximum Surge Location |
|------|-------------------|------|-------------------|--|
| 1 | 13.7 ^a | 1899 | Mahina | Bathurst Bay, QLD, Australia |
| 2 | 9.20 ^c | 1882 | Unnamed | Near Cossack, WA, Australia |
| 3 | 9.10 ^a | 1934 | Unnamed | Bailey Creek, QLD, Australia |
| 4 | 7.60 ^c | 1880 | Unnamed | Yammadery Bank, WA, Australia |
| 5 | 7.00 ^a | 2010 | Tomas | Lau Island Group, Fiji |
| 6 | 6.70 ^b | 1931 | Unnamed | Groote Eylandt, NT, Australia |
| 7 | 6.60 ^a | 1923 | Douglas Mawson | Groote Eylandt, NT, Australia |
| 8 | 6.05 ^a | 1925 | Unnamed | Roebourne, WA, Australia |
| 9 | 6.00 ^c | 2000 | Rosita | West of Thangoo Station, WA, Australia |
| 9 | 6.00 ^b | 2006 | Monica | Junction Bay, NT, Australia |

Water Height: a = Storm Surge; b = Storm Tide; c= Storm Tide + Waves

Uncertainty surrounds several unusually high storm surges during the early portion of Australia's surge archive. The highest profile of these events was TC Mahina, which supposedly generated the highest-magnitude event in Australia's history in 1899, when a 13.7-m storm surge was observed near Barrow Point, south of Bathurst Bay

(Nelson 1975). Although more literature is available for this surge event than any other in the region, some uncertainty exists regarding the actual storm surge height. This phenomenal storm surge was witnessed first-hand by Constable J.M. Kenny, who was camped 12.19 m (40 feet) above sea level, on a ridge near Ninian Bay, adjacent to Barrow Point (Anonymous 1899; Nott and Hayne 2000; Emergency Management Australia 2006). TC Mahina struck during his first night at this campsite and inundated this ridge with waist-high water levels (Anonymous 1899). The Disasters Database provided by Emergency Management Australia (2006) reported that large quantities of fish were found at 15 m above sea level and several kilometers inland, while dolphins were found 15.2 m up on the cliffs at Flinders. Granger and Smith (1995) provide a storm tide estimate of 14 m and suggest that this extreme magnitude represents a 1 in 1000 to 1 in 10,000 year event for this region. Observations from other sources range from 12.19 to 14 m (Whittingham 1958; Harper 1998; Terry 2007)

However, some doubt exists over the actual water level generated by Mahina. Nelson (1975) indicates that this water level estimate is unreliable. Notation from Harper (1998, pg. 22) indicates that Mahina's reported storm surge height is, "unknown, unreliable or an estimate only." Nott and Hayne (2000) have cast some doubt upon this extraordinary storm surge magnitude after conducting field surveys in the region around Ninian Bay. Multiple transects in this area show that marine deposits were not found greater than 5 m above HAT. Such findings support the notion that Mahina's storm surge was less than 5 m, with the exception of some areas of wave run-up. Numerical models support these lower storm surge heights (Nott and Hayne 2000).

Several other storm surge levels from the early portion of Australia's surge history are uncertain as well. In 1882, a 9.2-m storm tide described as a tidal wave submerged the Twin Islands near Cossack, in Western Australia (Nelson 1975). Based on this description, it is possible that this water level includes waves or wave run-up. Some uncertainty also surrounds a potentially massive storm surge that may have struck near Cape Tribulation, Queensland, in 1934. Two government sources provide a storm surge height of 9.1 m for this event (Emergency Management Australia 2006; Australia Bureau of Meteorology 2014), however, Harper (1998) provides a surge height of $\geq 1.8\text{m}$ for this event in a thorough list of Queensland storm surge observations. However, It is possible that the observation from Harper (1998), which was provided for Port Douglas, is an accurate water level but not the maximum storm surge level for this event. Maximum water levels of 9.2 and 9.1 m were added to SURGEDAT for these storms, however, I was less certain of these water levels than events in which multiple, credible sources confirm similar surge heights and locations.

The islands of Oceania located farthest from the Equator experience more TCs and storm surges than those islands at lower latitudes (De Scally 2008). This pattern likely occurs because the Coriolis effect, which enables TCs to spin, is stronger at higher latitudes and negligible near the Equator.

The highest observed water levels in Oceania generally range from 4-6 m. In some cases, such storm surge heights may completely wash over low-lying islands (Spennemann 1996; De Scally 2008). Six of the seven highest storm surge observations in the region range from four to 5.5 m. The 7-m storm surge observed in Fiji's Lau Island Group during TC Tomas in 2010 (Anonymous 2010) is noticeably higher than the other

observations and an outlier for this region. As this record was provided in a news article rather than a scientific source, the confidence of this observation is somewhat lower than other data in the region.

TCs often produce tremendous wave heights in Oceania, which may flood locations that are inland or elevated above the storm surge level. For example, in February 1990, TC Ofa made a direct hit on the island of Upolu in Samoa. Although the storm surge level on Upolu was only 1.6 m (Rearic 1990; Solomon and Forbes 1999), coastal flooding was severe, particularly east of Apia, where coastal protection was limited and the reef was narrow. Significant wave heights were 8.1 m at a buoy south of Samoa (Solomon and Forbes 1999). Wave heights on the island of Niue were approximately 18 m, comparable to the height of cliffs at some locations (Solomon and Forbes 1999). In 1987, TC Sally generated a maximum wave height of 12 m at a buoy off the north coast of Raratonga in the Cook Islands (Croad 1989; Barstow and Haug 1994; Solomon and Forbes 1999).

Although TCs sometimes impact New Zealand, storm surges are not considered a major hazard in comparison to other countries (Heath 1979; Murty and Flather 1994; Goring 1995; De Lange and Gibb 2000). Storm surges in New Zealand are generally considered to be an order of magnitude less than surges in the most active basins, like the Bay of Bengal, Gulf of Carpentaria and Gulf of Mexico (De Lange and Gibb 2000). For example, Heath (1979) lists several of New Zealand's highest-magnitude tropical and extra-tropical storm surge events, all of which are < 1 m high. Observations indicate that extra-tropical cyclones actually have produced the largest storm surges at Bay of Plenty and Tauranga Harbor (De Lange and Gibb 2000). A similar pattern is observed along

Australia's southern coast, where mid-latitude storms and cold fronts generate the largest storm surges (McInnes et al. 2008).

2.6.3 Storm Surge Impacts

The most deadly storm surge events in this region have occurred when surges and treacherous seas have sunk vessels near the Australian coast, sometimes causing more than 100 deaths. The extraordinary storm surge generated by TC Mahina inflicted the most destruction, as the storm surge and rough seas sank more than 100 vessels in a pearling fleet near Bathurst Bay (Australian Emergency Management 2013a), killing more than 300 people (Whittingham 1958; Granger and Smith 1995; Australian Emergency Management 2013a; Australia Bureau of Meteorology 2013b). Two separate TCs sank pearling fleets in Western Australia, both killing approximately 140 people. The first of these events occurred on April 22, 1887, off Ninety Mile Beach, while the second event occurred on March 26-27, 1935, near the Lacepede Islands (Australia Bureau of Meteorology 2013b). A storm surge at Port Douglas, Queensland, sank a pearl lugger fleet in March, 1934, killing 75 people (Australian Emergency Management 2013b). Some other surge events impacted passenger vessels not involved with pearl lugging. For example, in March, 1934, a TC in Western Australia generated a large storm surge and destructive waves, which sank several passenger vessels, killing more than 150 people (Australia Bureau of Meteorology 2013b). Approximately 140 of these people drowned on the vessel *Koombana*, which sank while en route from Port Hedland to Broome.

Storm surges have also inflicted agricultural losses in coastal areas. A repetitive theme in the anecdotal literature is the loss of cattle in Western Australia from drowning

in storm surge. The greatest documented loss of life occurred in 1994, when storm surge from Severe TC Annette drowned 500 cattle near Mandorah Station (Australia Bureau of Meteorology 1994). These cattle were driven to the sea by the strong winds, then drowned in the surging waters. In 2000, storm surge from Severe TC Rosita killed 200 head of cattle, mostly from drowning in storm surge (Australia Bureau of Meteorology 2000). The storm surge from Severe TC Quenton drowned 50 cattle that were trapped on a beach near Anna Plains Station in 1983 (Australia Bureau of Meteorology 1983a). Quantitative cattle losses are unavailable for some other TCs that drowned cattle, such as Severe TC Amy in 1980 (Australia Bureau of Meteorology 1980a) and Severe TC Jane in 1983 (Australia Bureau of Meteorology 1983b). Financial losses are provided for Severe TC Enid, which inflicted \$200,000 worth of cattle losses in 1980 at Wallal Station (Australia Bureau of Meteorology 1980b). Historical literature also provides documentation of a storm surge killing large numbers of sheep in Western Australia. In 1894, a TC generated a substantial storm surge, which washed away the sea wall at Cossack and killed 15,000 sheep (Australia Bureau of Meteorology 2013c.)

Although the highest magnitude storm surges in Oceania tend to be smaller than those in Australia, the impacts of storm surge on the island nations of the Pacific are severe. Populations living on the numerous atolls in the Pacific have no escape from storm surges, as the elevation of such islands is often less than 2 m above high water (Spennemann 1996). Although volcanic islands have higher average elevations, populations in these locations are still vulnerable to storm surge because most people live near the coast. For example, most of the population and economic activity in Fiji, Tonga and Western Samoa are located on low-lying coastal areas, even though these islands are

mountainous and comparatively large (Mimura 1999). Historical literature does not document many cases of storm surge causing high fatality totals in this region, however, a TC in the Cook Islands killed 1,000-2,000 people more than 400 years ago (De Scally 2008).

TC-generated storm surges and waves also contribute to coastal erosion in Oceania. Such erosion is often localized and may be more severe in locations with narrow reefs or limited coastal protection. Types of erosion include sand removal and the breaking of coral, which may be deposited as coral rubble in towns or villages (Solomon and Forbes 1999). Erosion in this region threatens coastal buildings and infrastructure, while reducing the size and extent of beaches. Such impacts will likely have widespread economic impacts on places such as Fiji, which is highly dependent on tourism (Gravelle and Mimura 2008).

Storm surges in Oceania also destroy long-term food and water supplies. These impacts are pronounced because such resources are often vulnerable to coastal inundation, particularly on low-lying atolls. In such locations, fresh water supplies are limited and often found in underground fresh water lenses, which are vulnerable to salt-water contamination following coastal flood events. Storm surges can contaminate these aquifers for at least 10 months (Terry and Falkland 2010).

Such impacts were experienced in the atoll nation of Tokelau, following TC Percy in 2005. The cyclone generated large waves that attacked the islands from both lagoon and ocean sides, meeting in the middle of islands and completely inundating villages (United Nations Office for the Coordination of Humanitarian Affairs 2005; Terry and Falkland 2010). This inundation drastically reduced the food supply, as 50% of the pigs

were lost and fish harvests were reduced following the storm at Fafafo atoll, in the Tokelau Island Group (United Nations Office for the Coordination of Humanitarian Affairs 2005). The surge also contaminated drinking water, requiring a shipment of water to be urgently transported from American Samoa (Terry and Falkland 2010). Overflowing septic tanks and trash that was washed out of landfills contributed to the contamination and pollution of Tokelau following this surge event (United Nations Office for the Coordination of Humanitarian Affairs 2005).

2.7 Southwest Indian Ocean

2.7.1. Storm Surge Literature

The Tropical Cyclone Centre at Réunion provides summaries of TC seasons in French and English from 1990/1991- 2009/2010, with the exception of 2002/2003, 2004/2005 and 2007/2008 (Meteo France 2013). These reports provide a comprehensive overview of TC seasons for the entire Southwest Indian Ocean, including Mauritius, Réunion, Madagascar and Mozambique. Detailed observations are provided, including cyclone tracks and intensity, as well as related hazards, such as wind speeds, rainfall, swell heights and storm surge inundation.

The Mauritius Meteorological Services provide a list of more than 40 historic TCs that impacted the Republic since 1892 (Mauritius Meteorological Services 2012). This resource provides the names, dates and years of TCs, as well as the closest distance they passed to Mauritius, the highest wind gusts and lowest pressure in each event. However, this archive does not provide any information about historic storm surge events.

Mayoka (1998) provides a publication in French that gives a comprehensive overview of TCs that have impacted the French island Réunion. This publication

provides a list of 10 historic cyclones that impacted the island from 1948-1997, including the name and year of the cyclone, the closest distance each cyclone came to the island, the minimum air pressure, maximum wind gusts and maximum rainfall. The number of fatalities and amount of damage are also provided. However, this list provides no storm surge observations or impacts.

The national center for meteorological services in Madagascar is called Direction de la Météorologie et de l'Hydrologie, according to the World Meteorological Organization's French language website (Organisation Météorologique Mondiale 2013). This organization does not currently maintain a website in French or English, or disseminate any information related to storm surge. However, several peer-reviewed journal articles provide some details about storm surge observations and impacts on the island, such as Naeera and Jury (1998), and Chang-Seng and Jury (2010).

The Instituto Nacional de Meteorologia (2013) provides weather and climate information in Portuguese for the country of Mozambique, but provides no archive of TC reports or information related to storm surges. A thorough search of academic literature provides no publications with information related to storm surge observations or impacts for this country. Although Chemane et al. (1997) provide a comprehensive overview of vulnerability in the Mozambique coastal zone, including potential impacts from sea-level rise, they do not provide any historical storm surge observations.

2.7.2 Storm Surge Observations

Relatively deep bathymetry off the coast of Réunion suppresses storm surge levels along the coast of this island (Mayoka 1998). However, storm swells which form into large waves impact the island, particularly along the northern and eastern coasts

(Mayoka 1998). Swells from Cyclone Colina in 1993 exceeded 9 m in height just 2 km off the north shore of Réunion (Mayoka 1998).

Heavy rainfall has historically threatened Réunion more than storm surge or high waves. In fact, TCs that have struck Réunion have produced some world record rainfall totals. For example, TC Denise in 1966 dumped more than 1.8 m of rain in 24 hours at a settlement called Foc-Foc, which is a world record one-day rainfall total (Cervený et al. 2007). Cyclone Hyacinthe dumped more than 5 m of rain on the same location in a 12-day period in January, 1980 (Mayoka 1998).

Although Madagascar experiences the most intense TC strikes in this region, few storm surge observations are available. A modeling analysis of three tropical separate cyclones in early 1994 estimates that each storm produced storm surge elevations of at least 4 m, with combined surge and wave setup elevations reaching 5 m in each event (Naeraa and Jury 1998). Peak surge levels may have reached 6 m, while waves that inundated the coast may have reached 10 m on Madagascar during that catastrophic cyclone season (Naeraa and Jury 1998; Chang-Seng and Jury 2010). However, independent observations are not available to validate these modeling results.

Although TCs sometimes strike Mozambique, this country observes a relatively modest amount of TC activity when compared to other locations in this basin, like Madagascar. Less than 5% of TCs in the South Indian Ocean basin make landfall on the mainland of southeast Africa, and those that strike are generally weak (Bettinger and Merry 2012).

Nonetheless, historical literature documents 13 intense TCs that have struck Mozambique from 1956-2008 (Queface and Tadross 2009; INGC 2009). In the absence

of observed storm surge observations in the literature, the Sea, Lake, and Overland Surge from Hurricanes (SLOSH) model has been used to estimate storm surge potential along the Mozambique coast (Neumann et al. 2013). Storm surge levels in Mozambique may be lower than other countries along the Southwest Indian Ocean because TCs tend to approach the country from the east or northeast, and often cross Madagascar and weaken before striking the African mainland. Also, Madagascar may block large swells and storm surge that develop in the Indian Ocean, thereby shielding the African coast from much of the displaced water. However, rising sea levels threaten to exacerbate future coastal flooding associated with storm surges in Mozambique (Chemane et al. 1997; Dasgupta et al. 2009).

2.7.3 Storm Surge Impacts

Wind and heavy rainfall have produced the most fatalities and damage at Réunion associated with TCs. An unnamed cyclone in 1948 inflicted 165 fatalities, which is the most in the modern history of the island (Mayoka 1998). Winds in this event were estimated at 250 km/ hr. Cyclone Hyacinthe killed 25 people in 1980, mostly from floods associated with torrential rains (Mayoka 1998). The literature does not provide any record of deaths from storm surge, but large waves from Cyclone Gamède in 2007 produced severe coastal erosion at Saint Paul Bay, in the northwest portion of the island (Dossier Départemental des Risques Majeurs 2011).

The 1994 TC season was very severe for portions of Eastern Madagascar. TCs Daisy, Geralda and Litanne all made landfall around the same region between January 13 and March 15 (Naeraa and Jury 1998). TC hazards, including storm surge, created much destruction at Tamatave Harbor, making it inoperable for nearly a year (Chang-Seng and

Jury 2010). Damage at this location greatly impacted the country, because Tamatave is the most important harbor and contains the only large oil refinery in Madagascar (Le Goff 1994; Naeraa and Jury 1998). Such destruction had wide-reaching impacts, as the country faced a petroleum shortage and experienced a 10% deflation in the gross domestic product (Chang-Seng and Jury 2010).

Although storm surge levels have been relatively modest along the Mozambique coast, the high coastal population density places many people at risk of inundation. Approximately 40% of the country's population lives in coastal districts (Chemane et al. 1997), which places Mozambique among the top five low-income countries worldwide with population exposed to coastal inundation (Dasgupta et al. 2011). Such vulnerability has substantial economic impacts. The coastal zone provides important resources for this low-income nation (Chemane et al. 1997), and more than 25% of the gross domestic product in the coastal region is produced in locations vulnerable to surge (Dasgupta et al. 2011). Sea-level rise also threatens some coastal cities, like Beira, where most of the city is below the high water level (Chemane et al. 1997). Such locations are vulnerable to inundation from even small storm surge events.

2.8 Global Comparison

This comprehensive literature review makes it possible to compare storm surge literature, observations and impacts by region. These comparisons are only as strong as the supporting literature. In other words, the number of available storm surge observations for a given region is dependent on both the climatology and the available literature, and some areas with fewer identified storm surge events may lack a robust

dataset because of sparse literature, while a less active storm surge climate may explain why other regions observed fewer surges.

2.8.1 Comparing Global Surge Literature

Federal government sources provide the most comprehensive storm surge data in United States, Australia, and the Philippines. The U.S. government provides the greatest quantity of storm surge data in the world; this source provides maximum storm surge heights for the United States, as well as some data for Mexico, Central America and the Caribbean. Most of these data are provided by the National Hurricane Center, United States Geologic Survey (USGS), U.S. Army Corps of Engineers, and the Federal Emergency Management Agency (FEMA). The Australia Bureau of Meteorology provides TC summaries for Queensland, Western Australia, Northern Territory and New South Wales, as well as more than 400 TC reports from 1970-2011. The Philippine Atmospheric, Geophysical and Astronomical Services Administration, or PAGASA, provides vital storm surge data for the Philippines, including a map of historical storm surge events that have been observed in the Archipelago. The National Maritime Institute of China provides a useful statistical summary of observed storm surges in China from 1949-1998, however, limited data are provided in English or in documents with English titles or abstracts from the Chinese government.

Academic sources provide excellent information on storm surge observations and impacts for various regions. For example, peer-reviewed journal articles provide most of the historic storm surge data for China in literature in English or with English titles or abstracts. Harper (1998) provides a comprehensive list of observed storm surge data for Queensland, Australia, which supplements government sources to provide a robust

dataset for that region. Dube et al. (1997) provide the most comprehensive data for the Northern Indian Ocean, as they provide the maximum water levels for more than 35 TCs that impacted Bangladesh and India. The SURGEDAT project at Louisiana State University provides a comprehensive storm surge database for the U.S. Gulf Coast (Needham and Keim 2012), as well as a global storm surge database comprised of surge events since 1880 (Needham et al. 2013). This project compiles data from many sources, including governmental organizations, peer-reviewed literature and historic newspapers.

2.8.2 Comparing Global Surge Observations

The global storm surge literature review discovered 702 unique storm surge or storm tide events around the world since 1880 (Table 2.10). The majority of these events came from the Western North Atlantic basin, which observed 388 events, or approximately 56% of the total.

Table 2.10. Numeric counts of storm surge and storm tide observations by basin. Taken from SURGEDAT database.

| Region/ Basin | Storm Surge | Storm Tide | Storm Tide + Waves | Total | Pct of Total |
|------------------------|-------------|------------|--------------------|-------|--------------|
| Western North Pacific | 73 | 45 | 1 | 119 | 16.9 |
| Northern Indian Ocean | 14 | 43 | 1 | 58 | 8.3 |
| Western North Atlantic | 175 | 214 | 0 | 388 | 55.3 |

Table 2.10 (continued). Numeric counts of storm surge and storm tide observations by basin. Taken from SURGEDAT database.

| | | | | | |
|--------------------------|-----|-----|---|-----|------|
| Eastern North Pacific | 2 | 0 | 0 | 2 | 0.3 |
| Australia, N.Z., Oceania | 105 | 25 | 4 | 134 | 19.1 |
| Southwest Indian Ocean | 1 | 0 | 0 | 1 | 0.1 |
| Total | 370 | 327 | 6 | 702 | 100 |

Australia and Oceania observed 134 events, or approximately 19% of global surges, while 119 events, or approximately 17% of the total, came from the Western North Pacific (Figure 2.2). Storm surge literature provided few events for the Eastern North Pacific and Southwest Indian oceans, as only three events, or less than one-half of one percent of the observations came from these regions.

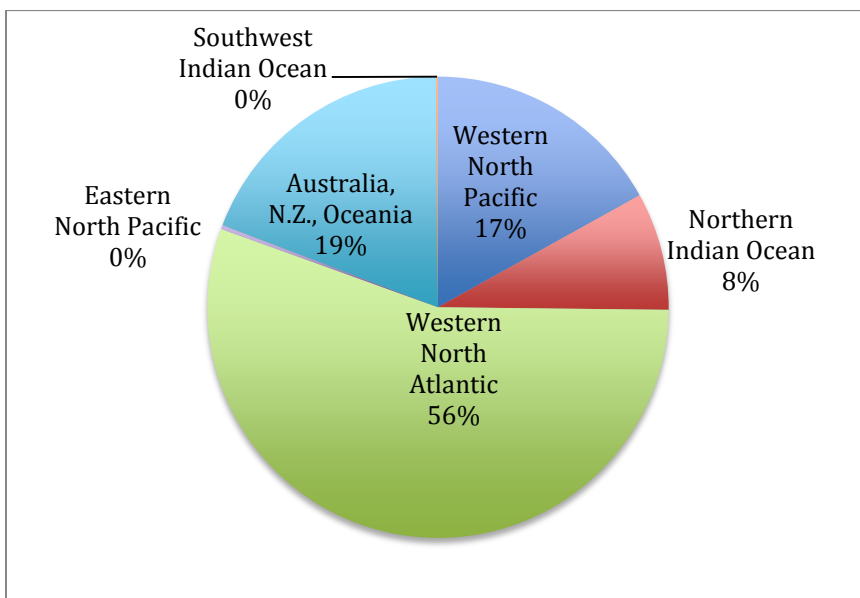


Figure 2.2. Global storm surge distribution graph.

A breakdown of these surge observations in the four major storm surge basins reveals that one region or country in each basin typically provides more than half of the observations in that basin, while other sub-basins or countries divide the remaining observations. For example, the majority of high-water levels in the Western North Pacific come from China, where peer-reviewed journal articles provided an abundance of surge data, accounting for 64% of observed water levels in this basin (Figure 2.3).

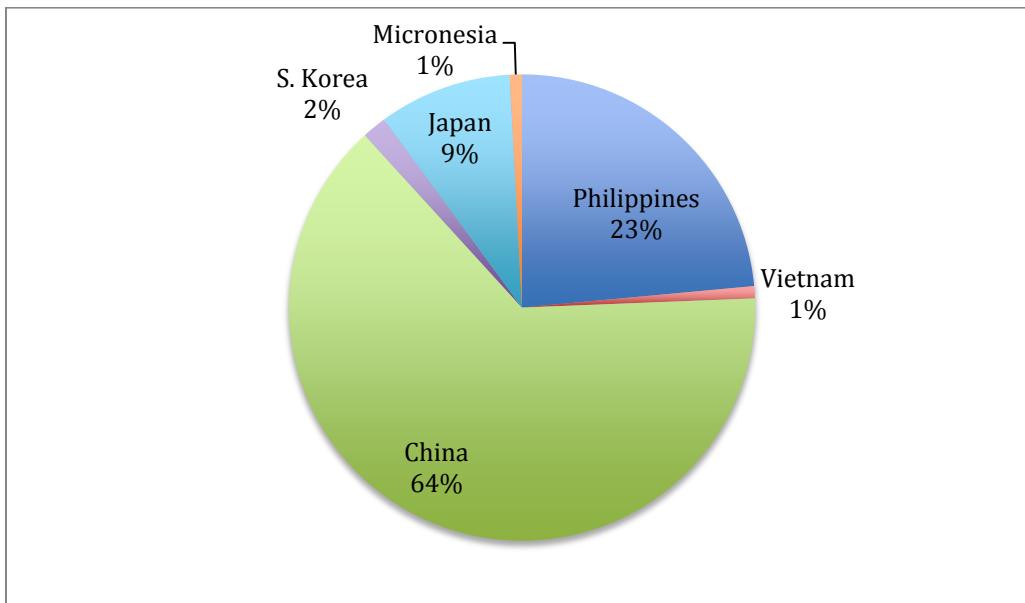


Figure 2.3. Western North Pacific storm surge distribution graph.

The Philippines provides nearly one-quarter of the observations in this basin. Slightly more than half of the observed water levels in Australia and Oceania come from Queensland, while nearly one-quarter of the events were located in Western Australia (Figure 2.4).

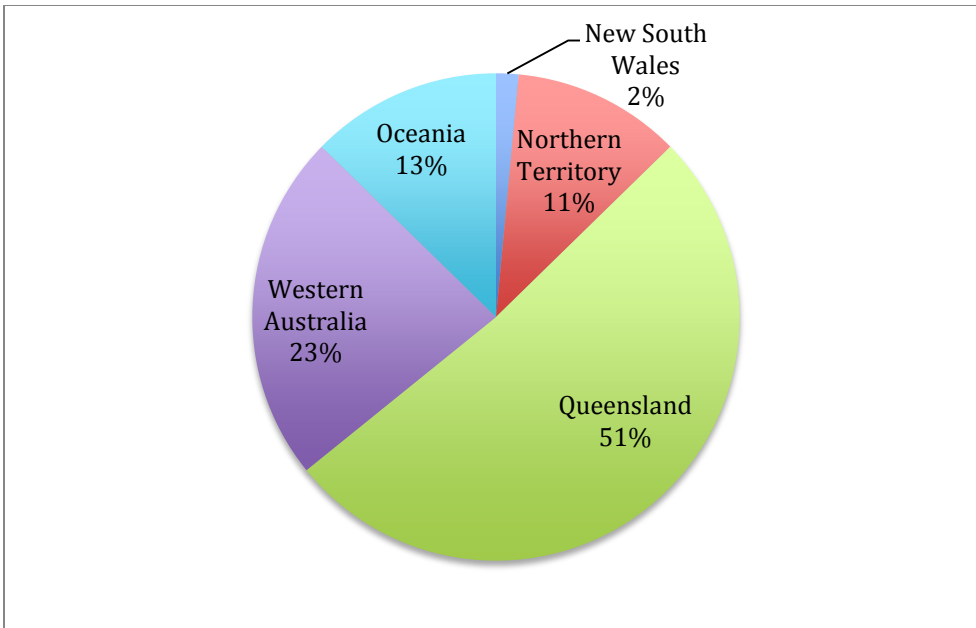


Figure 2.4. Australia and Oceania storm surge distribution graph.

Storm surge and storm tide observations in Bangladesh account for more than half of the total observations in the Northern Indian Ocean, while the Indian Coast along the Bay of Bengal accounts for approximately one-third of the events (Figure 2.5).

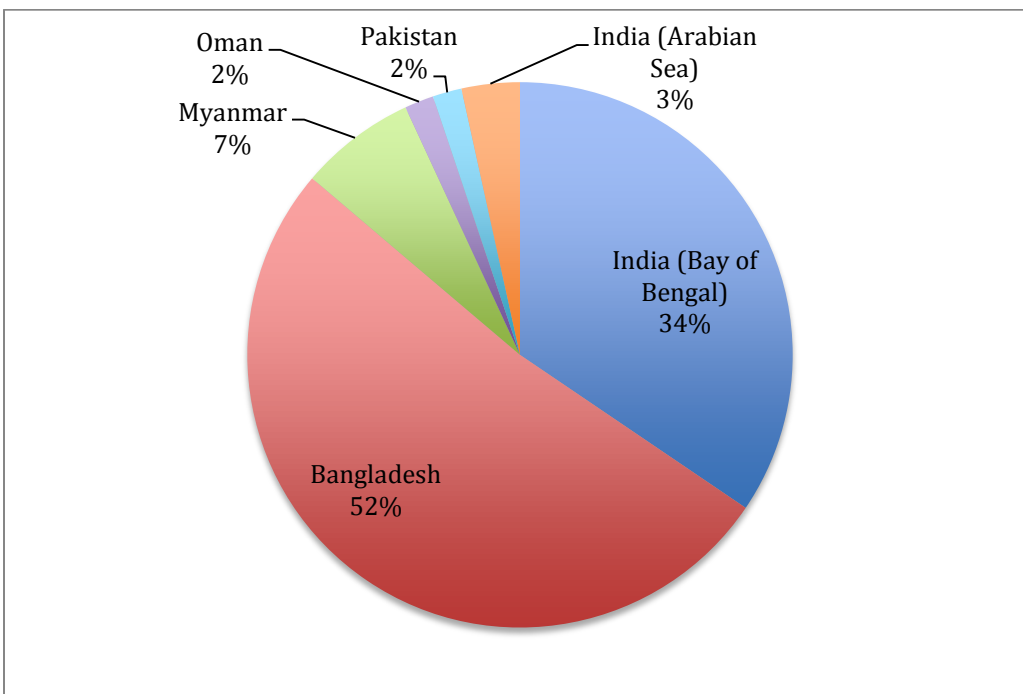


Figure 2.5. Northern Indian Ocean storm surge distribution graph.

Finally, the U.S. Gulf Coast provides 62% of the observations in the Western North Atlantic, followed by the U.S. Atlantic Coast, which provides 28% of the water levels (Figure 2.6). The Caribbean Sea, Central America and Eastern Canada collectively provide the remaining 10% of the observations in this basin.

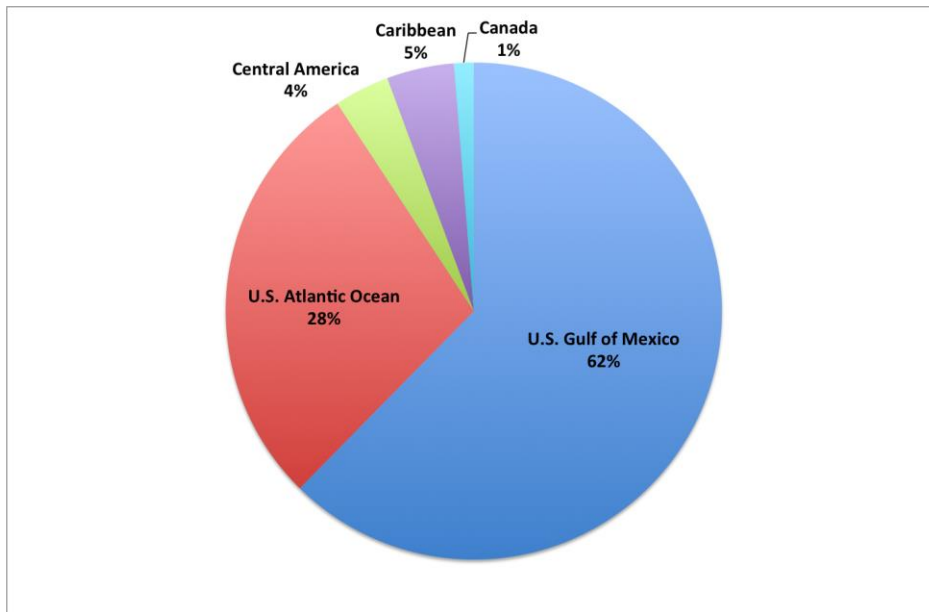


Figure 2.6. Western North Atlantic storm surge distribution graph.

A basin-by-basin comparison of storm surge heights is challenging because data availability varies considerably between basins. Therefore, a lack of observations over a period of time in a given basin may be identifying a lull in tropical weather, or potentially reveal a lack data for surge events that actually occurred. In many cases, data availability likely relates to both climatic and social factors.

Fortunately, comprehensive storm surge data are available for several sub-basins over a period of at least 50 years, enabling comparisons between some of the regions that are most prone to tropical storm surge inundations. These data are provided as either summary statistics for a sub-basin or actual storm surge and storm tide observations taken from SURGEDAT.

The summary statistics provided by China’s National Maritime Bureau provide counts of storm surges in China that exceeded 1m, 2m, and 3m during the 50-year period from 1949-1998 (Tang et al. 2011). The most comprehensive data for the Bay of Bengal is available for the 54-year period from 1958-2011, made available largely due to the contributions of Dube et al. (1997) and Dube et al. (2008). The best-developed storm surge archive from Australia and Oceania is the record from Queensland, Australia, beginning in 1934, made available through Harper (1998) and many documents from the Australia Bureau of Meteorology. SURGEDAT data for the U.S. Gulf Coast are most comprehensive from 1931-2013, as only 5.3% of potential surge events during this period are missing from the archive. The best dataset for the U.S. Atlantic Coast also comes from SURGEDAT, and begins in 1940.

Table 2.11 provides the quantity of storm surge and storm tide events that exceed 1m, 2m, 3m and 5m in each of these sub-basins. I chose the lowest three threshold levels to match the statistics provided by China’s National Maritime Bureau, and I added the 5m-threshold to capture the highest magnitude storm surges in each of these sub-basins.

Table 2.11. Summary statistics for storm surge observations in selected basins. Surge counts indicate the number of surge events that have exceeded the threshold. Counts of 1, 2, and 3 m surges in China provided by Tang et al. (2011). All other data provided by SURGEDAT database.

| Region/ Basin | Year Range | No. of Years | ≥ 1m | ≥ 2m | ≥ 3m | ≥ 5m |
|------------------|-------------|-----------------|------|------|------|------|
| China | 1949 - 1998 | 50 | 270 | 48 | 15 | 2 |
| Bay of Bengal | 1958-2011 | 54 | 45 | 40 | 39 | 27 |

Table 2.11 (continued). Summary statistics for storm surge observations in selected basins. Surge counts indicate the number of surge events that have exceeded the threshold. Counts of 1, 2, and 3 m surges in China provided by Tang et al. (2011). All other data provided by SURGEDAT database.

| | | | | | | |
|--------------------------|-----------|----|-----|----|----|---|
| Queensland, Australia | 1934-2011 | 57 | 31 | 14 | 8 | 3 |
| U.S. Gulf of Mexico | 1931-2013 | 84 | 151 | 67 | 36 | 8 |
| U.S. Atlantic | 1940-2013 | 74 | 66 | 40 | 24 | 5 |

The number of coastal flooding events exceeding each threshold was then converted to the number of events per decade in each sub-basin, using the number of exceedences and the length of data record for guidance (Table 2.12, Figure 2.7).

Table 2.12. The number of storm surge/ storm tide events per decade exceeding various threshold levels. Rates of 1, 2, and 3 m storm surges in China derived from Tang et al. (2011). All other values derived from SURGEDAT database.

| Region/ Basin | Year Range | No. of Years | $\geq 1\text{m}$ | $\geq 2\text{m}$ | $\geq 3\text{m}$ | $\geq 5\text{m}$ |
|--------------------------|----------------|-----------------|------------------|------------------|------------------|------------------|
| China | 1949 - 1998 | 50 | 54 | 9.6 | 3 | 0.4 |
| Bay of Bengal | 1958-2011 | 54 | 8.3 | 7.4 | 7.2 | 5.0 |
| Queensland, Australia | 1934-2011 | 78 | 5.4 | 2.5 | 1.4 | 0.5 |
| U.S. Gulf of Mexico | 1931-2013 | 84 | 18 | 8 | 4.3 | 1.0 |
| U.S. Atlantic | 1940-2013 | 74 | 8.9 | 5.4 | 3.2 | 0.7 |

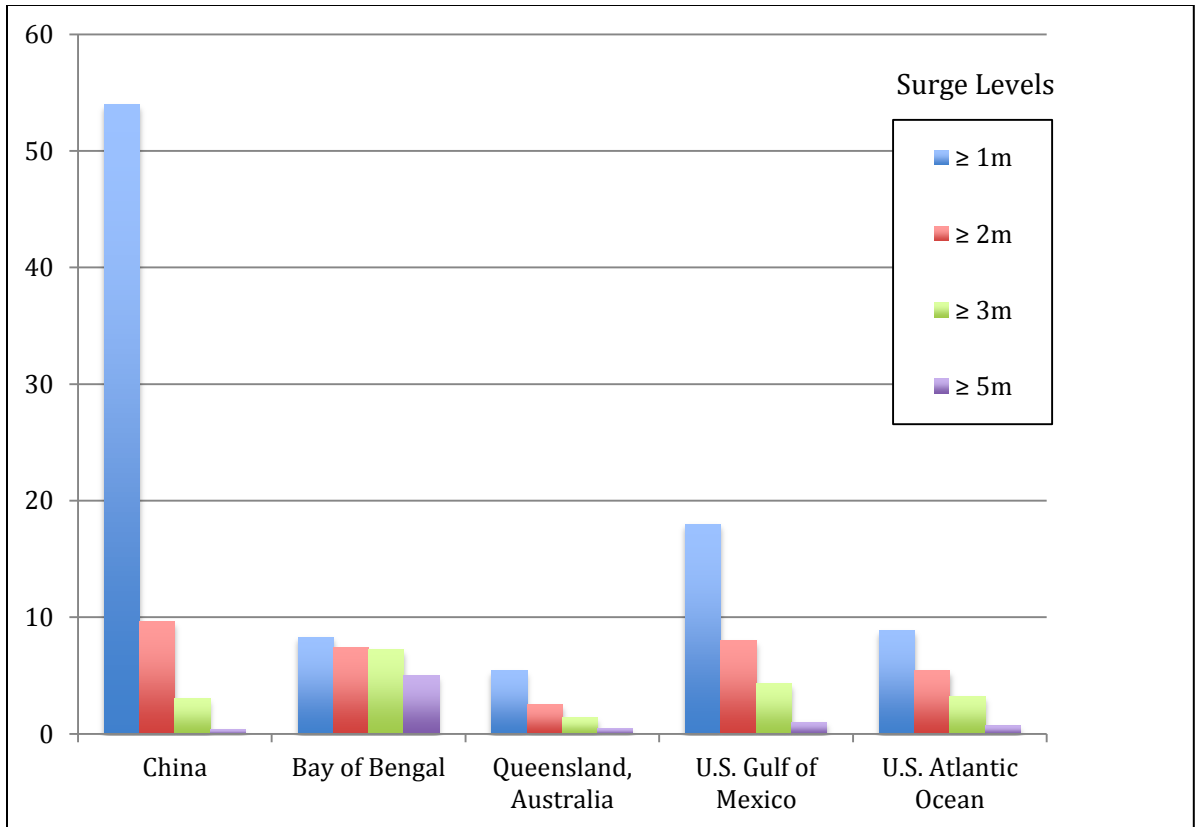


Figure 2.7. The number of storm surge events per decade exceeding various thresholds in selected regions/ ocean basins.

This comparison reveals that China observes more low-magnitude storm surge events than any other sub-basin, as the country averaged 54 storm surge events exceeding 1m per decade. These results seem reasonable, as the Western North Pacific observes more TCs than any other basin in the world (Table 2.1), but the relatively deep bathymetry in the region usually hinders the development of high-magnitude storm surges. The number of low-magnitude storm surges may be even greater in the Philippines, which observe more landfalling typhoons than China (Soriano 1992; Xuejie et al. 2002), however, long-term summary statistics or comprehensive storm surge data are not available yet for the Philippines to make this comparison.

The Bay of Bengal observes more high-magnitude storm surge events than any other sub-basin (Figure 2.8), even though the region ranks fourth out of five sub-basins for the rate of low-magnitude storm surges. During the 54-year-period from 1958-2011, the Bay of Bengal averaged a rate of five storm surges per decade exceeding 5m and 7.2 surge events per decade exceeding 3m. By contrast, the Western North Pacific only observes 0.4 surge events exceeding 5m every decade.

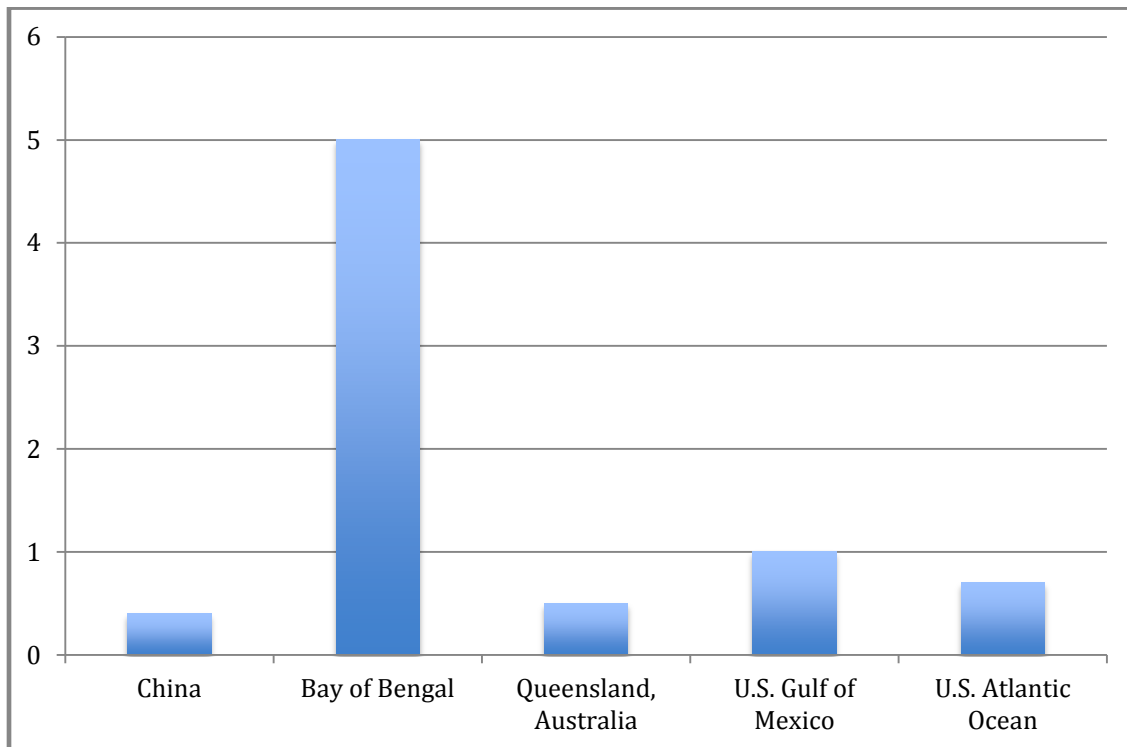


Figure 2.8. Count of storm surges per decade that equal or exceed 5m for selected regions/ ocean basins.

The U.S. Gulf Coast ranks second for both high- and low-magnitude storm surges. This basin observes 18 surges $\geq 1m$ per decade, which is one-third the rate of China. However, this rate is more than double the rate observed by the other sub-basins. The U.S. Gulf Coast also places second for high-magnitude storm surges, as the basin observes one surge event $\geq 5m$ per decade. However, this rate is only one-fifth the rate of 5m surges in the Bay of Bengal.

A time series of storm surge and storm tide events reveals temporal variability of global storm surge observations (Figure 2.9). These observations are plotted for the four ocean basins with the most available storm surge data: 1) The Western North Pacific; 2) The Northern Indian; 3) The Western North Atlantic; and 4) Australia and Oceania. Most striking is the extraordinary variability in the Northern Indian Ocean between different time periods. During the 66-year period from 1886-1951, a literature review provides no storm surge observations for this basin.

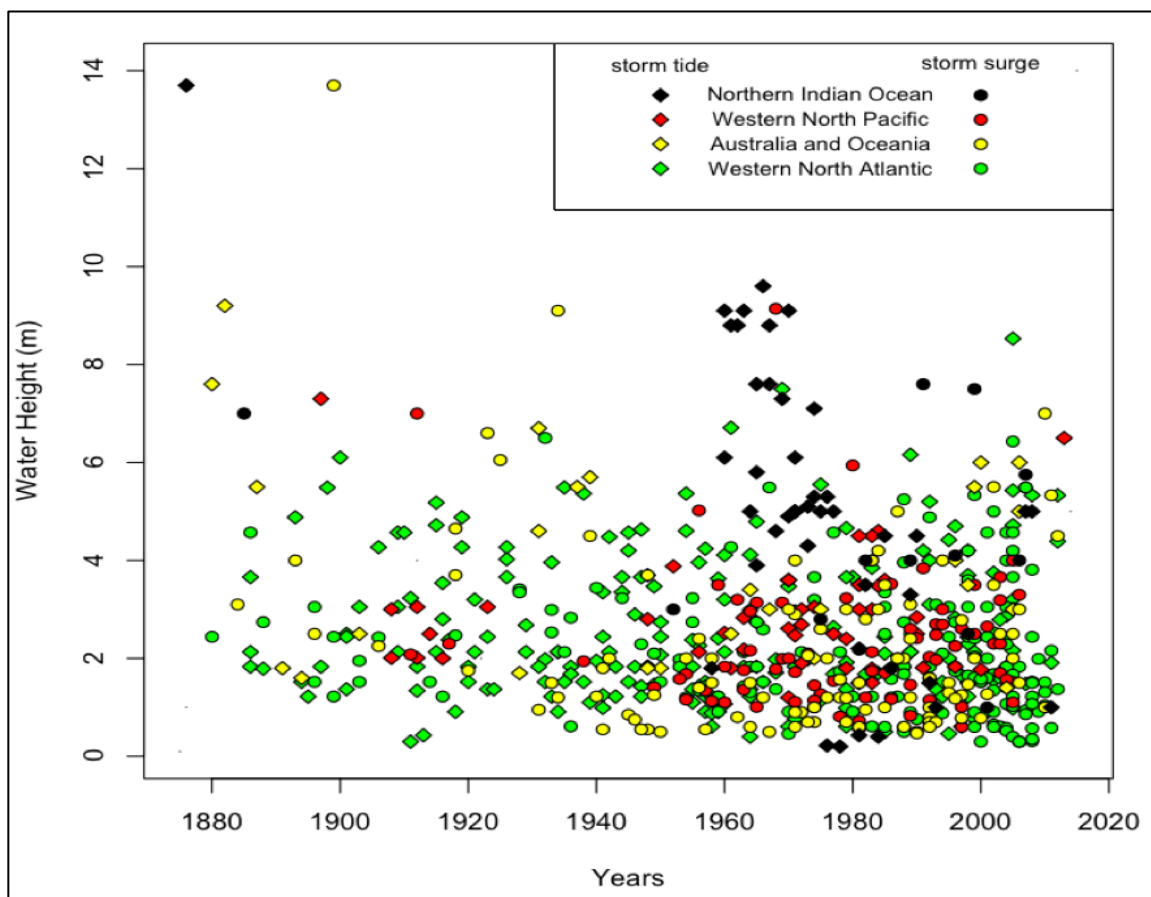


Figure 2.9. Time series of storm surge and storm tide observations for the four major basins that are impacted by tropical cyclone-generated storm surges.

Two events are provided for the 1950s, followed by an extremely active period beginning in 1960. In the 18-year period from 1960-1977, 23 surge events $\geq 5\text{m}$ were observed in this basin, including an 11-year period from 1960-1970, in which seven

storm tide magnitudes were $\geq 8.8\text{m}$. By comparison, these seven surge events all exceed Hurricane Katrina's 8.53-m storm tide in 2005, which was the highest-magnitude coastal flooding event ever recorded in the Western Hemisphere. Since 1977, the Bay of Bengal has been less active, although two storm surges in the 1990s exceeded 7m.

Several adjustments were made to Figure 2.9 to better depict storm surge vulnerability in the Bay of Bengal. For visual effects, an 8.8-m storm surge in 1961 was plotted as a 1962 event because another surge event in 1961 also reached 8.8 m. This adjustment enables both events to be visible in this figure. Amazingly, both of these massive storm surges occurred in Bangladesh during the month of May, 1961. Although SURGEDAT data starts in 1880, I plotted a 13.7-m storm tide in Bangladesh from 1876 to depict the extraordinary surge potential in this basin. I did not plot 12-m storm surges in this region from 1864 or 1737.

This time series also reveals a relative quiet period of storm surge observations in East Asia from approximately 1920-1950, as well as a downward trend in storm surge and storm tide magnitudes over time in Australia and Oceania. It is unknown whether this downward trend is actually a climate signature, or if it is the result of overestimating the height of surge events in the earlier portion of the record. As the actual storm surge/storm tide heights of Australia's three highest-magnitude coastal flooding events remains uncertain, it is possible that the water levels from these events include waves or wave run-up, or simply overestimate the actual water levels. Nonetheless, these events are archived as the best estimate of historic storm surge levels.

Storm surges in each of these four basins obtain heights well beyond the highest surge levels produced by extra-tropical cyclones in high latitudes. The highest storm

surges in regions that observe deep extra-tropical lows, like the North Sea, reach approximately 3 m (Nicholls 2006), however, a few extraordinary surges have reached slightly higher levels. An intense storm in January, 1953, produced a devastating storm surge in the North Sea that reached 3.5 m at Norfolk, United Kingdom, and drowned more than 1,800 people in the Netherlands (Risk Management Solutions 2003). A deep low-pressure system in the Alaskan and Canadian Beaufort Sea in the fall of 1970 produced a storm surge as high as 3 m and driftwood lines as high as 3.4 m in northern Alaska. (Reimnitz and Maurer 1979). Storm surges have reached at least twice as high as these levels in each of the four most active basins that observe TC-generated surges.

2.8.3 Comparing Global Surge Impacts

Storm surge kills more people in the Northern Indian Ocean, specifically along the shores of the Northern Bay of Bengal, than anywhere else in the world. Bangladesh and India have experienced 15 of the 21 TCs that have generated 5,000 or more fatalities through the late 1990s (Dube et al. 1997, see Table 2.13), and the 138,000 casualties inflicted by Cyclone Nargis in 2008 in Myanmar (Fritz et al. 2009), reveals the vulnerability of the eastern Bay of Bengal as well. From another perspective, six TCs in the Bay of Bengal have killed at least 138,000 people (Dube et al. 1997; Fritz et al. 2009). The extraordinary fatality totals in this region is best captured by the fact that cyclones in the Bay of Bengal inflict approximately 80-90% of worldwide TC fatalities, although TCs in this region account for only 5-6% of the global total (Chowdhury 2002; Paul 2009). Storm surges are the predominant reason for these extraordinary fatality totals, as the majority of cyclone-related deaths in this region are caused by drowning due to storm surge (Ikeda 1995; Chowdhury et al. 2007).

The Western North Pacific ranks second in the world for storm surge fatalities. The most severe events have occurred in China, where TCs killed 60,000 people in 1922 and 50,000 in 1912 (National Oceanic and Atmospheric Administration 1999). Storm surge appears to be the major cause of death in the 1922 event, however, it is unclear how many people were killed by the 1912 surge. More recently, Super Typhoon Haiyan killed approximately 8,000 people, mostly due to drowning near the city of Tacloban, in the Philippines (Aon Benfield 2014).

The Western North Atlantic ranks third for storm surge fatalities in a global context. The most deadly surge events in this basin have occurred along the U.S. Gulf Coast, where the 1900 Galveston Hurricane killed more than 8,000 people (Blake et al. 2011), and several other hurricanes killed more than 1,000 people. Islands in the Caribbean have also experienced deadly storm surges, such as the 1932 surge in Santa Cruz del Sur, Cuba, which caused nearly 3,000 deaths (Pielke et al. 2003). However, the deadliest hazard associated with TCs in this basin has been flooding from heavy rains on steep mountains in the Caribbean Sea and Central America.

Table 2.13. Deaths in tropical cyclones since 1700-1997, from Dube et al. (1997).

| Rank | Year | Countries | Deaths |
|------|------|---------------------|---------|
| 1 | 1970 | Bangladesh | 300,000 |
| 1 | 1737 | India | 300,000 |
| 1 | 1886 | China | 300,000 |
| 4 | 1923 | Japan | 250,000 |
| 5 | 1876 | Bangladesh | 200,000 |
| 6 | 1897 | Bangladesh | 175,000 |
| 7 | 1991 | Bangladesh | 140,000 |
| 8 | 1833 | India | 50,000 |
| 8 | 1864 | India | 50,000 |
| 10 | 1822 | Bangladesh | 40,000 |
| 11 | 1780 | Antilles (W. Indes) | 22,000 |
| 12 | 1965 | Bangladesh | 19,279 |
| 13 | 1963 | Bangladesh | 11,520 |

Table 2.13 (continued). Deaths in tropical cyclones since 1700-1997, from Dube et al. (1997).

| | | | |
|----|------|------------|--------|
| 14 | 1961 | Bangladesh | 11,466 |
| 15 | 1985 | Bangladesh | 11,069 |
| 16 | 1961 | India | 10,000 |
| 16 | 1977 | India | 10,000 |
| 18 | 1963 | Cuba | 7,196 |
| 19 | 1900 | USA | 6,000 |
| 20 | 1960 | Bangladesh | 5,149 |
| 21 | 1960 | Japan | 5,000 |
| 21 | 1973 | India | 5,000 |

By contrast, Australia and Oceania have observed the lowest fatality totals of the four major basins that are most prone to storm surge inundation. The most deadly surge events in Australia have occurred when storm surge and rough seas have sunk vessels off the coast. TC Mahina in 1899 was the most deadly of these events, as more than 300 people drowned in sinking vessels (Whittingham 1958; Granger and Smith 1995; Australian Emergency Management 2013a; Australia Bureau of Meteorology 2013a). A literature review of this region does not provide many high fatality totals from storm surge events in Oceania, however, a TC killed 1,000-2,000 people in the Cook Islands more than 400 years ago (De Scally 2008).

Although storm surge magnitudes in Oceania are comparatively lower than other regions that observe frequent storm surge inundations, surges that wash over low-lying islands inflict long-term problems that are more pronounced than in other basins. These surge events can contaminate drinking water supplies and drastically reduce food resources, which may be difficult to replace on small islands. For example, after TC Percy's storm surge contaminated the drinking water supply in the atoll nation of Tokelau in 2005, a shipment of water was urgently transported from American Samoa (Terry and Falkland 2010). This story makes the point that storm surge impacts are not necessarily

correlated with storm surge magnitudes, as some areas that observe lower-magnitude surge levels may actually be more vulnerable to the impacts of surge than other regions that observe higher surge magnitudes.

This literature review also reveals common storm surge impacts that are experienced by coastal areas in different regions of the world. For example, the states of Texas and Louisiana along the U.S. Gulf Coast share storm surge impacts with locations many thousands of kilometers away. Agricultural losses from storm surge in this region include large cattle losses and a reduction in rice productivity following saltwater inundation. Extensive cattle losses are also a common impact of storm surge in Western Australia, while low-lying coastal areas in Vietnam have reported severe impacts of storm surge on rice production. Storm surge along the U.S. Gulf Coast has also severely affected the energy industry, which is a common impact shared with Madagascar and China. TCs in China have damaged infrastructure on oil fields and have threatened thermal and nuclear plants, while TCs in 1994 severely damaged the only large oil refinery in Madagascar. The discovery of these common impacts could help foster collaboration between coastal stakeholders and researchers who may face common problems in different parts of the world.

2.9 Discussion

The time series of global storm surge observations (Fig. 9) shows considerable variability of surge events over time for some basins. For example, no storm surge observations are available from 1886-1951 for the Northern Indian Ocean, however, from 1960-1977 the basin observed 23 storm surge and storm tide events ≥ 5 m. We are led to wonder what proportion of this pattern shift is due to actual meteorological and

oceanographic variability, and what proportion may be due to changes in the recording and dissemination of storm surge observations.

The quantity of observations per basin likely depends on three factors: 1) The amount of TC activity in each basin; 2) The percentage of TCs that interact with land, particularly in populated areas where people would observe a storm surge; and 3) Societal factors that lead to the documentation and dissemination of scientific observations, such as the presence of conflicts or wars, the structure of local and regional governments, the quality of physical and technological infrastructure, as well as local education and literacy levels. It stands to reason that regions with established local and regional government agencies that are involved with disaster management activities would likely provide more storm surge observations than areas with less structured governmental support. Likewise, people in areas with higher levels of physical and technological infrastructure are able to connect easier with the outside world, and thereby share storm surge observations with a larger audience. Natural hazard observations would also likely increase in areas with higher education and literacy rates, as a higher proportion of the population could record and communicate localized coastal flooding information through verbal and written media.

A combination of these factors likely explains why so few storm surge observations are available for the North East Pacific and Southwest Indian Oceans. Although the North East Pacific Ocean observes approximately 19% of global TCs per year (Landsea and Delgado 2013), which is the second highest value of any basin in the world, many of these cyclones live out their entire lifespan over the vast expanse of the Eastern Pacific, without ever hitting land. Those that interact with land often hit the West

Coast of Mexico, where storm surge observations are not often recorded or made available to the outside world, or Hawaii, where TCs tend to produce high waves but modest surge levels, and water levels are typically reported as surf heights. The Southwest Indian Ocean observes approximately 11% of global TCs per year (Landsea and Delgado 2013), but many of these cyclones either stay out over open water, or strike areas in which surge observations are either not recorded or not widely disseminated, like Madagascar, Mozambique, or the islands of Réunion or Mauritius.

Although abundant coastal flooding observations are available for other basins, data are often missing for smaller regions and sub-basins within these areas. For example, while 56% of global storm surge observations are located in the Western North Atlantic, data are sparse for most Caribbean islands, as well as the coast of Mexico and Central America. Despite the inclusion of 119 observations from the Western North Pacific, SURGEDAT is still missing the majority of low-magnitude coastal flooding events in this region. Of the 270 surge events ≥ 1 m along the China coast from 1949-1998 (Tang et al. 2011), SURGEDAT has only identified the height and location of 65 of these surges, or approximately 24% of these events. An even higher proportion of data are likely missing from the Philippines, as this archipelago observes more landfalling typhoons than China (Soriano 1992; Xuejie et al. 2002), and SURGEDAT has only archived data for 28 coastal flooding events in this country. A greater proportion of high-level storm surges have been identified in East Asia. For example, of the 15 storm surges ≥ 3 m that were observed in China between 1949-1998 (Tang et al. 2011), SURGEDAT has identified 11 surges, or 73% of these events.

The surge data identified from this review should provide insight into storm surge characteristics for various ocean basins. For example, the Western North Pacific observes a high quantity of low- and medium-magnitude storm surges, although localized high-magnitude storm surges have sometimes suddenly struck the Philippines. Frequent, high-magnitude storm surges have devastated the Northern Indian Ocean over a period of nearly two decades in the historical record, preceded by and followed by less active decades. This pattern reveals that although the Northern Indian Ocean observes less TC activity than the other basins, numerous catastrophic storm surges may strike within relatively short time periods.

Future research should investigate the climatological pattern that led to the hyperactive TC period in the Northern Indian Ocean during the 1960s and 1970s. Data from recent decades have shown that correlations exist between TC activity in this basin and atmospheric teleconnections. For example, TC activity from October - December in the Northern Indian Ocean has been correlated with the El Nino Southern Oscillation (ENSO) pattern, as El Nino signals typically suppress TC activity in this basin, while La Nina signals tend to enhance activity, using data from 1993-2010 (Girishkumar and Ravichandran 2012), and 1983-2008 (Ng and Chan 2012). Also, the negative phase of the Indian Ocean Dipole leads to warmer SSTs in the Bay of Bengal and enhanced tropical cyclogenesis, according to data from 1993-2010 (Girishkumar and Ravichandran 2012), and 1981-2010 (JunPeng and Jie 2013).

While a record of historic storm surge levels is useful for understanding coastal flooding vulnerability in various regions, future surge events may have even greater impacts due to rising sea levels. Locations with high relative sea-level rise rates, such as

cities established on river deltas, are particularly vulnerable to the effects of this phenomenon. Sea-level rise will exacerbate coastal flooding problems in some locations that are already susceptible to high storm surge levels, like Bangladesh and the U.S. State of Louisiana. Bangladesh is likely to see more land loss from sea-level rise than any other location in South Asia (Dasgupta et al. 2007), while Louisiana experiences the fastest rates of coastal erosion in North America, as some coastal locations in this state observe rising sea-level rates exceeding 1m/ century (Penland and Ramsey 1990). Sea-level rise may also increase the frequency of coastal flooding events on some regions that do not regularly observe high storm surges. For example, Vietnam experiences less frequent and less severe storm surges than nearby countries, like China and the Philippines, however, the low elevation and rapid subsidence rates of the Mekong Delta will make Vietnam more susceptible to coastal flooding in the future.

While the observations archived in this study improve our understanding of storm surge potential in several regions of the world, storm surge modeling is important for predicting surge potential in regions with sparse observed data, like the Eastern North Pacific, Southwest Indian Ocean, and coastlines around the Caribbean Sea. Models may also play an important role for improving knowledge of storm potential in Australia, where details remain unclear about several massive surges that may have struck in the late 1800s and early 1900s. Surge models are also essential for predicting inundations in regions that rarely experience landfalling TCs, but have the physical characteristics to generate high-magnitude storm surges. For example, a 3.2-m storm tide in 1921 (Landsea et al. 2009) was the only coastal flooding event > 2.5 m in Tampa, Florida, since the SURGEDAT archive begins in 1880. Although this city has experienced many

hurricanes, the tracks of these storms have rarely enabled prolonged hurricane-force winds to blow water into Tampa Bay. However, surge models have predicted that if a hurricane tracked east across the Gulf of Mexico and made landfall north of Tampa, surge heights in Tampa Bay and Hillsborough Bay could reach as high as 6 m (Weisberg and Zheng 2006). The absence of similar storm surges in the historic archive does not eliminate the potential for a future catastrophic storm surge in this region.

2.10 Summary and Conclusion

TC-generated storm surges are among the most destructive and deadly natural hazards. This chapter provides the first review of global storm surge observations, providing a comprehensive overview of data sources, observed surge heights and regional impacts. The review was conducted in English, Spanish, French, Portuguese, as well as Chinese for articles that provided English titles or abstracts. The basins included in this analysis are: 1) Western North Pacific Ocean; 2) Northern Indian Ocean; 3) Western North Atlantic Ocean; 4) Eastern North Pacific Ocean; 5) Australia, New Zealand and Oceania, including the Southwest Pacific Ocean and Southeast Indian Ocean; and 6) The Southwest Indian Ocean. Storm surge observations are added to SURGEDAT, a global storm surge database (Needham et al. 2013).

A review of storm surge data sources reveals that federal government sources provide the most comprehensive data for Australia, the Philippines and the United States. Academic sources, such as peer-reviewed journal articles, provide most of the available data for the Northern Indian Ocean, and portions of East Asia, such as China. The SURGEDAT project at Louisiana State University provides a comprehensive storm surge

database for the U.S. Gulf Coast (Needham and Keim 2012), as well as a global storm surge database of surge events since 1880 (Needham et al. 2013).

This literature review identified 702 storm surge observations since 1880. Approximately 56% of these events were in the Western North Atlantic Basin, followed by 19% of the events in Australia and Oceania, and 17% of the events in the Western North Pacific. Storm surge observations were sparse in Eastern North Pacific and Southwest Indian Ocean basins, as these regions combined to provide only three high-water marks. Such geographic variability is greatly impacted by regional differences in data recording and dissemination, however, the number of TCs that strike populated areas in each region also contributes to these differences.

Five sub-basins with comprehensive storm surge statistics were selected for regional comparisons of storm surge frequency. These sub-basins were: 1) China; 2) Bay of Bengal; 3) Queensland, Australia; 4) The U.S. Gulf Coast; and 5) The U.S. Atlantic Coast. Although SURGEDAT is missing the majority of storm surge events in East Asia, China's National Maritime Bureau provided 50 years of surge summary statistics, which enabled China to be included in this analysis, and provide insight into the storm surge climatology of East Asia. This regional comparison revealed that East Asia observes more low- and medium- magnitude storm surges than any other area, as China averaged 54 surges per decade ≥ 1 m. The Bay of Bengal observes the highest rate of high-magnitude storm surges; from 1958-2011, this sub-basin averaged five storm surge events per decade ≥ 5 m. The U.S. Gulf Coast observes the second highest rate of low- and high-magnitude storm surges, as this region averaged 18 storm surges per decade ≥ 1 m and one surge event per decade ≥ 5 m, from 1931-2013.

The deadliest storm surges in world history have consistently occurred in the Bay of Bengal. Approximately 80-90% of worldwide TC fatalities occur in this sub-basin, although this region only experiences 5-6% of the world's TCs (Chowdhury 2002; Paul 2009). Bangladesh and India have experienced 15 of the 21 TCs that killed at least 5,000 people through the late 1990s (Dube et al. 1997), and in 2008, Cyclone Nargis killed 138,000 people in Myanmar, in the eastern portion of the Bay of Bengal (Fritz et al. 2009). Most TC deaths in this basin come from storm surge drowning (Ikeda 1995; Chowdhury et al. 2007). The Western North Pacific ranks second for cumulative storm surge deaths, followed by the Western North Atlantic. Although Australia and Oceania have observed the fewest number of storm surge fatalities, storm surge inflicts long-term impacts on islands in Oceania that experience overwashing of sea water during TCs. Such events contaminate fresh water drinking supplies and destroy food stocks, sometimes requiring urgent shipments of food or water from the outside.

This review also uncovered common storm surge impacts that afflict locations separated by thousands of kilometers. For example, storm surge along the U.S. Gulf Coast impacts the energy industry, as well as various components of the agricultural industry, such as cattle ranching and rice production. The impacts on cattle ranching are shared with Western Australia, impacts on rice production are also observed in Vietnam, and storm surge damage to energy infrastructure has also been observed in coastal China and the port city of Tamatave, the most important harbor in Madagascar.

Although this literature review and the associated SURGEDAT database provide the most comprehensive data on global storm surge observations, most data are still missing for the Eastern North Pacific Ocean, Southwest Indian Ocean, and the Caribbean

Sea. Also, the majority of low-magnitude surge events are missing from the Western North Pacific basin, and many events are potentially missing from the Northern Indian Ocean, as the literature provides no storm surge observations in this basin for the 66-year period from 1886-1951. Therefore, this data archive should be viewed as a starting point, rather than a finished product, and international collaboration will be vital to improve this global storm surge database.

2.11 References

Ali, A., 1996: Vulnerability of Bangladesh to climate change and sea level rise through tropical cyclones and storm surges. *Water, Air, and Soil Pollution*, 92, 171-179.

American Meteorological Society, 1973: Policy statement of the American Meteorological Society on hurricanes, as adopted by the Council on October 20, 1972. *Bulletin of the American Meteorological Society*, 54, 45-47.

Anonymous, 1922a: Typhoon death list now 50,000 at Swatow. *The New York Times*, Written by anonymous Associated Press author on August 11, 1922, published on the Web at: <http://query.nytimes.com/mem/archive-free/pdf?res=9F01EEDB1339EF3ABC4952DFBE668389639EDE>.

Anonymous, 1922b: The Swatow Typhoon of August, 1922. *Monthly Weather Review*, 50, Page 435.

Anonymous, 1899: *The Outridge Report- The Pearling Disaster, 1899*, Outridge Printing Company, Brisbane, Australia.

Anonymous, 1931: 100 Trapped Cattle Drown Near Frenier. *The Times-Picayune*, July 16, 1931. New Orleans, Louisiana.

Anonymous, 2007, Hurricane Dean Weakens, Expected to Spare Texas. *National Public Radio*. Written by anonymous National Public Radio author on August 21, 2007, published on the web at: <http://www.npr.org/templates/story/story.php?storyId=13817871>.

Anonymous, 2010: 'Few' deaths, 18,000 evacuated as Tomas smashes Fiji. *The New Zealand Herald*, March 16, 2010. Article available on the web at: http://www.nzherald.co.nz/world/news/article.cfm?c_id=2&objectid=10632415&pnum=0.

Aon Benfield, 2014: *Annual Global Climate and Catastrophe Report*. Available at: http://thoughtleadership.aonbenfield.com/Documents/20140113_ab_if_annual_climate_catastrophe_report.pdf.

Arafiles, C.P., and C.P. Alcances, Jr., 1978: *Storm Surge Potentials of Selected Philippine Coastal Basins*. Available on the Web at: <http://www.pagasa.dost.gov/ph/research.shtml>.

Arafiles, C.P., L.A. Amadore, C.S. Doctor, and C.L. Davis, 1984: Vulnerability of the Philippines to Storm Surges. *Proceedings of the Second Symposium on Tropical Cyclones in the South China Sea and Western North Pacific Ocean*. Quezon City, Philippines, 11-13 December 1984. Pages 142-151.

Ascharyapotha, N., P. Wongwises, U.W. Humphries, and S. Wongwises, 2011: Study of storm surge due to Typhoon Linda (1997) in the Gulf of Thailand using a three dimensional ocean model. *Applied Mathematics and Computation*, 217, 21, 8640-8654.

Australia Bureau of Meteorology, 1980a: Severe Tropical Cyclone Amy, 5-11 January 1980. Report made available by the Commonwealth of Australia and published on the web at: <http://www.bom.gov.au/cyclone/history/amy.shtml>.

Australia Bureau of Meteorology, 1980b: Severe Tropical Cyclone Enid, 15-18 February 1980. Report made available by the Commonwealth of Australia and published on the web at: <http://www.bom.gov.au/cyclone/history/enid.shtml>.

Australia Bureau of Meteorology, 1982: Severe Tropical Cyclone Dominic, 5-7 April 1982. Report made available by the Commonwealth of Australia and published on the web at: <http://www.bom.gov.au/cyclone/history/dominic82.shtml>.

Australia Bureau of Meteorology, 1983a: Severe Tropical Cyclone Quenton, 26-30 November 1983. Report made available by the Perth Tropical Cyclone Warning Centre and published on the web at: <http://www.bom.gov.au/cyclone/history/pdf/quenton83.pdf>.

Australia Bureau of Meteorology, 1983b: Severe Tropical Cyclone Jane, 2-10 January 1983. Report made available by the Perth Tropical Cyclone Warning Centre and published on the web at: <http://www.bom.gov.au/cyclone/history/pdf/jane83.pdf>.

Australia Bureau of Meteorology, 1994: Severe Tropical Cyclone Annette, 15-19 December 1994. Report made available by the Commonwealth of Australia and published on the web at: <http://www.bom.gov.au/cyclone/history/annette.shtml>.

Australia Bureau of Meteorology, 1996: Tropical Cyclone Barry, 4-7 January 1996. Report made available by the Commonwealth of Australia and published on the web at: <http://www.bom.gov.au/cyclone/history/barry.shtml>.

Australia Bureau of Meteorology, 2000: Tropical Cyclone Rosita, 17-21 April 2000. Report made available by the Commonwealth of Australia and published on the web at: <http://www.bom.gov.au/cyclone/history/wa/rosita.shtml>.

Australia Bureau of Meteorology, 2006: Severe Tropical Cyclone Monica, 17-25 April 2006. Report made available by the Commonwealth of Australia and published on the web at: <http://www.bom.gov.au/cyclone/history/monica.shtml>.

Australia Bureau of Meteorology, 2007: Tropical Cyclone George, 3-10 March 2007. Report made available by the Commonwealth of Australia and published on the web at: <http://www.bom.gov.au/cyclone/history/wa/george.shtml>.

Australia Bureau of Meteorology, 2013a: Previous Tropical Cyclones. Report made available by the Commonwealth of Australia and published on the web at: www.bom.gov.au/cyclone/history/index.shtml.

Australia Bureau of Meteorology, 2013b: Tropical Cyclone Extremes. Report made available by the Commonwealth of Australia and published on the web at: <http://www.bom.gov.au/cyclone/about/extremes.shtml>.

Australia Bureau of Meteorology, 2013c: Tropical Cyclones Affecting the Karratha/Dampier/Roebourne region. Report made available by the Commonwealth of Australia and published on the web at: <http://www.bom.gov.au/cyclone/history/wa/roebourne.shtml>.

Australian Emergency Management, 2013a: Documentation of Impacts from Tropical Cyclone Mahina. Available on the web at: <http://www.ema.gov.au/ema/emadisasters.nsf/0/40e758f025b7a858ca25d3300057CD3?OPENDOCUMENT>.

Australian Emergency Management, 2013b: Documentation of the Impacts from the 1934 Tropical Cyclone. Available on the web at: <http://www.ema.gov.au/ema/emadisasters.nsf/c85916e930b93d50ca256d050020cb1f/75c4edcd7d9ad39cca256d3300057de9?OpenDocument>.

Australia Bureau of Meteorology, 2014: Historical Impacts along the East Coast. Available on the Web at: <http://www.bom.gov.au/cyclone/history/eastern.shtml>.

AXCO, 2009: *Insurance Market Report: Japan Non-Life (P&C)*. London. Axco Insurance Information Services.

Baade, R.A., R. Baumann, and V. Matheson, 2007: Estimating the economic impact of natural and social disasters, with an application to Hurricane Katrina. *Urban Studies*, 44, 11, 2061-2976.

Bangladesh Meteorology Department, 2013: Main website, available at: <http://www.bmd.gov.bd/>.

Bankoff, G., 2003: *Cultures of Disaster: Society and Natural Hazard in the Philippines*. Published by RoutledgeCurzon, London, United Kingdom. 232 pp.

Barstow, S.F. and O. Haug, 1994: The wave climate of the Cook Islands. Suva: SOPAC. Technical Report 200, 1994. 26 pp.

Beckage, S., 2012: *An analysis of tropical storm surge trends for the Atlantic coast of the United States*. Master's thesis defended May, 2012. Louisiana State University.

Belize National Meteorological Service, 2013: List of Historical Storms. Available on the Web at: www.hydromet.gov.bz/tropical-weather/list-of-historical-storms.

Berg, R., 2009: National Hurricane Center Tropical Cyclone Report on Hurricane Ike (AL092008), updated January 23, 2009. Published on the Web at http://www.nhc.noaa.gov/pdf/TCR-AL092008_Ike.pdf.

Bernstein, A., 2013: U.S. Transportation Secretary LaHood Announces \$3.7 Billion in Additional Hurricane Sandy Disaster Relief Aid for Transit Agencies. United States Department of Transportation document *DOT 46-13*. Available on the Web at: <http://www.dot.gov/briefing-room/us-transportation-secretary-lahood-announces-37-billion-additional-hurricane-sandy>.

Bettinger, P., and K.L. Merry, 2012: Relative vulnerability of the forests along southeastern African coasts to cyclones. *Singapore Journal of Tropical Geography*, 33, 320-334.

Blake, E.S., E. J. Gibney, D. P. Brown, M. Mainelli, J. L. Franklin, and T. B. Kimberlain, G.R. Hammer, 2009: Tropical Cyclones of the Eastern North Pacific Basin, 1949-2006. Prepared by the National Climatic Data Center, Asheville, North Carolina, in cooperation with the National Hurricane Center, Miami, Florida, USA. Document available on the web at: http://www.nhc.noaa.gov/pdf/TC_Book_Epac_1949-2006_hires.pdf.

Blake, E.S., C.W. Landsea, and E.J. Gibney, 2011: The Deadliest, Costliest, and Most Intense United States Tropical Cyclones from 1851 to 2010 (And Other Frequently Requested Hurricane Facts). *NOAA Technical Memorandum NWS NHC-6*. This publication is available on the Web at: <http://www.nhc.noaa.gov/pdf/nws-nhc-6.pdf>.

Blake, E.S., T.B. Kimberlain, R.J. Berg, J.P. Cangialosi, and J.L. Beven II, 2013: *Tropical Cyclone Report, Hurricane Sandy, (AL182012), 22-29 October 2012*. National Hurricane Center, Miami, Florida, USA. Available on the Web at: http://www.nhc.noaa.gov/data/tcr/AL182012_Sandy.pdf.

Blumenstock, D.I., 1957: The 1957 Central Pacific Tropical Cyclone Season. National Weather Service – Central Pacific Hurricane Center, Honolulu, Hawaii. Available on the Web at: <http://www.prh.noaa.gov/cphc/summaries/1957.php>.

Bowyer, P., 2003: The Storm Surge and Waves at Halifax with Hurricane Juan. Prepared October 17, 2003 and archived by Environment Canada. Available on the Web at: www.ec.gc.ca/ouragans-hurricanes/default.asp?lang=EN&n=BAAEAC12-1.

Boyd, E., 2011: Fatalities Due to Hurricane Katrina's Impacts on Louisiana. Dissertation successfully defended April 20, 2011. Louisiana State University Department of Geography and Anthropology, Baton Rouge, Louisiana.

Canadian Hurricane Centre, 2014: Environment Canada – Canadian Hurricane Center Website. Available on the Web at: <http://www.ec.gc.ca/ouragans-hurricanes/>.

Central Pacific Hurricane Center, 1972: The Central Pacific Tropical Cyclone Season of 1972. National Weather Service – Central Pacific Hurricane Center, Honolulu, Hawaii. Available on the Web at: <http://www.prh.noaa.gov/cphc/summaries/1972.php>.

Central Pacific Hurricane Center, 1988: The 1988 Central Pacific Tropical Cyclone Season. National Weather Service – Central Pacific Hurricane Center, Honolulu, Hawaii. Available on the Web at: <http://www.prh.noaa.gov/cphc/summaries/1988.php>.

Central Pacific Hurricane Center, 1992: The 1992 Central Pacific Tropical Cyclone Season. National Weather Service- Central Pacific Hurricane Center, Honolulu, Hawaii. Available on the Web at <http://www.prh.noaa.gov/cphc/summaries/1992.php>.

Central Pacific Hurricane Center, 2012: Previous Tropical Systems in the Central Pacific. Tropical cyclone summaries for selected storms from 1832-1956, and for all storms from 1957-present. National Weather Service – Central Pacific Hurricane Center, Honolulu, Hawaii. Available on the Web at: www.prh.noaa.gov/cphc/summaries.

Cervený, R.S., J. Lawrimore, R. Edwards, and C. Landsea, 2007: Extreme Weather Records. *Bull. Amer. Meteor. Soc.*, 88, 853–860. Doi: <http://dx.doi.org/10.1175/BAMS-88-6-853>

Chang-Seng, D.S., M.R. Jury, 2010: Tropical cyclones in the SW Indian Ocean. Part 2: structure and impacts at the event scale. *Meteorology and Atmospheric Physics*, 106, 163-178.

Chemane, D., H. Motta, and M. Achimo, 1997: Vulnerability of coastal resources to climate changes in Mozambique: a call for integrated coastal zone management. *Ocean and Coastal Management*, 37, 1, 63-83.

Chen, Q., L. Wang, H. Zhao, S.L. Douglass, 2007: Prediction of storm surges and wind waves on coastal highways in hurricane-prone areas. *Journal of Coastal Research*, 23, 1304-1317.

China Meteorological Administration, 2014: CMA Tropical Cyclone Data Center for the western North Pacific Basin. Available on the Web at: tcd.data.typhoon.gov.cn/en/.

Chinapost, 2003: Report from September 14, 2003. Available on the Web at: <http://www.chinapost.com.tw>.

Chittibabu, P., S.K. Dube, A.D. Rao, P.C. Sinha, and T.S. Murty, 2000: Numerical simulation of extreme sea levels using location specific high resolution model for Gujarat coast of India. *Mar Geod*, 23, 133-142. DOI: 10.1080/01490410050030698.

Cho, Y-S., L. Chokkalingam, B.-H. Choi, T-M. Ha, 2008: Observations of run-up and inundation levels from the teletsunami in the Andaman and Nicobar Islands: A field report. *Journal of Coastal Research*, 24, 216-223.

Chowdhury, KMMH, 2002: Cyclone preparedness and management in Bangladesh. In: BPATC (ed) Improvement of early warning system and responses in Bangladesh towards total disaster risk management approach. BPATC, Savar, Dhaka, pp 115-119.

Chowdhury, A.M.R., A.U. Bhuyia, A.Y. Choudhury, and R. Sen, 2007: The Bangladesh Cyclone of 1991: Why So Many People Died. *Disasters*, 17, 291-304.

Croad, R.N., 1989: Wave climate at Avatiu Harbour, Rarotonga, 8 March 1985 to 29 April 1989. New Zealand Works, Consultancy Services, Central Laboratories Report 89-A7304, 1989. 33 pp.

Cruz, A.M., and E. Krausmann, 2008: Damage to offshore oil and gas facilities following hurricanes Katrina and Rita: An overview. *Journal of Loss Prevention in the Process Industries*, 21, 620-626.

Danard, M., A. Munro, and T. Murty, 2003: Storm Surge Hazard in Canada. *Natural Hazards*, 28, 407-431.

Das, P.K., 1994: On the prediction of storm surges. *Sadhana*, 19, 583-595.

Dasgupta, S., B. Laplante, C. Meisner, D. Wheeler, and J. Yan, 2007: *The Impact of Sea Level Rise on Developing Countries: A Comparative Analysis*. World Bank Policy Research Working Paper 4136, February 2007. Available on the Web at: http://www-wds.worldbank.org/servlet/WDSContentServer/WDSP/IB/2007/02/09/000016406_20070209161430/Rendered/PDF/wps4136.pdf.

Dasgupta, S., B. Laplante, S. Murry, and D. Wheeler, 2009: Sea-Level Rise and Storm Surges: A Comparative Analysis of Impacts in Developing Countries. Policy Research Working Paper 4901. Washington, DC. World Bank.

Dasgupta, S., B. Laplante, S. Murry, and D. Wheeler, 2011: Exposure of developing countries to sea-level rise and storm surges. *Climatic Change*, 106, 567-579.

De Lange, W.P., and J. G. Gibb, 2000: Seasonal, interannual, and decadal variability of storm surges at Tauranga, New Zealand. *New Zealand Journal of Marine and Freshwater Research*, 34, 419-434.

De Scally, F.A., 2008: Historical tropical cyclone activity and impacts in the Cook Islands. *Pacific Science*, 62, 443-459.

Denny, W.J., 1972: Eastern Pacific Hurricane Season of 1971. *Monthly Weather Review*, 100, 4, 276-293. Document available on the web at: <http://docs.lib.noaa.gov/rescue/mwr/100/mwr-100-04-0276.pdf>.

Disaster Management Working Group, 2005: Joint Assessment of Disaster and Needs 2005. Rapid Needs Assessment of Typhoon Damrey.

Donovan, M., and P. Grossi, 2009: 1959 Super Typhoon Vera: 50-Year Retrospective. *RMS Special Report*. Publication produced by Risk Management Solutions, Inc. Available on the Web at: https://support.rms.com/publications/1959_Typhoon_Vera.pdf.

Dossier Départemental des Risques Majeurs, 2011: Le risqué houle, maree de tempete et tsunami. Available on the web at: <http://www.reunion.pref.gouv.fr/ddrm/2011/risque02.html>.

Drye, W., 2007: Hurricane Felix Barrels into Nicaragua. National Geographic News, September 4, 2007. Available on the Web at: <http://news.nationalgeographic.com/news/2007/09/070904-felix-landfall.html>.

Dube, S.K., P.C. Sinha, A.D. Rao, and G.S. Rao, 1985: Numerical modeling of storm surges in the Arabian Sea. *Applied Mathematical Modeling*, **9**, 289-294. DOI: 10.1016/0307-904X(85)90067-8.

Dube, S.K., A.D. Rao, P.C. Sinha, T.S. Murty, N. Bahulayan, 1997: Storm surge in the Bay of Bengal and Arabian Sea: The problem and its prediction. *Mausam*, 48, 283-304.

Dube, S.K., A.D. Rao, P.C. Sinha and P. Chittibabu, 2008: Storm Surges: Worst Coastal Marine Hazard. Chapter 9, pp. 125-140, in: Murthy, C.R., P.C. Sinha, and Y.R. Rao, *Modelling and Monitoring of Coastal Marine Processes*. Co-published by Springer and Capital Publishing Company, 246 pp.

Dube, S.K., I. Jain, A.D. Rao, and T. Murty, 2009: Storm surge modeling for the Bay of Bengal and Arabian Sea. *Natural Hazards*, 51, 3-27.

Dunn, G.E., and Staff at the U.S. Weather Bureau, 1964: The Hurricane Season of 1963. *Monthly Weather Review*, 92, 3, 128-138.

Dunnavan, G.M., and J.W. Diercks, 1980: An analysis of Super Typhoon Tip (October 1979). *Monthly Weather Review*, 108, 1915-1923.

Earth Institute Columbia University, 2007: New Research Analyzes Countries at Greatest Risk from Climate Change Impacts. News story posted on March 29, 2007. Available on the web at: <http://www.earth.columbia.edu/news/2007/story03-29-07.php>.

Eaton, J.P., D.H. Richter, and W.U. Ault, 1961: The tsunami of May 23, 1960, on the Island of Hawaii. *Bulletin of the Seismological Society of America*, 61, 2, 135-157.

Elsner, J.B., and K. Liu, 2003: Examining the ENSO-typhoon hypothesis. *Climate Research*, 25, 43-54.

Emanuel, K., 2005: *Divine Wind-The History and Science of Hurricanes*. Oxford University Press, 296 pp. ISBN-10: 0195149416. ISBN-13: 9780195149418.

Emergency Management Australia, 2006: EMA Disasters Database. Available on the Web at: <http://www.ema.gov.au/ema/emadisasters.nsf/>.

Federal Emergency Management Agency, 2008: Hurricane Ike in Texas and Louisiana. Mitigation Assessment Team Report. Available on the web at: http://www.fema.gov/library/file?type=publishedFile&file=757_ape_final.pdf&fileid=71147ed0-b6a2-11df-97ce-001cc4568fb6.

Fengshu, L., and W. Xinian, 1989: A review of storm-surge research in China. *Natural Hazards*, 2, 17-29.

Fiji Meteorological Service, 2013: RSMC Nadi-Tropical Cyclone Centre. Available on the web at: www.met.gov.fj/index.php.

Frank, N.L., and S.A. Husain, 1971: Deadliest tropical cyclone in history. *Bulletin of the American Meteorological Society*, 52, 438-&.

Franklin, J.L., 2002: Tropical Cyclone Report, Hurricane Kenna, 22-26 October 2002. National Hurricane Center, Miami, Florida, USA. Report available online at: <http://www.nhc.noaa.gov/2002kenna.shtml>.

Franklin, J.L., 2004: Tropical Cyclone Report, Hurricane Marty, 18-24 September 2003. National Hurricane Center, Miami, Florida, USA. Report available online at: <http://www.nhc.noaa.gov/2003marty.shtml?>

Franklin, J.L., 2009: Tropical Cyclone Report, Hurricane Norbert, (EP152008), 4-12 October 2008. National Hurricane Center, Miami, Florida, USA. Report available online at: http://www.nhc.noaa.gov/pdf/TCR-EP152008_Norbert.pdf.

Fritz, H.M., C. Blount, R. Sokoloski, J. Singleton, A. Fuggle, B.G. McAdoo, A. Moore, C. Grass, and B. Tate, 2007 : Hurricane Katrina storm surge distribution and field observations on the Mississippi Barrier Islands. *Estuarine, Coastal and Shelf Science*, 74, 12-20.

Fritz, H.M., C.D. Blount, S. Thwin, M.K. Thu, and N. Chan, 2009 : Cyclone Nargis storm surge in Myanmar. *Nature Geoscience*, 2, 448-449.

Fritz, H.E., C. Blount, F.B. Albusaidi, and A.H.M. Al-Harthy, 2010: Cyclone Gonu Storm Surge in the Gulf of Oman. Published in Charabi, Y., *Indian Ocean Tropical Cyclones and Climate Change*. Published by Springer Science and Business Media.

Garriott, E.B., 1898: The West Indian Hurricane of September 29-October 2. *Monthly Weather Review*, 26, 10, 439-440.

Garriott, E.B., 1900: West Indian hurricane of September 1-12, 1900. *Monthly Weather Review*, 28, 371-378.

Gilmore, R.E., R.E. Englebretson, R.G. Handlers, and S. Brand, 1995: Typhoon Havens Handbook for the Western Pacific and Indian Oceans Change 4. Report NRL/PU/7543—95-0023. Naval Research Laboratory, Monterey, Calif., USA.

Girishkumar, M.S., and M. Ravichandran, 2012: The influences of ENSO on tropical cyclone activity in the Bay of Bengal during October-December. *Journal of Geophysical Research-Oceans*, 117, article number C02033.

Goring, D.G., 1995: Short-term variations in sea level (2-15 days) in the New Zealand region. *New Zealand Journal of Marine and Freshwater Research*, 29, 69-82.

Granger, K.J., and D.I. Smith, 1995: Storm Tide Impact and Consequence Modelling: Some Preliminary Observations. *Mathl. Comput. Modelling*, 21, 9, 15-21.

Gravelle, G., and N. Mimura, 2008: Vulnerability assessment of sea-level rise in Viti Levu, Fiji Islands. *Sustainability Science*, 3, 171-180.

Grossman, M., and M. Zaiki, 2009: Reconstructing typhoons in Japan in the 1880s from documentary records. *Weather*, 64, 12, 315-322.

Guiney, J.L., and M.B. Lawrence, 1999: Preliminary Report, Hurricane Mitch, 22 October – 05 November 1998. National Hurricane Center, Miami, FL, USA. Available on the Web at: www.nhc.noaa.gov/1998mitch.html.

Gunn, A.M., 2008: *Encyclopedia of disasters: environmental catastrophes and human tragedies*. Greenwood Press, 130-131.

Haigh, I.D., L.R. MacPherson, M.S. Mason, E.M.S. Wijeratne, C.B. Pattiaratchi, R.P. Crompton, and S. George, 2013: Estimating present day extreme water levels exceedance probabilities around the coastline of Australia: tropical cyclone-induced storm surges. *Climate Dynamics*. Published online February 1, 2013. DOI: 10.1007/s00382-012-1653-0.

Han, M., J. Hou, and L. Wu, 1995: Potential Impacts of Sea-Level Rise on China's Coastal Environment and Cities: A National Assessment. *Journal of Coastal Research*, SI 14, 79-95.

Hanh, P.T.T., and M. Furukawa, 2007: The impact of sea level rise on coastal zone of Vietnam. *Bull. Fac. Sci. Ryukyus*, 84, 45-59.

Harper, B.A., 1998: *Storm tide threat in Queensland: history, prediction and relative risks*. Department of Environment and Heritage, Conservation Technical Report No. 10, Brisbane, Australia.

Harris, D.L., 1963. *Characteristics of the Hurricane Storm Surge*. United States Weather Bureau, Technical Paper No. 48. Available on the web at: http://www.csc.noaa.gov/hes/images/pdf/CHARACTERISTICS_STORM_SURGE.pdf.

Harvey, N., 1974: *An Analysis of Storm Surges Associated with Tropical Cyclones in North-East Australia*. Honours Thesis. Department of Geography, James Cook University. Nov 1974.

Heath, R. A., 1979: Significance of storm surges on the New Zealand coast. *New Zealand Journal of Geology and Geophysics*, 22, 259-266.

Hebert, P.J., 1976: Atlantic Hurricane Season of 1975. *Monthly Weather Review*, 104, 453-474.

Henderson, F.I., 1988: Philippines: A Country Profile. Office of Foreign Disaster Assistance, Agency for International Development, Washington, DC, United States. 184 pp.

Henry, A.J., 1929 : Tropical Cyclones of the Eastern North Pacific Ocean. *Monthly Weather Review*, 57, 2, 43-49. Available on the web at : <http://docs.lib.noaa.gov/rescue/mwr/057/mwr-057-02-0043.pdf>.

Himoto, K., 2007: Risk of fire spread in densely built environments- a review emphasizing cities in Japan-. *Journal of Disaster Research*, 2, 276-283.

Holthouse, H., 1971: *Cyclone*. Published by Rigby. Adelaide, Australia.

Ikeda, K., 1995: Gender Differences in Human Loss and Vulnerability in Natural Disasters: A Case Study from Bangladesh. *Indian Journal of Gender Studies*, 2, 171-195.

India Meteorological Department, 2013: Cyclone Page. Available on the web at: <http://www.imd.gov.in/section/nhac/dynamic/cyclone.htm>.

INGC, 2009: Synthesis Report. *INGC Climate Change Report: Study on the impact of climate change on disaster risk in Mozambique*. Van Logchen, B., and R. Brito (eds), INGC, Mozambique.

Instituto de Meteorologia de la Republica de Cuba, 2014: Resumen de Temporadas de Ciclones. Disponible en al Web en: www.met.inf.cu/asp/genesis.asp?TB0=PLANTILLAS&TB1=TEMPORADA&TB2=/Temporadas/.

Instituto Nacional de Meteorologia, 2013: Website available at the following link: <http://www.inam.gov.mz/>.

Instituto Nicaraguense de Estudios Territoriales, 2013: Available on the Web at: www.ineter.gov.ni.

Intergovernmental Panel on Climate Change, 1994: *Preparing to meet the coastal challenges of the 21st century*. Conference report, World coast conference 1993. Ministry of Transport, Public Works and Water Management, The Hague.

Jakobsen, F., M.H. Azam, M.M.Z. Ahmed, M. Mahboob-ul-Kabir, 2006: Cyclone storm surge levels along the Bangladeshi coastline in 1876 and 1960-2000. *Coastal Engineering Journal*, 48, 295-307.

Japan Meteorological Agency, 2008: *Number of typhoons approaching the Japan Main Islands (Honshu, Hokkaido, Kyushu, Shikoku)*. Available on the Web at: <http://www.data.jma.go.jp/fcd/yoho/typhoon/statistics/average/average.html>.

Japan Meteorological Agency, 2009: *Climatology of tropical cyclones*. Available on the Web at: <http://www.jma.go.jp/jma/jma-eng/jma-center/rsmc-hp-pub-eg/climatology.html>.

Johnson, J.M., and K. Satake, 1997 : Estimation of seismic moment and slip distribution of the April 1, 1946, Aleutian tsunami earthquake. *Journal of Geophysical Research*, 102, B6, 11,765-11,774.

Joint Typhoon Warning Center, 1959 : *1959 Annual Typhoon Report*. U.S. Navy : JTWC Annual Tropical Cyclone Reports. Retrieved from http://metocph.nmci.navy.mil/jtwc/atcr/1959atcr/pdf/1959_complete.pdf.

Joint Typhoon Warning Center, 1960: *Annual Typhoon Report, 1960*. Available on the Web at: http://www.usno.navy.mil/NOOC/nmfc-ph/RSS/jtwc/atcr/1960atcr/pdf/1960_complete.pdf.

Joint Typhoon Warning Center, 2007: *Northern Indian Ocean Tropical Cyclone Best Track Data*. Retrieved on 4 June 2007.

Joint Typhoon Warning Center, 2014: *Annual Tropical Cyclone Reports, 1959- 2012*. Available on the Web at: <http://www.usno.navy.mil/JTWC/annual-tropical-cyclone-reports>.

Jordan II, M.R., and C.A. Clayson, 2008: Evaluating the usefulness of a new set of hurricane classification indices. *Monthly Weather Review*, 136, 5234-5238.

JunPeng, Y., and C. Jie, 2013: North Indian Ocean tropical cyclone activities influenced by the Indian Ocean Dipole mode. *Science China-Earth Sciences*, 56, 5, 855-865.

Kalsi, S.R., and M. Gupta, 2003: *Success and Failure of Early Warning Systems: A Case Study of the Gujarat Cyclone of June, 1998*. Published in Zschau, J., and A.N. Koppers, 2003: *Early warning systems for natural disaster reduction*. Published by Springer-Verlag. Printed in Italy. 837 pp.

Kang, S.-W., K.-C. Jun, K.-S. Park, and S.-D. Han, 2009: Storm Surge Hindcasting of Typhoon Maemi in Masan Bay, Korea. *Marine Geodesy*, 32, 218-232.

Kates, R.W., C.E. Colten, S. Laska, and S.P. Leatherman, 2006: Reconstruction of New Orleans after Hurricane Katrina: A research perspective. *Proceedings of the National Academy of Sciences of the United States of America*, 103, 14653-14660.

Kawai, H., 1999: Storm surge in Ise and Mikawa Bay caused by typhoon. *Proceedings of the Joint Meeting of the U.S.-Japan Cooperative Program in Natural Resources Panel on Wind and Seismic Effects, Journal Code: S0735A*, 31, 320-332.

Kawai, H., N. Hashimoto, and M. Yamashiro, 2009: Real-time Probabilistic Prediction of Storm Water Level at Japanese Ports. *Proceedings of the Nineteenth (2009) International Offshore and Polar Engineering Conference, Osaka, Japan, June 21-26, 2009*. International Society of Offshore and Polar Engineers (ISOPE).

Keim, B.D., and R.A. Muller, 2009: *Hurricanes of the Gulf of Mexico*. Louisiana State University Press, 216 pp.

Kessler, R.C., S. Galea, R.T. Jones, and H.A. Parker, 2006: Mental illness and suicidality after Hurricane Katrina. *Bulletin of the World Health Organization*, 84, 12, 930-939.

Knabb, R.D., J.R. Rhome, D.P. Brown, 2011: National Hurricane Center Tropical Cyclone Report on Hurricane Katrina. Published on the Web at: http://www.nhc.noaa.gov/pdf/TCR-AL122005_Katrina.pdf.

Knowles, T.N., 2009: *Category 5: The Labor Day Hurricane*. University Press of Florida, 350 pp.

Kohno, N., K. Kamakura, H. Minematsu, and D. Ueno, 2009: Case Study of the Storm Surges in the Seto Inland Sea Caused by Typhoon Chaba. *Marine Geodesy*, 32, 151-165.

Kurth, M.M., and D.V. Burckel, 2006 : *The Rita Report : A summary of the social and economic impact and recovery of Southwest Louisiana one year after Hurricane Rita*. 58 pp. Report developed for the Louisiana Recovery Authority and made available on the Web at : <http://instructor.mstc.edu/instructor/randers/Reports/RitaReportFinal091806.pdf>.

Lander, J.F., and P.A. Lockridge, 1989: *United States Tsunamis (Including United States Possessions) 1690-1988*, 265 pp., National Geophysical Data Center, Boulder, Colorado, 1989.

Landsea, C.W., C. Anderson, N. Charles, G. Clark, J. Dunion, J. Fernandez-Partagas, P. Hungerford, C. Neumann, M. Zimmer, 2004: The Atlantic Hurricane Database Reanalysis Project: Documentation for 1851-1910 Alterations and Additions to the HURDAT database. Published in Murnane, R. J. and K.B. Liu, *Hurricanes and Typhoons: Past, Present and Future*, Columbia Press 2004. Landsea et. al contributed pgs 178- 221. This document is published on the Web at: <http://www.aoml.noaa.gov/hrd/Landsea/rpibook-final04.pdf>.

Landsea, C., C. Anderson, W. Bredemeyer, C. Carrasco, N. Charles, M. Chenoweth, G. Clark, J. Dunion, R. Ellis, J. Fernandez-Partagas, S. Feuer, J. Gamache, D. Glenn, L. Hufstetler, C. Mock, C. Neumann, R. Perez Suarez, R. Prieto, J. Sanchez-Sesma, A. Santiago, D. Thomas, L. Woolcock, and M. Zimmer, 2009: Documentation of Atlantic Tropical Cyclones Changes in HURDAT. Atlantic Oceanographic and Meteorological Laboratory, Hurricane Research Division, Re-Analysis Project. Published on the Web at: http://www.aoml.noaa.gov/hrd/hurdat/metadata_jun09.html

Landsea, C., and S. Delgado, 2013: Record number of storms by basin. Table published on the Web through the Atlantic Oceanographic and Meteorological Laboratory,

Hurricane Research Division at: <http://www.aoml.noaa.gov/hrd/tcfaq/E10.html>. Last updated May 31, 2013.

Le, K., 2000: An Analysis of the Recent Severe Storm Surge Disaster Events in China. *Natural Hazards*, **21**, 215-223.

Le, K., 2002: Severe Storm Surge Disasters and Strategic Measures. *Marine Forecasts*, **19**, 1, 9-15.

Le, T.V.H., N.H. Nhan, E. Wolanski, T.T. Cong, and H. Shigeko, 2007: The combined impact on the flooding in Vietnam's Mekong River delta of local man-made structures, sea level rise, and dams upstream in the river catchment. *Estuarine, Coastal and Shelf Science*, **71**, 110-116.

Lee, J.-C., K.-S. Park, J.-I. Kwon, and S.-I. Kim, 2009: Storm Surge Calculations Using Sea Level Data. *Marine Geodesy*, **32**, 108-117.

LeDang, T.R.U.N.G, 2013: *Economic and Welfare Impacts of Disasters in East Asia and Policy Responses: The Case of Vietnam*. No. DP-2013-11. Economic Research Institute for ASEAN and East Asia (ERIA).

Le Goff, 1994: *Saison Cyclonique, 1993-1994, dans le Sud-Ouest de L'Ocean Indien*. Meteo France. Published in Reunion. 108 pp.

Liu, F., and X. Wang, 1989: A Review of Storm-Surge Research in China. *Natural Hazards*, **2**, 17-29.

Liu, J., 2002: Feature and Varied Rule of Typhoon Storm Surge along the Coast of South East China Sea. *Marine Forecasts*, **19**, 81-88.

Louisiana State University Ag Center, 2014: Louisiana Summary, Agriculture and Natural Resources. Annual agriculture summaries available on the Web at: www.lsuagcenter.com/agsummary/.

Ma, J., 2003: A Review of Preventing and Reducing the Storm Surge Disaster in Guangdong Province. *Marine Forecasts*, **2**, 34-40.

Ma, J., 2004: Analysis and Summary of Storm Surge in 2003 and Their Forecast. *Marine Forecasts*, **21**, 2, 78-85.

Mai, C.V., P.H.A.J.M. van Gelder, and J.K. Vrijling, 2006: Safety of coastal defences and flood risk analysis. *Safety and Reliability for Managing Risk*, **2**, 1355-1366.

Mai, C.V., P. Van Gelder, J.K. Vrijling, and T.C. Mai, 2008: Risk Analysis of Coastal Flood Defences- A Vietnam Case. Fourth International Symposium on Flood Defence: Managing Flood Risk, Reliability and Vulnerability. Toronto, Canada, May 6-8, 2008.

Mandia, S.A., 2010: The Long Island Express: The Great Hurricane of 1938. Suffolk County Community College. Available on the Web at: <http://www.sunysuffolk.edu/index.asp>.

Masters, J., 2013: Super Typhoon Haiyan: Strongest Landfalling Tropical Cyclone on Record. *Dr. Jeff Masters' Wunderblog*, November 7, 2013. Available on the Web at: <http://www.wunderground.com/blog/JeffMasters/super-typhoon-haiyan--strongest-landfalling-tropical-cyclone-on-recor>.

Mauritius Meteorological Services, 2012: List of historical cyclones. This resource is available on the web at: <http://metSERVICE.intnet.mu/?cat=28>.

Mayoka, Mireille, 1998: Les Cyclones à la Réunion. Meteo-France press, 48 pp.

MCEER, 2014: Major Japanese Earthquakes of the 20th Century. Database and Website provided by the Research Foundation of the State of New York. Available on the Web at: https://mceer.buffalo.edu/infoservice/reference_services/japanese_earthquake.asp.

McGee, B.D., B. B. Goree, R. W. Tollett, B.K. Woodward, and W.H. Kress, 2013: Hurricane Rita Surge Data, Southwestern Louisiana and Southeastern Texas, September to November 2005. U.S. Geological Survey. Data Series 220. Page last modified January 13, 2013. Available on the Web at: pubs.usgs.gov/ds/2006/220/index.htm#desc.

McInnes, K.L., G.D. Hubbert, I. Macadam, and J.G. O'Grady, 2008: Assessing the Impact of Climate Change on Storm Surges in Southern Australia, mimeo.

McTaggart-Cowan R., G.D. Deane, L.F. Bosart, C.A. Davis, T.J. Galarneau, Jr., 2008: Climatology of tropical cyclogenesis in the North Atlantic (1948-2004). *Monthly Weather Review*, 136, 1284-1304.

MetService, 2013: Weather Warnings. Web page for severe weather warnings provided by the Meteorological Service of New Zealand. Available on the web at: www.metservice.com/national/warnings/index.

Meteo France, 2013: Ministère de L'Écologie, du Développement durable et de L'Énergie. Available on the web at: [www.meteo.fr/temps/domtom/La Reunion/meteoreunion2/](http://www.meteo.fr/temps/domtom/La_Reunion/meteoreunion2/).

Meyer-Arendt, K.J., 1991: Hurricane Gilbert: The Storm of the Century. *GeoJournal*, 23, 323-325.

Mimura, N., 1999: Vulnerability of island countries in the South Pacific to sea level rise and climate change. *Climate Research*, 12, 137-143.

Mimura, N., K. Yasuhara, S. Kawagoe, H. Yokoki, and S. Kazama, 2011: Damage from the Great East Japan Earthquake and Tsunami – A Quick Report. *Mitigation Adaptation Strategies Global Change*, 16, 803-818.

Minerals Management Service, 2006: Impact Assessment of Offshore Facilities from Hurricanes Katrina and Rita, New Release 3486, May 1, 2006.

Moon, I.-J., I.S. Oh, T. Murty, and Y.-H. Youn, 2003: Causes of the Unusual Coastal Flooding Generated by Typhoon Winnie on the West Coast of Korea. *Natural Hazards*, 29, 485-500.

Mori, N., T. Takahashi, T. Yasuda, and H. Yanagisawa, 2011: Survey of 2011 Tohoku earthquake tsunami inundation and run-up. *Geophysical Research Letters*, 38, L00G14, doi: 10.1029/2011GL049210.

Murty, T.S., and A.D. Greenberg, 1987: Numerical simulation of the storm surge of January 1982 on the South Coast of Newfoundland. *Atmosphere-Ocean*, 25, 1, 46-59.

Murty, T.S., 1988: List of Major Natural Disasters, 1960-1987. *Natural Hazards*, 1, 303-304.

Murty, T.S., and R.A. Flather, 1994: Impact of storm surges in the Bay of Bengal. In: Finkl, C.W.J. *ed.* Coastal hazards: perception, susceptibility and mitigation, Special Issue No. 12. Charlottesville, Coastal Education and Research Foundation. Pp. 149.161.

Myanmar Department of Meteorology and Hydrology, 2011: Tropical Cyclone Disasters. Available on the web at: http://www.dmh.gov.mm/index.php?option=com_content&view=article&id=36&Itemid=37&lang=en.

Naeraa, M. and M.R. Jury, 1998: Tropical Cyclone Composite Structure and Impacts over Eastern Madagascar During January-March 1994. *Meteorology and Atmospheric Physics*, 65, 43-53.

National Geophysical Data Center, 2012: *March 11, 2011 Japan Earthquake and Tsunami*. Available on the Web at: http://www.ngdc.noaa.gov/hazard/tsunami/pdf/2011_0311.pdf.

National Hurricane Center, Miami, Florida, 1988: Preliminary Report, Hurricane Gilbert, 08-19 September 1988. Published on the Web at: http://www.nhc.noaa.gov/archive/storm_wallets/atlantic/atl1988-prelim/gilbert/prelim02.gif.

National Hurricane Center, 2013: NHC Data Archive. Available on the Web at: <http://www.nhc.noaa.gov/data/>.

National Oceanic and Atmospheric Administration, 1999: NOAA releases century's top weather, water and climate events. Published on the Web at: <http://www.noaanews.noaa.gov/stories/s334.htm>.

National Oceanic and Atmospheric Administration, 2014: Storm Surge and Coastal Inundation. Summary of extratropical storm surge events available on the Web at: www.stormsurge.noaa.gov/event_history.html.

National Weather Service Lake Charles, 2003a: Louisiana Hurricane History: Late 19th Century. Published on the Web at <http://www.srh.noaa.gov/lch/research/lalate19hu4.php>.

National Weather Service Lake Charles, 2003b: Louisiana Hurricane History: Late 20th Century. Published on the Web at: <http://www.srh.noaa.gov/lch/research/lalate20hur2.php>

National Weather Service, 2013: The 1993 Storm of the Century. Web page developed by the National Weather Service Weather Forecast Office for the Tampa Bay Area. Available on the Web at: <http://www.srh.noaa.gov/tbw/?n=93storm>.

Needham, H.F. and B.D. Keim, 2011: Storm surge: physical processes and an impact scale. In *Recent Hurricane Research- Climate, Dynamics, and Societal Impacts*, Lupo E (ed). Intech Open Access: Croatia.

Needham, H.F., and B.D. Keim, 2012: A Storm Surge Database for the U.S. Gulf Coast. *International Journal of Climatology*, 32,14,2108-2123. DOI: 10.1002/joc.2425.

Needham, H.F., B.D. Keim, D. Sathiaraj, and M. Shafer, 2013: A Global Database of Tropical Storm Surges. *EOS, Transactions American Geophysical Union*, 94, 24, 213-214.

Needham, 2013: Haiyan Storm Surge Estimates Improve through Shared Observations. Blog post on *Hurricane Hal's Storm Surge Blog*, November 15, 2013. Available on the Web at: <http://stormsurge2010.blogspot.com/2013/11/haiyan-storm-surge-estimates-improve.html>.

Needham, H.F., and B.D. Keim, 2014: Correlating Storm Surge Heights with Tropical Cyclone Winds at and before Landfall. *Earth Interactions*, **18**, 1-26.

Nelson, R.C., 1975: Tropical Cyclone Storm Surges in Australia 1880 to 1970. *Proceedings from Second Australian Conference for Coastal and Ocean Engineering*, IE Aust.

Neumann, J.E., K.A. Emanuel, S. Ravela, L.C. Ludwig, and C. Verly, 2012: Risks of Coastal Storm Surge and the Effect of Sea Level Rise in the Red River Delta, Vietnam. Working Paper No. 2012/81, United Nations University/ World Institute for Development Economics Research.

Neumann, J.E., K.A. Emanuel, S. Ravela, L.C. Ludwig, and C. Verly, 2013: *Assessing the risk of cyclone-induced storm surge and sea level rise in Mozambique*. WIDER Working Paper No. 2013/03. UNU-WIDER, World Institute for Development Economics Research.

Ng, E.K.W., and J.C.L. Chan, 2012: Interannual variations of tropical cyclone activity over the north Indian Ocean. *International Journal of Climatology*, 32, 6, 819-830.

Nicholls, R.J., 2003: *An Expert Assessment of Storm Surge "Hotspots"*. Final Report (Draft Version) to Center for Hazards and Risk Research, Lamont-Dohert Observatory, Columbia University.

Nicholls, R.J., 2006: *Storm Surges in Coastal Areas. Natural Disaster Hot Spots Case Studies*. Chapter 3. Margaret Arnold et al. 2006. The World Bank.

Nott, J., and M. Hayne, 2000: How high was the storm surge from Tropical Cyclone Mahina? North Queensland, 1899. *The Australian Journal of Emergency Management*, 15, 11-13.

NOVA, 2014: PBS Documentary, *Killer Typhoon*. Available on the Web at: <http://www.pbs.org/wgbh/nova/earth/killer-typhoon.html>.

Oh, I.S., J.K. Lee, and H.S. An, 1993: A study of storm surges of the seas in north eastern Asia. *Journal of Korean Earth Science Society*, 14, 467-481.

Organisation Météorologique Mondiale, 2013: Site principal en Français. Disponible sur le Web a: www.wmo.int/pages/index_fr.html.

PAGASA, 1987: *Program for Disseminating Public Information on Natural Hazards*. (Proposal to USAID/OFDA for Funding).

PAGASA, 2014: Philippine Atmospheric, Geophysical and Astronomical Services Administration. Links to scientific literature available on the Web at: <http://www.pagasa.dost.gov/ph/research.shtml>.

Paul, B.K., 2009: Why relatively fewer people died? The case of Bangladesh's Cyclone Sidr. *Natural Hazards*, 50, 289-304.

Peek, K.M., and R.S. Young, 2013: Understanding the Controls on Storm Surge through the Building of a National Storm Surge Database. *Journal of Coastal Research*, In-Press. DOI: <http://dx.doi.org/10.2112/JCOASTRES-D-12-00249.1>.

Penland, S., and K.E. Ramsey, 1990: Relative Sea-Level Rise in Louisiana and the Gulf of Mexico: 1908-1988. *Journal of Coastal Research*, 6, 323-342.

Perez, R.T., L. A. Amadore, and R.B. Feir, 1999: Climate change impacts and responses in the Philippines coastal sector. *Climate Research*, 12, 97-107.

Perez, M.B., and J.R. Torres, 2013a: Resumen de Temporada. Disponible en la Web en: www.met.inf.cu/asp/genesis.asp?TB0=PLANTILLAS&TB1=TEMPORADA&TB2=/Temporadas/temporada2003.htm.

Perez, M.B., and J.R. Torres, 2013b: Resumen de Temporada. Disponible en la Web en: www.met.inf.cu/asp/genesis.asp?TB0=PLANTILLAS&TB1=TEMPORADA&TB2=/Temporadas/temporada2005.htm.

Pielke, R.A., J. Rubiera, C. Landsea, M.L. Fernandez, and R. Klein, 2003: Hurricane Vulnerability in Latin America and The Caribbean: Normalized Damage and Loss Potentials. *Natural Hazards Review*, 4, 101-114.

Pine, J.C., 2006: Hurricane Katrina and Oil Spills: Impact on Coastal and Ocean Environments. *Oceanography*, 19, 37-39.

Post, Buckley, Schuh & Jernigan, Inc., 1993: *Hurricane Iniki Assessment, Review of Hurricane Evacuation Studies and Information Dissemination*. Report prepared for the U.S. Army Corps of Engineers, Federal Emergency Management Agency, and State of Hawaii, Department of Defense. Report available online at: http://www.csc.noaa.gov/hes/docs/postStorm/H_INIKI_ASSESSMENT_REVIEW_HES_UTILIZATION_INFO_DISSEMINATION.pdf.

Primavera, J.H., 2000: Development and conservation of Philippine Mangroves: institutional issues. *Ecological Economics*, 35, 91-106.

Queface, A. and M. Tadross, 2009: Main report: INGC Climate Change Report: Study on the impact of climate change on disaster risk in Mozambique. [Asante, K., Brito, R., Brundrit, G., Epstein, P., Fernandes, A., Marques, M.R., Mavume, A., Metzger, M., Patt, A., Queface, A., Sanchez del Valle, R., Tadross, M., Brito, R. (eds.)]. INGC, Mozambique.

Rappaport, E.N., and J. Fernandez-Partagas, 1995: The deadliest Atlantic tropical cyclones, 1492-1994. *NOAA Technical Memorandum NWS NHC-47*, National Hurricane Center, Pgs. 1-41.

Rearic, D.M., 1990: Survey of Cyclone Ofa damage to the north coast of Opolu, Western Samoa. Suva: SOPAC. Technical Report 118, 1991. 22 pp.

Reimnitz, E., and D. K. Maurer, 1979: Effects of Storm Surges on the Beaufort Sea Coast, Northern Alaska. *Arctic*, 32, 329-344.

Risk Management Solutions, 2003: *1953 U.K. Floods: 50-Year Retrospective*. 11 pp. Report available on the Web at: https://support.rms.com/publications/1953_Floods_Retrospective.pdf.

Sanh, N.V., V. T. Xuan, and T.A. Phong, 1998: 'History and Future of Farming Systems in the Mekong Delta', in Xuan, Vo-Tong and Matsui, Shigeo (eds.), *Development of Farming Systems in the Mekong Delta of Vietnam*, H.M.C. Publishing House, Ho Chi Minh City, Vietnam, pp. 17-80.

Schencking, J.C., 2008: The Great Kanto Earthquake and the culture of catastrophe and reconstruction in 1920s Japan. *The Journal of Japanese Studies*, 34, 295-331.

Schuck-Kolben, R.E., 1990: Storm-Tide Elevations Produced by Hurricane Hugo along the South Carolina Coast, September 21-22, 1989. *U.S. Geological Survey, Open-File Report 90-386*. Prepared in cooperation with the Federal Emergency Management Agency. Columbia, South Carolina. 50 pp. Available on the Web at: <http://sc.water.usgs.gov/hurricane/pubs/OFR90-386.pdf>.

Servicio Meteorológico Nacional, 2013: Tropical cyclone reports provided from 1997-present. Web site hosted by Comisión Nacional Del Agua (Conagua). Available on the Web at: http://smn.cna.gob.mx/index.php?option=com_content&view=article&id=38&Itemid=46

Servicio Meteorologico Nacional de Honduras, 2013: Main site available on the Web at: www.smn.gob.hn.

Siddiqui, Z.A., 2009: Storm Surge Forecasting for the Arabian Sea. *Marine Geodesy*, 32, 199-217.

Simpson, R. H., A.L. Sugg, and Staff at National Hurricane Center, 1970: The Atlantic hurricane season of 1969. *Monthly Weather Review*, 98, 293-306.

Singh, O.P., T.M.A. Khan, M.S. Rahman, 2001: Has the frequency of intense tropical cyclones increased in the north Indian Ocean? *Current Science*, 80, 575-580.

Smith, D.K., 1989: *Natural Disaster Reduction: How Meteorological and Hydrological Services Can Help*, Publication No. 722, World Meteorological Organisation, Geneva, Switzerland.

Solomon, S.M., and D.L. Forbes, 1999: Coastal hazards and associated management issues on South Pacific Islands. *Ocean and Coastal Management*, 42, 523-554.

Soriano, B., 1992: Tropical Cyclone, Statistics in the Bicol Region. *Ang Tagamasid*, 20, 15 pp.

Soriano, B., 2003: A Tribute to a Great Filipino Weatherman. Available on the Web at: <http://kidlat.pagasa.dost.gov.ph/angtagamasid/obituary.html>.

Spennemann, D.H.R., 1996: Nontraditional settlement patterns and typhoon hazard on contemporary Majuro Atoll, Republic of the Marshall Islands. *Environmental Management*, 20, 337-348.

Streatfield, P.K., and Z.A. Karar, 2008: Population Challenges for Bangladesh in the Coming Decades. *Journal of Health, Population and Nutrition*, 26, 261-272.

Sugg, A.L., 1967: The Hurricane Season of 1966. *Monthly Weather Review*, 95, 3, 131-142. Available on the Web at: <http://www.aoml.noaa.gov/general/lib/lib1/nhclib/mwreviews/1966.pdf>.

Sugg, A.L., and J.M. Pelissier, 1968: The hurricane season of 1967. *Monthly Weather Review*, 96, 242-259.

Sumner, H.C., 1944: North Atlantic Hurricanes and Tropical Disturbances of 1943. *Monthly Weather Review*, 71, 11, 179-183.

Syvitski, J.P., A.J. Kettner, I. Overeem, E.W. Hannon, M.T. Brakenridge, and J. Day, 2009: Sinking Deltas Due to Human Activities. *Nature Geoscience*, 2, 10, 681-686.

Tang, L., J.M. Zhan, and Y.Z. Chen, 2011: Typhoon Process and Its Impact on the Surface Circulation in the Northern South China Sea. *Journal of Hydrodynamics*, 23, 1, 95-104.

Terry, J.P., 2007: *Tropical Cyclones, Climatology and Impacts in the South Pacific*. Published by Springer Science and Business Media, LLC. New York, New York, USA. 224 pp.

Terry, J.P., and A.C. Falkland, 2010: Responses of atoll freshwater lenses to storm-surge overwash in the Northern Cook Islands. *Hydrogeology Journal*, 18, 749-759.

Thuy, V.T.T., 2003: *Storm Surge Modelling for Vietnam's Coast*. M.S. Thesis, International Institute for Infrastructural Hydraulic and Environmental Engineering. Delft University, Netherlands.

U.S. Army Corps of Engineers, 1972: *History of Hurricane Occurrences along Coastal Louisiana*. U.S. Army Engineer District, New Orleans Corps of Engineers, New Orleans, Louisiana. 43 pp. text, 20 maps.

U.S. Army Engineer District, 1962: *Hurricane Carla, September 9-12, 1961*. Report made available from U.S. Army Corps of Engineers, Galveston, Texas. [NUMBER] pp.

U.S. Corps of Engineers, 1935: Map of Storm Tide Levels in Labor Day Hurricane. Chart File No. 3-16-10,409, created October 21, 1935.

U.S. Department of Commerce, 1993: *Natural Disaster Survey Report, Hurricane Iniki, September 6-13, 1992*. Report available online at: <http://www.nws.noaa.gov/om/assessments/iniki/iniki1.pdf>.

U.S. Energy Administration, 2010: Independent Statistics and Analysis. National maps of energy distribution, refineries, power plants, coal mines and renewable energy, available on the Web at: <http://www.eia.doe.gov/state/>.

U.S. Geological Survey, 2013: Inland Storm-Tide Monitoring Program. Available on the web at: http://water.usgs.gov/osw/programs/storm_surge1.html.

Unisys Corporation, 2013: Hurricane/Tropical Data. Available on the Web at: <http://weather.unisys.com/hurricane/index.php>.

United Nations Office for the Coordination of Humanitarian Affairs, 2005: Cook Islands and Tokelau: Tropical Cyclone Percy- OCHA Situation Report No. 5. Published on the Web at: <http://reliefweb.int/report/cook-islands/cook-islands-and-tokelau-tropical-cyclone-percy-ocha-situation-report-no-5>.

URS, 2006a: Final Coastal and Riverine High Water Mark Collection for Hurricane Katrina in Mississippi. Prepared by URS Group, Inc. for the Federal Emergency Management Agency. Final edition completed March 14, 2006. Available at: https://www.fema.gov/pdf/hazard/flood/recoverydata/katrina/katrina_ms_hwm_public.pdf.

URS, 2006b: High Water Mark Collection for Hurricane Katrina in Louisiana. Prepared by URS Group, Inc. for the Federal Emergency Management Agency. Final edition completed March 30, 2006. Available on the web at: http://www.fema.gov/pdf/hazard/flood/recoverydata/katrina/katrina_la_hwm_public.pdf.

URS, 2006c: High Water Mark Collection for Hurricane Katrina in Alabama. Prepared by URS Group, Inc. for the Federal Emergency Management Agency. Final edition completed March 3, 2006. Available on the web at: http://www.fema.gov/pdf/hazard/flood/recoverydata/katrina/katrina_al_hwm_public.pdf.

URS, 2006d: *Hurricane Rita Rapid Response, Louisiana Coastal and Riverine High Water Mark Collection*. Final Report, Submitted to the Federal Emergency Management Agency, Region 4, Atlanta, Georgia. Available on the Web at: www.fema.gov/ped/hazard/flood/recoverydata/rita/rita_la_hwm_public.pdf.

United States Geological Survey, 2008: Largest and Deadliest Earthquakes by Year, Updated July 16, 2008. Published on the Web at: <http://earthquake.usgs.gov/eqcenter/eqarchives/year/byyear.php>.

Vongvisessomjai, S., 2007: Impacts of Typhoon Vae and Linda on wind waves in the Upper Gulf of Thailand and East Coast. *Songklanakarin Journal of Science and Technology*, 29, 5, 1199-1216.

Vongvisessomjai, S., 2009: Tropical cyclone disasters in the Gulf of Thailand. *Songklanakarin Journal of Science and Technology*, 31, 2, 213-227.

Wang, X., Q., Yin, and B. Zhang, 1991: Research and Applications of a Forecasting Model of Typhoon Surges in China. *Advances in Water Science*, 2, 1, 1-10.

Wang, Y.H., I.H. Lee, D.P. Wang, 2005: Typhoon induced extreme coastal surge: A case study at northeast Taiwan in 1994. *Journal of Coastal Research*, 21, 548-552.

Wassmann, N. X. Hien, C.T. Hoanh, and T. P. Tuong, 2004: Sea Level Rise Affecting the Vietnamese Mekong Delta: Water Elevation in the Flood Season and Implications for Rice Production. *Climatic Change*, 66, 89-107.

Weber, J., 2014: Interview on PBS Documentary, *Killer Typhoon*. Available on the Web at: <http://www.pbs.org/wgbh/nova/earth/killer-typhoon.html>.

Weisberg, R. H., and L. Zheng, 2006: Hurricane Storm Surge Simulations for Tampa Bay. *Estuaries and Coasts*, 29, 899 – 913.

Western States Seismic Policy Council, 2013: 1946 Aleutians Tsunami. Available on the Web at: www.wsspc.org/resources-reports/tsunami-center/significant-tsunami-events/1946-aleutians-tsunami/.

Whittingham, H.E., 1958: The Bathurst Bay hurricane and associated storm surge. *Australian Meteorological Magazine*, 27, 40-41.

Wolanski, E., N. Ngoc Huan, L. Trong Dao, N. Huu Nhan, and N. Ngoc Thuy, 1996: Fine-sediment dynamics in the Mekong River estuary, Vietnam. *Estuarine, Coastal and Shelf Science*, 43, 5, 565-582.

World Bank, 2009: 'Convenient Solutions to an Inconvenient Truth: Ecosystem-based Approaches to Climate Change'. Washington, DC: World Bank, Environment Department.

World Meteorological Organization, 2013: Latest Advisories on Current Tropical Cyclones Hurricanes Typhoons. Webpage providing a list of regional specialized meteorological centers and tropical cyclone warning centers. Available on the web at: www.wmo.int/pages/prog/www/tcp/Advisories-RSMCs.html.

Xuejie, G., Z. Zongci, and F. Giorgi, 2002: Changes of Extreme Events in Regional Climate Simulations over East Asia. *Advances in Atmospheric Sciences*, 19, 5, 927-942.

Ye, Q., 2004: Typhoon Rusa and Super Typhoon Maemi in Korea. Publication produced by NCAR/ ESIG. Available on the Web at: <http://ccb.colorado.edu/superstorm/ss-korea-v1.pdf>

Zhang, J., 2009: A Vulnerability Assessment of Storm Surge in Guangdong Province, China. *Human and Ecological Risk Assessment*, 15, 671-688.

CHAPTER 3. CORRELATING STORM SURGE HEIGHTS WITH TROPICAL CYCLONE WINDS AT AND BEFORE LANDFALL

3.1 Introduction

Scientific literature on the physical processes that generate storm surge has developed substantially in recent years, as researchers investigate the role that complex variables such as bathymetry (Weisberg and Zheng 2006; Westerink et al. 2008; Chen et al. 2008) and tropical cyclone size (Blain et al. 1998; Irish et al. 2008; Dietrich et al. 2011) have on storm surge development. Such research has shown that these factors contribute to the height, extent and timing of storm surge. However, one area that has not received much attention is the impact of pre-landfall hurricane winds on storm surge at coastlines.

To date, only Jordan and Clayson (2008) have investigated this topic in any depth. They found that surge magnitudes correlate better with pre-landfall winds than wind speeds at landfall, as they conducted a landfall/surge correlation analysis for 39 landfalling U.S. hurricanes from 1986-2007. They found that instantaneous wind speeds 12 hours before landfall and scaled, pre-landfall intensity 24 hours before landfall correlated best with surge heights.

Unfortunately, this important discovery has received little attention in the scientific literature. No other studies have investigated this topic in more depth or explained the physical processes responsible for this phenomenon, although it is thought that pre-landfall winds correlate better with surge heights because of the oceanic response time required to transfer energy from the atmosphere to the water column (Jordan and Clayson 2008).

Several Gulf Coast hurricanes have rapidly strengthened or weakened just before landfall, providing a unique opportunity to better understand the relationship between pre-landfall winds and peak surge heights. For example, Hurricane Lili in 2002 rapidly weakened just before landfall, but generated a higher surge than might have been anticipated. Although Lili made landfall as a category-1 hurricane, with maximum sustained winds of 148 km/hr (80 knots), the storm generated a 3.75-meter surge in South Louisiana (Pasch et al. 2004). Strong pre-landfall winds may explain how this hurricane generated such a large surge; while centered over the north central Gulf of Mexico, Lili was a category-4 hurricane with sustained winds of 232 km/hr (125 knots) (Pasch et al. 2004).

Two years after Lili, Hurricane Charley provided an example of a rapidly intensifying storm which generated a relatively small storm surge. Although Charley made landfall in Southwest Florida as a category-4 hurricane, with maximum sustained winds of approximately 241 km/hr (130 knots), the peak surge level observed in this storm was only 2.13 m at Sanibel and Estero Islands (Pasch et al. 2011). A storm tide at Fort Myers Beach was measured at 2.87 m above the National Geodetic Vertical Datum of 1929, but this observation was not adjusted for tides or datum (Wang et al. 2005). All of these observations were noticeably lower than the forecasted levels of 3.05 – 4.57 m provided by the National Hurricane Center (National Hurricane Center 2004) as Charley approached the coast. Weaker pre-landfall winds may have contributed to this relatively small magnitude surge. Less than eight hours before landfall, while passing over the Dry Tortugas, Charley's maximum sustained winds were 176 km/hr (95 knots) (Pasch et al.

2011), or 65 km/hr (35 knots) slower than at landfall. Charley's small size may have also contributed to the tempered surge levels (Franklin et al. 2006).

The next year, Hurricane Katrina struck coastal Louisiana and Mississippi generating a storm tide that reached a peak elevation of 8.53 m near Pass Christian, Mississippi (Knabb et al. 2011). This was the highest surge level in modern U.S. history (Needham and Keim 2012). In addition to Katrina's large size (Irish et al. 2008) and shallow bathymetry along the storm's track (Chen et al. 2008) strong pre-landfall winds likely also contributed to its massive storm surge. Katrina's peak winds in the Gulf of Mexico reached as high as 278 km/hr (150 knots) (Bevan II et al. 2008), placing the storm well over the minimum wind speed threshold of a category-5 hurricane. However, as Katrina approached the Louisiana and Mississippi Coasts, the storm weakened, making final landfall as a category-3 hurricane with maximum sustained winds of 194 km/hr (105 knots) (Knabb et al. 2011).

To better understand the role of wind timing in storm surge generation, this chapter investigates the role of pre-landfall winds as a predictor of storm surge height in more detail than previous research. I examine a storm surge dataset for the U.S. Gulf Coast that is substantially longer than the limited dataset employed by Jordan and Clayson (2008), thereby including a greater sample size of tropical storms and hurricanes. The two objectives are: 1) to produce a landfall/surge classification system that characterizes the location of landfall relative to the peak storm surge for hurricanes that impacted the U.S. Gulf Coast, and 2) to use this landfall classification to test the relationship between storm surge levels and wind speeds at 3-hour increments preceding landfall for tropical cyclones along the U.S. Gulf Coast.

3.2 Data

Tropical cyclone position and wind intensity data are provided by Elsner and Jagger (2013). This dataset contains hourly information on tropical cyclone position, maximum winds, forward speed and direction. The authors used spline interpolation to calculate non-linear tropical cyclone data from 6-hour observations provided by HURDAT.

Storm surge data are provided by SURGEDAT, a storm surge database that provides surge data for the U.S. Gulf Coast from 1880-2011 (Needham and Keim 2012). As of February, 2013, SURGEDAT has identified 189 surge events at least 1.22 m high along the U.S. Gulf Coast. SURGEDAT also provides envelopes of water for more than 150 U.S. surge events, supported by more than 7,600 high-water marks (Needham et al. 2013). As better data have become available, some adjustments have been made to the peak surge height and/ or location of maximum surge. An updated surge dataset is available for download at <http://surge.srcc.lsu.edu>.

Although Jordan and Clayson (2008) provided useful analysis on the wind/ surge relationship, some notable differences exist between their dataset and the data used in this chapter. One difference is that they incorporated landfall events from both the U.S. Atlantic and U.S. Gulf Coast, while I only included tropical cyclones that impacted the U.S. Gulf Coast. Despite the larger breadth of their study, they utilized a limited dataset of only 39 landfall events over a 22-year period from 1986 -2007. Also, their storm surge data came from only one source- the National Hurricane Center. In contrast, I utilize 189 surge events over a 130-year period. In addition, SURGEDAT compiles surge data from at least 62 separate sources (Needham and Keim 2012), including 28 federal sources,

numerous academic publications and more than 3,000 pages of historic newspaper, to provide a robust history of observed surge levels. As might be expected, in many cases, data from SURGEDAT differ considerably from surge levels utilized by Jordan and Clayson (2008). For example, Jordan and Clayson (2008) utilize a surge level of only 2.13 m for Hurricane Wilma's surge in southwest Florida in 2005, although multiple credible sources provide surge estimates of at least 4.72 m (Barnes 2007; Smith III et al. 2009).

Wind and surge data were analyzed for the period 1880-2011 (132 years), as well as a more recent, 52-year analysis, covering the years 1960-2011. This more recent time period is selected to validate the longer analysis. A start date of 1960 for the more recent analysis enables inclusion of the entire era of tropical satellite meteorology, which began operationally in the early 1960s (Fett 1964; Timchalk et al. 1965; Dvorak 1984). Improved hurricane tracking and intensity data from the satellite era should provide more accurate analysis related to the correlation of hurricane winds and surge heights. Also, several high-profile hurricanes struck the Gulf Coast in the 1960s, including Hurricanes Donna, Carla, Betsy, Beulah and Camille.

3.3 Methods

As this chapter correlates tropical cyclone winds and storm surge heights at landfall and at 3-hour pre-landfall increments, determining the precise time and location of landfall is crucial. Although the National Hurricane Center defines the term landfall to be, "The intersection of the surface center of a tropical cyclone with a coastline" (National Hurricane Center 2012a), determining the exact time and location of a hurricane landfall is sometimes ambiguous.

Hurricanes that move very slowly or remain stationary near the coast provide cases in which the time and location of landfall may be unclear. This may be especially true if the coastal zone contains wetlands, marshes or estuaries, as these features make it difficult to determine the boundary between land and sea. Hurricane Isaac in 2012 provides such an example, as the storm remained stationary near the Southeast Louisiana coast for a period of time between its first and second landfall (National Hurricane Center 2012b). As this portion of coastline contains many wetlands and small islands, it is possible that Isaac technically made more than two landfalls.

Tropical cyclones that make several distinct landfalls make it difficult to determine which landfall relates best in time and space to the peak storm surge event. Such storms may loop as they approach the coast or may briefly track over peninsulas or other protrusions of land before re-emerging over water and making another landfall. For example, in 1985, Hurricane Juan made a series of loops that impacted South Louisiana (Case 1986). The storm made an initial loop off the Louisiana coast, before the first landfall. After this landfall, the storm moved inland and made a second loop around Lafayette, Louisiana, before re-emerging into the Gulf of Mexico as a tropical storm and moving northeast, making a second Louisiana landfall in Plaquemines Parish (Unisys Corporation 2013). The system then continued moving northeast, making its final landfall along the Alabama Coast.

SURGEDAT contains 12 storm surge observations from Hurricane Juan, the highest of which is 2.5 m at Bayou Bienvenue, Louisiana, near New Orleans. However, given the erratic nature of Juan's track, it is difficult to know which landfall associates closest with the peak storm surge level.

Other hurricanes make only one distinctive landfall, however, the time and location of the landfall are separated in time and space from the peak storm surge. This is especially likely to occur if the hurricane tracked near the coastline for several hours before making landfall. Hurricane Andrew's Louisiana landfall fits into this category. Andrew approached the Louisiana Coast as a category-4 hurricane. At 0300 UTC on August 26, 1992, Andrew was centered near latitude 28.84N, longitude 90.92W, or about 52 km (28 nmi) southwest of the location of peak storm surge. The maximum sustained winds at this time were 233 km/hr (126 knots) (Elsner and Jagger 2013). As the radius of maximum winds were 28 km (15 nmi), Andrew's eyewall made a direct hit on the location of peak surge, because the distance from the center of the eye to the location of peak surge was less than double the radius of maximum winds (National Hurricane Center 2012a). However, the center of circulation remained offshore for more than five more hours after this closest approach to the location of peak surge. When the center of circulation finally crossed the coast, after 0800 UTC, the maximum sustained winds had dropped to 202 km/hr (109 knots) and the distance from the center of circulation to the location of peak storm surge had increased to 94 km (51 nmi). As such, Andrew's position and intensity related better to the location of peak storm surge when it was passing just off the coast from this location, than when the storm officially made landfall. It should be noted that the location of peak storm surge was accurately observed, and not influenced by a scarcity of storm surge data. SURGEDAT provides 74 high-water marks in this region from Hurricane Andrew, many of which are closer to the official landfall location than the peak surge location (Figure 3.1).

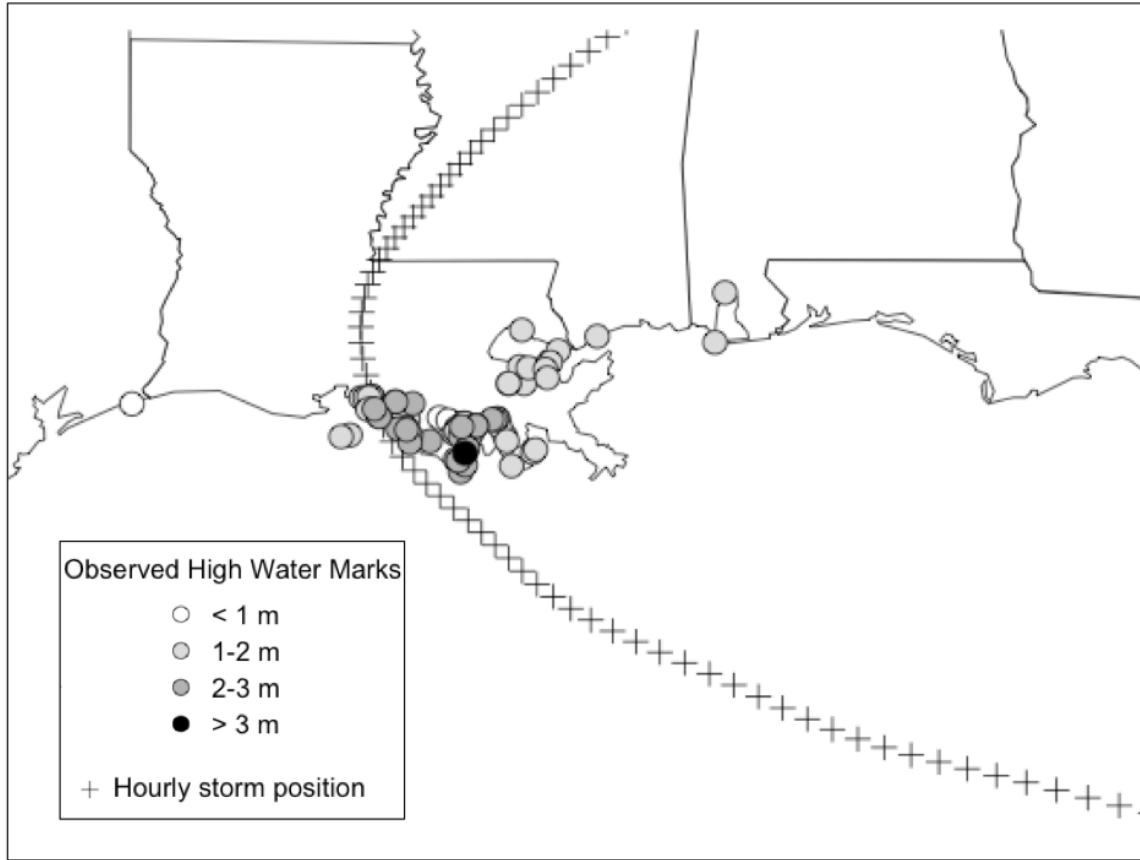


Figure 3.1. Hourly storm position and observed high water marks for Hurricane Andrew. The storm passed closest to the location of peak surge more than five hours before the center of circulation actually crossed the coast.

These examples introduce problems with using the standard landfall definition to study the correlation between storm surge magnitudes and hurricane winds at landfall and incremental time periods approaching landfall. Therefore, I developed a unique classification system that categorizes storm surge events into one of 14 landfall/surge categories. The spatial relationship between hourly hurricane positions and the location of peak storm surge determine the class identification.

I utilized the R Program for Statistical Software (R Development Core Team 2010) to plot the location of peak storm surge and hourly tropical cyclone locations. A minimum distance function was then incorporated to determine the closest hourly storm

observation to the location of peak storm surge. For many cases, I classified this Closest Hourly Observation (CHO) as the time of landfall. However, in some cases, CHO occurs after the tropical cyclone has crossed land. This introduces problems to the classification of landfall, particularly if the cyclone has been inland for at least several hours before CHO is classified. As such, I visually determined the Closest Offshore Observation (COO) as the offshore observation closest in time to CHO, and considered COO to be the time of landfall for cases in which CHO occurred inland.

This methodology produced 14 types of landfall/surge events based upon the timing of CHO and COO, as well as the movement of the tropical cyclone and the spatial comparison between the location of peak storm surge and hourly tropical cyclone locations. Table 3.1 provides a list of these event types, the number of events for each type, and an example tropical cyclone for each type. Of the 14 types, 10 were included in the statistical analysis (types 1-10), which comprised 117 landfall/ surge events. Four types (types 11-14) were not included in this analysis, removing 72 landfall/ surge events.

Table 3.1. Frequency of the 14 landfall classes, with a determination of inclusion/exclusion in this study.

| Type | Description of the Closest Hourly Observation (CHO) | Number of Events | Included or Excluded | Example Storm |
|------|--|------------------|----------------------|---------------|
| 1 | Last obs over water | 25 | Included | Bonnie |
| 2 | Obs over water- second or third obs before crossing land | 19 | Included | Lili |

Table 3.1 (continued). Frequency of the 14 landfall classes, with a determination of inclusion/ exclusion in this study.

| | | | | |
|----|--|----|----------|---------|
| 3 | Obs over water- more than three obs offshore | 16 | Included | Andrew |
| 4 | Second landfall- last obs over water | 1 | Included | Jerry |
| 5 | First inland obs | 27 | Included | Opal |
| 6 | Second inland obs | 7 | Included | Unnamed |
| 7 | Third inland obs | 6 | Included | Edith |
| 8 | Second landfall- first inland obs | 2 | Included | Katrina |
| 9 | Second landfall- second inland obs | 1 | Included | Allison |
| 10 | Florida Keys surge event | 13 | Included | Donna |
| 11 | "Landfall" four or more obs inland | 22 | Excluded | Matthew |
| 12 | Peak surge to left of landfall | 17 | Excluded | Unnamed |
| 13 | Peak surge and landfall locations "far" | 24 | Excluded | Gilbert |
| 14 | Tropical cyclone moving offshore | 9 | Excluded | Unnamed |

Types one through four represent events in which CHO occurs offshore, whereas types five through nine are events in which CHO occurred inland. Types 10 through 14 represent a variety of different landfall/ surge scenarios, which were removed from this analysis because of dissociation of the wind/surge relationship in space and/or time, as described below.

3.3.1 Landfall/ surge classification system

In Type 1 events, CHO is the last hourly observation before a tropical cyclone crosses the coastline. The timing of CHO is coordinated very well with the official landfall time in these events, producing a pattern that is generally considered to be a typical landfall. Hurricane Bonnie in 1986 (Figure 3.2a) is an example of this type, as CHO equals COO and occurs as the last hourly observation before the storm crosses the

southeast Texas coast. Bonnie generated a peak storm surge at Sabine Pass, Texas, a location just east of landfall.

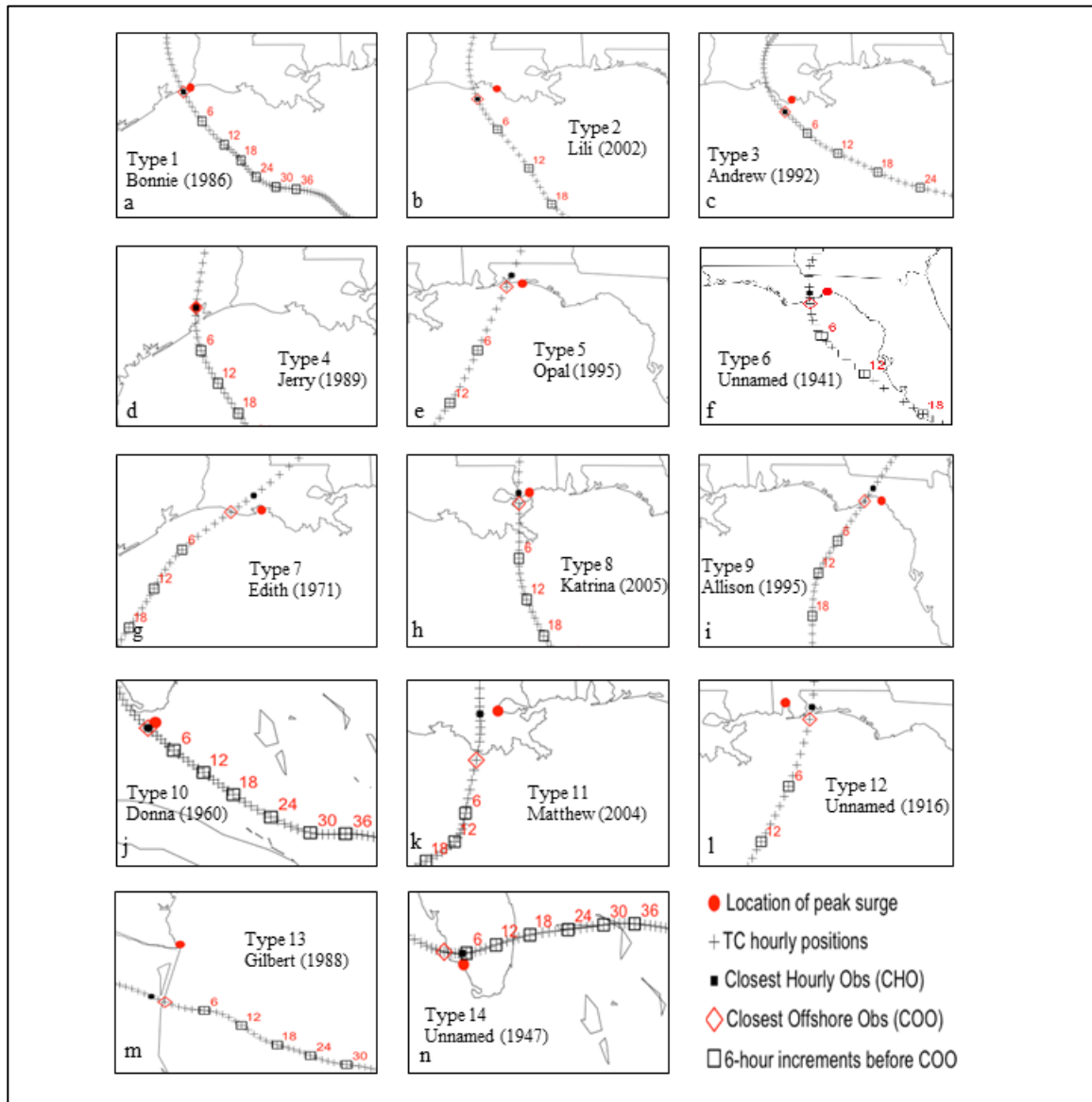


Figure 3.2. The 14 landfall/surge classification types. An example storm is provided for each type.

In Type 2 events, CHO occurs two or three observations before the tropical cyclone actually crosses the coast. In these cases CHO is also equal to COO. Hurricane Lili in 2002 (Figure 3.2b) is an example of a Type 2 event, as CHO occurred almost two hours before the center of Lili's circulation actually crossed the Louisiana Coast.

In Type 3 events CHO occurs more than three hours before the center of circulation crosses the coast. In these cases CHO is equal to COO. Hurricane Andrew in 1992 (Figure 3.2c) is an example of a Type 3 event, as CHO occurred more than five hours before the center of Andrew's circulation crossed the Louisiana Coast.

Type 4 events have multiple landfalls. In these cases, CHO is also an offshore observation, but this occurs after the tropical cyclone has previously made landfall. As such, in Type 4 events, CHO is equal to COO and occurs as the last offshore observation before the second landfall. Hurricane Jerry in 1989 (Figure 3.2d) is the example of this type, as the hurricane made landfall near Galveston Island, then briefly tracked inland west of Texas City, Texas, before emerging into Galveston Bay and generating a peak storm surge at Baytown, Texas.

Type 5 events typify cases in which the CHO is the first inland observation. In these events $CHO - COO = 1$, and the first observation before CHO is selected as the landfall observation. Hurricane Opal in 1995 (Figure 3.2e) is an example of this type. It should be noted that for cases in which CHO occurs inland, always use COO as the landfall observation, so an inland observation is never used to designate landfall.

Type 6 events are similar to type 5, however, CHO is the second inland observation. In these events $CHO - COO = 2$, and the second observation before CHO is selected as the landfall observation. An unnamed hurricane in 1941 (Figure 3.2f), which made landfall near Apalachicola, Florida, is an example of a Type 6 storm.

Type 7 events are similar to types 5 and 6, however, CHO is the third inland observation. In these events $CHO - COO = 3$, and the third observation before CHO is

selected as the landfall observation. Hurricane Edith in 1971 (Figure 3.2g) is an example of a Type 7 event.

In Type 8 events CHO is the first inland observation of the second landfall. Although only two events are classified in this type, these events are extremely important. Hurricanes Camille and Katrina (Figure 3.2h), were both type 8 events. These tropical cyclones produced the two highest storm surges in the past 130 years along the U.S. Gulf Coast (Needham and Keim 2012). Both of these hurricanes traversed open water of the Gulf of Mexico before making landfall along the Louisiana Delta. These storms then both re-emerged over water near Mississippi Sound and made a second landfall near the Louisiana- Mississippi border. In both cases, CHO is the first inland observation on the Louisiana or Mississippi mainland. Therefore, $CHO - COO = 1$ and the last observation before CHO is utilized as landfall.

Interestingly, Hurricane Camille's COO actually occurs over land, as the last observation before final landfall occurred while it was still over the Louisiana Delta. However, it is necessary to use this observation as landfall, as the storm emerged over the Mississippi Sound, and then made landfall again on the Mississippi mainland by the next hourly observation. This is a rare case where COO occurs over land, however, it is representative of the storm intensity as it emerged into Mississippi Sound. Hurricane Katrina was centered over Lake Borgne at COO, one hour before CHO, which occurred near Slidell, Louisiana.

Type 9 events are similar to Type 8 events, although CHO represents the second inland observation of the second landfall. In these cases $CHO - COO = 2$, so the second observation before CHO is used as the landfall observation. Tropical Storm Allison in

1995 (Figure 3.2i) is classified as a Type 9 event, as the storm briefly crossed Alligator Point, Florida, before reentering water and making a final landfall on the north shore of Apalachee Bay. Landfall in this case was defined as the second hourly observation before CHO.

In Type 10 events the peak storm surge occurred in the Florida Keys. These events were separated from surges that peaked on the mainland U.S. Coast or on barrier islands located just off the U.S. mainland. This decision was justified by the fact that landfall is difficult to define in island chains like the Florida Keys, as the center of circulation for many tropical cyclones crosses between islands, crosses the edges of islands, or may traverse many different islands. Hurricane Donna in 1960 (Figure 3.2j) is classified as a Type 10 event.

In Type 11 events CHO is classified as at least the fourth inland observation. Such events are not included in this analysis because the tropical cyclone makes its closest approach to the location of peak surge well after COO. It is reasonable to assume that the time of peak surge for many of these events occurred as the tropical cyclone passed closest to the location of peak surge. If the time of peak surge and COO are separated by four or more hours, the tropical cyclone conditions when the center of circulation actually crossed the coast are likely to be different than the tropical cyclone conditions four or more hours later.

The tropical cyclone in many of these cases makes landfall at an oblique angle to the coast, remaining near the coast for many hours after landfall. In other cases, the maximum surge occurs on the innermost portion of large bays or lakes, enabling the cyclone to continue approaching the location of peak storm surge many hours after it has

already made landfall. Tropical Storm Matthew in 2004 (Figure 3.2k) provides such an example, as the storm made landfall in South Louisiana, near Cocodrie, Louisiana, then continued to approach Frenier, the location of peak storm surge, for the next five hours. Matthew's center of circulation was inland during these five hours, but was still able to approach Frenier, as this small village is located near the westernmost portion of Lake Pontchartrain.

Type 12 events represent cases in which the location of peak storm surge was located to the left of the tropical cyclone track as the storm approached the coastline. In the Northern Hemisphere, storm surges generally peak to the right of the cyclone track, as these areas observe strong onshore winds from the counterclockwise wind flow around the cyclone. An unnamed hurricane that made landfall in the western Florida Panhandle in 1916 (Figure 3.2l) provides an example of this type of event. SURGEDAT provides a maximum surge height of 1.22 m in Mobile, Alabama, for this event, however, a higher storm surge may have occurred in the western Florida Panhandle, though no credible source of information is available.

In Type 13 events, the location of peak storm surge and the CHO are far enough apart that the timing of peak storm surge is not likely associated with the timing of landfall. An example of such events include tropical cyclones that generated storm surges in the United States, but made landfall far enough south of the Texas/ Mexico border that the eyewall never directly impacted the United States. This type also includes tropical cyclones that pass far enough south of the Florida Keys that the eyewall never crosses any islands, and tropical cyclones that are in proximity to the coast, though they parallel the coast in such a way that the peak surge is separated in space and time from landfall.

Hurricane Gilbert in 1988 (Figure 3.2m), for example, made landfall in Mexico, more than 200 km (108 nmi) south of the U.S. border, but still generated a storm surge of 1.83 m at South Padre Island, Texas (National Hurricane Center 1988). However, this surge height cannot be used in this analysis, because storm surge heights in Mexico were most likely larger than those in South Texas, estimated up to 3.96 m north of the landfall location (National Hurricane Center 1988).

I required COO to be located within 159 km (86 nmi) of the location of peak surge, effectively removing all events in which the tropical cyclone was too distant from the peak surge to associate the timing of landfall and peak surge. The size of this buffer corresponds to the average extent of tropical storm force winds in Category 1 and 2 hurricanes (Keim et al. 2007), which comprise most of the events in this analysis. An exception to this rule was made for Hurricane Emily, which was included as a Type 13 event even though the distance from COO to the location of peak surge was only 143.5 km (77.5 nmi). As Emily was a small storm, with a 28-km (15-nmi) radius of maximum winds (Demuth et al. 2006), and the storm made landfall well south of the Texas/ Mexico border, it is likely that surge levels in Mexico exceeded the 1.52-m surge measured at Boca Chica Beach, in South Texas.

Tropical cyclones that generated storm surges while moving offshore are classified as Type 14. These events are not included in the analysis because they are not making landfall in the Gulf of Mexico. Many of these events made landfall on the East Coast of Florida, then emerged into the Gulf after traversing the Peninsula. An unnamed hurricane in 1947 (Figure 3.2n) is an example of this type. This storm produced a 1.68-

meter surge in Everglades City as it emerged into the Gulf of Mexico after passing over South Florida.

3.3.2. Building a 3-hour incremental wind speed dataset

The maximum wind speed for each storm was recorded in a database, beginning at 36 hours before landfall and continuing at 3-hour increments until the time of landfall. In some cases, however, data were intentionally removed from one or more of the 3-hour pre-landfall increments.

One reason this occurs is that some storms developed into tropical storms less than 36 hours before making landfall. In these cases, observations are not included in the database until the system forms into a tropical storm. Hurricane Humberto (Figure 3.3) provides an example of this phenomenon, as this storm only formed into a tropical storm 24 hours before the time of COO. For this reason, wind data are removed for 27, 30, 33 and 36-hours before landfall.

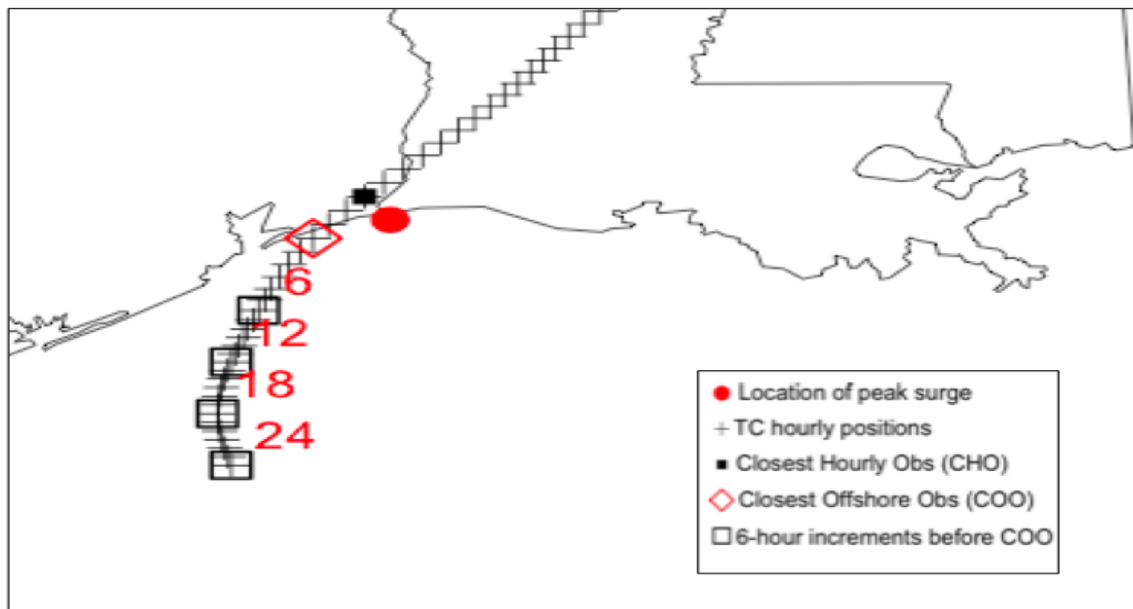


Figure 3.3. Hurricane Humberto formed into a tropical storm 24 hours before the time of COO. Therefore, no observations are available for 27, 30, 33 and 36 hours before landfall.

Another reason data may be missing from one or more of the 3-hour observations is that a tropical cyclone was not centered over the Gulf of Mexico at the time of the observation. If the cyclone was centered over land, such as Florida or Cuba, or centered over water outside the Gulf of Mexico, such as the Atlantic Ocean or Caribbean Sea, observations were not included. For example, no observations are provided for Hurricane Charley from 15 to 36 hours preceding landfall in Southwest Florida, as the hurricane was centered over the Caribbean Sea, south of Cuba, during these intervals (Figure 3.4). An exception was made for tropical cyclones centered over the Atlantic Ocean if the cyclone was moving towards a peak storm surge location in the Florida Keys.

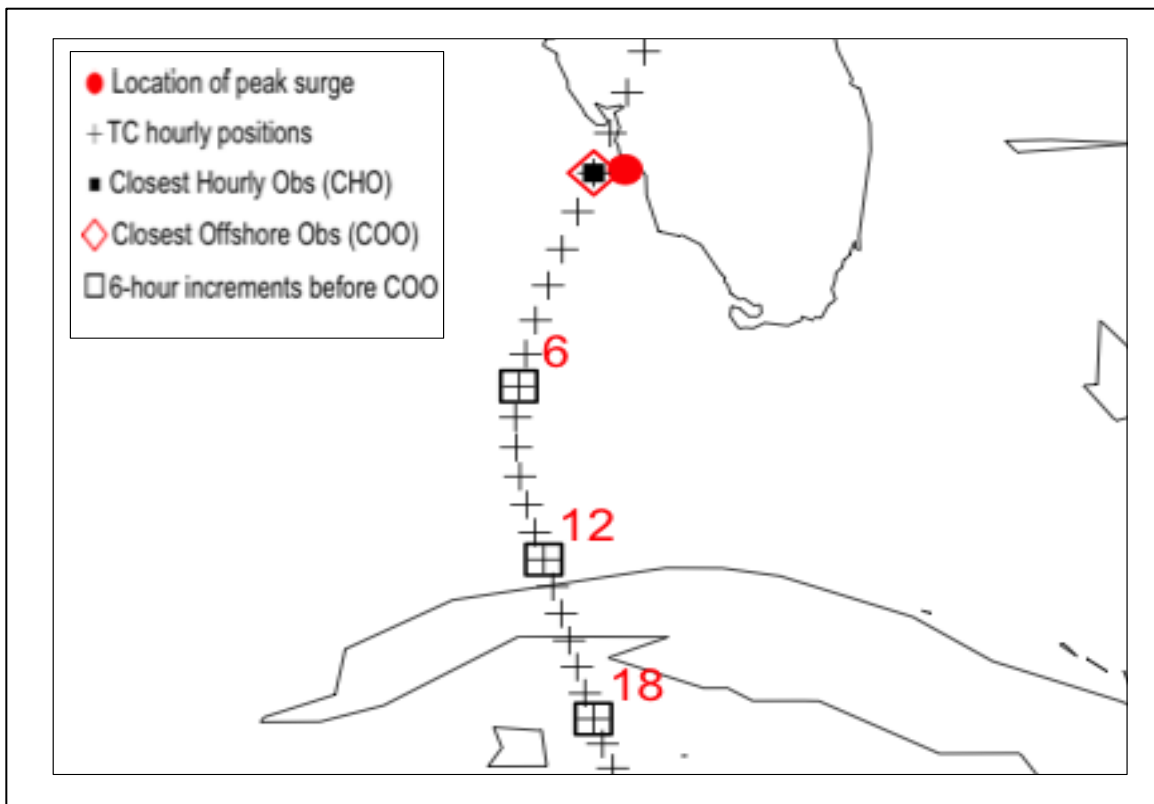


Figure 3.4. Hurricane Charley was centered over the Gulf of Mexico for approximately 12 hours before COO in Southwest Florida. Therefore, no observations are included in the analysis from 15 through 36 hours before landfall, when the cyclone was centered over the Caribbean Sea.

3.4 Results

3.4.1. LOESS and linear regression models

Analysis run on 117 tropical cyclones, from 1880-2011, reveals that pre-landfall wind speeds correlate better with surge magnitudes than wind speeds at landfall (Table 3.2). LOESS regression modeling methods, which use localized regression analysis to find the optimal fit for non-linear relationships, find the correlation between wind speeds and surge magnitudes from three to 30 hours before landfall fit better than wind speeds at landfall. For the wind/ surge relationship at each time increment, I calculated the Residual Standard Error (RSE), sometimes called Residual Standard Deviation (National Institute of Standards and Technology 2013) or Standard Error of Estimate (Spiegel 1961). Lower RSE values indicate a better fit (National Institute of Standards and Technology 2013). I found the optimal wind/ surge correlation occurs 18 hours before landfall, when RSE values drop to .897. The RSE values at landfall were 1.109.

Table 3.2. Residual Standard Error (RSE) between surge heights and wind speeds at landfall and 18 hours before landfall. Lower values indicate better correlation.

| Hours before landfall | Number of Observations | | RSE | |
|-----------------------|------------------------|-----------|-----------|-----------|
| | 1880-2011 | 1960-2011 | 1880-2011 | 1960-2011 |
| 0 | 117 | 63 | 1.109 | 1.187 |
| 3 | 117 | 63 | 1.03 | 1.089 |
| 6 | 117 | 63 | .9866 | 1.036 |
| 9 | 117 | 63 | .9503 | .9731 |
| 12 | 116 | 63 | .9294 | .9464 |
| 15 | 113 | 60 | .92 | .8984 |
| 18 | 109 | 59 | .897 | .8579 |
| 21 | 106 | 56 | .936 | .9338 |
| 24 | 104 | 55 | .9927 | 1.026 |

Table 3.2 (continued). Residual Standard Error (RSE) between surge heights and wind speeds at landfall and 18 hours before landfall. Lower values indicate better correlation.

| | | | | |
|----|----|----|-------|-------|
| 27 | 97 | 53 | 1.051 | 1.087 |
| 30 | 95 | 53 | 1.087 | 1.118 |
| 33 | 92 | 50 | 1.157 | 1.213 |
| 36 | 89 | 48 | 1.174 | 1.251 |

Also, the wind and surge observations 18 hours before landfall clearly fit tighter to a LOESS regression line and have fewer outliers than wind speeds at landfall (Figures 3.5a and 3.5b). The observations for Hurricane Katrina fit well into this pattern, as the higher wind speeds 18 hours before landfall shift this observation to the right in the graphic, making it fit much better with the regression model.

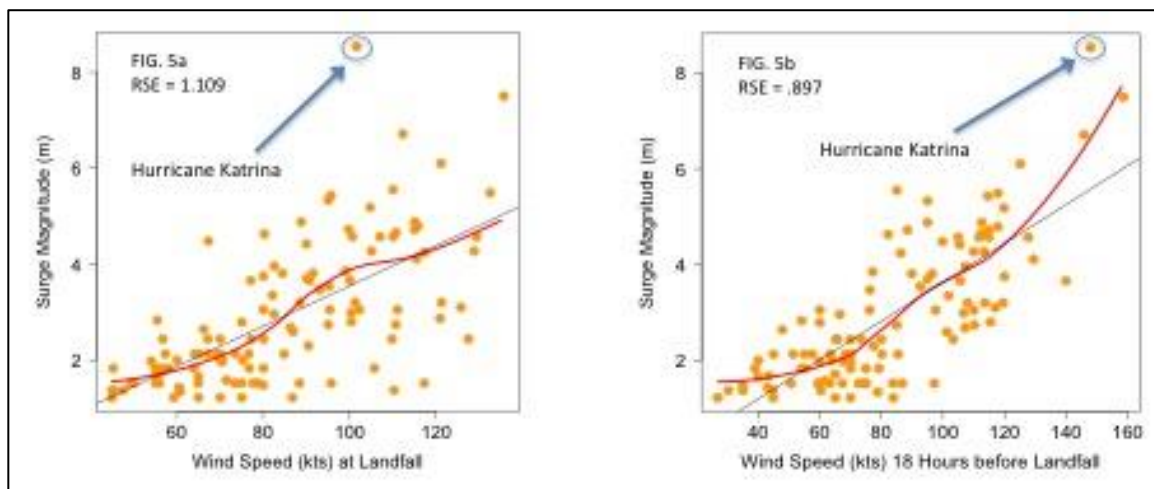


Figure 3.5a (left) and 3.5b (right): LOESS (red line) and linear (black line) regression models for relationship between maximum sustained wind speeds and surge magnitudes. Orange circles depict observed events.

Interestingly, a linear regression model does not fit the data as well as the LOESS model. RSE values for the linear model at 18 hours before landfall only fell to .9431. This outcome supports the notion that wind and surge relationships are non-linear, as the RSE value from the LOESS method was lower (more optimal) than that of the linear

regression. The relationship between maximum sustained winds and storm surge heights for both the LOESS and linear regression models are significant at the 99% confidence level.

Analysis of more recent landfall/surge events revealed similar results. LOESS regression modeling of wind and surge from 63 tropical cyclones between 1960-2011 revealed lowest RSE values at 18 hours before landfall as well, while values from three to 30 hours before landfall were lower than values at landfall. RSE values at 18 hours before landfall are .8579, which indicate a more optimal fit than on the 1880-2011 data. Interestingly, RSE values at landfall are 1.187, which is less optimal than the 1880-2011 values (Figure 3.6). The RSE values for linear regression in the more recent data are also higher (less optimal) than non-linear regression modeling. The RSE values for the linear regression at 18 hours before landfall are .9398. All values are significant at the 99% confidence level.

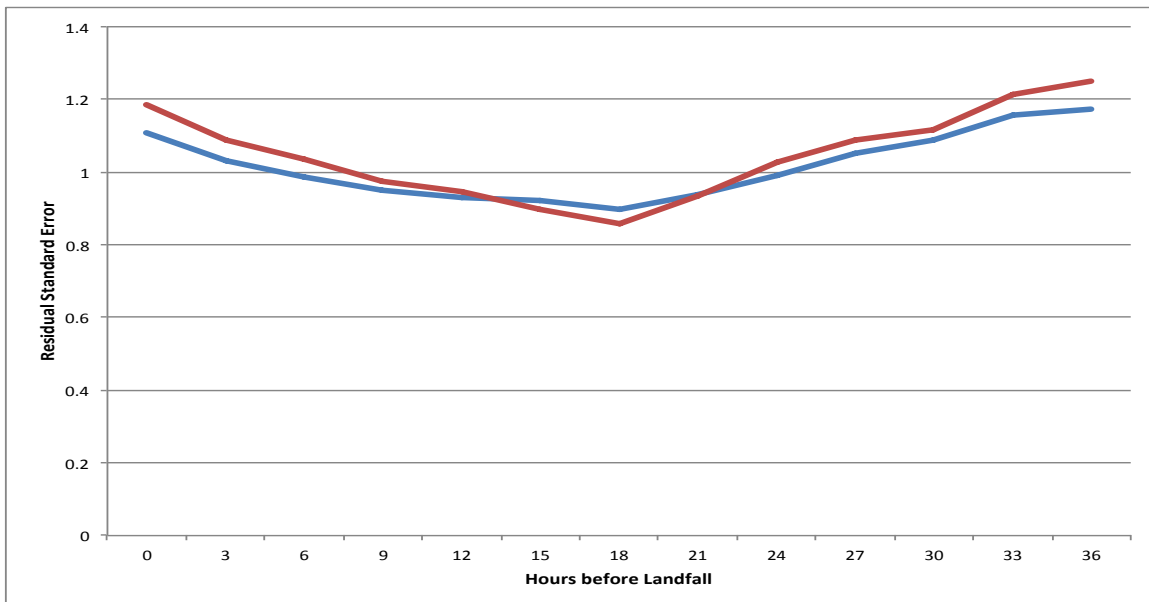


Figure 3.6. Residual Standard Error values from LOESS regression model investigating the relationship between maximum sustained winds and peak surge magnitudes at 3-hour increments before landfall. Values depicted for years 1880-2011 (blue) and 1960-2011 (red). Lower values indicate better correlation.

Multiple R-squared correlation tests find similar results. Correlations improve at each 3-hour interval before landfall until reaching an optimal correlation 18 hours before landfall, then begin to drop off as the time before landfall exceeds 18 hours. R-squared values peaked at .6012 for data from 1880-2011 and 0.663 for data from 1960-2011. These correlations are noticeably better than correlations at landfall, which were only .4299 for the longer dataset and .4369 for the most recent data. Although multiple R-squared values at 18 hours before landfall are noticeably higher than R-square values at landfall, the confidence interval function in R, $CI.Rsq()$, indicated that overlap exists in the 95% confidence level error bounds for these correlations, using both the shorter and longer dataset. This means these R-squared values are not significantly different within their entire error bounds.

Table 3.3 and Figure 3.7a provide comparisons of R-squared values at 3-hour intervals leading up to landfall for both of these time periods. As time before landfall increases, the difference in correlation values between the older and newer datasets increases, presumably because offshore tropical cyclone data have improved substantially during the era of satellite meteorology. These improved correlations between surge heights and pre-landfall winds in the newer dataset result in every 3-hour interval having better correlations than the correlation between surge and wind speeds at landfall.

Table 3.3. Multiple R-Squared values correlating storm surge heights vs. winds at 3-hour increments preceding landfall. Correlation tests were run on data from 1880-2011 (117 events) and 1960-2011 (63 events). These values are plotted in Figure 3.7a.

| Hours before landfall | 1880-2011 (117 events) | 1960-2011 (63 events) |
|-----------------------|------------------------|-----------------------|
| 0 | 0.4299 | 0.4369 |
| 3 | 0.5086 | 0.5341 |

Table 3.3 (continued). Multiple R-Squared values correlating storm surge heights vs. winds at 3-hour increments preceding landfall. Correlation tests were run on data from 1880-2011 (117 events) and 1960-2011 (63 events). These values are plotted in Figure 3.7a.

| | | |
|----|--------|--------|
| 6 | 0.5433 | 0.5793 |
| 9 | 0.557 | 0.6004 |
| 12 | 0.5693 | 0.6138 |
| 15 | 0.5717 | 0.6379 |
| 18 | 0.6012 | 0.663 |
| 21 | 0.5868 | 0.6473 |
| 24 | 0.5508 | 0.6124 |
| 27 | 0.5162 | 0.5657 |
| 30 | 0.4832 | 0.5408 |
| 33 | 0.4317 | 0.4932 |
| 36 | 0.3964 | 0.4698 |

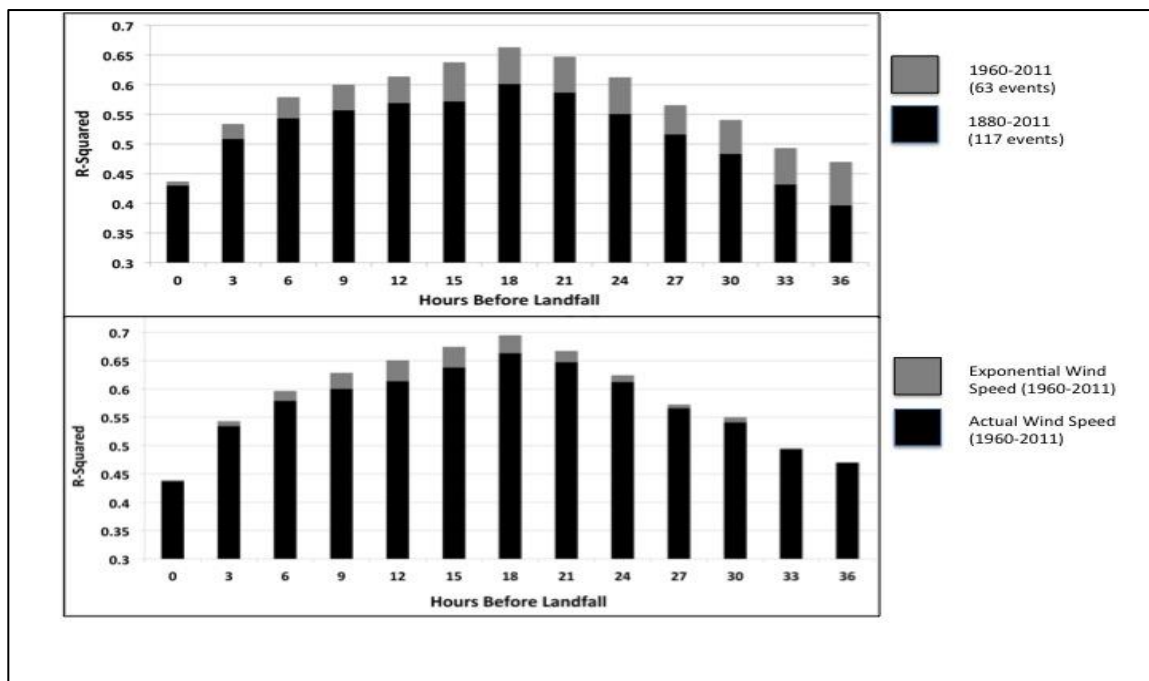


Figure 3.7a (Top): Correlation of surge height vs. wind speeds at 3-hour intervals for data from 1880-2011 (117 events) and 1960-2011 (63 events). Figure 3.7b (Bottom): Correlation of surge heights vs. actual and exponential wind speeds at 3-hour intervals for data from 1960-2011.

3.4.2 Non-linear wind/ surge relationship

The RSE LOESS and linear regression models show that the relationship between maximum wind speeds and storm surge magnitudes is non-linear. I investigated this topic in more depth by raising the array of wind speeds at each 3-hour interval to various exponential powers, then finding which power produced the best fit on a linear regression.

Surprisingly, raising wind arrays to an exponential power greater than two produces the highest R-squared values. Optimal fitting occurs when wind speeds 18 hours before landfall are raised to an exponential value of 2.2. When conducted on data from 1960-2011, raising wind speeds to an exponent of 2.2 increased multiple R-squared values from .6630 to .6948. Surge heights fit best with wind speeds 12 and 15 hours before landfall when these wind values were raised to a power of 2.4. Table 3.4 provides a list of R-squared values correlating surge heights to actual winds and winds raised to exponential powers for each 3-hour interval for the 1960-2011 dataset, which are graphed in Figure 3.7b.

Table 3.4. Multiple R-Squared values of surge vs. actual and exponential wind speeds for data from 1960-2011 (63 events). The exponential power that produced optimal fit is also listed.

| Hours before landfall | R-Squared of surge vs. actual winds | R-squared of surge vs. exponential winds | Optimal Exponent |
|-----------------------|-------------------------------------|--|------------------|
| 0 | 0.4369 | 0.4392 | 1.5 |
| 3 | 0.5341 | 0.543 | 1.74 |
| 6 | 0.5793 | 0.5968 | 1.88 |
| 9 | 0.6004 | 0.6287 | 2.17 |
| 12 | 0.6138 | 0.6507 | 2.4 |

Table 3.4 (continued). Multiple R-Squared values of surge vs. actual and exponential wind speeds for data from 1960-2011 (63 events). The exponential power that produced optimal fit is also listed.

| | | | |
|----|--------|--------|------|
| 15 | 0.6379 | 0.6745 | 2.4 |
| 18 | 0.663 | 0.6948 | 2.2 |
| 21 | 0.6473 | 0.6671 | 1.92 |
| 24 | 0.6124 | 0.6244 | 1.65 |
| 27 | 0.5657 | 0.5729 | 1.53 |
| 30 | 0.5408 | 0.5497 | 1.62 |
| 33 | 0.4932 | 0.4954 | 1.32 |
| 36 | 0.4698 | 0.4703 | 1.15 |

Although raising wind speeds to exponential powers maximizes the difference between multiple R-squared values at landfall and 18 hours before landfall, the confidence interval function in R once again indicates overlap in the error bounds for the 95% confidence level. However, this overlap does not exist for the 90% confidence level, in which the bounds for R-squared values at landfall range from .2935 to .5849, and the bounds for R-squared values 18 hours before landfall range from .5921 to .7975. This test shows a statistically significant difference in the R-squared values of these datasets at the 90% confidence level, when tropical cyclone wind speeds are raised to exponential powers.

These results may seem improbable because wind force is proportional to the square of the maximum wind speed. It may appear that optimal fitting would occur when the wind array is squared, however, when we consider that the transfer of energy from air to water is not perfectly efficient, it seems reasonable that the optimal exponent should be less than two (Jordan and Clayson 2008). So how is it possible that an exponent greater than two produces the best fit?

One possible explanation for this result is the inverse barometer effect. Because surge levels rise in a dome as air pressure near the eye of the hurricane becomes lower, wind stress is not the only physical parameter forcing storm surge. Increased surface roughness provides another possible explanation. As winds increase, wave heights increase as well, increasing the surface roughness of the water. This may increase friction between air and water, making it more efficient for the wind to move more water, thereby increasing the surge height. Other physical parameters may include the geometry of the coastline and bathymetry of water near the coast, which may amplify the buildup of water that is already displaced by the wind. Another possible explanation is that hurricanes displace water over a period of time, which may enhance the buildup of water along the coast from hurricanes that have stronger pre-landfall winds. Water displaced while the hurricane is approaching landfall will accumulate at the coast over time due to the geostrophic effect and it makes sense that more water would accumulate if pre-landfall winds were higher. By contrast, pre-landfall winds should not directly cause wind damage at the coast because they are blowing over water and not directly impacting structures on the coast. All of these potential reasons for the non-linear relationship between pre-landfall winds and surge magnitudes are speculative and should be investigated by scientists in the geophysical research community who specialize in atmospheric and oceanographic physics.

These findings are important because they reveal that changes in pre-landfall hurricane wind speed may impact surge height greater than previously expected. This may be especially important for the most intense tropical cyclones, which may displace more water than previously realized. For example, doubling the maximum wind speed

increases the wind force by a factor of four, but increases the surge potential by a factor of 4.59.

However, the accuracy of these may be limited because this chapter only considers the relationship between surge heights and maximum sustained wind speeds, while, in reality, many variables influence surge heights. Therefore, other unaccounted factors may influence these results. For example, hurricanes Katrina and Camille both produced the highest two storm surges in the region and also produced the highest wind speeds 18 hours before landfall. Data from these storms support the notion that the relationship between pre-landfall winds and surge heights are highly non-linear. However, both of these hurricanes produced peak surge levels in Mississippi, where shallow bathymetry and coastal shape exacerbates surge levels (Needham and Keim 2011). If these storms had struck areas with deeper bathymetry, like South Florida or South Texas, surge heights would have been lower, supporting a more linear relationship between pre-landfall winds and storm surge heights.

3.5 Discussion

These results are timely as the scientific community is re-evaluating the tropical cyclone parameters that are most influential on storm surge generation. For decades, the National Hurricane Center associated wind categories on the Saffir-Simpson Scale with potential storm surge heights, assuming higher category hurricanes will typically generate larger storm surges. This association was discontinued after Hurricane Ike made landfall as a category-2 hurricane but generated a massive 5.33-meter surge along the Texas Coast in 2008 (Berg 2010). At the time, the Saffir-Simpson Scale generalized category-2 hurricanes as having the potential to generate a surge of 1.8-2.4 m (Irish et al. 2008).

Ike's surge occurred approximately three years after Hurricane Katrina made landfall as a category-3 hurricane but generated the largest storm surge in modern U.S. history (Needham and Keim 2012). Katrina's surge of 8.47 m (Knabb et al. 2011) was noticeably larger than the 7.5-meter surge generated by Hurricane Camille in 1969 (Simpson et al. 1970), which made landfall as a category-5 hurricane in the same region.

Hurricanes Katrina and Ike revealed the importance of hurricane size on storm surge generation, as the size of these storms likely contributed to their large surge magnitudes (Irish et al. 2008; Berg 2010). While centered over the northern Gulf of Mexico, Katrina was a large and powerful hurricane. At 18 hours before landfall in Mississippi, the radius of 93 km/hr (50-kt) winds extended 222 km (120 nmi) and the radius of 119 km/hr (64-kt) winds extended 167 km (90 nmi) from the center of circulation, while maximum sustained winds were around 269 km/hr (145 knots) (Demuth et al. 2006). Hurricane Ike's size was even more impressive, when it traversed the Gulf of Mexico in 2008. The radius of 93 km/hr (50-kt) winds was 278 km (150 nmi) and the radius of 119 km/hr (64-kt) winds was 194 km (105 nmi) approximately 18 hours before landfall on the northern end of Galveston Island (Demuth et al. 2006).

Some may argue that Katrina and Ike revealed that hurricane size and bathymetry are the most important parameters for storm surge generation, as these large storms generated high-magnitude surges in areas with shallow bathymetry. Such conclusions may leave readers skeptical of my results, as it may appear that wind speeds do not correlate well with surge magnitudes.

In order to validate my results, I further investigated the characteristics of some tropical cyclones that generated surge events near each other in space. Analyzing surge

events that were proximal to each other limits the influence of bathymetry, enabling the roles of hurricane size and wind speeds to be more visible. I compared hurricanes Danny and Lili, which impacted South Central Louisiana in 1985 and 2002, The 1900 Galveston Hurricane and Hurricane Ike, which impacted the Houston-Galveston area in 1900 and 2008, as well as storm surge events that impacted the Florida Keys. These comparisons confirm that pre-landfall wind speeds are an important factor for generating high-magnitude storm surges, and may generally be as important as storm size.

Hurricane Danny followed a similar track as Lili, as both storms moved northwest from the Central Gulf of Mexico and made landfall just west of Vermillion Bay, Louisiana. Danny's 80-knot maximum sustained wind at landfall (National Hurricane Center 1985) also matched Lili's landfall wind speed (Pasch et al. 2004). However, Danny's peak surge was only 2.44 m (National Hurricane Center 1985), or about 1.31 m lower than Lili's peak surge of 3.75 m (Pasch et al. 2004).

How did Lili generate a storm surge more than 50% higher than Danny, when both storms made landfall with identical wind speeds? The physical profile of the coastal region, including bathymetry, proximity to the coastal shelf, as well as the shape and geometry of the coastline, does not likely explain the difference. These variables should have been nearly constant in these two storms, although changes in the coastline over time from coastal erosion, subsidence and other issues related to the coastal morphodynamics in this region may have had a slight influence on surge heights.

Hurricane size does not explain this difference either, because Danny's geographic size was comparable or larger than Lili's, even though it generated the smaller storm surge. Hurricane Lili was a small hurricane; the radius of maximum wind

was only 19 km (10 nmi) (Demuth et al. 2006). Unfortunately, published hurricane size data were unavailable for Hurricane Danny. To compensate for this lack of data, I utilized thermal infrared satellite imagery to measure the distance from the warmest hurricane eye pixel to the pixel with the coldest cloud-top temperature in this storm. This methodology had previously been used to estimate the size of Hurricane Lili. The distance from between Lili's warmest eye pixel and coldest cloud-top pixel measured 29.1 km (15.7 nmi) (Hsu and Babin 2005).

I measured these distances for both Danny and Lili in Louisiana State University's Earth Scan Lab. Satellite images were provided by the National Oceanic and Atmospheric Administration's (NOAA) Comprehensive Large Array-Data Stewardship System (CLASS) program (2013). I utilized GOES 08 and 10 infrared satellite imagery to measure the size for Hurricane Lili. The temporal resolution was 12 images per hour and the pixel size was 4 x 8 km. I obtained a distance of 45 km (24.3 nmi) between the eye and coldest cloud-top at 18 hours before landfall and 39 km (21 nmi) at 16.25 hours before landfall, which was approximately the same time that Hsu and Babin (2005) made their measurement. The distance I measured was slightly larger than the distance provided by Hsu and Babin (2005). No eye was visible on thermal infrared imagery for Lili at the time of landfall. I utilized GOES 06 infrared satellite imagery, with 30-min temporal resolution and pixel size of 4 x 8 km to measure the size of Hurricane Danny. No eye was clearly visible 18 hours before landfall, however, a discernible eye was visible at the time of landfall, and a distance of 56.5 km (30.5 nmi) was measured. Although these results make it difficult to make an exact size comparison between Danny and Lili, because they were measured at different time intervals before landfall, they do

suggest that Danny was comparable in size or larger than Lili, which rules out the possibility that size differences contributed to the differences in surge magnitudes.

As various parameters, such as storm size, bathymetry and landfall wind speeds are eliminated as the explanation in the difference of these two surge magnitudes, the difference in pre-landfall wind speeds emerges as the most likely explanation. Although the maximum sustained wind speeds of these storms were identical at landfall, Lili was a powerful category-4 hurricane with winds of 232 km/hr (125 knots) while centered over the north central Gulf of Mexico (Pasch et al. 2004), while Danny strengthened as it approached the coast, reaching its peak intensity around the time of landfall (National Hurricane Center 1985).

The difference in seasonal timing may have also contributed to the differences between these two storm surge events, as Danny struck Louisiana in mid-August, and Lili in early October. Cool waters near the northern Gulf Coast likely contributed to Lili's rapid weakening, however, it is possible that cool water temperatures were caused by the passage of Tropical Storm Isidore shortly before Lili (Shay and Uhlhorn 2007), and not from seasonal cooling.

A comparison between Hurricane Ike and the 1900 Galveston Hurricane also supports the importance of pre-landfall winds for generating high-magnitude storm surges. Both of these storms made landfall on Galveston Island and generated destructive surges. Hurricane Ike was the larger of the two storms, with an R_{max} size of 93 km (50 nmi) at 18 hours before landfall and 56 km (30 nmi) at landfall (Demuth et al. 2006). In contrast, the 1900 Galveston Hurricane was a relatively small storm, with an R_{max} size of 26 km (14 nmi) (Ho et al. 1975; Simpson and Riehl 1981; Landsea et al. 2003).

Although the 1900 Galveston Hurricane was a smaller storm, it generated a higher storm surge, which reached a height of 6.1 meters (Garriott 1900). This was slightly higher than Hurricane Ike's peak surge, which reached 5.33 m (Berg 2010). Pre-landfall winds emerge as the most likely reason that the 1900 Galveston Hurricane generated a higher surge. The storm was a powerful category-4 hurricane with a maximum sustained wind speed of 232 km/hr (125 knots) at 18 hours before landfall, which enabled the storm to produce large swells and thunderous surf that were observed on Galveston Island well before the strong winds arrived (Garriott 1900; Larson 1999; Keim and Muller 2009). Hurricane Ike, however, was a category-2 hurricane with a maximum sustained wind speed of 176 km/hr (95 knots) at 18 hours before landfall, and oscillated between category-2 and category-3 intensity as it approached the coast. The bathymetry related to both storms should have been relatively constant.

The storm surge history of the Florida Keys further supports the notion that pre-landfall winds are important for generating high surges. In particular, the 1935 Labor Day Hurricane provides clear evidence of the potential for compact, intense hurricanes to generate catastrophic surges. This cyclone generated a 5.49-m surge in the Florida Keys (U.S. Corps of Engineers 1935), which is the highest modern-day storm surge in this region (Needham and Keim 2012). Interestingly, this storm was also the smallest tropical cyclone to strike this region. The Rmax size of this storm was only 11 km (6 nmi) (Ho et al. 1975), which made it one of the smallest tropical cyclones to ever strike the United States. Intense, pre-landfall winds likely explain how this small storm was able to generate such a high storm surge. This storm was a category-4 hurricane 18 hours before

landfall, and generally strengthened as it approached the Keys, reaching category-5 strength approximately six hours before landfall (Elsner and Jagger 2013).

While these comparative storm surge events provide substantial evidence that pre-landfall winds are important for storm surge generation, they also demonstrate that we must be careful about categorizing hurricanes by their landfall intensities when referring to coastal flooding. For example, both hurricanes Danny and Lili made landfall as category-1 hurricanes in South Louisiana, but Lili was a category-4 hurricane before landfall and produced a storm surge height 50% higher than Danny. Suggesting that both of these storm surges were generated by category-1 hurricanes may mislead readers into believing that little relationship exists between maximum wind velocity and storm surge heights.

Although Hurricane Ike is usually referred to as a category-2 hurricane that generated a massive storm surge, spline-interpolated wind and position data indicate that the storm actually crossed the category-3 threshold multiple times as it approached the Texas coast (Elsner and Jagger 2013). Meanwhile, Hurricane Charley is often referred to as a category-4 hurricane that generated a small surge. However, nine hours before landfall the storm was only a category-2 hurricane and at 18 hours before landfall, when the strongest relationship exists between surge heights and maximum sustained winds, Charley was centered in the Caribbean Sea, south of Cuba, and was therefore displacing only a minimal amount of water in the Gulf of Mexico. While differences in storm size and bathymetry surely enabled Ike to generate a larger surge than Charley, the importance of these parameters is likely overemphasized when referring to Ike as a category-2 hurricane and Charley as a category-4 hurricane. A comparison of these

storms further supports the importance of pre-landfall winds, as Ike was actually a more intense tropical cyclone than Charley at nine hours before landfall (Elsner and Jagger 2013), and Charley was not even centered over the Gulf of Mexico 18 hours before landfall.

Some may argue that Charley generated a relatively small surge because the bathymetry off the coast of southwest Florida is too deep to enable hurricanes to produce high storm surges in this region. However, other coastal flooding events in this region prove that relatively high storm surge levels can be reached in southwest Florida. In 1992, hurricane Andrew generated a 4 m storm tide at North Highland Beach (Risi et al. 1995; Tedesco et al. 1995; Smith III et al. 2009), and Hurricane Wilma in 2005 generated a storm surge of at least 4.72 m between Lostman's Ranger Station and Big Sable Creek, in extreme southwest Florida (Barnes 2007; Smith III et al. 2009). Both of these sites are located within 140 km (76 nmi) of the peak surge location for Hurricane Charley. Also, storm surge modelers must recognize the potential for relatively high storm surges in this region because the National Hurricane Center forecasted Hurricane Charley's peak storm surge to reach between 3.05 – 4.57 m (National Hurricane Center 2004). If deep bathymetry off the coast of southwest Florida eliminated the potential for relatively high storm surges in this region, surge models could not have predicted a surge of this magnitude for Hurricane Charley. These various factors indicate that while bathymetry might have played a role in Charley's storm surge magnitude, the relatively low surge level was most likely due to a combination of small storm size and modest pre-landfall wind speeds, which were much less intense than the wind speeds at landfall.

Comparisons between hurricanes Katrina and Camille provide a final but important example of hurricane classifications that may unintentionally mislead people, when related to coastal flooding. Katrina is often referred to as a category-3 hurricane, based on its landfall intensity. When compared with Hurricane Camille, which made landfall as a category-5 hurricane in the same region, yet generated a lower storm surge, one may conclude that tropical cyclone wind speeds do not correlate well with surge heights. Difference in storm size emerges as the best explanation for these storm surge heights once maximum sustained winds are eliminated as a factor, because the bathymetry and coastal geomorphology near these two surge events should have been relatively constant. While storm size likely was an important factor that enabled Katrina to generate a high storm surge, the importance of size may be overestimated if Katrina's intense, pre-landfall winds are overlooked. Katrina's maximum sustained wind speed of 274 km/hr (148 knots) (Elsner and Jagger 2013) at 18 hours before landfall, was ranked second for all storms in this study, exceeded only by Hurricane Camille. In fact, the pre-landfall wind speeds of these two storms were comparable, as Camille's sustained winds only exceeded Katrina's by 20 km/hr (11 knots) at 18 hours before landfall (Elsner and Jagger 2013).

I am not suggesting that pre-landfall wind speed is the predominant variable that influences storm surge height, not do I imply that other physical parameters have little influence in generating storm surges. I simply suggest that the scientific community should be careful about characterizing past storms, and to make sure that pre-landfall wind speed is considered for cases in which tropical cyclones strengthened or weakened when approaching the coastline.

Comparison of historic storms, taken in conjunction with the statistical analysis of this study, suggest that the larger of two tropical cyclones with comparable pre-landfall winds will generate a larger storm surge, while the tropical cyclone with stronger pre-landfall winds will likely generate the larger storm surge if two storms have comparable sizes and relatively similar bathymetry.

These results should improve surge prediction as modelers give more weight to pre-landfall winds in storm surge forecasts. This will also improve surge prediction because pre-landfall wind forecasts should be more accurate, on average, than landfall forecasts. As a tropical cyclone approaches the coast, complex factors, such as the effect of dry-air entrainment and sea surface temperature changes become more prominent, making wind speed forecasts more difficult. However, wind speed forecasts are generally more accurate for tropical cyclones over open water.

Therefore, using pre-landfall winds as a predictor of surge heights should provide more accurate forecasts, because tropical cyclones are generally positioned well-offshore 18 hours before landfall. The average distance between the center of circulation at landfall and at 18 hours before landfall was 369 km (199 nmi) for wind/ surge events used in this analysis. The maximum distance was 739 km (399 nmi), produced by an unnamed cyclone in late September, 1924, that generated a peak surge height at Cedar Key, Florida. The minimum distance was approximately 67 km (36 nmi) produced by an unnamed tropical cyclone in late September, 1929, that generated a peak surge observation at Key Largo, Florida. Dividing these distances by 18 hours provides an average forward speed of 20.6 km/hr (11.1 knots), a maximum forward speed of 40.9 km/hr (22.1 knots) and a minimum forward speed of 5.9 km/hr (3.2 knots).

3.6 Summary and Conclusion

This chapter investigated relationships between storm surge heights and tropical cyclone winds at and before landfall. Elsner and Jagger (2013) provided a unique tropical cyclone dataset, which contained hourly tropical cyclone position and wind speed data. Maximum storm surge levels for 189 Gulf of Mexico surge events from 1880-2011 were provided by SURGEDAT (Needham and Keim 2012). A landfall/ surge classification was developed to determine the time of landfall and 3-hour increments preceding landfall.

LOESS regression modeling indicates that storm surge magnitudes correlate better with pre-landfall wind speeds than wind speeds at landfall, with wind speeds 18 hours before landfall producing the best correlation. These results were duplicated on tests of 63 wind/ surge events from 1960-2011. Wind speeds 18 hours before landfall also produced the best correlation and provided even better correlation than the longer dataset.

I validated these results by comparing some historical wind-surge events that occurred near each other spatially. Lili's strong pre-landfall winds likely enabled the storm to generate a surge more than 50% higher than Hurricane Danny, as the maximum sustained winds at landfall in these storms was equal, Danny was comparable in size or slightly larger, and bathymetry in the region of these storms was relatively constant. The intense pre-landfall winds of the 1900 Galveston Hurricane likely enabled this storm to generate a higher storm surge than Hurricane Ike, as both storms made landfall on Galveston Island, and the more intense, but smaller, Galveston Hurricane generated a higher-magnitude surge. Also, the 1935 Labor Day Hurricane was one of the smallest hurricanes to strike the United States, but it generated the highest-magnitude surge event

in the history of the Florida Keys. Pre-landfall winds likely influenced this surge height, as the storm approached the Keys as an intense tropical cyclone.

Although it appears that pre-landfall winds are important for generating high-magnitude storm surges, storm size is important for generating extensive surge events, which may actually inundate more area than a surge with a higher peak magnitude. Hurricane Ike's large size enabled this storm to inundate areas in Southeast Louisiana that were not likely flooded from the 1900 Galveston Hurricane. This observation provides an important caveat to this study- my results have only tested the relationship between pre-landfall winds and peak surge levels, but I have not considered the extent of storm surge or area of inundation. Emergency management personnel and other coastal stakeholders should be aware that tropical cyclones with large wind fields have the capacity to inundate long stretches of coastline, which may flood areas far from the region of landfall.

This study also found that the relationship between maximum winds and surge heights is more non-linear than previously expected. A test run on the 63 wind/ surge events since 1960 showed the wind/ surge relationship correlates best when wind values from 18 hours before landfall are raised to an exponential power of 2.2, producing an R-squared value of .6948. However, existing literature on this relationship suggested the optimal exponential power should be less than two (Jordan and Clayson 2008). The relationship between maximum sustained winds and peak surge levels is surprisingly non-linear, as these values indicate that doubling the maximum sustained winds of tropical cyclones increases surge potential by a factor of 4.59. As tropical cyclones may strengthen in a warmer climate (Emanuel 2005; Anthes et al. 2006; U.S. Global Change

Research Program 2009), this finding may have dire consequences for coastal regions, because even modest increases in tropical cyclone wind speeds would produce relatively large increases in surge height. Sea-level rise, which is accelerating at many locations (Zervas 2001), may also exacerbate storm surge inundations in the future.

These results will likely improve storm surge modeling as scientists give more weight to pre-landfall winds in surge forecasts. Although such models may utilize pre-landfall wind speeds 18 hours before landfall as an important indicator of storm surge potential, the forecasts may actually be issued at least several days before landfall. The scientific literature on the physical processes that generate storm surge contains little information on the importance of pre-landfall winds, so these results have not likely been incorporated into forecasting algorithms. These findings may help surge forecasts improve considerably, as pre-landfall tropical cyclone wind forecasts tend to be more accurate than landfall wind forecasts.

These results may have implications for disaster science/ emergency management professionals, especially for hurricanes that are rapidly strengthening or weakening just before landfall. Local authorities may want to prepare more for a wind event in storms that rapidly strengthen just prior to landfall, a surge event in storms that were once intense, but rapidly weaken before landfall, and both hazards for storms that hold consistent intensity as they approach the coast.

The benefits of improved evacuation decisions are substantial, as evacuations are costly. It is estimated that the cost to evacuate one mile of coastline is approximately 1 million U.S. dollars (Adams and Berri 1999; Whitehead 2003; Wolshon et al. 2005; Regnier 2008). The cumulative cost of false hurricane evacuations is staggering; such

false alarms cost an average of more than 1 billion U.S. dollars per year from 2000-2006 (Regnier 2008). Also, local authorities may lose credibility after false evacuation orders, making the public more likely to turn to other information sources in future storms (Dow and Cutter 1998).

Although this chapter focused on the influence of maximum sustained wind speeds for storm surge generation in tropical cyclones, future research could focus on the influence of multiple parameters for generating surge, including tropical cyclone size, forward speed, and pre-landfall wind velocity, as well as non-storm variables, such as bathymetry and coastal shape. Emerging fields in computer science, such as data mining, machine learning and geoinformatics, may be useful for such analyses, because multiple variables interact simultaneously to generate storm surge as a tropical cyclones approaches the coastline. Such methods could potentially unravel complex relationships between variables, such as the influence of tropical cyclone size for generating storm surge over shallow bathymetry, or the expected difference in surge heights from two storms with identical size and bathymetry but different pre-landfall wind speeds. Such data-driven research may offer new insights not provided by hydrodynamical models.

Future studies could also investigate the role of pre-landfall winds in other ocean basins vulnerable to tropical cyclone-generated storm surges. Such efforts may reveal how variations in coastal shape and bathymetry may affect the correlation between pre-landfall winds and storm surge magnitude. The potential for such projects exist in every ocean basin vulnerable to storm surge, as the SURGEDAT database develops internationally.

3.7 References

- Adams, C.R., and D.J. Berri, 1999: The economic cost of hurricane evacuations. *First U.S. Weather Res. Program Sci. Sympos.*, March 29-31, http://www.esrl.noaa.gov/research/uswrp/abstracts/Adams_Christopher.html.
- Anthes, R.A., R.W. Corell, G. Holland, J.W. Hurrell, M.C. MacCracken, and K.E. Trenberth, 2006: Hurricanes and Global Warming- Potential Linkages and Consequences. *Bulletin of the American Meteorological Society*, 87, 623-628.
- Barnes, J., 2007: *Florida's Hurricane History*, 3rd Edition, University of North Carolina Press, Chapel Hill, North Carolina, USA, 407 pp.
- Berg, R., 2010: Tropical Cyclone Report, Hurricane Ike. The National Hurricane Center, Miami, Florida, United States. Report made available on the Web at: www.nhc.noaa.gov/pdf/TCR-AL092008_Ike_3May10.pdf.
- Bevan II, J.L., L.A. Avila, E.S. Blake, D.P. Brown, J.L. Franklin, R.D. Knabb, R. J. Pasch, J.R. Rhome, and S.R. Stewart, 2008: Annual Summary, Atlantic Hurricane Season of 2005. *Monthly Weather Review*, 136, 1109-1173.
- Blain, C.A., J.J. Westerink, and R.A. Luettich, 1998: Grid convergence studies for the prediction of hurricane storm surge. *International Journal of Numerical Methods Fluids*, 26, 369-401.
- Case, R.A., 1986: Annual Summary, Atlantic Hurricane Season of 1985. *Monthly Weather Review*, 114, 1390-1405.
- Chen, Q., L. Wang, and R. Tawes, 2008: Hydrodynamic response of northeastern Gulf of Mexico to hurricanes. *Estuaries and Coasts*, 31, 1098-1116.
- Demuth, J., M. Demaria, and J.A. Knaff, 2006: Improvement of advanced microwave sounder unit tropical cyclone intensity and size estimation algorithms. *Journal of Applied Meteorology*, 45, 1573-1581.
- Dietrich, J.C., M. Zijlema, J.J. Westerink, L.H. Holthuijsen, C. Dawson, R. A. Luettich, Jr., R. Jensen, J.M. Smith, G.S. Stelling, and G.W. Stone, 2011: Modeling Hurricane Waves and Storm Surge using Integrally-Coupled, Scalable Computations. *Coastal Engineering*, 58, 45-65.
- Dow, K., and S.L. Cutter, 1998: Crying wolf: Repeat responses to hurricane evacuation orders. *Coastal Management*, 26, 4, 237-252.
- Dvorak, V.F., 1984: Tropical Cyclone Intensity Analysis Using Satellite Data. NOAA Technical Report NESDIS 11. National Oceanic and Atmospheric Administration, U.S. Department of Commerce. Report available on the Web at: ftp://satepsanone.nesdis.noaa.gov/Publications/Tropical/Dvorak_1984.pdf.

Elsner, J.B., and T.H. Jagger, 2013: *Hurricane Climatology: A Modern Statistical Guide Using R*. Oxford University Press, New York, USA. 430 pp.

Emanuel, K., 2005: Increasing destructiveness of tropical cyclones over the past 30 years. *Nature*, 436, 686-688.

Fett, R.W., 1964: Some characteristics of the formative stage of typhoon development: A satellite study. National Conference on Physics and Dynamics of Clouds, Chicago, IL, March 24-26, U.S. Weather Bureau, U.S. Department of Commerce, National Oceanic and Atmospheric Administration, National Earth Satellite Service, Washington, D.C., 20233, 10 pp.

Franklin, J.L., R. J. Pasch, L.A. Avila, J.L. Bevin II, M.B. Lawrence, S.R. Stewart, and E.S. Blake, 2006: Annual Summary, Atlantic Hurricane Season of 2004. *Monthly Weather Review*, 134, 981-1025.

Garriott, E.B., 1900: West Indian Hurricane of September 1-12, 1900. Published in the *Monthly Weather Review*, 28, 371-377. Edited by C. Abbe. Available on the Web at: <http://www.aoml.noaa.gov/general/lib/lib1/nhclib/mwreviews/1900.pdf>.

Ho, F.P., R.W. Schwerdt, and H.V. Goodyear, 1975: *NOAA Technical Report NWS 15: Some Climatological Characteristics of Hurricanes and Tropical Storms, Gulf and East Coasts of the United States*. Washington, D.C., 87 pp.

Hsu, S.A., and A. Babin, 2005: Estimating the Radius of Maximum Winds Via Satellite During Hurricane Lili (2002) over the Gulf of Mexico. Unpublished paper made available by S.A. Hsu at Louisiana State University. Available on the Web at: www.nwas.org/ej/hsu/hsu_babin_2005.pdf.

Irish, J.L., D.T. Resio, and J.J. Ratcliff, 2008: The Influence of Storm Size on Hurricane Surge. *Journal of Physical Oceanography*, 38, 2003-2013.

Jordan, II, M.R., and C.A. Clayson, 2008: A new approach to using wind speed for prediction of tropical cyclone generated storm surge. *Geophysical Research Letters*, 35, doi: 10.1029/2008GL033564.

Keim, B., R. Muller, and G. Stone, 2007: Spatiotemporal Patterns and Return Periods of Tropical Storm and Hurricane Strikes from Texas to Maine. *Journal of Climate*, 20, 3498-3509.

Keim, B.D., and R.A. Muller, 2009: *Hurricanes of the Gulf of Mexico*. Louisiana State University Press, 216 pp.

Knabb, R.D. J.R. Rhome, and D.P. Brown, 2011: Tropical Cyclone Report, Hurricane Katrina, 23-30 August 2005. Report produced by the National Hurricane Center, Miami, Florida, and published on the Web at: http://www.nhc.noaa.gov/pdf/TCR-AL122005_Katrina.pdf.

Landsea, C.W., C. Anderson, N. Charles, G. Clark, J. Dunion, J. Fernandez-Partagas, P. Hungerford, C. Neumann, and M. Zimmer, 2003: The Atlantic Hurricane Database Re-analysis Project Documentation for 1851-1910 Alterations and Addition to the HURDAT Database. Revised 6 January 2003. Publication available on the Web at: www.aoml.noaa.gov/hrd/hurdat/Documentation.html.

Larson, E., 1999: *Isaac's Storm*. Crown Publishers. New York. 323 pp.

National Hurricane Center, Miami, Florida, 1985. Preliminary Report, Hurricane Danny, 12 to 20 August 1985. Published on the Web at: http://www.nhc.noaa.gov/archive/storm_wallets/atlantic/atl1985-prelim/danny/prelim01.gif.

National Hurricane Center, Miami, Florida, 1988. Preliminary Report, Hurricane Gilbert, 08-19 September 1988. Published on the Web at: http://www.nhc.noaa.gov/archive/storm_wallets/atlantic/atl1988-prelim/gilbert/prelim01.gif.

National Hurricane Center, Miami, Florida, 2004: Hurricane Charley Special Advisory Number 18 Correction, 2PM EDT, Fri Aug 13, 2004. Available on the Web at: <http://www.nhc.noaa.gov/archive/2004/pub/al032004.public.018.shtml?>

National Hurricane Center, Miami, Florida, 2012a: Glossary of NHC Terms. Available on the Web at: <http://www.nhc.noaa.gov/aboutgloss.shtml>.

National Hurricane Center, Miami, Florida, 2012b: Hurricane Isaac Intermediate Advisory Number 32B, 0200AM CDT, Wed Aug 29, 2012. Available on the Web at: http://www.nhc.noaa.gov/archive/2012/al09/al092012.public_b.032.shtml?

National Institute of Standards and Technology, 2013: *Engineering Statistics Handbook*. Available on the Web at: <http://www.itl.nist.gov/div898/handbook/eda/section3/eda33j.htm>.

National Oceanic and Atmospheric Administration Comprehensive Large Array-Data Stewardship System (CLASS), 2013: Web portal for satellite imagery. Available on the Web at: www.class.ngdc.noaa.gov/saa/products/welcome.

Needham, H.F. and B.D. Keim, 2011: Storm surge: physical processes and an impact scale. In *Recent Hurricane Research- Climate, Dynamics, and Societal Impacts*, Lupo E (ed). Intech Open Access: Croatia.

Needham, H.F., and B.D. Keim, 2012: A Storm Surge Database for the U.S. Gulf Coast. *International Journal of Climatology*, 32, 14, 2108-2123. DOI: 10.1002/joc.2425.

Needham, H.F., B.D. Keim, D. Sathiaraj, and M. Shafer, 2013: A Global Database of Tropical Storm Surges. *EOS, Transactions American Geophysical Union*, 94, 24, 213-214.

Pasch, R.J., M.B. Lawrence, L.A. Avila, J.L. Beven, J.L. Franklin, and S.R. Stewart, 2004: Atlantic Hurricane Season of 2002. *Monthly Weather Review*, 132, 1829-1859.

Pasch, R.J., D.P. Brown, and E.S. Blake, 2011: Tropical Cyclone Report, Hurricane Charley, 9-14 August 2004. National Hurricane Center, Miami, FL. Report available on the Web at: http://www.nhc.noaa.gov/pdf/TCR-AL032004_Charley.pdf.

R Development Core Team, 2010: *R: A Language and Environment for Statistical Computing*. Vienna, Austria: R Foundation for Statistical Computing. ISBN 3-900051-07-0.

Regnier, E., 2008: Public Evacuation Decisions and Hurricane Track Uncertainty. *Management Science*, 54, 1, 16-28.

Risi, J. A., H. R. Wanless, L. P. Tedesco, and S. Gelsanliter. 1995. Catastrophic sedimentation from Hurricane Andrew along the southwest Florida coast. *Journal of Coastal Research*, Special Issue 21:83-102.

Shay, L.K., and E.W. Uhlhorn, 2007: Loop Current Response to Hurricanes Isidore and Lili. *Monthly Weather Review*, 136, 3248-3274.

Simpson, R.H., A.L. Sugg and Staff, 1970: The Atlantic Hurricane Season of 1969. *Monthly Weather Review*, 98, 4, 293-306. The National Hurricane Center, Weather Bureau, ESSA, Miami, Florida, United States. Report available on the Web at: <http://www.aoml.noaa.gov/general/lib/lib1/nhclib/mwreviews/1969.pdf>.

Simpson, R.H., and H. Riehl, 1981: *The Hurricane and Its Impact*. Louisiana State University Press, Baton Rouge, Louisiana, 398 pp.

Smith, III, T.J., G.H. Anderson, K. Balentine, G. Tiling, G.A. Ward, and K.R.T. Whelan, 2009: Cumulative Impacts of Hurricanes on Florida Mangrove Ecosystems. *Wetlands*, 29, 1, 24-34.

Spiegel, M.R., 1961: *Schaum's Outline of Theory and Problems of Statistics*. Published in New York by McGraw-Hill Book Company. 359 pp.

Tedesco, L. P., H. R. Wanless, L. A. Scusa, J. A. Risi, and S. Gelsanliter. 1995. Impacts of Hurricane Andrew on south Florida's sandy coastlines. *Journal of Coastal Research*, Special Issue 21:59-82.

Timchalk, A., L. Hubert, and S. Fritz, 1965: Wind speeds from TIROS pictures of storms in the tropics. MSL Report No. 33, U.S. Weather Bureau, U.S. Department of Commerce, National Oceanic and Atmospheric Administration, National Earth Satellite Service, Washington, D.C., 20233, 33 pp.

Unisys Corporation, 2013: 1985 Hurricane/Tropical Data for Atlantic. Available on the Web at: <http://www.weather.unisys.com/hurricane/atlantic/1985/index.php>.

URS Corporation, 2008: *Texas Hurricane Ike Rapid Response Coastal High Water Mark Collection*. Prepared for FEMA. October 2008.

U.S. Corps of Engineers, 1935: 1935 Labor Day Hurricane, Limits of Destruction and Storm Surge Heights. Chart File No. 3-16-10,409 produced on October 21, 1935. Published in Knowles, T.N., 2009: *Category 5: The 1935 Labor Day Hurricane*. University Press of Florida, 350 pp.

U.S. Global Change Research Program, 2009: *Global Change Impacts in the United States*. Cambridge University Press, 188pp.

Wang, R., M. Manausa, and J. Cheng, 2005: *Hurricane Charley Characteristics and Storm Tide Evaluation*. Beaches and Shores Resource Center, Institute of Science and Public Affairs, Florida State University. Available on the Web at: <http://bcs.dep.state.fl.us/reports/strmtide/charley.pdf>.

Weisberg, R.H., and L. Zheng, 2006: Hurricane Storm Surge Simulations for Tampa Bay. *Estuaries and Coasts*, 29, 899-913.

Westerink, J.J., R.A. Luetich, J.C. Feyen, J.H. Atkinson, C. Dawson, H.J. Roberts, M.D. Powell, J.P. Dunion, E.J. Kubatko, and H. Pourtaheri, 2008: A Basin- to Channel-Scale Unstructured Grid Hurricane Storm Surge Model Applied to Southern Louisiana. *Monthly Weather Review*, 136, 833-864.

Whitehead, J.C., 2003: One million dollars per mile? The opportunity costs of hurricane evacuation. *Ocean Coastal Management*, 46, 11-12, 1069-1083.

Wolshon, B., E. Urbina, C. Wilmot, and M. Levitan, 2005: Review of Policies and Practices for Hurricane Evacuation. I: Transportation Planning, Preparedness, and Response. *Natural Hazards Review*. 6(3).

Zervas, C., 2001: Sea Level Variations of the United States 1854-1999. NOAA Technical Report NOS CO-OPS 36. Available on the Web at: <http://tidesandcurrents.noaa.gov/publications/techrpt36doc.pdf>.

CHAPTER 4. AN EMPIRICAL ANALYSIS ON THE RELATIONSHIP BETWEEN TROPICAL CYCLONE SIZE AND STORM SURGE HEIGHTS ALONG THE U.S. GULF COAST

4.1 Introduction

In the past decade, numerous tropical cyclones have generated destructive storm surges along the U.S. Atlantic and Gulf Coasts. While the maximum sustained wind speed of these storms differed considerably, large geographic cyclone size was a common feature among many of these high-profile storms. These disasters have made us reconsider how tropical cyclones generate storm surge.

In 2005, Hurricane Katrina generated a catastrophic storm surge that reached a maximum level of 8.47 m along the Mississippi Coast (Knabb et al. 2011). This was the highest modern-day storm surge level in the United States (Needham and Keim 2012). This storm surge overwhelmed many levees in southeast Louisiana, which led to the flooding of approximately 80% of New Orleans (Kates et al. 2006). The \$81 billion in damage from this storm (McTaggart-Cowan et al. 2008) ranks Katrina as the most costly natural disaster in U.S. history (Kessler et al. 2006). Katrina's large size contributed to this massive storm surge, enabling it to generate a higher storm surge than Hurricane Camille, even though Camille produced stronger winds when it struck the same area in 1969 (Irish et al. 2008).

Three years later, Hurricane Ike generated a 5.33-meter surge in Chambers County, Texas (Berg 2010). This surge level surprised many people, because Ike approached the Texas Coast as a category-2 hurricane on the Saffir-Simpson Scale, with maximum sustained winds of 176 km/hr (95 knots) (Berg 2010). At that time, the National Oceanic and Atmospheric Administration (NOAA) generalized category-2

hurricanes as having the potential to generate surge levels from 1.8 – 2.4 m (Irish et al. 2008). After Hurricane Ike, NOAA removed storm surge heights from the Saffir Simpson Scale, as it became apparent that maximum sustained wind speeds at landfall are not always a good indicator of surge potential. It is thought that Ike's large size contributed to this massive storm surge. As Ike approached the Texas Coast, tropical storm force winds extended as far as 296 km (160 nmi), and hurricane force winds extended as far as 204 (110 nmi) from the center of circulation (Demuth et al. 2006).

In 2012, Hurricane Isaac generated a large storm surge in Southeast Louisiana and Mississippi. Storm tide levels exceeded 3 m in at least two Mississippi counties and four Louisiana parishes east of the Mississippi River (McCallum et al. 2012). In portions of Plaquemines Parish, Louisiana, storm tide levels exceeded 4.3 m (McCallum et al. 2012). Isaac's large size likely contributed to this massive coastal flooding event, as the storm became a hurricane just hours before landfall in Southeast Louisiana (Berg 2013). Hurricane Isaac produced tropical storm force winds up to 333 km (180 nmi) from the center of circulation for several days before making landfall, and hurricane force winds up to 111 km (60 nmi) from the center of circulation in the hours before landfall (Demuth et al. 2006). Also, the slow forward movement of Isaac may have also contributed to the large surge, as the duration of persistently strong winds was high in certain locations.

Two months after Isaac, Hurricane Sandy generated a destructive storm surge that flooded much of the U.S. Mid-Atlantic Coast, including portions of the greater New York City metropolitan area. The storm caused approximately \$50 billion in economic losses and killed 147 people (Blake et al. 2012). Damage from Sandy's surge included more than \$5 billion in losses to mass transit infrastructure (Bernstein 2013), as the storm surge

inundated lower Manhattan and flooded the subway system. Sandy's large size likely contributed to its devastating storm surge. Several hours before landfall on the New Jersey Coast, Sandy generated a massive wind field, with tropical storm force winds extending 778 km (420 nmi) and hurricane force winds extending 333 km (180 nmi) from the center of circulation (Demuth et al. 2006). From another perspective, the diameter of tropical storm force winds was approximately 1519 km (820 nmi), which is greater than the driving distance from Atlanta to New York (Erdman 2012).

These surge events have attracted much attention, and several publications have now investigated the role of hurricane size for generating storm surge. For example, Irish et al. (2008) found that hurricane size plays a key role for storm surge generation, particularly over mildly-sloping bathymetry. They also estimate that differences in storm size may cause storm surge heights to vary as much as 30%. Nielsen (2009) stated that these observations are mimicked by a simple power fit, and further investigated the role of storm size on surge height using 1D and 2D analyses.

Although these papers provided new insights into the influence of tropical cyclone size on storm surge generation, the approach of these analyses relied heavily on modeling. A thorough literature review on this topic reveals that no studies have relied on empirical analysis to investigate this topic. As such, this chapter investigates the role of tropical cyclone size for generating storm surges along the U.S. Gulf Coast by: 1) building a comprehensive tropical cyclone size data set; 2) correlating various tropical cyclone size parameters with observed storm surge heights; and 3) investigating relationships between tropical cyclone size and maximum sustained wind speeds.

4.2 Data

4.2.1 Storm Surge Data

Storm surge data are provided by SURGEDAT, a global surge database that provides more than 7,600 high-water marks from storm surge events in the U.S. since 1880 (Needham and Keim 2012; Needham et al. 2013). I chose the U.S. Gulf Coast as the geographic region for this analysis based on the excellent quality of surge data provided by SURGEDAT for this region. The database provides the location and height of peak storm surge for 191 surge events along this coastline since 1880, as well as widespread coverage of observations for 110 individual Gulf Coast storms, supported by approximately 5,200 high-water marks. An updated surge dataset is available for download at <http://surge.srcc.lsu.edu>.

4.2.2 Tropical Cyclone Wind and Position Data

Tropical cyclone wind and position data are provided by Elsner and Jagger (2013). This dataset provides hourly information on tropical cyclone maximum sustained winds, forward speed, direction and position. The authors utilized spline interpolation to provide non-linear tropical cyclone data from 6-hour observations provided by HURDAT (Atlantic Oceanographic and Meteorological Laboratory 2006).

4.2.3 Tropical Cyclone Size Data

A thorough literature review reveals that many sources provide tropical cyclone size data. These sources provide a variety of temporal coverage, hurricane size parameters and units of measurement. The most common measurement type is radius of maximum wind (Rmax), which measures the distance from the center of the hurricane eye to the peak wind speed, usually observed in the eye wall. Distances are usually

provided in nautical miles, although some sources list distances in kilometers.

The Atlantic Oceanographic and Meteorological Laboratory (AOML) HURDAT Re-Analysis Project provides four datasets that include hurricane size information. These data provide a comprehensive reanalysis of hurricane characteristics, including the radius of maximum winds. AOML provides data for the years 1851-1910 (Landsea et al. 2003), 1911-1920 (Landsea et al. 2007), 1921-1930 (Landsea et al. 2011), and 1944-1953 (Hagen et al. 2012).

Various other sources provide hurricane size data, listed as radius of maximum wind. Simpson and Riehl (1981) provide data for 59 hurricanes from 1893-1979, Ho et al. (1975) provide data from 1900-1969, and Irish et al. (2008) provide data for 22 selected hurricanes from 1941-2005. All of these sources only provide the distance of Rmax. Powell and Reinhold (2007) provide storm size data for 18 hurricane landfalls in the U.S. from 1989-2005, as well as Hurricane Camille, in 1969. Data are provided as Rmax, as well as radius of 34-knot, 50-knot and 64-knot winds, all listed in kilometers. Demuth et al. (2006) provide hurricane size data in six-hour intervals for tropical systems from 1988- present, listed as Rmax, eye diameter, radius of the outer closed isobar, and radii of 34-knot wind, 50-knot wind and 64-knot winds, all in nautical miles. Although this source was originally published in 2006, the web site associated with this publication is updated annually. This is the only source that provides hurricane size data in various time intervals, providing insight into the variation of hurricane size over time for specific storms.

4.3 Methods

The first step in this analysis involved creating a comprehensive tropical cyclone size dataset because each of the (nine) size sources provides data for a select period of time, but no source provides a comprehensive archive of complete size data. I archived the size of R_{max} , as this measurement type is the most common in historical literature, as well as the radius of 63 km/hr (34-kt), 93 km/hr (50-kt), and 119 km/hr (64-kt) winds, even though these data are only available since 1988.

As this chapter investigates the role of tropical cyclone size for generating storm surge, it is only necessary to archive size data for storms with useable storm surge data. Although SURGEDAT provides peak storm-surge data for 191 events along the U.S. Gulf Coast since 1880, it is not necessary to obtain size data for all of these events because only surge events that are identified near the location of a tropical cyclone landfall will be used in this study. This methodology follows the approach used by in Chapter 3, where a landfall classification system that categorized surge events into 14 categories, depending on the relationship between the tropical cyclone track and peak surge location. Of the 189 surge events analyzed between 1880-2011, 117 provided useable data in which a peak storm surge position was located near a landfalling tropical cyclone, while 72 events were removed from the analysis, due to disconnects in time and space of the storm track and the surge event. A list of the event types that were removed from this analysis are provided in Table 4.1.

Table 4.1. Landfall/ surge event types that were removed from analysis in Chapter 3. A total of 72 events were removed from the analysis.

| Event Type | Number of Events | Storm Name (Year) |
|--|------------------|-------------------------------|
| Storm tracks closest to location of peak surge four or more hours after the Closest Offshore Observation (COO) | 22 | Tropical Storm Matthew (2004) |
| Peak surge located to the left of landfall | 17 | Unnamed (1916) |
| Landfall location “far” from location of peak surge | 24 | Gilbert (1988) |
| Tropical cyclone moving offshore as it generates peak surge | 9 | Unnamed (1947) |

This landfall classification system defined the landfall location as the Closest Offshore Observation (COO), which was the offshore tropical cyclone position closest to the location of peak storm surge. However, 22 tropical cyclones were removed because four or more hours passed between the time of COO and the time when the tropical cyclone actually tracked closest to the location of peak surge. In these cases, the tropical cyclone tracked inland toward the location of peak surge for at least four hours after COO, which means the storm conditions near the location of peak surge may have differed considerably from the conditions when the cyclone made landfall. In many of these cases, the peak surge occurred on a bay, enabling the storm track to make its closest approach to the location of peak surge while the storm was located inland for several

hours. Peak surge events that were located to the “left” of tropical cyclone tracks were also removed from this analysis. These 17 events were excluded from the study because peak surge heights usually occur to the “right” of tropical cyclone tracks in the Northern Hemisphere, so it is possible that SURGEDAT is missing the actual location and height of peak surge for these events, or extreme extenuating circumstances prevailed in the storm track and/or the coastal geomorphology. Tropical cyclones that tracked too far away from the location of peak surge were also excluded from this analysis. The 24 events that fall into this category often include tropical cyclones that made landfall far south of the Texas/ Mexico border, but still produced a surge observation in South Texas, as well as tropical cyclones that track well south of the Florida Keys, but still generate elevated seas along the island chain. Tropical cyclones that made landfall more than 159 km (86 nmi) from the location of peak surge were removed from this analysis, as this distance represents the average extent of tropical storm force winds in Category 1 and 2 hurricanes (Keim et al. 2007). The final event type that was removed from this analysis included cyclones that generated a peak surge along the West Coast of Florida as they tracked westward off the Peninsula. These nine events were removed because the tropical cyclones were not making landfall, but moving from land to water as they generated a storm surge event.

Although the landfall classification system adds some complexity, it improves the analysis by providing a consistent method for determining landfall, while removing missing or inaccurate surge data. The cyclone size analysis provides data for as many of the 117 useable surge events as possible, as well as Tropical Storm Debby and Hurricane Isaac, which both occurred in 2012 and were not included in the previous analysis.

Tropical cyclone size data were provided as a measure of Rmax size for 83 of these 119 surge events. Most sources provided one Rmax size per tropical cyclone, however, Demuth et al. (2006) provided values at 6-hour intervals for 31 out of 33 tropical cyclones since 1988. This source was missing Rmax data for hurricanes Chantal and Jerry, which both produced peak surge observations in Texas in 1989. For cases in which Rmax sizes changed as a tropical cyclone approached the coast, the Rmax size at 18 hours before landfall was utilized to represent the storm characteristics as the cyclone approached the coast. This specific time interval was determined because results in Chapter 3 proved that surge heights correlate best with wind speeds 18 hours before landfall.

Demuth et al. (2006) also provided the radius of 63 km/hr (34-kt), 93 km/hr (50-kt) and 119 km/hr (64-kt) winds for tropical cyclones from 1988-2012. These distances were archived at landfall and 18 hours before landfall. This source provided distance in nautical miles (nmi) to the northeast, southeast, southwest and northwest of the storm center. I chose the greatest distance and employed interpolation techniques if the time of landfall fell between 6-hour observations. Following the methodology established in Chapter 3, I did not archive data if the tropical cyclone was not centered over the Gulf of Mexico or approaching the Florida Keys from the Atlantic. As such, size observations were not archived for Hurricane Charley at 18 hours before landfall, as this storm was centered in the Caribbean Sea, south of Cuba, at this time. The Rmax size of Charley consistently remained at 19 km (10 nmi) from this time until it crossed Cuba and made landfall in Florida, so I used the Rmax size from the Florida landfall. Although Powell and Reinhold (2007) also provided the radius of 63 km/hr (34-kt), 93 km/hr (50-kt) and

119 km/hr (64-kt) wind fields for Hurricane Camille, these data were not utilized because they relied heavily on modeling, while this chapter relies on empirical observations.

After building this tropical cyclone size dataset, I identified the largest and smallest tropical cyclones, as well as the average size of these storms. I also analyzed the correlation between various tropical cyclone size parameters, as well as the relationship between those parameters and storm surge heights.

4.4 Results

4.4.1 Analysis of Rmax Size for Storm Surge Generation

The average Rmax size of the 83 events was 48.3 km (26.08 nmi). The 31 Rmax sizes provided by Demuth et al. (2006) show some change in size as tropical cyclones approach the coast. At landfall, the average Rmax size of these events was 61.41 km (33.16 nmi), while the average size at 18 hours before landfall was 67.1 km (36.23 nmi). These results may indicate that Rmax sizes tend to decrease as a tropical cyclone approaches the coast, however, these values were only calculated for a subset of storms for which accurate storm surge data were available, and may not represent patterns found in more extensive analyses. It is unclear why the average size of the storms provided by Demuth et al. (2006) is noticeably larger than the average size for the entire dataset. While changes in detection methodologies are a possible explanation, it is also noteworthy that many of the smallest tropical cyclones, like Hurricane Camille and the 1935 Labor Day Hurricane, occurred before 1988, so they are not included in the data provided by Demuth et al. (2006).

The three storms with the largest Rmax sizes were tropical storms that produced peak surge heights along the west coast of Florida. Tropical Storm Josephine had an

Rmax size of 167 km (90 nmi) in 1996, the Rmax size for Tropical Storm Keith in 1988 was 141 km (76 nmi), and Tropical Storm Debby's Rmax size was 139 km (75 nmi) in 2012.

The storms with the smallest Rmax sizes were intense tropical cyclones that made landfall as major hurricanes. The Rmax size of Hurricane Dennis in 2005 was 9 km (5 nmi), the 1935 Labor Day Hurricane had an Rmax size of 11 km (6 nmi), and Hurricane Camille had an Rmax size of 15 km (8 nmi) in 1969. The 1935 Labor Day Hurricane and Hurricane Camille both made landfall as category-5 hurricanes.

The pattern shown in these events reveals an inverse relationship between Rmax sizes and maximum sustained wind speeds.. The storms with the largest Rmax sizes tend to be less intense, while the most intense tropical cyclones that have struck the United States tended to have small Rmax sizes. This observation is supported statistically, as the Pearson correlation of Rmax sizes and maximum sustained wind speeds 18 hours before landfall is inverse. The r-value of this correlation is 0.46 and the correlation is significant at the 99.9% confidence interval.

The inverse relationship between Rmax sizes and maximum sustained wind speeds raises an interesting question related to storm surge generation. If tropical cyclone size, defined as the Rmax size, relates inversely with maximum sustained wind speeds, which of these two parameters correlates better with storm surge heights? Statistical analysis of these variables reveals that storm surge magnitudes correlate inversely with Rmax sizes, with a Pearson correlation r-value of 0.0902, significant at the 99% confidence level (Figure 4.1). These results indicate tropical cyclones with small Rmax sizes often produce larger storm surge magnitudes than tropical cyclones with large

Rmax sizes. However, a Pearson correlation test shows that storm surge heights correlate positively with maximum sustained winds 18 hours before landfall for these 83 tropical cyclones, producing an R-squared value of 0.62, significant at the 99.9% confidence level. These values are comparative to results provided in Chapter 3, where the relationship between storm-surge heights and pre-landfall winds produces R-squared values of 0.60 for 117 events from 1880-2011 and 0.66 for 63 events from 1960-2011.

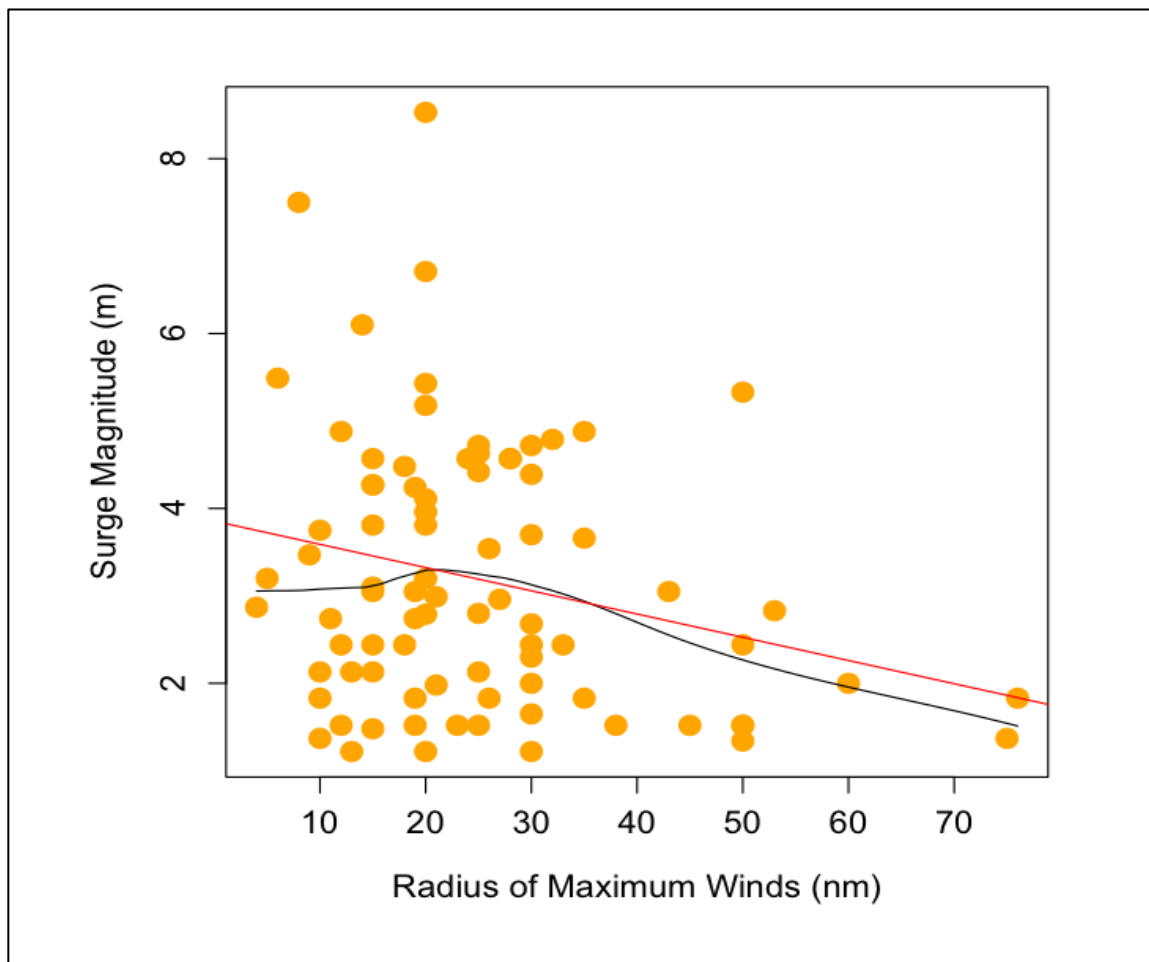


Figure 4.1. LOESS (black line) and linear (red line) regression models for the relationship between surge heights and the radius of maximum winds (nmi). Orange circles depict observed events.

Although it may seem counterintuitive that tropical cyclones with larger R_{max} sizes tend to generate smaller storm surges, historical examples support these results. For example, the three tropical cyclones with the largest R_{max} sizes, tropical storms Josephine, Keith and Debby, generated an average surge height of 2.01 m, while the three tropical cyclones with the smallest R_{max} sizes, Hurricane Dennis, the 1935 Labor Day Hurricane, and Hurricane Camille, generated an average surge magnitude of 5.40 m.

A comparison between the 1900 Galveston Hurricane and Hurricane Ike in 2008 provides a helpful comparison, because both storms tracked across the Gulf of Mexico from southeast to northwest and made landfall on Galveston Island, Texas. The 1900 Galveston Hurricane was a small storm, with a radius of maximum winds of 26 km (14 nmi) (Ho et al. 1975; Simpson and Riehl 1981; Landsea et al. 2003), while Hurricane Ike was larger. The radius of maximum winds for Hurricane Ike was 92 km (50 nmi) at 18 hours before landfall and 56 km (30 nmi) at landfall (Demuth et al. 2006). Although Ike was a larger storm, it generated a peak surge level of 5.33 meters in Chambers County, Texas (Berg 2010), while the 1900 Galveston Hurricane generated a peak surge of 6.1-meters (Garriott 1900), which devastated Galveston Island.

The storm surge history of the Florida Keys provides further evidence for the inverse relationship between surge magnitudes and R_{max} sizes. I have listed the surge magnitude, R_{max} size and the wind speed 18 hours before landfall for the 13 Florida Keys surge events analyzed in this study (Table 4.2). This region is chosen because this island chain has relatively consistent bathymetry, without the presence of large bays or sounds, which enhance surge heights (Needham and Keim 2011).

Table 4.2. Comparison of storm surge heights, hurricane size and maximum sustained wind speed at 18 hours before landfall for the 13 Florida Keys surge events analyzed in this study. Data compiled from Ho et al. (1975), Landsea et al. (2003), Demuth et al. (2006), Landsea et al. (2007), Landsea et al. (2011), and Hagen et al. (2012).

| Storm Name | Year | Peak Surge Location | Surge Height (m) | Rmax in km (nmi) | 18 hour wind in km/hr (kts) | Surge Rank | Wind Rank | Size Rank |
|------------|------|-----------------------|------------------|------------------|-----------------------------|------------|-----------|-----------|
| Unnamed | 1910 | Key West | 4.57 | 52 (28) | 237 (128) | 2 | 2 | 4 |
| Unnamed | 1919 | Cow Key | 4.27 | 28 (15) | 209 (113) | 3 | 4 | 9 |
| Unnamed | 1929 | Key Largo | 2.68 | 56 (30) | 198 (107) | 6 | 6 | 1 |
| Labor Day | 1935 | Lower Matecumbe | 5.49 | 11 (6) | 219 (118) | 1 | 3 | 12 |
| Unnamed | 1948 | Key West | 1.83 | 19 (10) | Outside GOM | 8 | - | 10 |
| Donna | 1960 | Upper Matecumbe | 4.11 | 37 (20) | 239 (129) | 4 | 1 | 6 |
| Isbell | 1964 | Key West | 1.37 | 19 (10) | Outside GOM | 11 | - | 10 |
| Betsy | 1965 | North Key Largo | 2.74 | 35 (19) | 204 (110) | 5 | 5 | 7 |
| Inez | 1966 | Big Pine Key | 1.52 | 35 (19) | 139 (75) | 9 | 8 | 7 |
| Floyd | 1987 | Lower and Middle Keys | 1.22 | No Data | Outside GOM | 12 | - | No Data |
| Gordon | 1994 | Upper FL Keys | 1.22 | 56 (30) | 83 (45) | 12 | 10 | 1 |
| Georges | 1998 | Florida Keys | 2.3 | 56 (30) | 144 (78) | 7 | 7 | 1 |
| Rita | 2005 | Key West | 1.52 | 46 (25) | 109 (59) | 9 | 9 | 5 |

The four hurricanes with the strongest pre-landfall winds in this region generated the four largest surge events, although not in rank order. However, the hurricanes with the four largest Rmax sizes generated the 6th, 7th, 9th and 12th largest surges. The 1935 Labor Day Hurricane was the smallest storm in this archive, but it produced the largest modern-day surge height in the Florida Keys. Although the radius of maximum winds for this event was only 11 km (6 nmi) (Ho et al. 1975), this storm generated a massive 5.49-meter surge (U.S. Corps of Engineers 1935), which was the sixth highest magnitude

surge event along the U.S. Gulf Coast in the past 132 years, according to the SURGEDAT database. This storm was a category-4 hurricane, with maximum sustained winds of 218 km/hr (118 knots), 18 hours before landfall. It further intensified into the first category-5 hurricane to make landfall in the United States (National Weather Service 2010).

4.4.2 Analysis of Wind Swath Size for Storm Surge Generation

Demuth et al. (2006) provided wind-swath data for tropical cyclones that impacted the U.S. Gulf Coast since 1988. These data are provided as radial distances of 63 km/hr (34-kt), 93 km/hr (50-kt), and 119 km/hr (64-kt) winds. SURGEDAT provided surge data for 33 storm surges located near landfalling tropical cyclones during this time period, making them suitable for analysis.

The size of each of these wind swaths was recorded at landfall and 18 hours before landfall. At landfall, 31 observations were provided for radius of 63 km/hr (34-kt) winds, 32 observations for radius of 93 km/hr (50-kt) winds, and 29 observations were available for radius of 119 km/hr (64-kt) winds (Table 4.3). Missing data explain why 33 observations are unavailable for each of these time periods. At 18 hours before landfall, 31 observations were available for 63 km/hr (34-kt) winds and 30 observations were available for both 93 km/hr (50-kt) and 119 km/hr (64-kt) winds (Table 4.3). Missing data account for some of the data loss; however, I intentionally excluded data from Hurricane Charley at 18 hours before landfall, because the storm was centered in the Caribbean Sea, south of Cuba, at this time.

Table 4.3. Spearman rank order correlations measuring the relationship between storm surge heights and radius of 63 km/hr (34-kt), 93 km/hr (50-kt), and 119 km/hr (64-kt) winds.

| Radius Measure | 63 km/hr (34-kt) winds at landfall | 63 km/hr (34-kt) winds at landfall – 18h | 93 km/hr (50-kt) winds at landfall | 93 km/hr (50-kt) winds at landfall - 18h | 119 km/hr (64-kt) winds at landfall | 119 km/hr (64-kt) winds at landfall – 18h |
|---------------------|------------------------------------|--|------------------------------------|--|-------------------------------------|---|
| No. of observations | 31 | 31 | 32 | 30 | 29 | 30 |
| R-Value | .6874 | .6069 | .7634 | .8158 | .7388 | .7935 |
| P-Value | .0000 | .0004 | .0000 | .0000 | .0000 | .0000 |

For observations 18 hours before landfall, the average extent of 63 km/hr (34-kt) winds was 278.5 km (150.4 nmi), the maximum radius was 463 km (250 nmi) in Hurricane Ivan in 2004, and the minimum distance was 74 km (40 nmi) in Tropical Storm Humberto in 2007. The average size of 93 km/hr (50-kt) winds was 166 km (89.9 nmi), the maximum size was 278 km (150 nmi) in Hurricane Ike in 2008, and the minimum distance was 0 km (0 nmi), which occurred for six tropical cyclones that did not reach this intensity. The average value was computed for the 24 events that generated winds of at least 93 km/hr (50 knots). The average radius of 119 km/hr (64-kt) winds among the 16 storms that generated hurricane-force winds was 113 km (60.8 nmi). The greatest extent was 217 km (117 nmi) in Hurricane Opal in 1995, and the smallest was 0 km (0 nmi), which occurred in 14 tropical cyclones that did not reach hurricane-force winds.

Statistical analysis determined positive correlations between storm surge heights and the radius of 63 km/hr (34-kt), 93 km/hr (50-kt) and 119 km/hr (64-kt) winds (Table 4.3). I used Spearman rank order correlations for these tests because of data constraints, as the value of some radii were listed as zero, such as the radius of 119 km/hr (64-kt) winds if the tropical cyclone was below the intensity of a hurricane. Correlation tests found the radius of 93 km/hr (50-kt) winds 18 hours before landfall produced the best correlation with surge heights ($r=0.82$; $p < 0.01$). I used linear and loess regression to depict this relationship graphically in Figure 4.2. The radius of 34-knot winds 18 hours before landfall produced the least optimal correlation ($r=0.61$; $p < 0.01$).

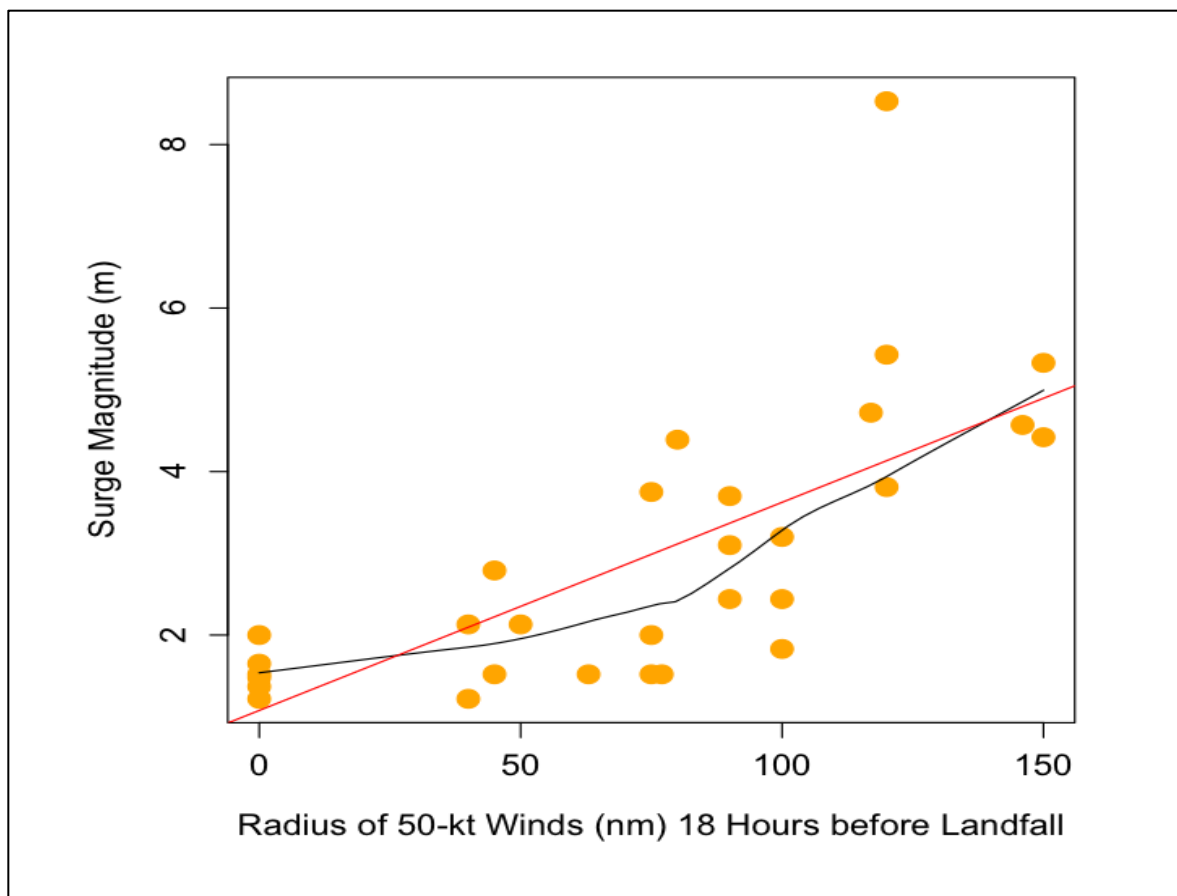


Figure 4.2. LOESS (black line) and linear (red line) regression models for the relationship between surge heights and radius of 93 km/hr (50-kt) winds (nmi) at 18 hours before landfall. Orange circles depict observed events.

Rmax sizes were inversely related to the radius of 63 km/hr (34-kt), 93 km/hr (50-kt) and 119 km/hr (64-kt) winds (Table 4.4). These results suggest that tropical cyclones with more compact eyewalls tend to cover larger areas with strong winds. This is logical when considering that storm surge magnitudes relate positively with the size of wind fields but negatively with Rmax sizes. The relationship between Rmax sizes and the size of the wind fields became increasingly inverse for stronger wind speeds. Also, this negative correlation was greater at 18 hours before landfall than at landfall for the area of 63 km/hr (34-kt), 93 km/hr (50-kt) and 119 km/hr (64-kt) winds. However, these results were only significant above the 90% confidence level for the relationship between Rmax sizes and 119 km/hr (64-kt) winds at landfall and 18 hours before landfall. Hurricanes Katrina and Rita are examples of such storms. Both of these hurricanes had Rmax sizes of 37 km (20 nmi), which is smaller than the average distance for the 83 storms with Rmax data, however, the radius of 119 km/hr (64-kt) winds for both of these hurricanes ranked in the top five, and both cyclones generated catastrophic storm surges along the northern Gulf Coast.

Many tropical cyclones in the past several decades reveal the importance of wind-swath area for generating storm surges. For example, the tropical cyclones with the six largest radii of 119 km/hr (64-kt) winds produced the six largest storm surges, although not in rank order. However, relatively low-magnitude storm surges were generated by the 14 tropical cyclones with no radius of 119 km/hr (64-kt) winds at 18 hours before landfall. These events were all tropical storms, with wind intensity less than hurricane force. From another perspective, 75% (12 of 16) of the tropical cyclones with non-zero radii of 119 km/hr (64-kt) winds at 18 hours before landfall generated surge heights of at

least 3 m, while none of the 14 storms with a zero value for the radius of 119 km/hr (64-kt) winds generated a surge exceeding 3 m.

Table 4.4. Correlation between Rmax sizes and the radius of 63 km/hr (34-kt), 93 km/hr (50-kt) and 119 km/hr (64-kt) winds. All of these correlations are inverse, meaning there is a negative relationship between the variables.

| Radius Measure | 63 km/hr (34-kt) winds at landfall | 63 km/hr (34-kt) winds at landfall – 18h | 93 km/hr (50-kt) winds at landfall | 93 km/hr (50-kt) winds at landfall - 18h | 119 km/hr (64-kt) winds at landfall | 119 km/hr (64-kt) winds at landfall – 18h |
|---------------------------------|------------------------------------|--|------------------------------------|--|-------------------------------------|---|
| R-Value for Rmax vs. Swath Size | -0.0458 | -0.1868 | -0.1208 | -0.2247 | -0.3306 | -0.4274 |
| P-value | .8088 | .3294 | .5233 | .2486 | .0804 | .0242 |

4.5 Discussion

This analysis reveals that we must be careful how we define tropical cyclone size when considering its role in storm surge generation. The size of Rmax correlates inversely with surge height, while the radii of 63 km/hr (34-kt), 93 km/hr (50-kt) and 119 km/hr (64-kt) winds correlate positively with surge magnitudes, indicating that surge potential is increased in tropical cyclones with small Rmax sizes or large swaths of strong winds. However, observations from some storms may appear to contradict these results. For example, Hurricane Katrina generated a larger storm surge than Hurricane Camille, although Camille had a smaller Rmax size. However, the swath size of Katrina’s wind

field was larger than the area covered by Hurricane Camille. It should also be noted that Katrina's maximum sustained winds were comparable to Camille's at 18 hours before landfall; the difference in wind speeds was only about 20 km/hr (11 knots). Such comparisons may reveal that the larger of two tropical cyclones with comparable pre-landfall wind speeds may generate the higher storm surge, while the stronger of two cyclones with comparable sizes may generate the larger surge.

We should use caution not to overestimate the role of tropical cyclone size. The comparison between Katrina and Camille may tempt us to do so, as Katrina is often referred to as a category-3 hurricane that generated a higher storm surge than a category-5 hurricane along the same stretch of coastline. As bathymetry and geomorphology were relatively constant for these two storms, we may overemphasize the importance of tropical cyclone size if we do not consider that Katrina's pre-landfall wind speeds were also intense and surge heights correlate better with pre-landfall winds than wind speeds at landfall (Jordan and Clayson 2008; see Chapter 3).

My analysis also further expands understanding of the importance of pre-landfall tropical cyclone characteristics for storm surge generation. Storm surge magnitudes correlated best with the radii of 93 km/hr (50-kt) winds and 119 km/hr (64-kt) winds at 18 hours before landfall, and these correlations were noticeably higher than the radii of those same wind fields at landfall. These results help us understand that maximum sustained winds are not the only tropical cyclone parameter that correlates better with surge heights before striking the coast than at landfall. The role of pre-landfall tropical cyclone size, particularly the area of 93 km/hr (50-kt) or 119 km/hr (64-kt) winds, appears to be comparable to the role of pre-landfall winds for storm surge generation. R-

values for the correlation of surge and pre-landfall winds were 0.7754 (R-squared was 0.60) in 117 wind/ surge events since 1880 and 0.81 (R-squared = 0.66) in 63 wind/ surge events since 1960 (see Chapter 3).

This study utilized peak storm surge heights and did not consider the full extent of storm surge inundation along a coastline. While small, intense tropical cyclones have sometimes generated high surge magnitudes, larger cyclones tend to inundate larger expanses of coastline. For example, although the 1900 Galveston Hurricane generated a higher peak surge than Hurricane Ike in 2008, Hurricane Ike's surge likely inundated a longer stretch of coastline (Needham and Keim 2011). Although Ike made landfall near Galveston, Texas, the storm produced a storm tide of 3.32 m south of New Orleans, in Plaquemines Parish, Louisiana (Federal Emergency Management Agency 2009), more than 463 km (250 nmi) east of Ike's landfall location. A thorough literature review does not provide any coastal flooding observations that far east from the 1900 Galveston Hurricane. Therefore, it appears as though Ike's massive size generated higher surge levels than the 1900 Galveston Hurricane outside the zone of peak surge. This comparison may provide an important insight into this study. While small, intense tropical cyclones sometimes generate high-magnitude storm surges, the extent of inundation along the coastline may be less than the surges produced by larger, less-intense cyclones.

4.6 Summary and Conclusion

This study provides the first empirical analysis on the relationship between tropical cyclone size and storm-surge heights. Storm surge is provided from SURGEDAT tropical cyclone position and intensity data are provided by Elsner and Jagger (2013), and

a tropical cyclone size dataset is built from nine separate sources.. Tropical cyclone size data were archived as the size of the radius of maximum winds (Rmax), as well as the radius of 63 km/hr (34-kt), 93 km/hr (50-kt) and 119 km/hr (64-kt) winds.

Rmax sizes correlated inversely with storm surge heights, pre-landfall wind speeds and the size of wind swaths. Historical examples support this statistical analysis. For example, the cyclones with the three largest Rmax sizes were all tropical storms that did not reach hurricane intensity, and generated average surge levels of approximately 2 m. However, the tropical cyclones with the three smallest Rmax sizes were all major hurricanes that generated large surges, averaging 5.4 m. The 1900 Galveston Hurricane, the 1935 Labor Day Hurricane and Hurricane Camille all had small Rmax sizes, but generated catastrophic storm surges.

Conversely, the size of tropical cyclone wind swaths correlated positively with surge heights. Storm surge magnitudes correlated best with the radius of 93 km/hr (50-kt) winds at 18 hours before landfall, when the Spearman correlation coefficient reached 0.8158,, followed by the radius of 119 km/hr (64-kt) winds at 18 hours before landfall. These results indicate that storm surge magnitudes relate to the pre-landfall size of tropical cyclone wind swaths about as well they do to the strength of pre-landfall winds. This study also reveals that storms with compact eyewalls and large wind fields tend to generate larger storm surges.

Such results may be helpful to the storm surge modeling community, as scientists are currently re-evaluating the role of various tropical cyclone parameters for storm surge generation. These results may also be important for the emergency management and disaster-science community for better understanding surge potential in specific types of

storms. As many of the recently destructive storm surges were generated by large tropical cyclones, it's important to realize that storms such as the 1900 Galveston Hurricane, the 1935 Labor Day Hurricane and Hurricane Camille, all generated catastrophic storm surges, even though they were all small storms, at least in regards to the Rmax size. Coastal stakeholders should take the utmost precautions for such events, as well as tropical cyclones with large pre-landfall radii of 93 km/hr (50-kt) or 119 km/hr (64-kt) winds, which tend to consistently generate large surge events.

4.7 References

Atlantic Oceanographic and Meteorological Laboratory, 2006: NOAA Revisits Historic Hurricanes. Tropical cyclone database and documentation available on the Web at: <http://www.aoml.noaa.gov/hrd/hurdat/>.

Berg, R., 2010: Tropical Cyclone Report, Hurricane Ike. The National Hurricane Center, Miami, Florida, United States. Report available on the Web at: www.nhc.noaa.gov/pdf/TCR-AL092008_Ike_3May10.pdf.

Berg, R., 2013: Tropical Cyclone Report, Hurricane Isaac. The National Hurricane Center, Miami, Florida, United States. Report available on the Web at: http://www.nhc.noaa.gov/data/tcr/AL092012_Isaac.pdf.

Bernstein, A., 2013: U.S. Transportation Secretary LaHood Announces \$3.7 Billion in Additional Hurricane Sandy Disaster Relief Aid for Transit Agencies. United States Department of Transportation document *DOT 46-13*. Available on the Web at: <http://www.dot.gov/briefing-room/us-transportation-secretary-lahood-announces-37-billion-additional-hurricane-sandy>.

Blake, E.S., T.B. Kimberlain, R.J. Berg, J.P. Cangialosi and J.L. Beven II, 2012: Tropical Cyclone Report, Hurricane Sandy, (AL182012), 22-29 October 2012. National Hurricane Center, Miami, Florida. Report available on the Web at: http://www.nhc.noaa.gov/data/tcr/AL182012_Sandy.pdf.

Demuth, J., M. Demaria, and J.A. Knaff, 2006: Improvement of advanced microwave sounder unit tropical cyclone intensity and size estimation algorithms. *Journal of Applied Meteorology*, 45, 1573-1581.

Elsner, J.B., and T.H. Jagger, 2013: *Hurricane Climatology: A Modern Statistical Guide Using R*. Oxford University Press, New York, USA. 430 pp.

Erdman, J., 2012: Superstorm Sandy: A Giant Circulation. Article published on The Weather Channel website on November 29, 2012. Available on the Web at:

<http://www.weather.com/news/weather-hurricanes/sandy-another-giant-storm-20121027>.

Federal Emergency Management Agency, 2009: Hurricane Ike in Texas and Louisiana, Mitigation Assessment Team Report. Available on the Web at: <https://www.fema.gov/media-library/assets/documents/15498>.

Gariott, E.B., 1900: West Indian Hurricane of September 1-12, 1900. Published in the *Monthly Weather Review*, 28, 371-377. Edited by C. Abbe. Available on the Web at: <http://www.aoml.noaa.gov/general/lib/lib1/nhclib/mwreviews/1900.pdf>.

Hagen, A.B., C.W. Landsea, D. Strahan, and C. Lueckett, 2012: A Reanalysis of the 1944-1953 Atlantic Hurricane Seasons – The First Decade of Aircraft Reconnaissance. Publication available on the Web at: [www.aoml.noaa.gov/hrd/data_sub/A_Reanalysis_of_the_1944-1953_Atlantic_Hurricane_Seasons - The First Decade of Aircraft Reconnaissance.pdf](http://www.aoml.noaa.gov/hrd/data_sub/A_Reanalysis_of_the_1944-1953_Atlantic_Hurricane_Seasons_-_The_First_Decade_of_Aircraft_Reconnaissance.pdf).

Ho, F.P., R.W. Schwerdt, and H.V. Goodyear, 1975: *NOAA Technical Report NWS 15: Some Climatological Characteristics of Hurricanes and Tropical Storms, Gulf and East Coasts of the United States*. Washington, D.C., 87 pp.

Irish, J.L., D.T. Resio, and J.J. Ratcliff, 2008: The Influence of Storm Size on Hurricane Surge. *Journal of Physical Oceanography*, 38, 2003-2013.

Jordan, II, M.R., and C.A. Clayson, 2008: A new approach to using wind speed for prediction of tropical cyclone generated storm surge. *Geophysical Research Letters*, 35, doi: 10.1029/2008GL033564.

Kates, R.W., C.E. Colten, S. Laska, and S.P. Leatherman, 2006: Reconstruction of New Orleans after Hurricane Katrina: A research perspective. *Proceedings of the National Academy of Sciences of the United States of America*, 103, 14653-14660.

Keim, B., R. Muller, and G. Stone, 2007: Spatiotemporal Patterns and Return Periods of Tropical Storm and Hurricane Strikes from Texas to Maine. *Journal of Climate*, 20, 3498-3509.

Kessler, R.C., S. Galea, R.T. Jones, and H.A. Parker, 2006: Mental illness and suicidality after Hurricane Katrina. *Bulletin of the World Health Organization*, 84, 12, 930-939.

Knabb, R.D. J.R. Rhome, and D.P. Brown, 2011: Tropical Cyclone Report, Hurricane Katrina, 23-30 August 2005. Report produced by the National Hurricane Center, Miami, Florida, and published on the Web at: http://www.nhc.noaa.gov/pdf/TCR-AL122005_Katrina.pdf.

Landsea, C.W., C. Anderson, N. Charles, G. Clark, J. Dunion, J. Fernandez-Partagas, P. Hungerford, C. Neumann, and M. Zimmer, 2003: The Atlantic Hurricane Database Re-analysis Project Documentation for 1851-1910 Alterations and Addition to the HURDAT

Database. Revised 6 January 2003. Publication available on the Web at: www.aoml.noaa.gov/hrd/hurdat/Documentation.html.

Landsea, C.W., D.A. Glenn, W. Bredemeyer, M. Chenoweth, R. Ellis, J. Gamache, L. Hufstetler, C. Mock, R. Perez, R. Prieto, J. Sanchez-Sesma, D. Thomas, and L. Woolcock, 2007: A Reanalysis of the 1911 to 1920 Atlantic Hurricane Database. *Journal of Climate* (In press). Publication available on the Web at: www.aoml.noaa.gov/hrd/Landsea/19111920jc-final.pdf.

Landsea, C.W., S. Feuer, A. Hagen, D.A. Glenn, N.T. Anderson, J. Sims, R. Perez, and M. Chenoweth, 2011: A Reanalysis of the 1921 to 1930 Atlantic Hurricane Database. Submitted to *Journal of Climate*, May 2011. This publication is available on the Web at: www.aoml.noaa.gov/hrd/Landsea/19211930jc-main.pdf.

McCallum, B.E., B.D. McGee, D.R. Kimbrow, M.S. Runner, J.A. Painter, E.R. Frantz, and A.J. Gotvald, 2012: Monitoring Storm Tide Flooding from Hurricane Isaac along the Gulf Coast of the United States, August 2012. Open-File Report 2012-1263. Available on the Web at: <http://pubs.usgs.gov/of/2012/1263/>.

McTaggart-Cowan, R., G.D. Deane, L.F. Bosart, C.A. Davis, and T.J. Galarneau, Jr., 2008: Climatology of tropical cyclongenesis in the North Atlantic (1948-2004). *Monthly Weather Review*, 136, 1284-1304.

National Weather Service, 2010: NWS Marks 75th Anniversary of the 1935 Labor Day Hurricane. Article provided by the Southern Region Headquarters of the National Weather Service. Available on the Web at: www.srh.noaa.gov/srh/srnews/stories/2010/1935.htm.

Needham, H., and B.D. Keim, 2011: Storm Surge: Physical Processes and an Impact Scale. *Recent Hurricane Research- Climate, Dynamics, and Societal Impacts*. E. Lupo (Ed.). Intech Open Access. Publisher: Croatia.

Needham, H.F., and B.D. Keim, 2012: A Storm Surge Database for the U.S. Gulf Coast. *International Journal of Climatology*, 32, 14, 2108-2123. DOI: 10.1002/joc.2425.

Needham, H.F., B.D. Keim, D. Sathiaraj, and M. Shafer, 2013: A Global Database of Tropical Storm Surges. *EOS, Transactions American Geophysical Union*, 94, 24, 213-214.

Nielsen, P., 2009: How storm size matters for surge height. *Coastal Engineering*, 56, 1002-1004.

Powell, M.D., and T.A. Reinhold, 2007: Tropical Cyclone Destructive Potential by Integrated Kinetic Energy. *Bulletin of the American Meteorological Society*, 88, 513-526.

Simpson, R.H., and H. Riehl, 1981: *The Hurricane and Its Impact*. Louisiana State University Press, Baton Rouge, Louisiana, 398 pp.

U.S. Corps of Engineers, 1935: 1935 Labor Day Hurricane, Limits of Destruction and Storm Surge Heights. Chart File No. 3-16-10,409 produced on October 21, 1935. Published in Knowles, T.N., 2009: Category 5: The 1935 Labor Day Hurricane. University Press of Florida, 350 pp.

CHAPTER 5. STORM SURGE RETURN PERIODS FOR THE U.S. GULF COAST

5.1. Introduction

Tropical cyclone-generated storm surges inflict catastrophic natural hazards along the U.S. Gulf Coast. Storm surge events in this region have produced the most deadly and costly natural disasters in U.S. history. The 1900 Galveston Hurricane struck Texas with a 6.1-meter storm surge (Garriott 1900) and killed at least 8,000 people (Blake et al. 2011), making it the deadliest natural disaster in the United States (Emanuel 2005). More recently, Hurricane Katrina inundated the northern Gulf Coast with the highest storm surge in the U.S. history (Needham and Keim 2012). This disaster killed more than 1,800 people (McTaggart-Cowan et al. 2008) and inflicted losses exceeding \$100 billion (Blake et al. 2011), making Katrina the most costly natural disaster in the United States (Baade et al. 2007).

High-magnitude coastal flooding events have occurred frequently in this region over the past decade, as six hurricanes generated storm surges measuring at least 4 m. In 2004, Hurricane Ivan made landfall as a category-3 hurricane, generating a storm surge of 4.57 m in Alabama and the Florida Panhandle (Stewart 2005). In 2005, hurricanes Katrina, Rita and Wilma all made landfall as major hurricanes along the U.S. Gulf Coast. Katrina generated a storm tide of 8.53 m at Hancock County, Mississippi (Knabb et al. 2011), Rita produced a 5.4-m storm tide in Cameron Parish, Louisiana (URS Group 2006), and Wilma inundated southwest Florida with a storm tide of at least 4.72 m (Barnes 2007; Smith III et al. 2009). In 2008, Hurricane Ike generated a storm tide of 5.33 m at Chambers County, Texas (Berg 2010), and in 2012, Hurricane Isaac flooded Southeast Louisiana with a storm tide as high as 4.39 m (McCallum et al. 2012).

These surge events inflicted tremendous financial losses in the region. Losses from Hurricane Katrina reached as high as \$148 billion, adjusted to 2013 dollars, which exceeds Hurricane Andrew, the second most costly hurricane, by more than \$100 billion (Smith et al. 2013). Collectively, hurricanes Ivan, Katrina, Rita, Wilma, Ike and Isaac inflicted more than \$235 billion in losses, adjusted to 2013 dollars (Smith et al. 2013). Storm surge was responsible for a substantial amount of these losses. The price tag from Katrina's surge alone was tremendous, as the massive storm surge breached levees and flooded approximately 80% of the New Orleans metropolitan area (Kates et al. 2006).

Insurance rates reacted to these catastrophes, as property insurance pricing increased after hurricanes Katrina and Ike (Aschkenasy 2014). Following Katrina, some carriers had increased rates up to 40% by 2006 (Warner 2007) and in Louisiana, the State Insurance Rating Commission approved premium increases ranging from 16-35% in 2007 (Green et al. 2007). Homeowners' insurance premiums also rapidly increased, as rates rose by 22% in Louisiana (Mowbray 2007), and residential wind insurance premiums increased by as much as 300 to 400 percent in some coastal zones (Kunreuther and Michel-Kerjan 2009).

These storm surge disasters also encouraged the insurance industry to re-evaluate place-based risk for locations in coastal zones. For example, in Louisiana, homeowners' insurance premiums increased the most in flood-prone or coastal parishes (Mowbray 2007). While some carriers raised prices in coastal areas, others decided to stop writing policies in flood-prone locations, like New Orleans (Green et al. 2007). Such practices have also been followed in surge-prone areas outside the Gulf Coast region; insurance

rates rose substantially for locations exposed to the flood zone in the Mid-Atlantic States following Hurricane Sandy's massive storm surge in 2012 (Aschkenasy 2014).

Destructive storm surges in the United States during the past decade have also influenced the planning sector to consider storm surge risk for future projects and long-term policies. For example, future building codes in New York City may require computer hardware, HVAC machinery, electrical systems, and other critical infrastructure to be elevated in buildings that are located in the coastal flood zone (Freedman 2013). Transportation infrastructure in the United States also must account for coastal flooding, which threatens approximately 97,000 km of roads (Environmental Protection Agency 2013). Such planning, however, relies on accurate mapping of coastal flood zones to determine the areas of greatest risk.

The Federal Emergency Management Agency (FEMA) has recently produced updated coastal flood maps, which will benefit coastal stakeholders in many sectors, including insurance and planning. These maps use computer models to find the maximum potential surge in coastal areas. In this project, FEMA's National Hurricane Program (NHP) collaborated with the National Hurricane Center's Storm Surge Unit to model surge with the Sea, Lake and Overland Surges from Hurricanes (SLOSH) model (Jennings 2013). This model ran thousands of possible hurricane scenarios that incorporated various hurricane categories, speeds and tracks to create Maximum Envelopes Of Water (MEOW) and Maximum Of MEOWs (MOM), which indicated flood potential for coastal areas. Such efforts were timely, as enrollment in FEMA's National Flood Insurance Program (NFIP), which handles flood insurance for the United States, grew substantially following the active 2004 and 2005 hurricane seasons. Between

2004 and 2007, for example, national enrollment increased by 20% and enrollment along the Gulf Coast increased by 41% (MacDonald et al. 2010).

In practice, these updated coastal flood maps are crucial for coastal planning. FEMA's coastal flood maps, called Flood Insurance Rate Maps (FIRM), designate Special Flood Hazard Areas (SFHAs), which are essentially zones of varying flood risk. The zones are assigned one or two letters, such as A, AE, AH, AO, V, and VE (Federal Emergency Management Agency 2013). Zones V and VE are coastal high velocity flood zones, which are subjected to high-velocity storm surges and waves (Federal Emergency Management Agency 2013). Structures in these zones must be elevated and may not be built on fill (Texas General Land Office and Texas Sea Grant College Program 2013). As coastal residents adhere to these building codes, the potential savings in economic and human losses are tremendous.

While these improved storm surge maps are beneficial, it is difficult to verify their accuracy because they rely entirely upon storm surge modeling. For short-term forecasts, storm surge models are crucial because each tropical cyclone is unique and dynamic, and it is difficult to analyze water level observations in near real-time to conduct empirical analyses as a storm is approaching the coast. However, an empirical approach offers potential for evaluating long-term coastal flood heights, provided storm surge observations sufficiently account for coastal flooding events over a period of record at a given location. Surprisingly, a thorough literature review reveals that no previous studies have utilized observed storm surge data to conduct an empirical analysis of coastal flooding return levels along the U.S. Gulf Coast. As such, the purpose of this chapter is to fill the gap in the literature by providing the first such analysis.

5.2 Data

Storm surge data are provided by SURGEDAT, a global surge database that provides more than 7,600 high-water marks for the United States since 1880, including approximately 5,400 high-water marks for the U.S. Gulf Coast (Needham et al. 2013). This dataset pulls observations from more than 60 separate sources (Needham and Keim 2012). An updated surge dataset is available for download at <http://surge.srcc.lsu.edu>.

SURGEDAT includes data on both storm surge and storm tide heights. Storm surge is the water height above predicted tide levels, while storm tide includes both storm surge and the tidal variation. For some observations, SURGEDAT provides both the storm surge and storm tide height, while for others either storm surge or storm tide levels are provided.

SURGEDAT also assigns a numeric confidence level for each observation, which provides an indication of the data quality. Confidence levels range from 1-5, with higher numbers assigned to better quality data. Higher confidence levels are assigned to tide-gauge data, as well as mudlines and watermarks inside structures. The lowest confidence levels are classified as Level 1, and are considered unsuitable for analysis. Observations affected by fresh water runoff, called riverine data, fit into this category. Field data that estimate water levels by measuring the height of rafted debris, tree bark removal, damage trimlines or exterior water marks on exposed structures, are also considered Level 1 data, because these types of high-water marks include the height of waves. Approximately 7% of Gulf Coast observations were assigned to Level 1 confidence, and were removed from this analysis.

When using observed data to estimate the occurrence of extreme values, it is important to also limit the amount of missing data in order to minimize analytical errors. Missing data creates an underestimation bias because extreme events that actually occurred are excluded from the analysis. SURGEDAT is missing accurate data on approximately 17% of potential surge events from 1880-2012. Most of these missing data were small-magnitude surge events that occurred in rural areas. However, the amount of missing data is reduced to 9% for the data record beginning in 1900, and 6% for the period commencing in 1910.

I chose to analyze data from the 114-year period of 1900-2013 for several reasons. Starting the analysis in 1900 limits the amount of missing data, while still including several high-profile surge events that impacted the Gulf Coast during the early 1900s. The 1900 Galveston Hurricane generated a 6.1-m storm tide that devastated the city of Galveston, Texas (Garriott 1900); a hurricane in September, 1903, produced a 3.05 m storm tide at Apalachicola, Florida (Barnes 2007); in September, 1906, a hurricane generated a storm tide of 4.27 m in Santa Rosa County, Florida (Williams and Duedall 2002; Barnes 2007); the Velasco Hurricane of July, 1909, produced a 3.05-m storm tide at Velasco and Galveston, Texas (Dunn and Miller 1960; Ellis 1988); and a hurricane in September, 1909, produced a 4.57-m storm tide near the mouth of Terrebonne Bay, Louisiana (Cline 1926). The 1900 storm tide in Galveston, Texas, produced the highest water mark on record for that city, while the 1903 storm tide in Apalachicola tied for the highest water mark in that location with Hurricane Elena's 3.05-m storm surge in 1985 (National Hurricane Center 1985).

A starting date of 1900 also provides a similar time frame with several studies that analyzed the risk of hurricane strikes or hurricane-related damage in the United States. Jarrell et al. (1992) provided a comprehensive list of hurricane strikes for counties from Texas to Maine, beginning in 1900. This list has been updated through 2009 (Atlantic Oceanographic and Meteorological Laboratory 2006). Pielke et al. (2008) also used data from 1900-2005 to normalize U.S. hurricane damage. Also, Keim et al. (2007) analyzed the return periods of tropical storm and hurricane strikes for 45 coastal locations from Texas to Maine, using data from approximately the same period, as their analysis considered tropical cyclones from 1901-2005.

5.3 Methods

5.3.1 Data Selection

The first step for data analysis involved selecting surge data for coastal locations. Ideally, I would have selected data from one geographic point in each community because storm surge heights are often localized and can vary considerably across short distances (Jarvinen and Neumann 1985; Needham and Keim 2011). Tide-gauge data are ideal for such analysis, because they constantly record water heights at a fixed location. SURGEDAT incorporates tide gauge data from the U.S. Army Corps of Engineers (USACE) and the National Ocean Survey (NOS), which are the two most prominent tide-gauge networks available for the U.S. Gulf Coast (Penland and Ramsey 1990).

Unfortunately, I could not rely solely on tide gauge data because of limited data coverage in both time and space. For example, although the USACE provides a dense network of tide gauge data for Louisiana, no sites provide data from before 1931, and only five sites provide data from before 1942 (Penland and Ramsey 1990). Some NOS

sites along the Gulf Coast have longer records, with the longest archive available for Galveston, Texas, where an NOS gauge began recording water levels in 1908 (Penland and Ramsey 1990). However, only eight NOS gauges along the Gulf Coast have long-term records that began by 1947, and only four of these sites provide data from before 1934 (Penland and Ramsey 1990). Such limited spatial coverage rarely captures the peak magnitude of a storm surge event.

Another limitation of tide gauge data is that gauges often malfunction or are destroyed in high-magnitude storm surge events. For example, the NOS tide gauge at Bay Waveland Yacht Club, Mississippi, lists a maximum water level of 2.79 m, recorded on September 1, 2008 (National Oceanic and Atmospheric Administration 2014), which corresponds with the timing of Hurricane Gustav. However, this gauge was established in May of 1978, and was operational when Hurricane Katrina made landfall close to this site, generating a storm tide level as high as 8.53 m in nearby Hancock County, Mississippi (Knabb et al. 2011). Katrina's record-setting storm surge presumably destroyed the gauge, making water level data unavailable at this site for this important surge event. The NOS gauge at Calcasieu Pass, Louisiana, malfunctioned during Hurricane Rita's storm surge in southwest Louisiana, just several weeks after Hurricane Katrina. Rita generated a 5.4-m storm tide in Cameron Parish (URS Group 2006), however, the NOS tide gauge malfunctioned during Rita's surge, soon after water levels exceeded Mean Sea Level (MSL) by a height of 1.22 m (National Oceanic and Atmospheric Administration 2014; Figure 5.1). In 2008, the NOS tide gauge at Galveston Pier 21, Texas, malfunctioned for at least four hours during the time of Hurricane Ike's peak storm surge (National Oceanic and Atmospheric Administration 2014; Figure 5.2),

making the peak water level at that site uncertain. Ike's surge did not destroy this gauge, and it began recording again when water levels fell below approximately 3.35 m.

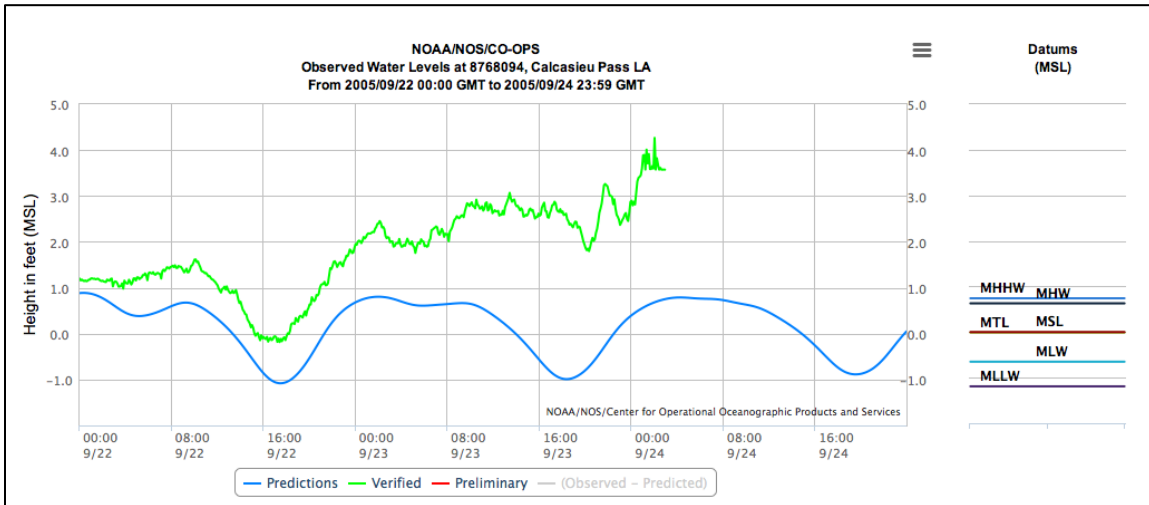


Figure 5.1. The NOS tide gauge at Calcasieu Pass, Louisiana, malfunctioned shortly after water levels exceeded 1.22 m (4 feet) on September 24, 2005, during Hurricane Rita's storm surge.

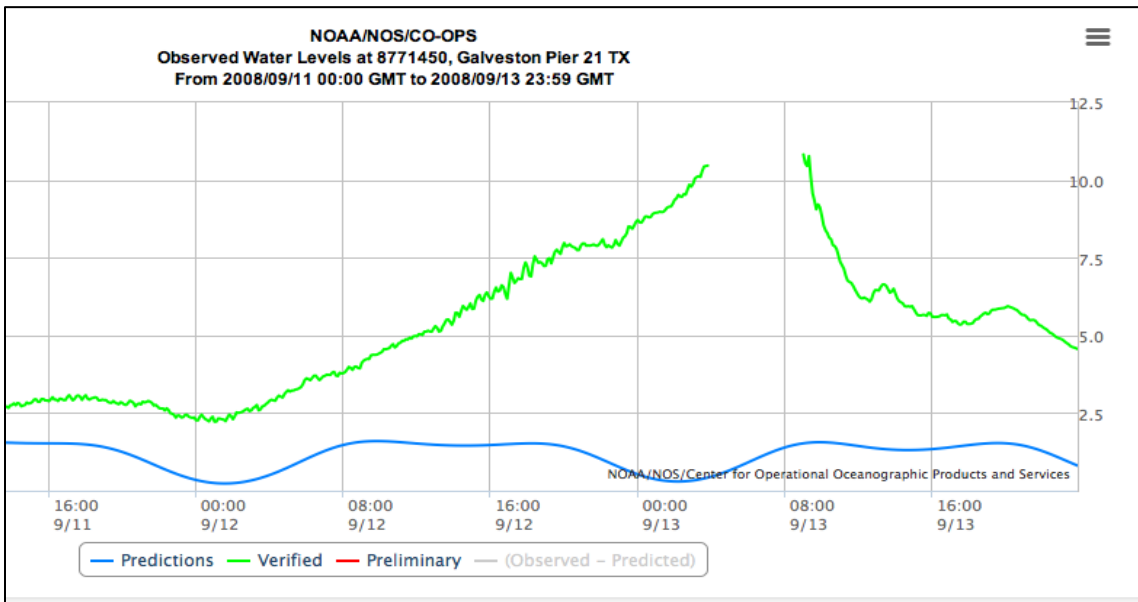


Figure 5.2. The NOS tide gauge at Galveston Pier 21, Texas, malfunctioned after water levels exceeded 3.05 m (10 feet) on September 13, 2008, during Hurricane Ike's storm surge. The gauge began recording water levels again once the peak surge passed.

Due to incomplete storm surge records available at fixed tide gauges in the region, it was necessary to construct storm surge history from a variety of sources. SURGEDAT contains abundant data from fixed and mobile tide gauges that have not failed in surge events, and high water marks that were measured after storm surges subsided. In many cases, high-water marks provide the most accurate data from the area of peak storm surge, while fixed tide gauges provide accurate data from lower-magnitude water levels, outside the region of peak storm surge. Mobile tide gauges also provide a network of accurate observations, however, coordinated efforts to collect such data are relatively new, as the United States Geological Survey (USGS) has deployed mobile tide gauges through the Inland Storm-Tide Monitoring Program, beginning with Hurricane Rita's storm surge in 2005 (U.S. Geological Survey 2013).

Therefore, I determined to analyze all reliable observations within geographic proximity to coastal communities, regardless of the data source. In order to conduct this analysis, a web-mapping tool was developed that enables users to create a circle on a map to define an area from which water height data are provided (Figure 5.3). Users customize the location and size of the circle by clicking on any location to define a circle's center point, while selecting the circle's radius size from a drop-down menu. Internally, the web-mapping tool uses the following: 1. A spatial database (Postgis, <http://www.postgis.net>) to store and spatially query storm surge observations. 2. Computational methodologies to compute peak storm surge values and conduct return frequency analyses (code was written using the programming language Python and scientific computing libraries, numpy and scipy). 3. For the web-based visualization, technologies such as Javascript and HTML5.

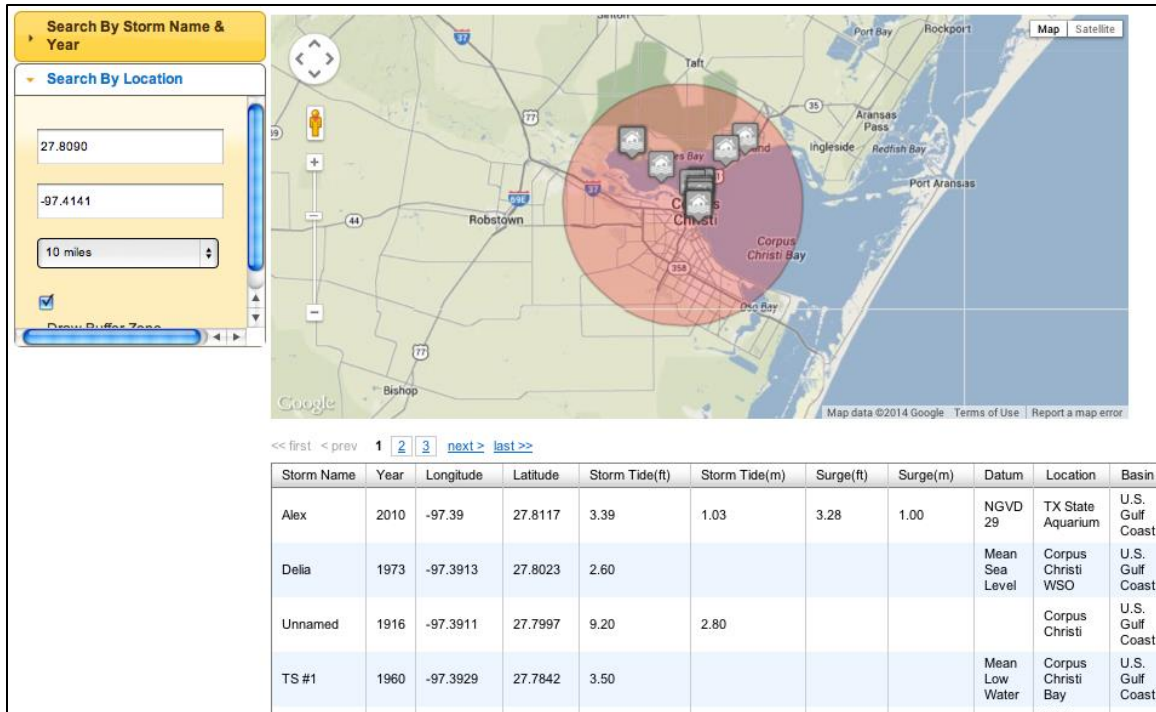


Figure 5.3. The storm surge web tool enables users to select surge data for coastal communities. In this screen shot, a user has selected all observed storm surge and storm tide heights within 16 km (10 miles) of Corpus Christi, Texas.

The tool provides a list of historical storm surge and storm tide data within each circle. If an observation contains both storm surge and storm tide data, I selected the surge height. However, if storm surge is unavailable for an observation, the storm tide height is selected. If a tropical cyclone generated multiple high watermarks within the circle, the highest-magnitude observation is listed. Following this methodology, this web-tool provides a comprehensive storm surge/ storm tide history for coastal locations.

I selected observations for 26 coastal communities from South Texas to the Florida Keys, including all of West Florida, but excluding Florida’s Atlantic Coast. These communities represent developed areas with sufficient storm surge history for statistical analysis. For these communities, we tested data-selection circles with 8-km (5-mile), 16-km (10 mile), and 40-km (25-mile) radii. We selected these radii sizes because circles

with 8-km (5-mile) radii represent areas approximately the size of many Gulf Coast communities, while circles with 16-km (10-mile) and 40-km (25-mile) radii provided regional coverage that typically extended beyond community borders. Large metropolitan areas, such as Houston, New Orleans and Tampa, are exceptions, as these cities sprawl beyond the borders of a circle with a 16-km (10-mile) radius.

As expected, larger circles usually provided more data than smaller circles, however, in some cases data quantity from circles of different sizes was identical. Table 5.1 provides a list of coastal communities and the number of observations provided by circles with 8-km (5-mile), 16-km (10-mile) and 40-km (25-mile) radii. Larger circles usually selected data that were less physically homogenous with each other than smaller circles. Homogeneity of data is important because observations from each coastal community will be combined into a statistical distribution to analyze storm surge return periods. If these data come from locations with different physical characteristics, they are essentially derived from different populations and make statistical analysis inaccurate.

Table 5.1. The number of observations provided by circles with 8-km (5-mile), 16-km (10-mile), and 40-km (25-mile) radii at 26 locations along the U.S. Gulf Coast. The latitude and longitude values depict the coordinates of circle centers.

| Location | State | Lat | Lon | Data | Data | Data |
|--------------------------------|-------|---------|----------|------|------|------|
| S Padre Island/ Port Isabel | TX | 26.0617 | -97.1906 | 23 | 23 | 24 |
| Corpus Christi | TX | 27.8026 | -97.4185 | 21 | 23 | 29 |
| Port Lavaca | TX | 28.611 | -96.622 | 14 | 14 | 19 |
| Freeport | TX | 28.9457 | -95.3503 | 21 | 21 | 25 |
| Galveston | TX | 29.3032 | -94.8148 | 47 | 50 | 51 |
| Baytown | TX | 29.7119 | -95.04 | 18 | 18 | 23 |
| Sabine Pass | TX | 29.7191 | -93.8892 | 16 | 30 | 39 |
| Cameron | LA | 29.7964 | -93.3259 | 24 | 25 | 31 |
| Morgan City | LA | 29.64 | -91.3 | 9 | 20 | 23 |
| Grand Isle | LA | 29.2427 | -89.9897 | 34 | 34 | 35 |

Table 5.1 (continued). The number of observations provided by circles with 8-km (5-mile), 16-km (10-mile), and 40-km (25-mile) radii at 26 locations along the U.S. Gulf Coast. The latitude and longitude values depict the coordinates of circle centers.

| | | | | | | |
|------------------------------------|----|---------|----------|----|----|----|
| Shell Beach | LA | 29.8508 | -89.6789 | 20 | 21 | 49 |
| New Orleans at L. Pontchartrain | LA | 30.0267 | -90.13 | 21 | 30 | 46 |
| Frenier | LA | 30.1047 | -90.4147 | 15 | 17 | 34 |
| Mandeville | LA | 30.3681 | -90.0961 | 24 | 24 | 39 |
| Slidell | LA | 30.2543 | -89.805 | 7 | 27 | 46 |
| Bay St. Louis/ Pass Christian | MS | 30.3255 | -89.3216 | 23 | 23 | 33 |
| Gulfport/ Biloxi | MS | 30.3942 | -88.9875 | 8 | 33 | 37 |
| Dauphin Island | AL | 30.2519 | -88.0994 | 19 | 21 | 21 |
| Mobile | AL | 30.6899 | -88.0417 | 31 | 31 | 33 |
| Pensacola | FL | 30.48 | -87.2589 | 11 | 32 | 38 |
| Panama City | FL | 30.176 | -85.806 | 7 | 22 | 23 |
| Apalachicola | FL | 29.7286 | -84.9847 | 26 | 27 | 32 |
| Cedar Key | FL | 29.1642 | -83.0457 | 21 | 21 | 27 |
| Tampa | FL | 27.9313 | -82.4689 | 25 | 25 | 33 |
| Fort Myers/ Cape Coral | FL | 26.6033 | -81.9086 | 18 | 27 | 30 |
| Key West | FL | 24.5609 | -81.7754 | 29 | 32 | 34 |

In order to evaluate homogeneity of selected data, I created a Physical Homogeneity Index (PHI). The PHI classifies the physical homogeneity of selected data sets into four categories: excellent, good, fair and poor. “Excellent” data are considered physically homogenous. Examples of these data are observations that come from the same side of a barrier island or the same area of a bay. “Good” data generally maintain physical homogeneity, however, slight differences in physical geography exist. An example would be data that come from different areas of the same barrier island. “Fair” data maintain some physical homogeneity, although some obvious differences exist in the physical settings of selected data. For example, data that come from both a barrier island and the mainland, or a barrier island and the seaward portion of a bay would be classified

in this category. “Poor” data are considered inhomogenous. Examples include data that are pulled from both barrier islands and the inward portion of a bay, or data that come from opposite sides of a levee system, such as the levees along the Mississippi River in Plaquemines Parish, Louisiana. I assigned a PHI value to each data selection circle for all 26 coastal communities from which I selected data (Table 5.2).

Table 5.2. Physical Homogeneity Index (PHI) classification provided by circles with 8-km (5-mile), 16-km (10-mile), and 40-km (25-mile) radii.

| Location | State | Lat | Lon | Data Quantity 5-mile Radius | Data Quantity 10-mile Radius | Data Quantity 25-mile Radius |
|------------------------------------|-------|---------|----------|-----------------------------|------------------------------|------------------------------|
| S Padre Island/ Port Isabel | TX | 26.0617 | -97.1906 | Fair | Fair | Poor |
| Corpus Christi | TX | 27.8026 | -97.4185 | Good | Good | Poor |
| Port Lavaca | TX | 28.611 | -96.622 | Good | Good | Poor |
| Freeport | TX | 28.9457 | -95.3503 | Good | Fair | Fair |
| Galveston | TX | 29.3032 | -94.8148 | Good | Fair | Poor |
| Baytown | TX | 29.7119 | -95.04 | Fair | Fair | Fair |
| Sabine Pass | TX | 29.7191 | -93.8892 | Good | Fair | Poor |
| Cameron | LA | 29.7964 | -93.3259 | Good | Fair | Poor |
| Morgan City | LA | 29.64 | -91.3 | Good | Fair | Poor |
| Grand Isle | LA | 29.2427 | -89.9897 | Good | Fair | Poor |
| Shell Beach | LA | 29.8508 | -89.6789 | Good | Fair | Poor |
| New Orleans at L. Pontchartrain | LA | 30.0267 | -90.13 | Good | Fair | Poor |
| Frenier | LA | 30.1047 | -90.4147 | Good | Good | Poor |
| Mandeville | LA | 30.3681 | -90.0961 | Fair | Fair | Poor |
| Slidell | LA | 30.2543 | -89.805 | Fair | Fair | Poor |
| Bay St. Louis/ Pass Christian | MS | 30.3255 | -89.3216 | Fair | Fair | Fair |
| Gulfport/ Biloxi | MS | 30.3942 | -88.9875 | Fair | Fair | Fair |
| Dauphin Island | AL | 30.2519 | -88.0994 | Fair | Fair | Poor |
| Mobile | AL | 30.6899 | -88.0417 | Fair | Fair | Poor |
| Pensacola | FL | 30.48 | -87.2589 | Good | Fair | Poor |
| Panama City | FL | 30.176 | -85.806 | Excellent | Fair | Fair |

Table 5.2 (continued). Physical Homogeneity Index (PHI) classification provided by circles with 8-km (5-mile), 16-km (10-mile), and 40-km (25-mile) radii.

| | | | | | | |
|------------------------|----|---------|----------|-----------|-----------|------|
| Apalachicola | FL | 29.7286 | -84.9847 | Good | Fair | Poor |
| Cedar Key | FL | 29.1642 | -83.0457 | Excellent | Excellent | Good |
| Tampa | FL | 27.9313 | -82.4689 | Fair | Fair | Poor |
| Fort Myers/ Cape Coral | FL | 26.6033 | -81.9086 | Good | Fair | Poor |
| Key West | FL | 24.5609 | -81.7754 | Fair | Fair | Fair |

After sampling the 26 locations for data quantity and homogeneity of data, I determined that data selection circles with radii of 16 km (10 miles) provided optimal data. Such circles provided sufficient data quantity, as these circles returned a total of 677 high watermarks at 26 locations, or an average of approximately 26 observations per site. Also, the data quality of these observations was adequate, as none of these datasets contained “poor” homogeneity.

Although circles with 40-km (25-mile) radii provided more data than circles with 16-km (10-mile) radii, 19 of the 26 sites contained “poor” data homogeneity at this scale, making analysis at this scale unsuitable. Circles with 8-km (5-mile) radii often provided better homogeneity than circles with 16-km (10-mile) radii, however, insufficient data quantity limited the number of sites for analyses, as only 18 of the 26 sites contained at least 20 observations.

Data selection circles were typically centered along the waterfront near the center of coastal communities, however, some exceptions were made to improve homogeneity. For example, a 16-km (10-mile) circle centered at the New Canal Station tide gauge in New Orleans, near Lake Pontchartrain, provides high-water marks from both the Lake Pontchartrain shorefront, on the north side of the city, and the Mississippi River Gulf Outlet (MRGO), on the east side of New Orleans. These two locations experience storm

surge from different directions, and are therefore inhomogenous. I shifted the data selection circle slightly to the west of New Canal Station, so New Orleans data were entirely selected from the Lake Pontchartrain waterfront, and canals that connect to Lake Pontchartrain. I also established a data selection site at Shell Beach, Louisiana, to analyze surge levels that approach New Orleans from the east. The 16-km (10-mile) data selection circle for Shell Beach provides “fair” data homogeneity, as this circle does not extend to Lake Pontchartrain or the levees along the Mississippi River.

I also intentionally shifted the data selection circle at Pensacola, Florida, to improve data homogeneity. A 16-km (10-mile) radius circle centered near Pensacola’s waterfront covers both the barrier island near Pensacola Beach, and the inward portions of Pensacola and Escambia Bays. Combining data from both of these locations creates an inhomogenous dataset. As such, I shifted the circle slightly north to eliminate observations from the barrier island. This shift enables the circle to select data entirely from the western side of Pensacola and Escambia Bays, near the city of Pensacola. The data in Tables 5.1 and 5.2 account for these shifted data-selection circles.

In other cases, I shifted the centers of data selection circles away from city centers in order to combine cities that were near each other into the same circle. For example, data selection circles with 16-km (10-mile) radii, centered on Gulfport and Biloxi, Mississippi, overlap each other. Therefore, I created a circle that is centered between these two cities and contains data for both locations. I also created circles that combine data from Bay St. Louis and Pass Christian, Mississippi, as well as Cape Coral and Fort Myers, Florida, for the same reason.

Following these steps, I created a list of observed high water marks for 26 locations along the U.S. Gulf Coast. I also decided to add estimated water levels for two major surge events that likely impacted Baytown, Texas. From an industrial and economic perspective, Baytown is one of the most important cities in the region, as it contains one of the largest petrochemical complexes in the world. However, storm surge data are unavailable at Baytown for the category-4 hurricane that struck Galveston in 1900, or the major hurricane that struck south of Galveston in 1915. Storm tides at Galveston reached 6.1 m in 1900 (Garriott 1900), and 4.72 m in 1915 (Connor 1956; Landsea et al. 2008). These events produced the two highest watermarks at Galveston (Needham and Keim 2012). Both of these hurricanes likely generated massive storm surges at Baytown, as well, where storm surge heights exceed levels in Galveston when hurricanes make landfall between Galveston and Corpus Christi. I identified seven tropical cyclones that made landfall between Corpus Christi and Galveston, and for which observed water levels are available at both Baytown and Galveston in SURGEDAT. The water level at Baytown exceeded levels in Galveston for all of these events, and the average difference was approximately 37% (Table 5.3). As such, I estimated the maximum storm tide of the 1900 and 1915 hurricanes to be 37% higher at Baytown than Galveston, producing storm tide estimates of 8.38 m in 1900, and 6.49 m in 1915, at Baytown. These are the only two values in this analysis that were not observed, but derived, however, given the economic importance of Baytown, I felt it was best to estimate water levels for these events. These events increased the quantity of coastal flood events at Baytown from 18 to 20.

Table 5.3. Comparison of water levels at Galveston and interior portions of Galveston Bay, from tropical cyclones that made landfall between Corpus Christi and Galveston, Texas, and produced at least 2 m storm surge/ storm tide in Galveston Bay. Adapted from Zoch (1949); U.S. Weather Bureau (1959); U.S. Army Engineer District- Galveston, Texas (1962); Harris (1963); National Hurricane Center (1983); National Hurricane Center (1989); Federal Emergency Management Agency (2009).

| Year | Storm Name | Water Level at | Water Level at | Percent Greater |
|------|------------|----------------|-----------------|-----------------|
| 1942 | Unnamed | 1.92 | 2.44 | 27.1 |
| 1949 | Unnamed | 2.13 | 3.47 | 62.9 |
| 1959 | Debra | 1.49 | 2.41 | 61.7 |
| 1961 | Carla | 3.13 | 4.45 | 42.2 |
| 1983 | Alicia | 2.9 | 3.69 | 27.2 |
| 1989 | Jerry | 1.83 | 2.44 | 33.3 |
| 2008 | Ike | 3.52 | 3.79 | 7.7 |
| | | | Avg. Difference | 37.4 |

5.3.2 Adjusting for Geodetic and Tidal Datums

Storm tide observations measure the total water level above a datum, or vertical reference line. SURGEDAT references high water marks to both geodetic and tidal datums. Approximately 85% of Gulf Coast storm tide observations in SURGEDAT are tied to such geodetic and tidal datums.

5.3.2.1 Adjusting Geodetic Datum References

The most common geodetic datums referenced in SURGEDAT are the National Geodetic Vertical Datum of 1929 (NGVD 29) and the North American Vertical Datum of 1988 (NAVD88). These datums reference the approximate MSL for the years 1929 and 1988. Observations measured from geodetic datums overestimate the actual storm tide height because sea levels along the U.S. Gulf Coast are rising relative to the height of land. The term most commonly used in the scientific literature for this phenomenon is

Relative Sea-Level Rise (RSLR), which combines eustatic, or global, sea-level elevation changes, with localized changes in land elevation. Relative sea levels are rising faster along much of the U.S. Gulf Coast than the global average because land elevations at many locations are subsiding, or sinking, due to various factors, including sediment compaction of deltas (Penland and Ramsey 1990) and extraction of subterranean fluids, like oil, gas or water (Galloway et al. 1999; Nicholls and Cazenave 2010).

In order to remove errors introduced by geodetic datum references, I acquired annual RSLR rates for all locations and multiplied those rates by the number of years that passed between storm surge events and the establishment of referenced vertical datums. I then subtracted this value from observed storm tide heights in SURGEDAT to obtain adjusted water levels that provide water heights above MSL for the year of each surge event, which I defined as a new reference line, called “annual datum.”

Various sources provided data for localized sea-level trends (Table 5.4). A list of MSL trends provided by the National Oceanic and Atmospheric Administration (2013) reveals the rate of RSLR in mm/year for 14 sites included in this study. Most of these 14 sites reference unique RSLR values, however, both Corpus Christi and Port Lavaca, Texas, reference the sea-level trend for Rockport, Texas, which is located between these two cities. Two RSLR values are provided for Galveston, Texas; I referenced the RSLR rate at Galveston Pleasure Pier because this site is located on the Gulf side of Galveston, where higher storm surges have historically occurred. Sea-level trends are also listed for both Padre Island and Port Isabel, Texas, which both fall within the same data-selection circle in South Texas. I referenced the sea-level trend at Padre Island because SURGEDAT provides more comprehensive data at this site than at Port Isabel. I used

tide gauge data for St. Petersburg, Florida, for datum adjustments at Tampa, because the St. Petersburg gauge provides the most extensive sea-level trend data for the Tampa Bay area. This gauge provides 60 years of data (National Oceanic and Atmospheric Administration 2013) and is located on the western shore of Tampa Bay (Penland and Ramsey 1990).

Table 5.4. Sea-level trends for 26 locations along the U.S. Gulf Coast. Data provided by Penland and Ramsey (1990); Galloway et al. (1999); National Oceanic and Atmospheric Administration (2013); and U.S. Department of Transportation (2013).

| Location | State | Sea-Level Trend Location | Yrs of Sea-Level Trend Data | Sea-Level Trend (cm/ yr) | Source |
|------------------------------------|-------|------------------------------------|---|---------------------------------|------------------------------|
| S Padre Island/ Port Isabel | TX | Padre Island | 49 | 0.348 | NOAA (2013) |
| Corpus Christi | TX | Rockport | 59 | 0.516 | NOAA (2013) |
| Port Lavaca | TX | Rockport | 59 | 0.516 | NOAA (2013) |
| Freeport | TX | Freeport | 53 | 0.435 | NOAA (2013) |
| Galveston | TX | Galveston Pleasure Pier | 50 | 0.684 | NOAA (2013) |
| Baytown | TX | Baytown- Laporte | 108 | 1.19* | Galloway et al. (1999) |
| Sabine Pass | TX | Sabine Pass | 49 | 0.566 | NOAA (2013) |
| Cameron | LA | Calcasieu Pass | 47 | 0.57 | Penland and Ramsey (1990) |
| Morgan City | LA | Calumet and Morgan City | 47 and 45 | 1.77 and 1.26 | Penland and Ramsey (1990) |
| Grand Isle | LA | Grand Isle | 60 | .924 | NOAA (2013) |
| Shell Beach | LA | South Shore and Little Woods | 38 and 47 (Used 2 tide gauges) | 1.05 (Avg. of two values) | Penland and Ramsey (1990) |
| New Orleans at L. Pontchartrain | LA | West End | 57 | .40 | Penland and Ramsey (1990) |
| Frenier | LA | Frenier | 54 | .36 | Penland and Ramsey (1990) |

Table 5.4 (continued). Sea-level trends for 26 locations along the U.S. Gulf Coast. Data provided by Penland and Ramsey (1990); Galloway et al. (1999); National Oceanic and Atmospheric Administration (2013); and U.S. Department of Transportation (2013).

| | | | | | |
|----------------------------------|----|------------------|---------|------|---------------------------|
| Mandeville | LA | Mandeville | 58 | .45 | Penland and Ramsey (1990) |
| Slidell | LA | Mandeville | 58 | .45 | Penland and Ramsey (1990) |
| Bay St. Louis/ Pass Christian | MS | Biloxi | Unknown | .15 | Penland and Ramsey (1990) |
| Gulfport/ Biloxi | MS | Biloxi | Unknown | .15 | Penland and Ramsey (1990) |
| Dauphin Island | AL | Dauphin Island | 41 | .298 | NOAA (2013) |
| Mobile | AL | 4 km E of Mobile | Unknown | .09 | U.S. DOT (2013) |
| Pensacola | FL | Pensacola | 84 | .21 | NOAA (2013) |
| Panama City | FL | Panama City | 34 | .075 | NOAA (2013) |
| Apalachicola | FL | Apalachicola | 40 | .138 | NOAA (2013) |
| Cedar Key | FL | Cedar Key | 93 | .18 | NOAA (2013) |
| Tampa | FL | St. Petersburg | 60 | .24 | NOAA (2013) |
| Fort Myers/ Cape Coral | FL | Fort Myers | 42 | .24 | NOAA (2013) |
| Key West | FL | Key West | 94 | .224 | NOAA (2013) |

* This value represents the average sea-level trend for the entire record, but rates varied through different periods.

Penland and Ramsey (1990) provided sea-level trend data for coastal Mississippi and Louisiana, including multiple sites around Lake Pontchartrain. This source provided data for the U.S. Army Corps tide gauge at West End, which were used to estimate the RSLR rate at New Orleans, for storm surges that approach the city from the north. Penland and Ramsey (1990) also provided sea-level trend data for Mandeville and Frenier, along the shores of Lake Pontchartrain. Mandeville data were used to estimate the sea-level trend at Slidell, Louisiana, even though the city of Slidell is closer to the

U.S. Army Corps tide gauge at South Shore, Louisiana. The South Shore tide gauge is located less than 10 km south of Slidell's waterfront, whereas Mandeville is located approximately 30 km to the west. However, the geomorphology of Slidell relates better to Mandeville than South Shore. Slidell and Mandeville are both located on Lake Pontchartrain's North Shore, and have slower subsidence rates than the South Shore tide gauge, which is located on the St. Bernard Delta Plain, and observes a rapid RSLR rate of 1.01 cm/ year (Penland and Ramsey 1990).

However, data from the South Shore tide gauge were used to estimate sea-level trends at Shell Beach, Louisiana. Penland and Ramsey (1990) concluded that out of 10 U.S. Army Corps tide gauges on the St. Bernard Delta Plain, only South Shore and Little Woods tide gauges provided adequate data to analyze sea-level trends in this region. They provide a RSLR rate of 1.09 cm/ year at Little Woods and 1.01 cm/ year at South Shore. The average of these two values provide an estimated sea-level trend of 1.05 cm/ year at Shell Beach, which is also located on the St. Bernard Delta Plain.

In South Central Louisiana, Penland and Ramsey (1990) provided sea-level trends for Morgan City and Calumet. Trends for both of these sites were used for datum adjustments, and each high water mark in this area was matched with sea-level trend data for either Morgan City or Calumet, depending on the location of the observation. Although these two locations both fall within the Morgan City data-selection circle, and have noticeably different RSLR rates. Calumet has observed a RSLR rate of 1.77 cm/yr, while the rate at Morgan City is 1.26 cm/yr (Penland and Ramsey 1990).

RSLR rates in Mississippi are considerably lower than much of South Louisiana because of differences in geomorphology. The sea-level trend at Biloxi, Mississippi is

only 0.15 cm/year (Penland and Ramsey 1990). This trend was used for datum adjustments at both the Biloxi/ Gulfport and Bay St. Louis/ Pass Christian locations.

The U.S. Department of Transportation (2013) provides vertical land elevation changes from benchmark surveys for more than 60 sites in Mobile and Baldwin Counties, Alabama. Site BH0144 is located less than 4 km east of the Mobile waterfront, near the junction of the Mobile River and Mobile Bay. This site was selected for datum adjustments at Mobile because of its proximity to the city.

Datum adjustments near Baytown, Texas, were the most complicated because rapid subsidence rates occurred throughout much of the 20th century near this location due to the extraction of subterranean fluids, such as oil, gas and water. Subsidence rates also changed over time in this area, as ground elevations responded to localized fluid extraction. Oil extraction in the region began in 1917, when the Goose Creek Oil Field was developed near the modern-day Houston Ship Channel (Galloway et al. 1999). By 1926, localized subsidence in this area already reached 0.91 m (Galloway et al. 1999). Subsidence continued through the 1970s, reaching at least 1.83 m along the Houston Ship Channel, between Houston and Bayport (Galloway et al. 1999). By 1979, 5,150 square km of land had subsided at least 0.3 m and maximum subsidence levels reached as high as 3.05 m (Galloway et al. 1999). In nearby Pasadena, cumulative subsidence exceeded 3.05 m between 1906-1995 (Stork and Sneed 2002).

The drowning of the Brownwood subdivision in Baytown provides an excellent example of the local impacts of rapid subsidence in this area. This subdivision was constructed in 1938 and consisted of approximately 500 single-family homes (Galloway et al. 1999). Although portions of Brownwood were located as high as 3.05 m above sea

level, flooding from high tides and storm surge occurred frequently after more than 2.44 m of subsidence occurred (Galloway et al. 1999). The entire community was abandoned (Galloway et al. 1999) after Hurricane Alicia generated a 3.69-m storm tide near the entry to the Houston Ship Channel in 1983 (National Weather Service 2011).

I referenced subsidence maps provided by the Harris-Galveston Coastal Subsidence District and published in Galloway et al. (1999), in order to make datum adjustments of storm tide heights in this region. These maps provide regional subsidence trends for the time periods 1906-1943, 1943-1973, and 1973-1995. They depict total subsidence levels, from which I calculated average annual subsidence rates. I estimated subsidence trends for the area where the present-day Houston Ship Channel divides the cities of Baytown from Laporte, because most of the observations from the Baytown data-selection circle come from one of these two cities. For the years 1995-2013, I used the 1906-1943 rates, because recent subsidence rates relate better to the 1906-1943 era, before rapid industrialization caused the most rapid subsidence. In recent decades, subsidence rates have been arrested, due to laws restricting and prohibiting the extraction of fluids (Stork and Sneed 2002), so the use of the slower subsidence rates for this period is appropriate.

Table 5.5 provides the total subsidence and annual subsidence rates for Baytown/Laporte during the four time periods. The total amount of subsidence estimated in this region between 1906-2013 is 1.28 m, which provides an annual sea-level trend of 1.19 cm/yr. This is a conservative estimate that represents the general subsidence in this area, although localized maximum levels in the region have reached as high as 3.05 m (Galloway et al. 1999). Adjustments of storm tide observations in SURGEDAT were

customized depending on the number of years that transpired between the coastal flooding event and the year of the datum reference.

Table 5.5. Subsidence rates near Baytown, Texas, from 1906-2013.

| Year Range | Number of Years | Total Elevation Change (m) | Annual Subsidence Rate (cm/yr) |
|------------|-----------------|----------------------------|--------------------------------|
| 1906-1943 | 37 | .0914 | .25 |
| 1943-1973 | 30 | .9144 | 3.05 |
| 1973-1995 | 22 | .2286 | 1.04 |
| 1995-2013 | 19 | .0475 | .25 |
| | | | Average: 1.19 |

For all coastal locations included in this analysis, the average annual RSLR rate was .46 cm/yr. The highest rate was 1.77 cm/yr at Calumet, Louisiana, which falls inside the Morgan City data-selection circle. The lowest sea-level trend was .09 cm/yr at Mobile, Alabama. From 1943-1973, the rate near Baytown, Texas, was 3.05 cm/yr.

Hurricane Rita’s storm tide in Galveston, Texas, provides an example of a geodetic datum adjustment. The maximum water level at Galveston Pleasure was measured as 1.43 m (4.69 ft) above NGVD 29 (Knabb et al. 2006). However, 76 years passed from the establishment of this datum and Rita’s storm surge in 2005. I estimate that the sea level in Galveston rose 0.52 m relative to the land during this period because the linear MSL trend at Galveston Pleasure Pier during the period 1957-2006 averaged 0.0064 m/yr (National Oceanic and Atmospheric Administration 2013). I therefore subtracted 0.52 m from the observed storm tide level to obtain an adjusted storm tide level of 0.91 m above the “annual datum,” or the mean sea level for 2005 (Figure 5.4).

This adjusted water level is not a storm surge because the time of the peak water level is unknown, so I cannot remove the tidal influence from the day of the storm tide event.

5.3.2.2 Adjusting Tidal Datum References

The most common tidal datums include Normal Astronomical Tide (NAT), Mean Sea Level (MSL), Mean Low Water (MLW), and Mean Lower Low Water (MLLW). Observations measured above NAT already remove the tidal component of the water level, essentially classifying such observations as storm surges. Water heights measured above MSL were left as unadjusted storm tides, as I assumed the MSL level to refer to the year of the surge event. Numerical adjustments were made, however, for observations referenced to MLW and MLLW, as it was necessary to convert these datums to MSL. In all of these cases, such datum adjustments lowered the observed water level.

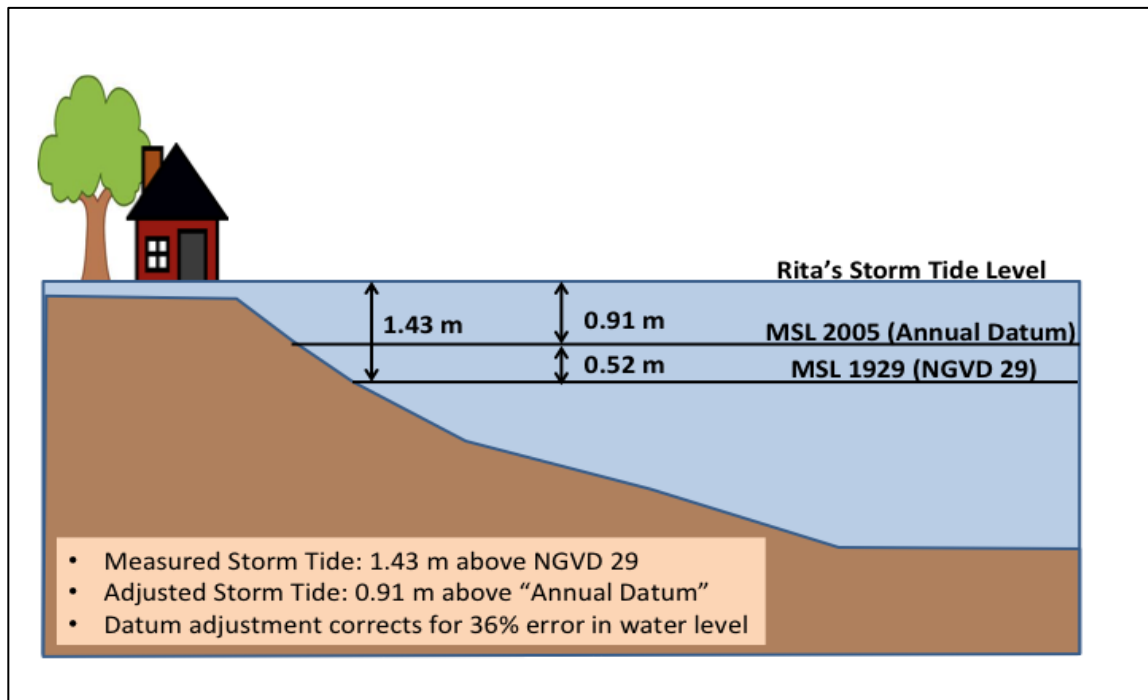


Figure 5.4. A geodetic datum adjustment at Galveston, Texas, reduced the storm tide level for Hurricane Rita from 1.43 m above NGVD29 to 0.91 m above the "annual datum" of 2005. Rita's storm surge impacted Texas and Louisiana on September 23-24, 2005. Data adapted from Knabb et al. (2006) and National Oceanic and Atmospheric Administration (2013).

For tidal datum adjustments, I used tide data from the NOAA Tides and Currents Web Portal, provided by the National Oceanic and Atmospheric Administration (2014). Each referenced tide gauge had a customized graphic and table that provided the heights of various tidal datum. All of these data referenced the Present Epoch, which extended from 1983-2001. I assumed stationarity of tidal data over time, which enabled me to use data from the Present Epoch to make tidal datum adjustments for surge events at any time in the data record. This assumption is reasonable, as the range of tidal cycles should stay approximately stationary, even as sea levels rise relative to the elevation of land.

A storm tide generated by Hurricane Alma in 1966 in the Florida Keys provides an example of a tidal datum adjustment. This storm generated a 1.07-m storm tide above MLW at Key West (Sugg 1967). The difference between MSL and MLW at Key West is 0.20 m, according to data from the Present Epoch, provided by the National Oceanic and Atmospheric Administration (2014). I therefore reduced the water level of this event by 0.20 m, adjusting the storm tide height from 1.07 to 0.87 m (Figure 5.5). The adjusted level represents a storm tide height above MSL.

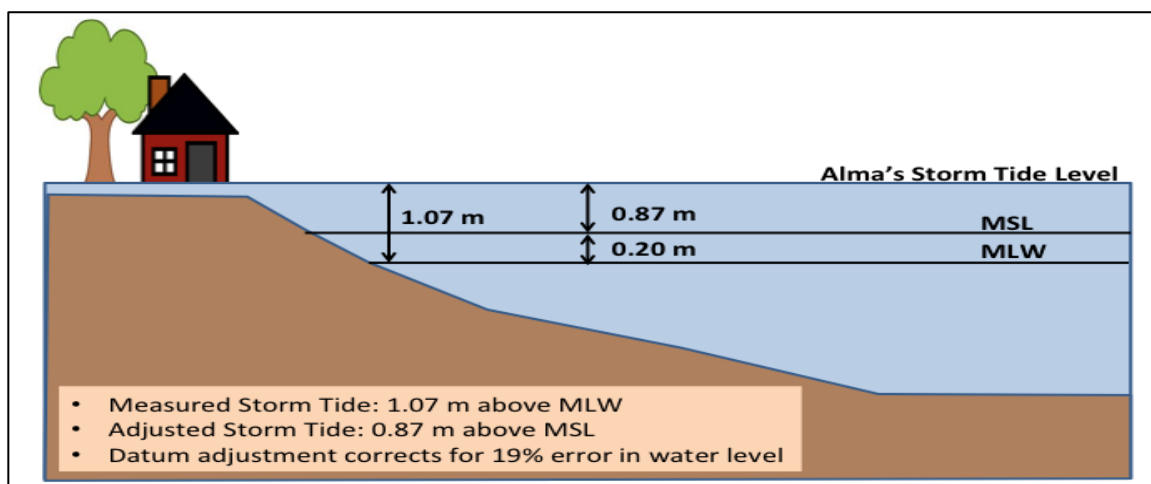


Figure 5.5. Tidal datum adjustment at Key West reduced the storm tide for Hurricane Alma from 1.07 m above MLW to 0.87 m above MSL. Data adapted from Sugg (1967) and National Oceanic and Atmospheric Administration (2014).

Table 5.6 provides a list of tidal datum heights at all 26 coastal locations. As the National Oceanic and Atmospheric Administration (2014) lists these datums as height in meters above the station datum, considerable differences in the datum elevations sometimes exist. For example, the elevation of MSL at Galveston is listed as 1.404 m, while the elevation of MSL at Cameron is 8.553 m. These are heights above arbitrary station datums that vary considerably between locations. Therefore, the higher value at Cameron does not refer to the gauge height above MSL but the height above Cameron's station datum. For purposes of tidal adjustment, the actual elevation values were unimportant, as I used the difference between MSL and MLW or MSL and MLLW to adjust water levels.

Table 5.6. The height of MSL, MLW and MLLW at locations along the U.S. Gulf Coast. The difference between MSL and MLW or MSL and MLLW were used for tidal datum adjustments. Data provided by National Oceanic and Atmospheric Administration (2014).

| Site Location | Tide Gauge Location | MSL | MLW | MLLW | MSL-MLW | MSL-MLLW |
|--------------------------------|---|-------|-------|-------|---------|----------|
| S Padre Island/ Port Isabel | South Padre Island Coast Guard Station | 1.351 | 1.157 | 1.114 | .194 | .237 |
| Corpus Christi | Bob Hall Pier | 6.635 | 6.421 | 6.353 | .214 | .282 |
| Port Lavaca | Port Lavaca | 1.081 | .949 | .931 | .132 | .15 |
| Freeport | Freeport | 1.525 | 1.317 | 1.234 | .208 | .291 |
| Galveston | Galveston Pleasure Pier | 1.404 | 1.185 | 1.066 | .219 | .338 |
| Baytown | Morgans Point | 1.807 | 1.625 | 1.59 | .182 | .217 |
| Sabine Pass | Sabine Pass North | 1.343 | 1.174 | 1.05 | .169 | .293 |
| Cameron | Calcasieu Pass | 8.553 | 8.355 | 8.19 | .198 | .363 |
| Morgan City | Berwick | 6.088 | 6.01 | 5.996 | .078 | .092 |
| Grand Isle | Grand Isle | 1.980 | 1.820 | 1.817 | .16 | .163 |

Table 5.6 (continued). The height of MSL, MLW and MLLW at locations along the U.S. Gulf Coast. The difference between MSL and MLW or MSL and MLLW were used for tidal datum adjustments. Data provided by National Oceanic and Atmospheric Administration (2014).

| | | | | | | |
|----------------------------------|----------------------------|-------|-------|-------|------|------|
| Shell Beach | Shell Beach | 9.765 | 9.554 | 9.542 | .211 | .223 |
| New Orleans at L. Pontchartrain | New Canal Station | 1.380 | 1.301 | 1.305 | .079 | .075 |
| Frenier | Unavailable* | | | | | |
| Mandeville | Unavailable* | | | | | |
| Slidell | Unavailable* | | | | | |
| Bay St. Louis/ Pass Christian | Bay Waveland Yacht Club | .994 | .763 | .728 | .231 | .266 |
| Gulfport/ Biloxi | Biloxi | 6.548 | 6.317 | 6.272 | .231 | .276 |
| Dauphin Island | Dauphin Island | 1.049 | .88 | .877 | .169 | .172 |
| Mobile | Point Clear, Mobile Bay | 8.821 | 8.588 | 8.583 | .233 | .238 |
| Pensacola | Pensacola | 2.757 | 2.578 | 2.569 | .179 | .188 |
| Panama City | Panama City | 1.222 | 1.033 | 1.019 | .189 | .203 |
| Apalachicola | Apalachicola | 1.584 | 1.429 | 1.307 | .155 | .277 |
| Cedar Key | Cedar Key | 1.171 | .743 | .550 | .428 | .621 |
| Tampa | Tampa, Ballast Point | .758 | .445 | .312 | .313 | .446 |
| Fort Myers/ Cape Coral | Fort Myers | 1.522 | 1.376 | 1.329 | .146 | .193 |
| Key West | Key West | 1.662 | 1.463 | 1.390 | .199 | .272 |
| Average | --- | --- | --- | --- | .196 | .256 |
| | | | | | | |

* All datum adjustments were geodetic

The average difference between MSL and MLW for the coastal locations included in this study was 0.1964 m, and the average difference between MSL and MLLW was

0.2555 m. The highest tidal range for these communities is observed at Cedar Key, Florida, where the difference between MSL and MLW is 0.428 m, and the difference between MSL and MLLW is 0.621 m. The lowest tidal range was observed at New Orleans on Lake Pontchartrain, where the difference between MSL and MLW was 0.79 m and the difference between MSL and MLLW was 0.75 m. This was the only location where the elevation of MLW was lower than MLLW.

Tidal datum adjustments did not account for tidal oscillations on the date of storm tide events, which means that adjusted water levels are not storm surges, but storm tides measured above MSL. The timing of such storm tides affects maximum water levels; a storm surge inundating one location at the time of high tide will produce a higher total water level than a storm surge of equal magnitude inundating a different location at the time of low tide. As such, tidal oscillations introduce errors for storm tide observations, because the timing of most observed storm surge events is unknown in SURGEDAT. Fortunately, the Gulf of Mexico is a microtidal basin, where tidal ranges are < 1 m (Stumpf and Haines 1998).

5.3.3 Statistical Analysis

5.3.3.1 Extreme Value Theory

Storm surges are rare events and historical storm surge measurements in most locations only extend back less than 125 years, providing sparse data for building reliable empirical models for events that exceed the data record. Extreme value theory has often been used as an alternative to estimate the probability of rare events, including extreme hurricane winds (Chu and Wang 1998; Jagger and Elsner 2006; Elsner et al. 2008; Emanuel and Jagger 2010), volcanoes (Mendoza-Rosas and De la Cruz-Reyna 2008;

Sobradelo et al. 2011), and wildfires (Jiang and Zhuang 2011). Extreme value theory is a powerful tool for analyzing extreme events because it attempts to model only the tail end of a distribution, or in other words, the distribution of the extreme events only (Coles 2001). Through the use of mathematical limit arguments, extreme value models allow for the study of events that are much greater than what have already been observed (Coles 2001). The ability to extrapolate from observed levels out to higher, unobserved levels is important when considering a location's storm surge risk, because it is likely that storm surge heights greater than what have been observed in the historical record will occur in the future.

5.3.3.2 Point Process Model for Extreme Values

The Point Process (PP) representation of extreme value behavior is one of a variety of different approaches to extreme value modeling (Coles 2001). Pickands III (1971) was the first to introduce the PP approach for use in extreme value statistics, and Smith (1989) was one of the first to develop the theory needed to apply the approach. For the derivation of the PP model for extreme values, and its connection to other extreme value distributions, see Coles (2001). The PP extreme value model is a physically appropriate model for storm surge, because it enables surge occurrence to be modeled separately from surge height. In addition, in contrast to some other extreme value methods, an annual return rate for extreme surge can be obtained, rather than just a return rate per surge occurrence. For these reasons, the PP approach to extreme value statistics has been used to model similar types of phenomena, such as hurricane wind speeds (Jagger and Elsner 2006).

The PP approach is based on the theory that for very high values above a threshold u , the frequency of extreme events follows a Poisson distribution with mean exceedance rate λ_u , and the threshold excesses, or the magnitudes of the events, follow a generalized Pareto distribution with parameters location μ , scale σ , and shape ξ . The choice of a threshold u is important. Choosing a high threshold reduces the risk of bias, but the threshold exceedances may be too few to create a meaningful model (Coles 2001). Therefore, it is common to fit the model at various thresholds and choose the highest threshold at which there is some stability in the parameter estimations, though this distinction is somewhat subjective. An additional consideration in this study was the desire to choose a common threshold among all 26 cities to standardize the data analysis.

Figure 5.6 shows the threshold analysis for Galveston, Texas. This location provides a good indicator of parameter behavior for various thresholds because more storm surge data are available for Galveston than any other location along the U.S. Gulf Coast. This plot shows the range of parameter values for location, scale and shape. Lower threshold values produce more stable results, as the range of parameter estimates is smaller than the parameter range of higher thresholds. For example, the range of parameter estimates for both location and scale begin to increase substantially for surge thresholds ≥ 1.2 m. Also, the difference in parameter estimates between consecutive threshold values is lower for low thresholds.

After reviewing these plots, several advantages became apparent for using a threshold of 0.91 m. At this level, there appears to be stability in the parameter estimates. Also, some National Weather Service websites suggest that a threshold of 0.91 m (3 ft) may provide a practical upper-limit for minor coastal flood levels, in terms of flood

impacts in hurricane-prone areas of the United States. The National Weather Service Office in Tampa Bay, Florida, defines low-impact coastal floods as events with storm tides ≤ 0.91 m (National Weather Service- Tampa Bay 2014). Also, the National Weather Service Forecast Office at Wakefield, Virginia, defines a minor coastal flood as an event with a storm tide ≤ 0.61 m and a moderate coastal flood as an event with a storm tide magnitude from 0.61-0.91 m (National Weather Service– Wakefield 2014).

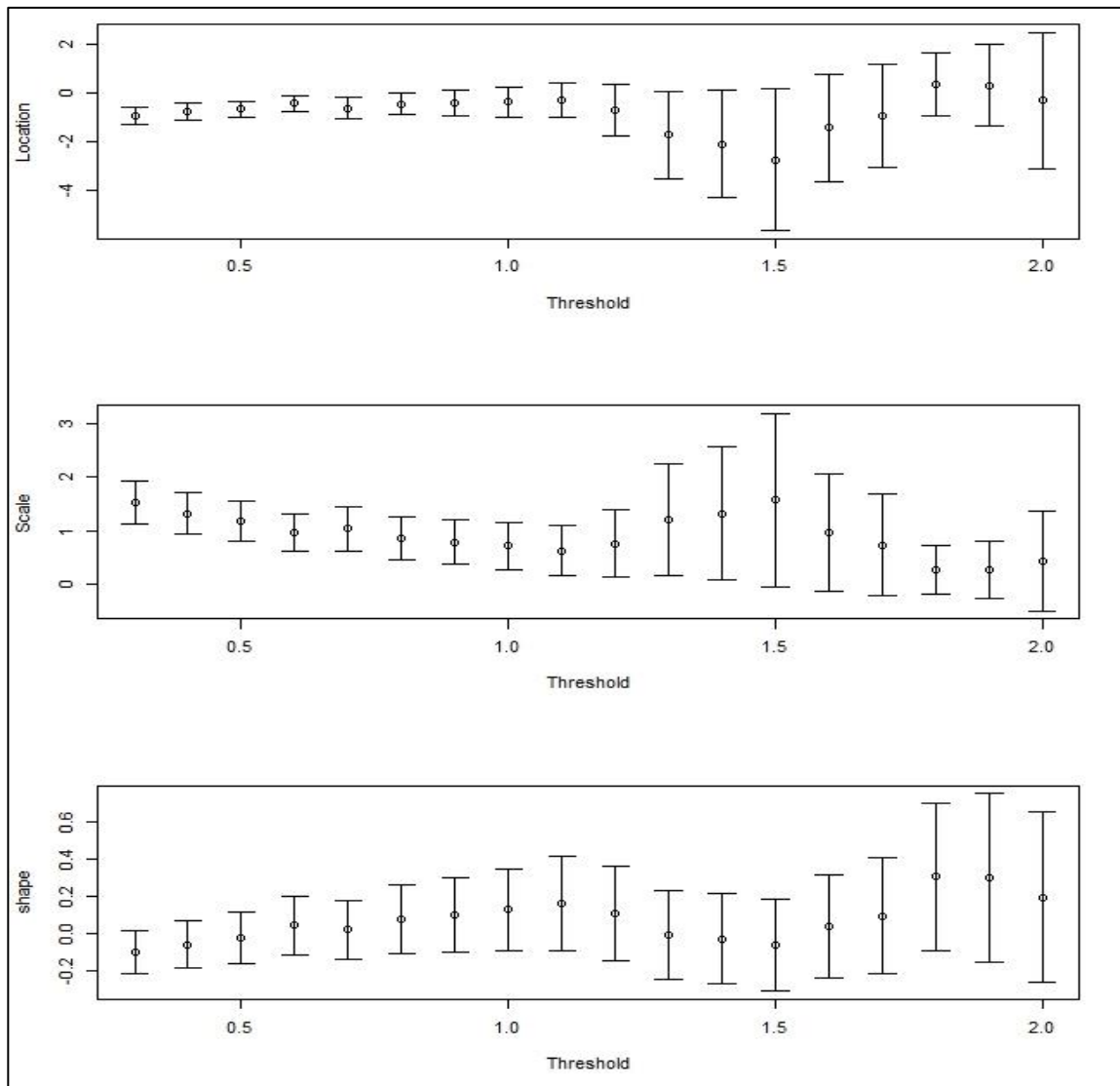


Figure 5.6. Parameter estimates of location μ , scale σ , and shape ξ determined by fitting the point process model at various thresholds. Vertical bars show the standard error of each parameter estimate.

A threshold of 0.91 m is also proximal to 1 m, which is a water level that has already been used to investigate topics related to coastal flooding and sea-level rise. For example, Strauss et al. (2012) concluded that 3.7 million people in the U.S. would be inundated by a 1 m sea level rise. Nicholls et al. (1999) estimates that a 1 m sea level rise would increase the global population in coastal flood hazard zones by 25%.

A threshold of 0.91 m provides more data in this study than a threshold of 1 m, because high water marks in this region have usually been recorded in feet, and numerous observations have magnitudes of 0.91 m (3 ft). Approximately 85% of the locations (22 of 26) contain more data with a threshold of 0.91 m than 1 m, and the number of observations at Slidell, Louisiana, increases from 19 to 24 when using the lower threshold. Before applying the threshold, the average location in this study contained approximately 26 observations, but a threshold of 0.91 m decreases the average number of observations to 19.3, while a threshold of 1 m reduces the average to 17.7 (Table 5.7).

Table 5.7. Comparison of observed storm surge/ storm tide events at each location and the number of events \geq than the 0.91 m threshold used in the Point Process method.

| Location | State | All High | High Water | High Water |
|--------------------------------|-------|----------|------------|------------|
| S Padre Island/ Port Isabel | TX | 23 | 14 | 12 |
| Corpus Christi | TX | 23 | 13 | 10 |
| Port Lavaca | TX | 14 | 10 | 9 |
| Freeport | TX | 21 | 18 | 16 |
| Galveston | TX | 50 | 34 | 32 |
| Baytown | TX | 20* | 17* | 16* |
| Sabine Pass | TX | 30 | 22 | 21 |
| Cameron | LA | 25 | 15 | 13 |
| Morgan City | LA | 20 | 15 | 12 |
| Grand Isle | LA | 34 | 24 | 23 |
| Shell Beach | LA | 21 | 20 | 20 |
| New Orleans | LA | 30 | 26 | 25 |
| Frenier | LA | 17 | 17 | 17 |

Table 5.7 (continued). Comparison of observed storm surge/ storm tide events at each location and the number of events \geq than the 0.91 m threshold used in the Point Process method.

| | | | | |
|------------------|----|----|----|----|
| Mandeville | LA | 24 | 24 | 22 |
| Slidell | LA | 27 | 24 | 19 |
| Bay St. Louis/ | MS | 23 | 28 | 25 |
| Gulfport/ Biloxi | MS | 33 | 29 | 28 |
| Dauphin Island | AL | 21 | 18 | 14 |
| Mobile | AL | 31 | 21 | 21 |
| Pensacola | FL | 32 | 20 | 20 |
| Panama City | FL | 22 | 13 | 10 |
| Apalachicola | FL | 27 | 22 | 21 |
| Cedar Key | FL | 21 | 15 | 14 |
| Tampa | FL | 25 | 18 | 17 |
| Ft Myers | FL | 27 | 13 | 10 |
| Key West | FL | 32 | 13 | 12 |

* Includes estimates of two events that were observed at Galveston, Texas.

Although an average quantity of 19 observations per site may be inadequate for traditional statistics, extreme value analysis is useful for analyzing datasets that are short or incomplete (Davison and Smith 1990; Coles 2001; Beguería 2005; Sobradelo et al. 2011). The precedent has also been set for analyzing datasets with similar or less data quantity; for example, (Sobradelo et al. 2011) utilized extreme value theory to analyze volcanic activity in the Canary Islands using only 15 historical observations. Approximately 73% (19 of 26) of the locations in this study have at least 15 observations after applying the 0.91 m threshold, and 96% of locations (25 of 26) have at least 13 observations. Port Lavaca, Texas, has only 10 observations after introducing the threshold, however, it is important to include this site in the study, as it fills a geographic gap along the Texas Coast, and is the site of Hurricane Carla's peak storm tide level,

which reached 6.71 m (U.S. Army Engineer District- Galveston, Texas, 1962). However, this short dataset may introduce analytical errors at this site.

Given a storm surge event that is above the threshold u , the probability that the surge height is greater than some magnitude v is expressed as:

(Equation 1)

$$\left[1 + \frac{\xi}{\sigma}(v - u)\right]^{-1/\xi}$$

To estimate the parameters μ , σ , ξ for each city's surge data, Maximum Likelihood Estimation (MLE) is used to evaluate Equation 1 to find the parameter combination that maximizes the function. There are other ways to estimate the parameters, but MLE is the most commonly used method because it provides standard errors for the parameter estimates. After obtaining the parameter estimates, the annual number of storm surges that exceed the threshold can then be modeled as a thinned Poisson process with mean exceedance rate:

(Equation 2)

$$\lambda_v = \lambda_u \left[1 + \frac{\xi}{\sigma}(v - u)\right]^{-1/\xi}$$

Using the exceedance rate from equation 2 and the GPD parameters, the return level for a given return period x is expressed as

(Equation 3)

$$rl(x) = u + \frac{\tilde{\sigma}}{\xi} \left[(x\lambda_v)^\xi - 1 \right]$$

where $\tilde{\sigma} = \sigma + \xi(u - \mu)$.

Therefore, these equations can be used to estimate return levels for any return period- even periods of time that extend well beyond the length of observed data. This is

important because coastal planning and engineering projects often reference long-term return periods, sometimes exceeding hundreds of years. For example, FEMA has delineated the 500-year flood plain on localized maps, and has determined that areas outside this zone have minimal flood risk (Federal Emergency Management Agency 2013). The Netherlands has extended flood analyses for even longer periods, as the country has developed some of the best flood defenses in the world, and portions of the country are now protected by dykes built to the 10,000-year flood level (Vermeer 2005).

The return periods for which I estimate surge heights are 10-, 25-, 50-, 100-, 200-, and 500-years (Table 5.8). Extending the analysis to 500 years enables the prediction of return levels for a time period beyond the length of the observed data, while matching the longest time period included in Flood Insurance Rate Maps (FIRM) provided by FEMA (Federal Emergency Management Agency 2013). Analyzing the 10-year flood enables me to match the period of this analysis with Flood Insurance Study (FIS) reports, which provide flood elevations to FEMA for the 10-year flood through 500-year flood (Federal Emergency Management Agency 2013b). These flood quantiles provide values for a wide range of projects. Estimates of the 500-year flood are helpful for planning of critical facilities, like power plants and wastewater treatment plants. Data on the 50-year flood are useful for transportation infrastructure, like bridges, and estimates of the 10-year flood are useful for planning smaller infrastructure, like septic systems (Federal Emergency Management Agency 2013b).

Table 5.8. Storm surge return levels (m) for 26 locations along the U.S. Gulf Coast, using the Point Process Model.

| Location | 10-Yr | 25-Yr | 50-Yr | 100-Yr | 200-Yr | 500-Yr |
|----------------------------------|-------|-------|-------|--------|--------|--------|
| South Padre Island | .52 | 1.66 | 2.37 | 2.97 | 3.48 | 4.04 |
| Corpus Christi | .55 | 1.33 | 2.03 | 2.82 | 3.74 | 5.17 |
| Port Lavaca | -.55 | 1.4 | 2.77 | 4.05 | 5.25 | 6.71 |
| Freeport | 1.55 | 2.96 | 3.65 | 4.12 | 4.44 | 4.72 |
| Galveston | 1.61 | 2.57 | 3.34 | 4.16 | 5.02 | 6.22 |
| Baytown | 1.4 | 3.26 | 4.63 | 5.96 | 7.26 | 8.93 |
| Sabine Pass | 1.22 | 2.21 | 2.86 | 3.44 | 3.95 | 4.53 |
| Cameron | .69 | 1.6 | 2.38 | 3.26 | 4.24 | 5.71 |
| Morgan City | .66 | 1.83 | 2.22 | 2.41 | 2.51 | 2.56 |
| Grand Isle | 1.24 | 1.91 | 2.39 | 2.85 | 3.29 | 3.84 |
| Shell Beach | 1.91 | 3.28 | 4.06 | 4.67 | 5.14 | 5.6 |
| New Orleans Lakefront | 1.73 | 2.52 | 2.96 | 3.29 | 3.54 | 3.78 |
| Frenier | 1.3 | 2.36 | 2.97 | 3.45 | 3.83 | 4.21 |
| Mandeville | 1.83 | 2.48 | 2.76 | 2.93 | 3.04 | 3.13 |
| Slidell | 1.56 | 2.38 | 2.91 | 3.38 | 3.78 | 4.25 |
| Bay St. Louis/ Pass Christian | 2.01 | 3.56 | 5.01 | 6.76 | 8.87 | 12.35 |
| Gulfport/ Biloxi | 2.06 | 3.45 | 4.57 | 5.74 | 6.97 | 8.7 |
| Dauphin Island | 1.09 | 1.81 | 2.59 | 3.65 | 5.1 | 7.83 |
| Mobile | 1.28 | 2.41 | 2.95 | 3.31 | 3.55 | 3.75 |
| Pensacola | .98 | 1.72 | 2.37 | 3.09 | 3.9 | 5.13 |
| Panama City | .6 | 1.35 | 1.99 | 2.7 | 3.49 | 4.67 |
| Apalachicola | 1.25 | 1.94 | 2.34 | 2.65 | 2.9 | 3.15 |
| Cedar Key | .85 | 1.53 | 1.89 | 2.15 | 2.36 | 2.54 |
| Tampa | .99 | 1.51 | 1.87 | 2.21 | 2.52 | 2.89 |
| Fort Myers/ Cape Coral | .74 | 1.04 | 1.39 | 1.88 | 2.56 | 3.9 |
| Key West | .11 | 1.07 | 1.81 | 2.56 | 3.34 | 4.38 |

5.3.3.3 Logarithmic Plotting

As this is the first study that employs Extreme Value Theory to estimate storm surge return levels from observed data along the U.S. Gulf Coast, it is difficult to evaluate the accuracy of the results. As such, I also determined to estimate storm surge return periods in this region with Logarithmic Plots (LP), which are useful for fitting trend lines to historical observations. Such plots have been used in a wide variety of studies (Huff and Angel 1992; Faiers et al. 1997; Sindhu and Unnikrishnan 2012).

Huff and Angel (1992), and Faiers et al. (1997) have produced such plots by incorporating the Weibull plotting position formula:

$$\textit{Exceedence Probability} = \textit{Rank} / (n+1)$$

where “n” is the number of years in the data record. Makkonen (2008) provides a detailed discussion of plotting position formulas and their limitations in engineering design. Exceedence probabilities were then utilized to calculate return periods in years, utilizing the formula:

$$\textit{Return Period} = 1 / \textit{Exceedence Probability}$$

The Huff-Angel linear regression technique, used by Huff and Angel (1992), utilizes a log-log scale (for the x and y axes), thereby graphing and linearizing the surge events in their appropriate Weibull plotting position. Faiers et al. (1997) also utilized a linear regression procedure, with a log scale on the x-axis (return period), and a linear scale on the y-axis (event magnitude). I determined to use the log-linear method employed by Faires et al. (1997) after visually assessing the fit provided by both of these methods.

Figure 5.7 provides an example of logarithmic plotting for Morgan City, Louisiana. Table 5.9 lists the storm surge return levels for each of the 26 coastal locations using the LP method.

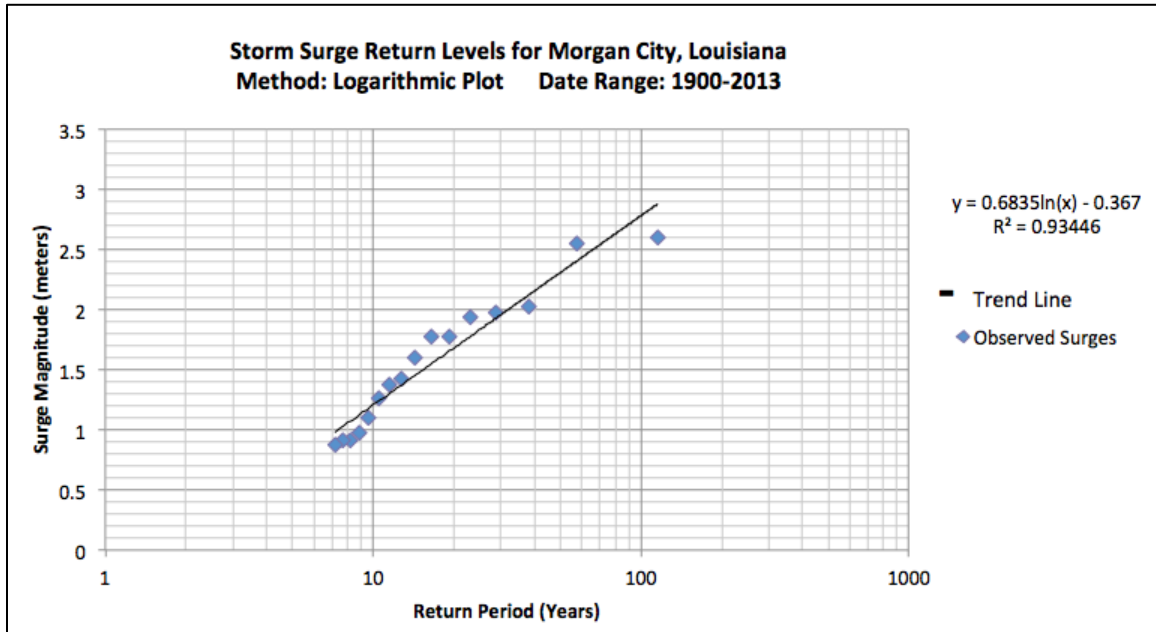


Figure 5.7. Logarithmic plot of storm surge return periods and storm surge magnitudes (m) for Morgan City, Louisiana.

Table 5.9. Storm surge return levels (m) for 26 locations along the U.S. Gulf Coast, using Logarithmic Plotting.

| Location | 10-Yr | 25-Yr | 50-Yr | 100-Yr | 200-Yr | 500-Yr |
|--------------------|-------|-------|-------|--------|--------|--------|
| South Padre Island | 1.13 | 2.27 | 3.14 | 4 | 4.86 | 6 |
| Corpus Christi | 1 | 2.28 | 3.26 | 4.23 | 5.21 | 6.49 |
| Port Lavaca | 0.6 | 2.71 | 4.3 | 5.9 | 7.49 | 9.6 |
| Freeport | 1.86 | 3.04 | 3.94 | 4.83 | 5.73 | 6.91 |
| Galveston | 2 | 3.34 | 4.35 | 5.36 | 6.38 | 7.71 |
| Baytown | 1.71 | 4.03 | 5.78 | 7.54 | 9.29 | 11.61 |
| Sabine Pass | 1.56 | 2.68 | 3.54 | 4.39 | 5.24 | 6.36 |
| Cameron | 1.14 | 2.58 | 3.67 | 4.76 | 5.85 | 7.29 |
| Morgan City | 1.21 | 1.83 | 2.31 | 2.78 | 3.25 | 3.88 |
| Grand Isle | 1.44 | 2.27 | 2.91 | 3.54 | 4.17 | 5.01 |
| Shell Beach | 2.09 | 3.29 | 4.19 | 5.1 | 6 | 7.2 |

Table 5.9 (continued). Storm surge return levels (m) for 26 locations along the U.S. Gulf Coast, using Logarithmic Plotting.

| | | | | | | |
|----------------------------------|------|------|------|------|------|-------|
| New Orleans Lakefront | 1.85 | 2.56 | 3.1 | 3.65 | 4.19 | 4.9 |
| Frenier | 1.49 | 2.43 | 3.14 | 3.84 | 4.55 | 5.49 |
| Mandeville | 1.79 | 2.36 | 2.79 | 3.22 | 3.65 | 4.22 |
| Slidell | 1.68 | 2.85 | 3.74 | 4.63 | 5.51 | 6.68 |
| Bay St. Louis/ Pass Christian | 2.15 | 4.46 | 6.2 | 7.95 | 9.69 | 12 |
| Gulfport/ Biloxi | 2.13 | 4.12 | 5.63 | 7.13 | 8.64 | 10.63 |
| Dauphin Island | 1.22 | 2.44 | 3.37 | 4.3 | 5.23 | 6.45 |
| Mobile | 1.76 | 2.64 | 3.3 | 3.97 | 4.64 | 5.52 |
| Pensacola | 1.34 | 2.46 | 3.3 | 4.14 | 4.98 | 6.09 |
| Panama City | 0.99 | 2.17 | 3.07 | 3.97 | 4.87 | 6.05 |
| Apalachicola | 1.44 | 2.08 | 2.56 | 3.04 | 3.52 | 4.16 |
| Cedar Key | 1.15 | 1.7 | 2.12 | 2.53 | 2.95 | 3.49 |
| Tampa | 1.18 | 1.77 | 2.21 | 2.65 | 3.1 | 3.68 |
| Fort Myers/ Cape Coral | 0.88 | 1.76 | 2.43 | 3.09 | 3.76 | 4.64 |
| Key West | 1.03 | 2.31 | 3.28 | 4.25 | 5.22 | 6.5 |

5.4 Results

5.4.1 Comparing Estimates from the PP and LP Methods

Storm surge return levels estimated by the PP and LP methods are depicted in Figures 5.8 and 5.9 as vertical bars that stack return levels for each city on a Gulf Coast map. Individual storm surge and storm tide observations are plotted as red dots on top of the black and blue bars in these figures.

These graphics and tables show considerable geographic variability in storm surge return levels between different cities. In general, both methods portray a bi-modal pattern, with maximum return levels estimated for the Mississippi Coast and the areas near Galveston and Matagorda Bays in Texas. The lowest levels are found on the West Coast of Florida, and near Morgan City, Louisiana.

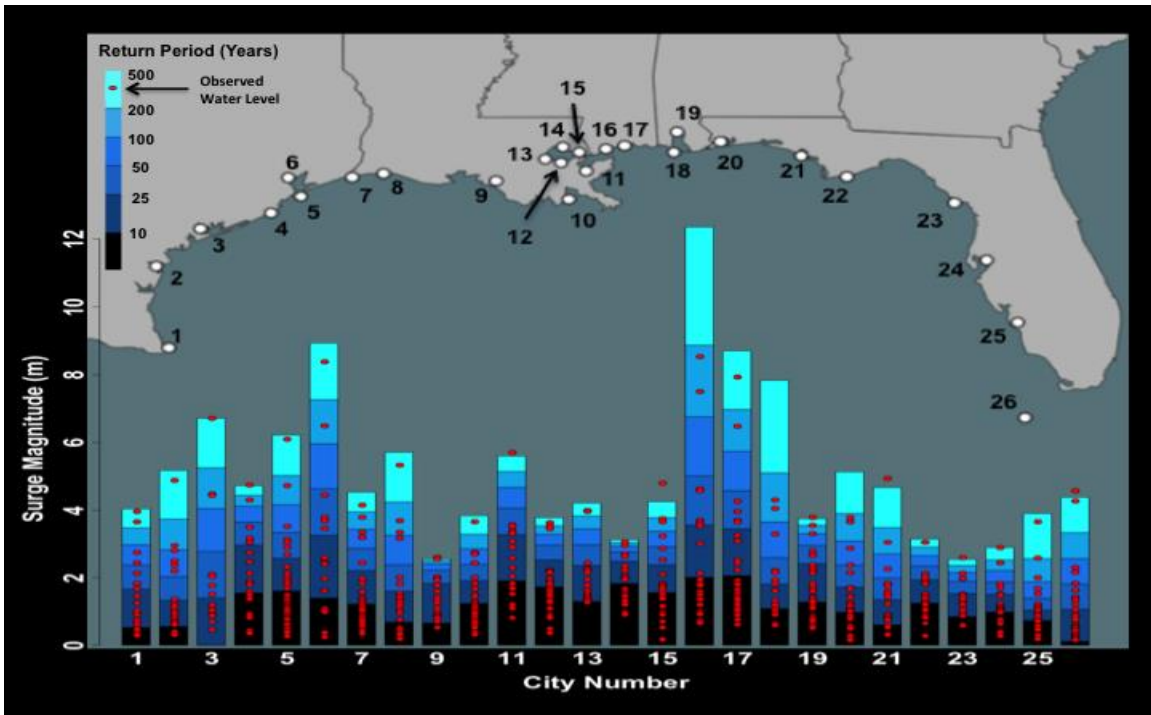


Figure 5.8. Storm surge return levels and observed storm surges for the U.S. Gulf Coast produced by the Point Process Model.

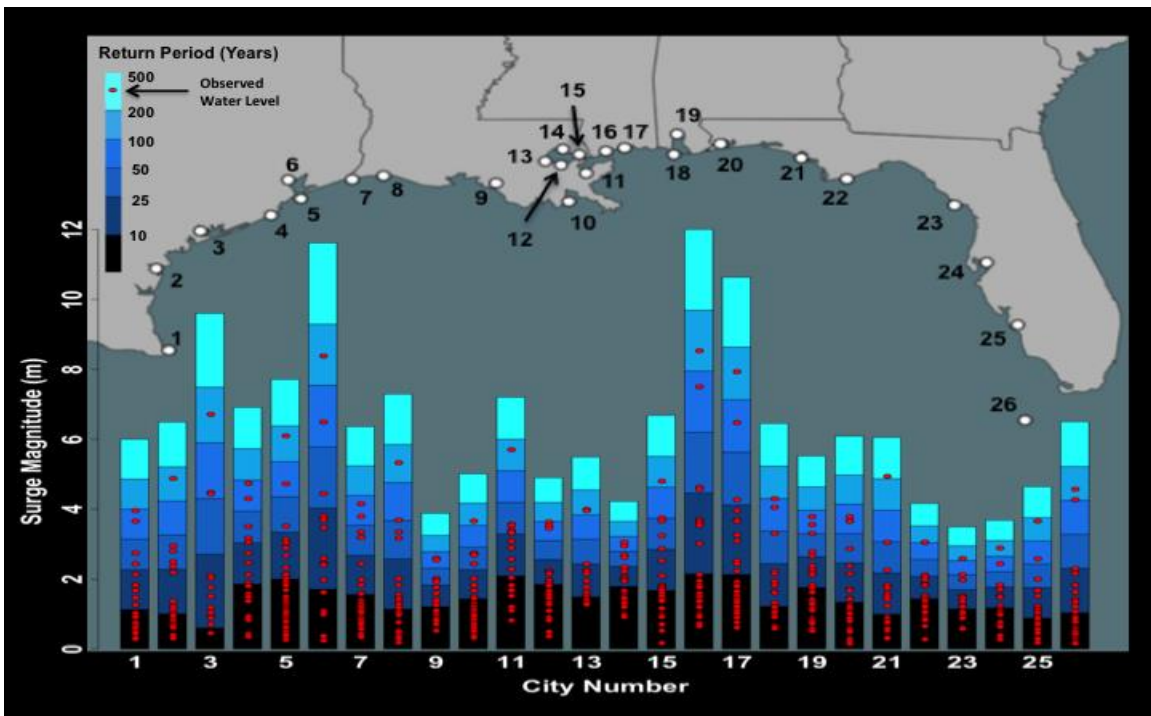


Figure 5.9. Storm surge return levels and observed storm surges for the U.S. Gulf Coast produced by Logarithmic Plotting.

More specifically, both methods estimate the highest water levels at Bay St. Louis/ Pass Christian, Mississippi, followed by Baytown, Texas, and then Gulfport/ Biloxi, Mississippi. The PP method estimates a 500-year storm surge of 12.35 m and a 100-year storm surge of 6.76 m at Bay St. Louis/ Pass Christian, while the LP method predicts a lower 500-year level of 12 m at this site, but a higher 100-year level of 7.95 m. Both methods estimate the lowest return levels at Cedar Key, Florida, followed by Tampa, Florida, and then Morgan City, except for the 500-year level for the PP method, which is lower at Morgan City than Tampa. At Cedar Key, the PP method estimates return levels of 2.54 and 2.15 m for the 500-year and 100-year return period, respectively, while the LP method estimates 3.49 and 2.53 m for the same return periods.

A distinctive pattern is visible for the PP plots found in Figures 5.9a and 5.9b. Water levels for cities with high return levels continue rising substantially after the 100-year period on the x-axis. However, the slope of the return levels flattens out considerably by the 100-year return period for cities with lower 100- and 500-year return levels. This is apparent on the graphs for Freeport, Morgan City, Mobile, Cedar Key and Tampa, and explains the small size of bars for the 200- and 500-year levels at these cities in Figure 5.8.

While the general pattern produced by these two methods is similar, the actual predicted water levels are quite different. The PP method estimates lower water levels than the LP method at all locations, with the exception of Bay St. Louis/ Pass Christian and Dauphin Island. Differences typically increase for higher return periods. For example, the LP method estimates a water level 1.03 m higher than the PP method for the 100-year return period at South Padre Island, but this difference increases to 1.96 m for

the 500-year return period. This pattern is especially pronounced on the Texas Coast, where the difference in the 100-year water level exceeds 1 m and the difference in the 500-year water level ≥ 1.83 m (6 ft) at 71% of the sites (5 out of 7). The largest differences between these methods are visible for the 500-year return periods at Port Lavaca and Baytown, where the LP method estimates higher return levels of 2.89 and 2.68 m, respectively.

Large proportional differences between these methods are apparent at locations where the PP method flattens out the return level plot, producing relatively low 100-, 200- and 500-year water levels. For example, the slope of the PP plot at Morgan City approaches zero as time increases; the difference between the 200-year and 500-year water level is only 0.05 m at this location. However, the LP method estimates that water levels will continue to rise for time periods beyond 100 years, and the difference between the 100-year and 500-year level at this location is 1.1 m (Figure 5.10). As absolute water levels at Morgan City are predicted to be relatively low by both methods, the predictive differences in these two methods are proportionally large. The LP method predicts a 500-year water level of 3.88 m at Morgan City, which is 66% higher than the 2.56-m water level estimated by the PP method. Similar differences are apparent at Freeport, Mobile, Cedar Key and Tampa.

From another perspective, the LP method reduces the difference between the most extreme water levels, as this approach decreases the return levels at Bay St. Louis/ Pass Christian, but increases the return levels at most other sites. The PP method estimates that the 500-year return level at Bay St. Louis/ Pass Christian is 4.86 times higher than at Cedar Key, while the LP method estimates that Bay St. Louis/ Pass Christian is only 3.44

times higher. In summary, the LP method estimates less difference between the cities with the highest and lowest water levels.

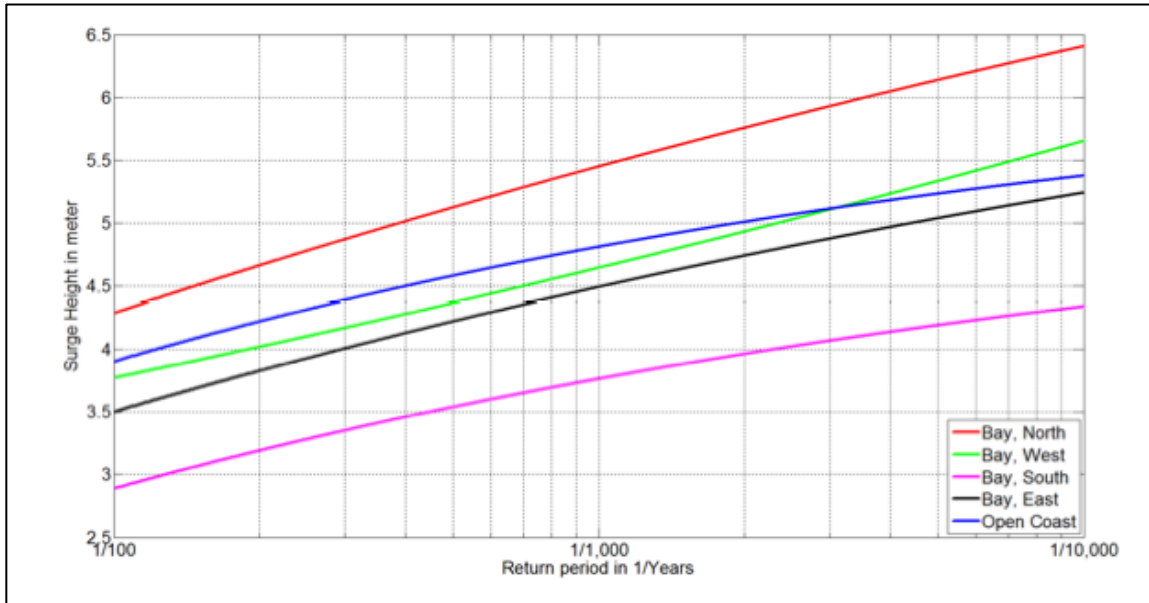


Figure 5.10. Return level plot using a probabilistic modeling approach on thousands of synthetic surge scenarios, provided by Stoeten (2013), page 56. The blue line estimates return levels at the Open Coast, which pertains to Galveston City, and the red line predicts storm surge levels closest to Baytown, Texas. These water levels are considerably lower than my data-driven estimates.

5.4.2 Evaluating the PP and LP Methods

Evaluation of these methods suggests the PP method usually underestimates storm surge return levels. I came to this conclusion after analyzing the return periods of the highest watermarks at each location, and applying the Kolmogorov-Smirnov test, which analyzes counts above specific return periods to test goodness-of-fit.

Table 5.10 provides a list of the highest watermarks at each location, as well as the return period of that event. The PP method estimates higher return periods than the LP method at every site. The differences in these values are substantial, and are most pronounced at Morgan City and Slidell. The PP method estimates a storm surge return period of 2.59×10^{15} for the 2.6-m storm tide produced by Hurricane Audrey at Morgan City

in 1957, whereas the LP method estimates this water level was a 77-year event. The PP method estimates Hurricane Katrina’s 4.8-m storm tide at Slidell was a 1,963-year event, whereas the LP method calculates this event as a 114-year flood.

The average return period of the highest watermark per location was approximately 468 years for the PP method and 123 years for the LP method, excluding Morgan City, because of the extraordinarily high return periods produced by the PP method at that site. From another perspective, the PP method estimated that 19 out of the 26 locations have already observed a 300-year event, whereas the LP method estimates that only one event, Hurricane Eloise, in Panama City, Florida, had a return period ≥ 200 years. Also, the numerous 300+ year events provided by the PP method were not caused by one extraordinary hurricane, but rather by 13 separate storms in 19 different locations, which indicates the PP method underestimates widespread return level values for many locations.

Table 5.10. Return periods of the maximum water level at each site using the Point Process Model and Logarithmic Plot.

| Location | State | Storm Name | Year | Water Level (m) | PP Return Pd. | LP Return Pd. |
|--------------------------------|-------|---------------------|------|-----------------|---------------|---------------|
| S Padre Island/ Port Isabel | TX | Unnamed | 1933 | 3.96 | 433 | 97 |
| Corpus Christi | TX | Unnamed | 1919 | 4.88 | 421 | 158 |
| Port Lavaca | TX | Carla | 1961 | 6.71 | 500 | 142 |
| Freeport | TX | Carla | 1961 | 4.74 | 547 | 93 |
| Galveston | TX | Galveston Hurricane | 1900 | 6.10 | 456 | 166 |
| Baytown | TX | Galveston | 1900 | 8.38 | 369 | 139 |
| Sabine Pass | TX | Carla | 1961 | 4.15 | 271 | 82 |
| Cameron | LA | Rita | 2005 | 5.33 | 400 | 144 |

Table 5.10 (continued). Return periods of the maximum water level at each site using the Point Process Model and Logarithmic Plot.

| | | | | | | |
|----------------------------------|----|-------------|------|------|---------|-----|
| Morgan City | LA | Audrey | 1957 | 2.6 | 2.59e15 | 77 |
| Grand Isle | LA | Katrina | 2005 | 3.66 | 366 | 114 |
| Shell Beach | LA | Katrina | 2005 | 5.7 | 631 | 159 |
| New Orleans at L. Pontchartrain | LA | Katrina | 2005 | 3.63 | 274 | 98 |
| Frenier | LA | Betsey | 1965 | 3.99 | 285 | 115 |
| Mandeville | LA | Katrina | 2005 | 3.06 | 231 | 78 |
| Slidell | LA | Katrina | 2005 | 4.80 | 1963 | 114 |
| Bay St. Louis/ Pass Christian | MS | Katrina | 2005 | 8.42 | 174 | 121 |
| Gulfport/ Biloxi | MS | Katrina | 2005 | 7.82 | 316 | 137 |
| Dauphin Island | AL | Katrina | 2005 | 4.3 | 140 | 100 |
| Mobile | AL | Katrina | 2005 | 3.78 | 618 | 82 |
| Pensacola | FL | Ivan | 2004 | 3.78 | 181 | 74 |
| Panama City | FL | Eloise | 1975 | 4.94 | 608 | 211 |
| Apalachicola | FL | Elena | 1985 | 3.05 | 334 | 101 |
| Cedar Key | FL | Alma | 1966 | 2.59 | 664 | 110 |
| Tampa | FL | Unnamed | 1921 | 2.89 | 499 | 145 |
| Fort Myers/ Cape Coral | FL | Great Miami | 1926 | 3.66 | 437 | 180 |
| Key West | FL | Unnamed | 1910 | 4.57 | 591 | 126 |

A count of exceedences above the 100-year return level also reveals that the PP method generally underestimates return levels. Approximately 88% (23 of 26) of the sites have observed at least two 100-year events, and 23% (6 of 26) have observed three events above the 100-year water level estimated by the PP method. The number of exceedences above the PP method's 100-year return level averages 2.11 for the 26 sites. By comparison, the LP method estimates that only three sites have experienced two 100-year

floods, and no sites have experienced three hundred year floods. The average number of exceedences per site above the LP method's 100-year water level is 0.81.

The Kolmogorov-Smirnov (KS) test provides a goodness-of-fit evaluation for each of these methods. This non-parametric test is used to compare an observed frequency distribution with a hypothetical (expected) frequency distribution (Kenkel 1984). This test also requires at least five cases, and my study compares six different return period lengths. Table 5.11 provides the expected number of exceedences for each return period, which was obtained by dividing the total number of years in the analysis (114) by the return period length. Tables 5.12 and 5.13 provide the actual number of exceedences above return levels at each site using the PP and LP methods. Table 5.14 provides the value of the two-tailed KS statistic at each site; lower values indicate a better fit. The LP method produced a better fit at 24 of the 26 sites. The PP method produced a better fit at Galveston, Texas, and both methods produced equally good fits at Key West, Florida. These results suggest that the LP method provided a better overall fit than the PP method.

Table 5.11. Expected water level exceedences above specific return periods.

| Return Period (Yr) | Expected Exceedences |
|--------------------|----------------------|
| 10 | 11.4 |
| 25 | 4.56 |
| 50 | 2.28 |
| 100 | 1.14 |
| 200 | 0.57 |
| 500 | 0.23 |

Table 5.12. Actual exceedences above return levels using the PP method.

| Location | 10-yr | 25-yr | 50-yr | 100-yr | 200-yr | 500-yr |
|------------------------------------|-------|-------|-------|--------|--------|--------|
| S Padre Island/ Port Isabel | 18 | 8 | 4 | 2 | 2 | 0 |
| Corpus Christi | 20 | 7 | 6 | 2 | 1 | 0 |
| Port Lavaca | 14 | 7 | 3 | 3 | 1 | 1 |
| Freeport | 13 | 6 | 2 | 2 | 1 | 1 |
| Galveston | 17 | 7 | 3 | 2 | 1 | 0 |
| Baytown | 13 | 6 | 2 | 2 | 1 | 0 |
| Sabine Pass | 17 | 6 | 5 | 2 | 1 | 0 |
| Cameron | 18 | 6 | 4 | 3 | 1 | 0 |
| Morgan City | 19 | 5 | 2 | 2 | 2 | 1 |
| Grand Isle | 14 | 7 | 6 | 1 | 1 | 0 |
| Shell Beach | 11 | 6 | 1 | 1 | 1 | 1 |
| New Orleans at L. Pontchartrain | 14 | 3 | 3 | 3 | 2 | 0 |
| Frenier | 16 | 3 | 2 | 2 | 2 | 0 |
| Mandeville | 11 | 4 | 2 | 2 | 1 | 0 |
| Slidell | 13 | 6 | 4 | 3 | 1 | 1 |
| Bay St. Louis/ Pass Christian | 10 | 7 | 2 | 2 | 0 | 0 |
| Gulfport/ Biloxi | 11 | 6 | 2 | 2 | 1 | 0 |
| Dauphin Island | 12 | 7 | 3 | 2 | 0 | 0 |
| Mobile | 19 | 5 | 3 | 3 | 2 | 1 |
| Pensacola | 20 | 6 | 5 | 3 | 0 | 0 |
| Panama City | 18 | 9 | 3 | 2 | 1 | 1 |
| Apalachicola | 15 | 5 | 2 | 2 | 2 | 0 |
| Cedar Key | 17 | 4 | 4 | 1 | 1 | 1 |
| Tampa | 17 | 8 | 2 | 2 | 1 | 0 |
| Fort Myers/ Cape Coral | 17 | 10 | 5 | 3 | 2 | 0 |
| Key West | 32 | 11 | 6 | 2 | 2 | 1 |

Table 5.13. Actual exceedences above return levels using the LP method.

| Location | 10-yr | 25-yr | 50-yr | 100-yr | 200-yr | 500-yr |
|------------------------------------|-------|-------|-------|--------|--------|--------|
| S Padre Island/ Port Isabel | 11 | 4 | 2 | 0 | 0 | 0 |
| Corpus Christi | 10 | 5 | 1 | 1 | 0 | 0 |
| Port Lavaca | 13 | 3 | 3 | 1 | 0 | 0 |
| Freeport | 10 | 6 | 2 | 0 | 0 | 0 |
| Galveston | 12 | 3 | 2 | 1 | 0 | 0 |
| Baytown | 11 | 3 | 2 | 1 | 0 | 0 |
| Sabine Pass | 11 | 5 | 2 | 0 | 0 | 0 |
| Cameron | 12 | 4 | 2 | 1 | 0 | 0 |
| Morgan City | 11 | 5 | 2 | 0 | 0 | 0 |
| Grand Isle | 12 | 6 | 1 | 1 | 0 | 0 |
| Shell Beach | 10 | 6 | 1 | 1 | 0 | 0 |
| New Orleans at L. Pontchartrain | 12 | 3 | 3 | 0 | 0 | 0 |
| Frenier | 12 | 3 | 2 | 2 | 0 | 0 |
| Mandeville | 11 | 4 | 2 | 0 | 0 | 0 |
| Slidell | 12 | 5 | 2 | 1 | 0 | 0 |
| Bay St. Louis/ Pass Christian | 9 | 4 | 2 | 1 | 0 | 0 |
| Gulfport/ Biloxi | 11 | 3 | 2 | 1 | 0 | 0 |
| Dauphin Island | 10 | 3 | 2 | 1 | 0 | 0 |
| Mobile | 10 | 5 | 2 | 0 | 0 | 0 |
| Pensacola | 10 | 4 | 3 | 0 | 0 | 0 |
| Panama City | 10 | 3 | 1 | 1 | 1 | 0 |
| Apalachicola | 11 | 3 | 2 | 2 | 0 | 0 |
| Cedar Key | 12 | 4 | 2 | 1 | 0 | 0 |
| Tampa | 10 | 3 | 2 | 1 | 0 | 0 |
| Fort Myers/ Cape Coral | 13 | 3 | 2 | 1 | 0 | 0 |
| Key West | 12 | 2 | 2 | 2 | 0 | 0 |

Table 5.14. Two-tailed KS Statistic. Lower values indicate a better fit between observed and expected values.

| Location | PP Method | LP Method |
|---------------------------------|-----------|-----------|
| S Padre Island/ Port Isabel | .08 | .06 |
| Corpus Christi | .08 | .05 |
| Port Lavaca | .13 | .04 |
| Freeport | .10 | .06 |
| Galveston | .04 | .06 |
| Baytown | .07 | .04 |
| Sabine Pass | .09 | .06 |
| Cameron | .08 | .02 |
| Morgan City | .11 | .06 |
| Grand Isle | .13 | .07 |
| Shell Beach | .10 | .06 |
| New Orleans at L. Pontchartrain | .15 | .06 |
| Frenier | .10 | .05 |
| Mandeville | .09 | .06 |
| Slidell | .15 | .02 |
| Bay St. Louis/ Pass Christian | .13 | .05 |
| Gulfport/ Biloxi | .11 | .04 |
| Dauphin Island | .11 | .02 |
| Mobile | .13 | .06 |
| Pensacola | .07 | .06 |
| Panama City | .08 | .07 |
| Apalachicola | .10 | .06 |
| Cedar Key | .08 | .02 |
| Tampa | .04 | .02 |
| Fort Myers/ Cape Coral | .15 | .07 |
| Key West | .06 | .06 |

5.5 Discussion

This analysis reveals that logarithmic plotting of observed storm surge data estimates higher storm surges than not only the point process model, but also other modeling and statistical techniques found in the literature. For example, the Interagency Performance Evaluation Task Force, Team Louisiana provided estimates for Hurricane Katrina's storm surge level in Southeast Louisiana and along the Mississippi Coast. They estimated that Katrina's surge was a 400-year event in coastal Mississippi, a 250-year event in St. Bernard Parish, and a 150-year event along New Orleans' lakefront (Interagency Performance Evaluation Task Force 2007; Swenson 2013). The results provided by logarithmic plotting in this chapter suggest that storm surge levels in this region are higher than the IPET estimates, making Katrina's storm surge less rare. This analysis estimates that Katrina's storm surge was a 121-year event in Bay St. Louis/ Pass Christian, Mississippi, a 250-year event in Shell Beach, which provides estimates of surge levels approaching St. Bernard Parish from the east, and a 150-year event at New Orleans' lakefront.

The difference between the results provided in this chapter and previous methodologies is also evident for Galveston, Texas. Table 5.15 provides a list of 100-year storm surge levels estimated for Galveston using different methodologies, adapted from Stoeten (2013). These methods include statistical analysis of tide records near Galveston and Bolivar Roads, as well as probabilistic modeling. The 100-year storm surge estimated in this study is noticeably higher than all of these other methods.

The probabilistic model provided by Stoeten (2013) provides a valuable contribution towards understanding storm surge in the region, however, it also reveals the

importance of validating models with observed data. This model estimated surge return levels by generating thousands of synthetic surges in the Galveston Bay area, and predicting a 100-year storm surge of ~ 3.95 m near Galveston and ~ 4.3 m near Baytown (Figure 5.11). This predicted level is 37% lower than my 100-yr estimate at Galveston and 57% lower than my 100-yr surge at Baytown, which are 5.36 m, and 7.54 m, respectively. I believe the model underestimates surge potential in the region, because the modeled 10,000-yr water level only reaches ~ 5.4 m at the city of Galveston, however, this location already observed a 6.1 m storm tide (Garriott 1900). According to the modeled plot, the storm tide produced by the 1900 Galveston Hurricane would have been at least a 100,000-year water level (if the plot is extrapolated), and the 4.72-m storm tide at Galveston in 1915 (Connor 1956; Landsea et al. 2008) was approximately an 800-year event. Nonetheless, modeling efforts are important, and future research will hopefully combine advanced modeling techniques with statistical analysis of observed surge data.

Table 5.15. Comparison of 100-yr water levels at Galveston. Adapted from Stoeten (2013), page 55. Original table included first three studies, and results referenced to Needham and Keim (2012), from presentation at Galveston in Oct. 2012. These results were for entire Upper Texas Coast, and have therefore been removed from this table.

| Source | Methodology | Time Period | 100-Year |
|----------------|---|-------------|----------|
| Bodine (1969) | Statistical analysis (POT) of tide records near Galveston | 1900-1963 | 3.6 m |
| Davis (1962) | Statistical analysis (POT) of tide records at Bolivar Roads inlet | 1900-1960 | 4.5 m |
| NOAA (2013) | GEV fit of annual maximum at Galveston Pleasure Pier | 1960-2012 | 2.7 m |
| Stoeten (2013) | Probabalistic modeling | Simulations | 3.9 m |
| Current Study | Statistical analysis using log plotting | 1900-2013 | 5.36 m |

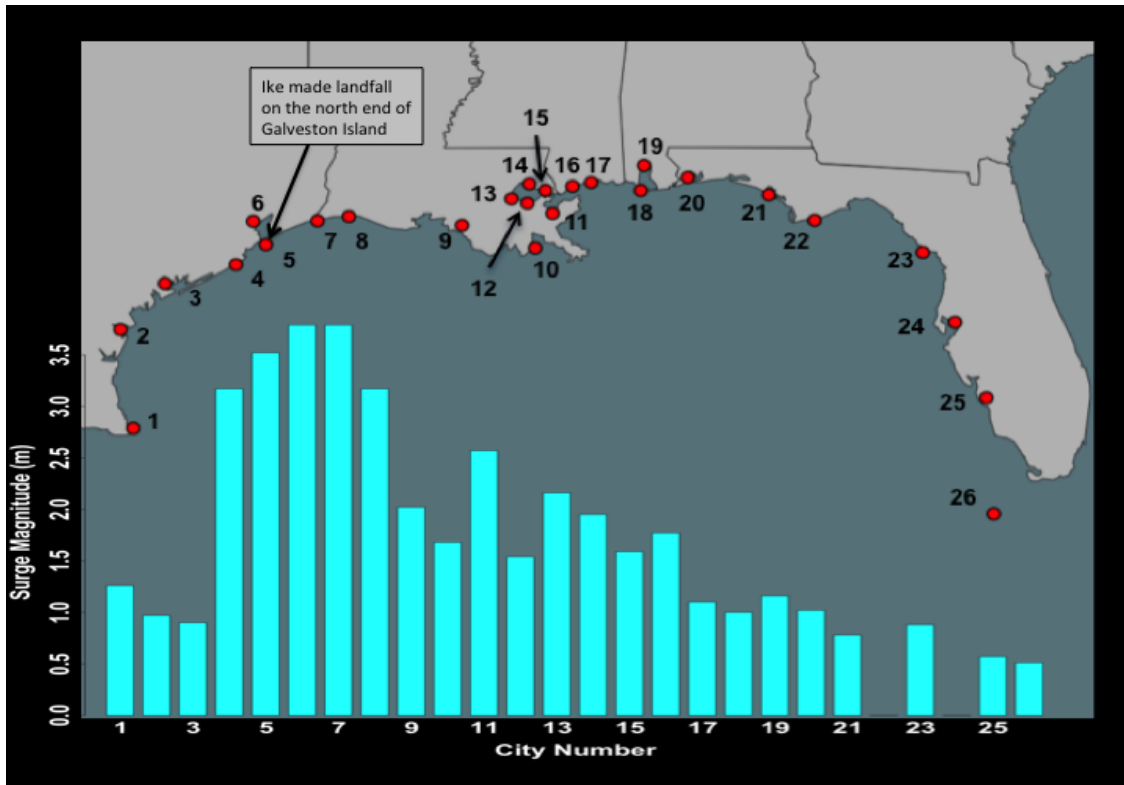


Figure 5.11. Water level heights generated by Hurricane Ike in 2008. This image shows that proximity to landfall is not the only important factor that influences surge heights. Note that Shell Beach (city 11) observed higher water levels than Morgan City (city 9) and Grand Isle (city 10), even though Ike made landfall at Galveston (city 5). Adapted from Doran et al. (2009); Federal Emergency Management Agency (2009); Berg (2010).

I cannot explain why the LP method also produced a better fit than the PP method, however, inadequate data quantity may provide a partial explanation. The LP method utilized more observed data because it fit all observations on logarithmic plots, and did not exclude data below a certain magnitude. The PP method, however, used a peaks-over-threshold approach and, in this case, eliminated all observations < 0.91 m. This truncation of the dataset reduced the number of surge observations for the PP method to approximately 19 observations per site, whereas the LP method plotted an average of 26 observations per site. Katz et al. (2002) indicate that the performance of the Maximum Likelihood approach, which was used in the PP method, may be erratic for

sample sizes ≤ 25 . However, the LP method also fit the data better at New Orleans, Bay St. Louis/ Pass Christian, and Gulfport/ Biloxi, even though more than 25 observations exceeded the truncation level at each of these sites. On the contrary, the PP method provided a better fit than the LP method at Galveston, Texas, the site with the most observed data, where 34 observations exceeded the truncation level.

These results may indicate that the observed storm surge record for the U.S. Gulf Coast is currently inadequate to predict storm surge return levels for time periods that exceed the data record. Such predictions are theoretically possible through Extreme Value Theory, but the PP analysis in this study produced unreliable results. Although the LP analysis provided a better fit to observed data, this method is not designed to predict return levels beyond the length of data record, but it still may be valuable for estimating the annual storm surge probability (Elsner et al. 2008). For example, estimates of 100-year storm surge return levels provided by the LP method should be credible, as this return period is less than the length of observed data, and the two-tailed KS Statistic indicated that the LP method provided a good fit to observed data. Such results are still valuable, as many flood protection projects, like the U.S. Army Corps of Engineers flood protection system around New Orleans, are designed to protect against the 100-year flood (U.S. Army Corps of Engineers 2011).

Estimates of 100-year storm surge levels also provide limits on analytical errors caused by tidal oscillations. Although I adjusted the data for geodetic and tidal datum references, these corrections set water marks above MSL for the year of the storm surge event, a reference line I called, “annual datum.” However, these adjustments did not account for the influence of tides on the day of the storm surge event.

Table 5.16 provides a comparison between the magnitude of tidal oscillations and 100-year storm surge return levels at each location. Tidal ranges are calculated by averaging the difference between MSL and both Mean High Water (MHW) and Mean Low Water (MLW), from tidal data provided by the National Oceanic and Atmospheric Administration (2014). Error estimates were then computed by dividing the average tidal range by the height of the 100-year storm surge level. Following this approach, tidal oscillations account for < 5% error of the 100-year surge height at 22 of 26 locations. Cedar Key and Tampa Bay were two outliers, as tidal ranges in these locations reached 17% and 11.3% of the 100-year storm surge level, respectively. These two sites have higher tidal ranges than the other locations and have observed relatively low-magnitude storm surges through the observation period. The lowest tidal error was 1.7% at Slidell.

Such estimates assume stationarity of tidal oscillations over time, however, sea-level rise is a problem that introduces non-stationarity of water levels over longer time periods. Although the geodetic datum adjustments corrected for errors in historic storm tide observations that were caused by relative sea-level rise, I have not accounted for the future influence of sea level rise on extreme water levels. A detailed investigation on this topic is beyond the scope of this chapter, however, a quick comparison of two extreme cases is useful.

Coastal Mississippi has observed slow RSLR rates of only 0.15 cm/yr (Penland and Ramsey 1990), but this area has observed the highest storm surges in the Western Hemisphere, and the 100-year storm surge return level at Bay St. Louis/ Pass Christian is estimated to be 7.95 m.

Table 5.16. Tidal errors as percentage of the 100-year water level. Tidal data provided by NOAA Tides and Currents.

| Location | 100-Yr Surge | Location of | Tidal Range | Pct. Tidal Error |
|----------------------------------|--------------|----------------------------|-------------|------------------|
| South Padre Is. | 4 | South Padre | .17 | 4.3 |
| Corpus Christi | 4.23 | Bob Hall Pier | .20 | 4.7 |
| Port Lavaca | 5.9 | Port Lavaca | .13 | 2.2 |
| Freeport | 4.83 | Freeport | .21 | 4.3 |
| Galveston | 5.36 | Galveston | .22 | 4.1 |
| Baytown | 7.54 | Morgans Point | .17 | 2.3 |
| Sabine Pass | 4.39 | Sabine Pass | .17 | 3.9 |
| Cameron | 4.76 | Calcasieu Pass | .20 | 4.2 |
| Morgan City | 2.78 | Berwick | .07 | 2.5 |
| Grand Isle | 3.54 | Grand Isle | .16 | 4.5 |
| Shell Beach | 5.1 | Shell Beach | .20 | 3.9 |
| New Orleans Lakefront | 3.65 | New Canal Station | .08 | 2.2 |
| Frenier | 3.84 | Tchefuncta R. | .09 | 2.3 |
| Mandeville | 3.22 | Tchefuncta R. | .09 | 2.8 |
| Slidell | 4.63 | Big Point | .08 | 1.7 |
| Bay St. Louis/ Pass Christian | 7.95 | Bay Waveland Yacht Club | .23 | 2.9 |
| Gulfport/ Biloxi | 7.13 | Biloxi | .24 | 3.4 |
| Mobile | 4.3 | Point Clear | .23 | 5.3 |
| Dauphin Island | 3.97 | Dauphin Island | .18 | 4.5 |
| Pensacola | 4.14 | Pensacola | .18 | 4.3 |
| Panama City | 3.97 | Panama City | .19 | 4.8 |
| Apalachicola | 3.04 | Apalachicola | .17 | 5.6 |
| Cedar Key | 2.53 | Cedar Key | .43 | 17.0 |
| Tampa | 2.65 | Ballast Point | .30 | 11.3 |
| Fort Myers/ Cape Coral | 3.09 | Fort Myers | .14 | 4.5 |
| Key West | 4.25 | Key West | .20 | 4.7 |

These values suggest that RSLR will have little influence on creating higher storm surges in coastal Mississippi in the future, as 100 years of RSLR at this rate accounts for

< 2% of the 100-year storm surge level. However, Morgan City has observed rapid RSLR, as the two locations that provide data near this city average RSLR rates of 1.52 cm/yr (Penland and Ramsey 1990). The 100-year storm surge at Morgan City is only 2.78 m, which is relatively low for the region. As such, RSLR will comprise a relatively large increase onto future surge levels at this location. Assuming that RSLR rates continue increasing at the same rate and storm surge observations remain stationary in the future, the Morgan City area would observe approximately 1.5 m of RSLR in the next 100 years, which accounts for > 50% of the 100-year storm surge level. This means the impact of sea-level rise on storm surge levels would be noticeably higher at locations like Morgan City than sites along the Mississippi Coast. Such comparisons are generalized and not precise, as future RSLR rates may differ considerably from historic rates. Although such considerations are important, it must be emphasized that the water level estimates provided in this chapter relate only to storm surge and storm tide levels, and do not incorporate rates of relative sea level rise.

This study also reveals that storm surge return levels vary considerably depending on location. For example, the 100-year return level at Bay St. Louis/ Pass Christian is at least three times as high as Tampa and Cedar Key. Although the frequency of hurricane strikes influences these results, this study suggests that storm surge climatology along the U.S. Gulf Coast is not merely an extension of hurricane-strike climatology. For example, major hurricanes strike Morgan City twice as often as Gulfport (Keim et al. 2007), however, the 100-year storm surge return level at Biloxi/ Gulfport is more than 2.5 times higher than Morgan City.

Expanding on this example, several factors beyond the frequency of hurricane strikes contribute to elevated storm surge levels along the Mississippi Coast and modest storm surge levels near Morgan City. Shallow bathymetry and coastal features that are efficient at trapping water near the Mississippi coast enhance surge heights in that region (Needham and Keim 2011). Water tends to funnel into Bay St. Louis, and the nearby Mississippi River Delta often traps water that is flowing from east to west as hurricanes approach the coastline. However, Morgan City is protected by more than 20 km of wetlands (Google Earth 2014), which usually reduce surge heights (Wamsley et al. 2010). Also, Morgan City and Grand Isle are protected to some degree by the extensive Mississippi River Delta, which serves to block storm surge that flows from east to west during hurricane events. In addition, the coastline closest to Morgan City faces southwest, so when hurricanes pass south of Morgan City, strong easterly winds blow offshore and moderate surge levels. For example, Hurricane Ike tracked northwest across the Gulf of Mexico in 2008, and made landfall near the northern end of Galveston Island, Texas. This massive hurricane produced strong east winds along much of the Northern Gulf Coast (Berg 2010), and this wind was blowing onshore at Shell Beach, but offshore at Morgan City. A map of observed water levels at cities along the Gulf Coast (Figure 5.12) reveals that Ike generated higher water levels at Shell Beach than Morgan City or Grand Isle, even though Shell Beach is located farther from Ike's landfall location than the other two cities. This example proves that comparatively low storm surge return levels in places like Morgan City and Grand Isle are not caused by lack of hurricane strikes, but because of coastal geography.

For cases in which hurricanes strike closer to Morgan City, the highest surge levels often do not occur as hurricanes make landfall, but rather after hurricanes pass the area, when wrap-around winds on the backside of the storm push water in from the west. Maximum sustained wind speeds are therefore usually less intense as the surge is peaking in this area, and this moderates surge levels. This exact scenario happened during Hurricane Andrew in 1992, when water levels in the region peaked more than four hours after Andrew's closest approach (Halford 1995). Although Andrew made landfall as a category-3 hurricane approximately 37 km west-southwest of Morgan City (Rappaport 1993), the highest water level close to Morgan City was a storm tide of 2.3 m above NGVD 29 at Calumet (Halford 1995), which reduces to 1.26 m above the annual datum after a geodetic datum adjustment. This pattern resembles storm surges that occur on the West Coast of Florida, when hurricanes enter the Gulf of Mexico from the Florida Peninsula, and wrap-around winds on the backside of these storms generate modest storm surges.

Although tropical storm surges on the West Coast of Florida tend to be modest by regional comparison, this region is also vulnerable to storm surges generated by extra-tropical low-pressure systems and frontal passages, particularly during the winter and spring. After cold fronts pass, prolonged onshore winds often produce storm surges in this region. Extra-tropical systems have generated the highest modern-day water levels at many locations along the West Coast of Florida, surpassing the highest storm surges generated by tropical cyclones. For example, the Storm of the Century, a massive mid-latitude cyclone that struck the Eastern United States in March, 1993, generated the highest modern-day storm surge in portions of Western Florida, north of Tampa. This

coastal flooding event drowned 13 people and caused extensive damage, as surge heights ranged from 2.74 – 3.66 m from Pasco to Taylor Counties (National Weather Service 2013). These water levels are higher than any tropical surges found in SURGEDAT in this region. The city of Cedar Key, one of the locations analyzed in this chapter falls in this region. The storm surge in March, 1993, reached 2.9 m, surpassing the 2.59-m surge generated by Hurricane Alma in 1966 (Sugg 1967), which is the highest tropical surge on record at this location.

Although this study reveals considerable geographic variability of storm surge return levels along the U.S. Gulf Coast, the analysis is based completely on historical storm surge observations from 1900-2013. Data from this time period indicate that modest storm surge levels have been observed at locations like Morgan City, Cedar Key and Tampa, where 100-year storm surge levels are less than 3 m. However, such results do not ensure the absence of catastrophic storm surges in these locations in the future. For example, models suggest that if a hurricane tracked east across the Gulf of Mexico and made landfall north of Tampa, surges in downtown Tampa could reach 6 m (Weisberg and Zheng 2006). Therefore, one should take caution when considering storm surge potential in locations with low return levels, like the West Coast of Florida.

5.6 Summary and Conclusion

This is the first analysis to use observed water level data to estimate storm surge return periods for the U.S. Gulf Coast. Data are provided by SURGEDAT, a global storm surge database that provides more than 7,600 high-water marks for the United States since 1880. This study analyzed 114 years of data, from 1900-2013, for 26 coastal locations.

A key step in this analysis involved building a web tool that returns historical storm surge and storm tide data for coastal locations. This tool enables users to define the center point and radius for a data-selection circle on a Gulf Coast map. After testing circles with 8-km, 16-km, and 40-km radii, I concluded that circles with 16-km radii are optimal for data selection. Circles with 40-km radii often combined data that are inhomogeneous, such as observations from barrier islands and the inner portion of bays, while circles with 8-km radii did not return enough data for statistical analysis. Circles with 16-km radii provided data with adequate homogeneity, and these circles returned 677 observations at 26 coastal locations, or an average of approximately 26 observations per site.

This web-tool provides a combination of storm surge and storm tide observations. Storm tide observations are total water levels above established geodetic and tidal datums. I adjusted these observations to the water level above the Mean Sea Level (MSL) for the year of the storm tide event. Observations measured above historical geodetic datums differ from heights above MSL for the year of the storm tide event because sea levels are rising relative to the elevation of land along the U.S. Gulf Coast. I obtained relative sea-level rise RSLR rates for coastal locations to estimate the difference between MSL for the year of the storm tide event and the elevation of the referenced datum. In order to make tidal datum adjustments, I subtracted from the storm tide observation the difference between MSL and the elevation of the tidal reference. Nearly all datum adjustments lowered observed storm tide heights. These procedures provided clean storm surge/ storm tide history for each location that removed errors from datum references.

I used the Point Process (PP) method of Extreme Value Theory to predict storm surge return levels for 10-, 25-, 50-, 100-, 200-, and 500-year return periods. This approach enabled me to obtain an annual return rate for extreme storm surges, and also allowed the prediction of return levels beyond the length of the observed dataset. This method follows a peaks-over-threshold approach, and theorizes that for very high values above a threshold, the frequency of extreme events follows a Poisson distribution, and the magnitudes of the events follow a Generalized Pareto Distribution, with parameters location μ , scale σ , and shape ξ . I selected a threshold of 0.91 m, as the parameters show stability at this threshold, and this water level represents the upper-limit of minor coastal flood magnitudes in the region. I also utilized Logarithmic Plotting (LP), which is a useful method of fitting trend lines to historical observations, to validate the results provided by the PP method.

Both methods show considerable geographic variability in storm surge return levels in the region, with the highest levels provided for the Mississippi Coast at both Bay St. Louis/ Pass Christian and Biloxi/Gulfport, as well as the Upper Texas Coast, at Baytown. The lowest levels were estimated along the West Coast of Florida, at Cedar Key and Tampa, as well as Morgan City, Louisiana. While these two methods provided similar return level patterns, the PP method provided lower return levels than the LP method at 24 of 26 sites, and likely underestimated water levels at most locations. The PP method indicated that 19 of the 26 sites have observed at least a 300-year surge event, with the average high water mark at each location producing a 468-year event. Also, according to this method, the average location has observed more than two 100-year surge events. The two-tailed Kolmogorov-Smirnov (KS) test indicates the LP method

provided a better fit to the data than the PP method at 24 of 26 sites. Inadequate data quantity may partially explain the inaccurate results of the PP method, as the use of the peaks-over-threshold method reduced the average number of observations at each site from approximately 26 to 19.

Although the LP method is not designed to predict return levels for time periods beyond the length of the dataset, this approach is still useful for estimating the 10-, 25-, 50-, and 100-year return levels in this study. These values are useful for many high-profile flood protection projects, like the U.S. Army Corps of Engineers flood protection system around New Orleans, which is designed to protect against the 100-year flood (U.S. Army Corps of Engineers 2011).

The results from this analysis provided higher storm surge return levels than previous studies. For example, these results provide higher return levels than both statistical and probabilistic modeling efforts for Galveston, Texas, while suggesting that Hurricane Katrina's storm surge in Southeast Louisiana and Mississippi was not as rare as indicated by synthetic modeling (Interagency Performance Evaluation Task Force 2007; Swenson 2013).

Estimates of the 100-year return levels also confirmed that tidal oscillations introduce only minor errors for storm surge statistics in this region, as the tidal range is < 5% of the 100-year water level at 22 of 26 locations. I also concluded that the influence of sea-level rise on storm surge heights varies dramatically for different locations. For example, if sea levels along the Gulf Coast rise over the next 100 years at the same rate as recent decades, rising seas would only increase the 100-year water levels by < 2% in

Bay St. Louis/ Pass Christian, but > 50% at Morgan City, where sea-level rise rates are rapid, but storm surge heights are relatively low.

This study also reveals that storm surge climatology in this region is not merely an extension of hurricane-strike climatology. For example, the 100-year storm surge return level at Gulfport/ Biloxi is 2.5 times as high as Morgan City, although major hurricanes strike Morgan City twice as often as Gulfport (Keim et al. 2007). Shallow bathymetry and coastal configuration of the Mississippi Coast tend to enhance surge heights, while Morgan City is protected by extensive wetlands, and is situated near a southwest-facing coast, which enables strong, easterly winds to blow offshore and moderate surge levels as hurricanes approach. Such patterns reveal that storm surge climatology is complex and localized, and may vary substantially over short distances.

Future research should investigate alternative statistical approaches that better estimate storm surge return levels using a limited record of observed data. Such improvements would be helpful for predicting return levels beyond the length of observed records. Nonetheless, this analysis provides the first empirical estimates for storm surge return levels to the 100-year return period along the U.S. Gulf Coast, which will benefit coastal planning and flood protection, as well as the storm surge modeling community.

5.7 References

Aschkenasy, J., 2014: P/C Rate Outlook. *Risk and Insurance*. Article published online February 6, 2014. Available on the Web at: <http://www.riskandinsurance.com/pc-rate-outlook/>.

Atlantic Oceanographic and Meteorological Laboratory, 2006: Hurricane Research Division, Hurricane Re-Analysis Project. Updated hurricane datasets provided on the Web at: www.aoml.noaa.gov/hrd/hurdat/Data_Storm.html.

Baade, R.A., R. Baumann, and V. Matheson, 2007: Estimating the economic impact of natural and social disasters, with an application to Hurricane Katrina. *Urban Studies*, 44, 11, 2061-2976.

Barnes, J., 2007: *Florida's Hurricane History*, 3rd Edition, University of North Carolina Press, Chapel Hill, North Carolina, USA, 407 pp.

Beguiría, S., 2005: Uncertainties in partial duration series modeling of extremes related of the choice of the threshold value, *Journal of Hydrology*, 303, 215–230.

Berg, R., 2010: Tropical Cyclone Report, Hurricane Ike. The National Hurricane Center, Miami, Florida, United States. Report available on the Web at: www.nhc.noaa.gov/pdf/TCR-AL092008_Ike_3May10.pdf.

Blake, E.S., C.W. Landsea, and E.J. Gibney, 2011: The Deadliest, Costliest, and Most Intense United States Tropical Cyclones from 1851 to 2010 (And Other Frequently Requested Hurricane Facts). *NOAA Technical Memorandum NWS NHC-6*. This publication is available on the Web at: <http://www.nhc.noaa.gov/pdf/nws-nhc-6.pdf>.

Bodine, B., 1969. Hurricane Surge Frequency Estimated For The Gulf Coast Of Texas. Washington, DC: U.S. Army Coastal Engineering Research Center.

Chen, Q., L. Wang, and R. Tawes, 2008: Hydrodynamic response of northeastern Gulf of Mexico to hurricanes. *Estuaries and Coasts*, 31, 1098-1116.

Chu, P.-S., and J. Wang, 1998: Modeling Return Periods of Tropical Cyclone Intensities in the Vicinity of Hawaii. *Journal of Applied Meteorology*, 37, 951-960.

Cline, I., 1926: *Tropical Cyclones*. First Edition Ed., The Macmillan Co., New York.

Coles, S., 2001: *An Introduction to Statistical Modeling of Extreme Values*. Springer, 208 pp.

Connor, W.C., 1956: Preliminary Summary of Gulf of Mexico Hurricane Data. Report from the New Orleans Forecast Office.

Davis, A.B., 1966: *Design of Hurricane flood protection works on the upper Texas coast*, Galveston, TX: USACE.

Davison, A. and R. Smith, 1990: Models for exceedances over high thresholds, *J. R. Stat. Soc.*, 52(B), 393–442.

Doran, K.S., N.G. Plant, H.F. Stockdon, A.H. Sallenger, and K.A. Serafin, 2009: Hurricane Ike: Observations and Analysis of Coastal Change. . Open-File Report 2009-1061. United States Geological Survey (USGS), Reston, Virginia Available on the Web at: <http://pubs.usgs.gov/of/2009/1061/pdf/ofr2009-1061.pdf>.

Dunn, G.E., and B.I. Miller, 1960: *Atlantic Hurricanes*. The Louisiana State University Press, Baton Rouge, Louisiana. 326 pp.

Ellis, M.J., 1988: *The Hurricane Almanac- 1988 Texas Edition*. Hurricane Publications, Inc.: Corpus Christi, Texas. 213 pp. ISBN 0-961 8707-1-0).

Elsner, J.B., T.H. Jagger, and K.-B. Liu, 2008: Comparison of Hurricane Return Levels Using Historical and Geological Records. *Journal of Applied Meteorology and Climatology*, 47, 368-374.

Emanuel, K., 2005: *Divine Wind-The History and Science of Hurricanes*. Oxford University Press, 296 pp. ISBN-10: 0195149416. ISBN-13: 9780195149418.

Emanuel, K., and T. Jagger, 2010: On Estimating Hurricane Return Periods. *Journal of Applied Meteorology and Climatology*, 49, 837-844.

Environmental Protection Agency, 2013: Climate Impacts on Transportation. Available on the Web at: <http://www.epa.gov/climatechange/impacts-adaptation/transportation.html>.

Faiers, G.E., B.D. Keim, and R.A. Muller, 1997: *Rainfall Frequency/ Magnitude Atlas for the South-Central United States*. SRCC Technical Report 97-1, published by the Southern Regional Climate Center, Department of Geography and Anthropology, Louisiana State University, Baton Rouge, Louisiana, 40 pp.

Federal Emergency Management Agency, 2009: Mitigation Assessment Team Report: *Hurricane Ike in Texas and Louisiana – Building Performance Observations, Recommendations and Technical Guidance*. Publication ID: FEMA P-757. Available on the Web at: <http://www.fema.gov/media-library/assets/documents/15498>.

Federal Emergency Management Agency, 2013: Flood Zones. Available on the Web at: <http://www.fema.gov/floodplain-management/flood-zones>.

Federal Emergency Management Agency, 2013b: Unit 3: NFIP Flood Studies and Maps. Available on the Web at: http://www.fema.gov/pdf/floodplain/nfip_sg_unit_3.pdf.

Freedman, A., 2013: Sandy: One Year Later. *Risk and Insurance*, October 1, 2013. Available on the Web at: <http://www.riskandinsurance.com/sandy-one-year-later/>.

Galloway, D., D.R. Jones, and S.E. Ingebritsen, (Eds.), 1999: Chapter titled Houston-Galveston, Texas, Managing Coastal Subsidence, in *Land Subsidence in the United States*. Circular 1182. U.S. Geological Survey. Available on the Web at: <http://pubs.usgs.gov/circ/circ1182/pdf/07Houston.pdf>.

Garriott, E.B., 1900: West Indian Hurricane of September 1-12, 1900. Published in the *Monthly Weather Review*, 28, 371-377. Edited by C. Abbe. Available on the Web at: <http://www.aoml.noaa.gov/general/lib/lib1/nhclib/mwreviews/1900.pdf>.

Google Earth, 2014: Landsat satellite image of the region near Morgan City, Louisiana. Image centered on: lat: 29.7041, lon: -91.2112. Imagery Date: April 9, 2013. Image Accessed: March 6, 2014.

Green, R., L.K. Bates, and A. Smyth, 2007: Impediments to recovery in New Orleans' Upper and Lower Ninth Ward: one year after Hurricane Katrina. *Disasters*, 31, 4, 311-335.

Halford, K.J., 1995: Estimating the dynamic water-level surfaces associated with Hurricane Andrew crossing the Louisiana coast. *Journal of Coastal Research*, Special Issue 21, 265-279.

Harris, D.L., 1963: Characteristics of the Hurricane Storm Surge. United States Weather Bureau, Technical Paper No. 48. Available on the Web at: http://www.csc.noaa.gov/hes/images/pdf/CHARACTERISTICS_STORM_SURGE.pdf.

Huff, F.A., and J.R. Angel, 1992: *Rainfall frequency atlas of the Midwest*. Bulletin 71, MCC Research Report 92-03. Published through the Midwestern Climate Center (NOAA), and Illinois State Water Survey, 141 pp.

Interagency Performance Evaluation Task Force, 2007: IPET Summary and Status Report. 23 pp. Presentation available on the Web at: http://www.iwr.usace.army.mil/Portals/70/docs/projects/29Jan07/IPET_Summary_USGS.pdf.

Jagger, T.H., and J.B. Elsner, 2006: Climatological Models for Extreme Hurricane Winds near the United States. *Journal of Climate*, 19, 3220-3236.

Jarrell, J.D., P.J. Hebert, and B.M. Mayfield, 1992: *Hurricane Experience Levels of Coastal County Populations – Texas to Maine*. NOAA Technical Memorandum NWS-NHC-46, 152 pp.

Jarvinen, B.J., and C.J. Neumann, 1985: An evaluation of the SLOSH storm surge model. *Bulletin of the American Meteorological Society*, 66, 1408-1411.

Jennings, R., 2013: Personal correspondence with R. Jennings, Hurricane Program Specialist with FEMA Region 4. Communication through e-mail, November 2013.

Jiang, Y., and Q. Zhuang, 2011: Extreme value analysis of wildfires in Canadian boreal forest ecosystems. *Canadian Journal of Forest Research*, 41, 1836-1851.

Kates, R.W., C.E. Colten, S. Laska, and S.P. Leatherman, 2006: Reconstruction of New Orleans after Hurricane Katrina: A research perspective. *Proceedings of the National Academy of Sciences of the United States of America*, 103, 14653-14660.

Katz, R.W., M.B. Parlange, P. Naveau, 2002: Statistics of Extremes in Hydrology. *Advances in Water Resources*, 25, 1287-1304.

Keim, B.D., R. Muller, and G. Stone, 2007: Spatiotemporal Patterns and Return Periods of Tropical Storm and Hurricane Strikes from Texas to Maine. *Journal of Climate*, 20, 3498-3509.

Kenkel, J.L., 1984: *Introductory Statistics for Management and Economics*. PWS Publishers. Boston, Massachusetts, USA. 837 pp.

Knabb, R.D., D.P. Brown, and J.R. Rhome, 2006: Tropical Cyclone Report, Hurricane Rita, 18-26 September 2005. National Hurricane Center, Miami, Florida. Report available on the Web at: www.nhc.noaa.gov/pdf/TCR-AL182005_Rita.pdf.

Knabb, R.D., J.R. Rhome, and D.P. Brown, 2011: Tropical Cyclone Report, Hurricane Katrina, 23-30 August 2005. National Hurricane Center, Miami, Florida. Available on the Web at: http://www.nhc.noaa.gov/pdf/TCR-AL122005_Katrina.pdf.

Kunreuther, H.C., and E.O. Michel-Kerjan, 2009: *At War with the Weather: Managing Large-Scale Risks in a New Era of Catastrophes*. MIT Press, Cambridge, Massachusetts.

Landsea C., C. Anderson, W. Bredemeyer, C. Carrasco, N. Charles, M. Chenoweth, G. Clark, J. Dunion, R. Ellis, J. Fernandez-Partagas, J. Gamache, D. Glenn, L. Hufstetler, C. Mock, C. Neumann, A. Santiago, D. Thomas, L. Woolcock, M. Zimmer, 2008: Documentation of Atlantic tropical cyclones changes in HURDAT. *Atlantic Oceanographic and Meteorological Laboratory*, Published on the Web at: http://www.aoml.noaa.gov/hrd/hurdat/metadata_19151920_new.html.

MacDonald, J.W., L. Dixon, and L. Zakaras, 2010: *Residential Insurance on the U.S. Gulf Coast in the Aftermath of Hurricane Katrina*. Restricted Draft produced for the Rand Corporation. 41 pp. Available on the Web at: <http://www.hhii.us/HHII%20images/Insurance/RandCorpWindStorm.pdf>.

Makkonen, L., 2008: Problems in the extreme value analysis. *Structural Safety*, 30, 405-419.

McCallum, B.E., B.D. McGee, D.R. Kimbrow, M.S. Runner, J.A. Painter, E.R. Frantz, and A.J. Gotvald, 2012: Monitoring Storm Tide Flooding from Hurricane Isaac along the Gulf Coast of the United States, August 2012. Open-File Report 2012-1263. Available on the Web at: <http://pubs.usgs.gov/of/2012/1263/>.

McTaggart-Cowan R., G.D. Deane, L.F. Bosart, C.A. Davis, T.J. Galarneau, Jr., 2008: Climatology of tropical cyclogenesis in the North Atlantic (1948-2004). *Monthly Weather Review*, 136, 1284-1304.

Mendoza-Rosas, A.T., and S. De la Cruz-Reyna, 2008: A statistical method linking geological and historical eruption time series for volcanic hazard estimations: Applications to active polygenetic volcanoes. *Journal of Volcanology and Geothermal Research*, 176, 277-290.

Mowbray, R., 2007: Insurance panel locked in struggle to survive; rate-control strategy

ineffective, some say. *Times-Picayune*. February 5.

National Hurricane Center, 1983: Preliminary Report, Hurricane Alicia, 15-21 August 1983. Miami, Florida, United States. Available on the Web at: http://www.nhc.noaa.gov/archive/storm_wallets/atlantic/atl1983-prelim/alicia/prelim02.gif.

National Hurricane Center, 1985: Preliminary Report, Hurricane Alicia, 28 August – 4 September. Miami, Florida, United States. Available on the Web at: http://www.nhc.noaa.gov/archive/storm_wallets/atlantic/atl1985-prelim/elena/prelim01.gif.

National Hurricane Center, 1989: Preliminary Report, Hurricane Jerry, 12-16 October 1989. Miami, Florida, United States. Available on the Web at: http://www.nhc.noaa.gov/archive/storm_wallets/atlantic/atl1989-prelim/jerry/.

National Oceanic and Atmospheric Administration, 2013: Linear mean sea level (MSL) trends and 95% confidence intervals in mm/yr. NOAA Tides and Currents, available on the Web at: www.tidesandcurrents.noaa.gov/sltrends/msltrendstable.htm.

National Oceanic and Atmospheric Administration, 2014: Water Levels – Station Selection. Datum and tidal data available for selected tide gauges. Available on the Web at: www.tidesandcurrents.noaa.gov/stations.html?type=Water+Levels.

National Weather Service, 2011: Hurricane History in Texas and Louisiana. Web page developed by the National Weather Service Forecast Office in Lake Charles, Louisiana. Available on the Web at: <http://www.srh.noaa.gov/lch/research/txlate20hur2.php>.

National Weather Service, 2013: The 1993 Storm of the Century. Web page developed by the National Weather Service Weather Forecast Office for the Tampa Bay Area. Available on the Web at: <http://www.srh.noaa.gov/tbw/?n=93storm>.

National Weather Service– Tampa Bay, 2014: National Weather Service Weather Forecast Office in Tampa Bay Area, Florida. Graphical Hazardous Weather Outlook, available on the Web at: <http://www.srh.noaa.gov/tbw/?n=ghwo-coastalflood>.

National Weather Service- Wakefield, 2014: National Weather Service Forecast Office in Wakefield, Virginia. Severe weather information webpage, available on the Web at: <http://www.erh.noaa.gov/er/akq/svrthun.php>.

Needham, H.F. and B.D. Keim, 2011: Storm surge: physical processes and an impact scale. In *Recent Hurricane Research- Climate, Dynamics, and Societal Impacts*, Lupo E (ed). Intech Open Access: Croatia.

Needham, H.F., and B.D. Keim, 2012: A Storm Surge Database for the U.S. Gulf Coast. *International Journal of Climatology*, 32, 14, 2108-2123. DOI: 10.1002/joc.2425.

Needham, H.F., B.D. Keim, D. Sathiaraj, and M. Shafer, 2013: A Global Database of Tropical Storm Surges. *EOS, Transactions American Geophysical Union*, 94, 24, 213-214.

Nicholls, R.J., F.M.J. Hoozemans, and M. Marchand, 1999: Increasing flood risk and wetland losses due to global sea-level rise: regional and global analyses. *Global Environmental Change*, 9, S69-S87.

Nicholls, R.J., and A. Cazenave, 2010: Sea-Level Rise and Its Impact on Coastal Zones. *Science*, 328, 1517-1520.

Penland, S., and K.E. Ramsey, 1990: Relative Sea-Level Rise in Louisiana and the Gulf of Mexico: 1908-1988. *Journal of Coastal Research*, 6, 323-342.

Pickands III, J., 1971: The Two-Dimensional Poisson Process and Extremal Processes. *Journal of Applied Probability*, 8, 4, 745-756.

Pielke, R.A., J. Gratz, C.W. Landsea, D. Collins, M.A. Saunders, and R. Musulin, 2008: Normalized Hurricane Damage in the United States: 1900-2005. *Natural Hazards Review*, 9, 1, 29-42.

Rappaport, E.N., 1993: Preliminary Report, Hurricane Andrew, 16-28 August 1992. National Hurricane Center, Miami, Florida. Report available on the Web at: http://www.nhc.noaa.gov/archive/storm_wallets/atlantic/atl1992/andrew/prenhc/prelim04.gif.

Sindhu, B., and A.S. Unnikrishnan, 2012: Return period estimates of extreme sea level along the east coast of India from numerical simulations. *Natural Hazards*, 61, 1007-1028.

Smith, R.L., 1989: Extreme Value Analysis of Environmental Time Series: An Application to Trend Detection in Ground-Level Ozone. *Statistical Science*, 4, 4, 367-393.

Smith, III, T.J., G.H. Anderson, K. Balentine, G. Tiling, G.A. Ward, and K.R.T. Whelan, 2009: Cumulative Impacts of Hurricanes on Florida Mangrove Ecosystems. *Wetlands*, 29, 1, 24-34.

Smith, A., N. Lott, T. Houston, K. Shein, and J. Crouch, 2013: Billion-Dollar U.S. Weather/Climate Disasters 1980-2013. National Climatic Data Center, Asheville, North Carolina. Report available on the Web at: <http://www.ncdc.noaa.gov/billions/events.pdf>.

Sobradelo, R., J. Martí, A.T. Mendoza-Rosas, and G. Gómez, 2011: Volcanic hazard assessment for the Canary Islands (Spain) using extreme value theory. *Natural Hazards and Earth System Sciences*, 11, 2741-2753.

Stewart, S.R., 2005: Tropical Cyclone Report, Hurricane Ivan, 2-24 September 2004. National Hurricane Center, Miami, Florida. Available on the Web at: http://www.nhc.noaa.gov/pdf/TCR-AL092004_Ivan.pdf.

Stoeten, K.J., 2013: Hurricane Surge Risk Reduction for Galveston Bay. MSc. Thesis. Faculty of Civil Engineering and Geosciences – Hydraulic Engineering, Delft University of Technology. Available on the Web at: http://repository.tudelft.nl/assets/uuid:3239a90e-42ef-485b-a73a-d39a99c1611a/Stoeten_KJ_-_Hurricane_Surge_Risk_Reduction_for_Galveston_Bay.pdf.

Stork, S.V., and M. Sneed, 2002: Houston-Galveston Bay Area, Texas, From Space- A New Tool for Mapping Land Subsidence. United States Geologic Survey and the U.S. Fish and Wildlife Service. Fact Sheet 110-02. Available on the Web at: <http://pubs.usgs.gov/fs/fs-110-02/Fact%20Sheet@10110-02.htm>.

Strauss, B.H., R. Ziemiński, J.L. Weiss, and J.T. Overpeck, 2012: Tidally adjusted estimates of topographic vulnerability to sea level rise and flooding for the contiguous United States. *Environmental Research Letters*, 7, 1, 014033.

Stumpf, R.P., and J.W. Haines, 1998: Variations in Tidal Level in the Gulf of Mexico and Implications for Tidal Wetlands. *Estuarine, Coastal and Shelf Science*, 46, 165-173.

Sugg, A.L., 1967: The Hurricane Season of 1966. *Monthly Weather Review*, 95, 3, 131-142. Available on the Web at: <http://www.aoml.noaa.gov/general/lib/lib1/nhclib/mwreviews/1966.pdf>.

Swenson, D., 2013: Hurricane Katrina flooding compared to a 500-year storm today: Graphic. Published on August 16, 2013 in *The Times-Picayune*. Available on the Web at: http://www.nola.com/hurricane/index.ssf/2013/08/hurricane_katrina_floodwater_d.html.

Texas General Land Office and Texas Sea Grant College Program, 2013: *Texas Homeowners Handbook to Prepare for Coastal Natural Hazards*. March, 2013. 78 pp. Available on the Web at: <http://www.glo.texas.gov/what-we-do/caring-for-the-coast/publications/homeowners-handbook-hurricanes.pdf>.

URS Group, 2006: *Hurricane Rita Rapid Response, Louisiana Coastal & Riverine High Water Mark Collection Final Report*, 79 pp. Available on the Web at: http://www.fema.gov/pdf/hazard/flood/recoverydata/rita/rita_la_hwm_public.pdf.

U.S. Army Engineer District- Galveston, Texas, 1962, Report on Hurricane Carla, 9-12 September, 1961: Galveston District Corps of Engineers, 29 pp.

U.S. Army Corps of Engineers, 2011: 100-Year Level of Protection. Website explains 100-year flood protection project for New Orleans, available on the Web at: www2.mvn.usace.army.mil/hps2/hps_100_year.asp.

U.S. Department of Transportation, 2013: Climate Variability and Change in Mobile, Alabama. Appendix D: Additional Information on the Sea Level Rise and Storm Surge

Analyses. Available on the Web at:
https://www.fhwa.dot.gov/environment/climate_change/adaptation/ongoing_and_current_research/gulf_coast_study/phase2_task2/mobile_variability/variable13.cfm.

U.S. Geological Survey, 2013: Inland Storm-Tide Monitoring Program. Available on the web at: http://water.usgs.gov/osw/programs/storm_surge1.html.

U.S. Weather Bureau, 1959: Hurricane Debra, July 24-26, 1959, A Preliminary Report and the Bulletins and Advisories Issued. Available on the Web at: http://www.nhc.noaa.gov/archive/storm_wallets/atlantic/atl1959/debra/prehnc/prelim1.gif

Vermeer, D., 2005: Climate Proofing the Netherlands. *Nature*, 438, 17.

Wamsley, T.Y., M.A. Cialone, J.M. Smith, J.H. Atkinson, and J.D. Rosati, 2010: The potential of wetlands in reducing storm surge. *Ocean Engineering*, 37, 1, 59-68.

Warner, C., 2007: Insurance rate increases ok'd: Coastal parishes to bear bulk of higher changes. Times-Picayune. May 1.

Weisberg, R.H., and L. Zheng, 2006: Hurricane storm surge simulations for Tampa Bay. *Estuaries and Coasts*, 29, 899-913.

Williams, J.M. and I.W. Duedall, 2002: *Florida Hurricanes and Tropical Storms, 1871-2001*, Expanded Edition. University of Florida Press, Gainesville, Florida. 167 pp.

Zoch, R.T., 1949: North Atlantic Hurricanes and Tropical Disturbances of 1949. *Monthly Weather Review*, 77, 12, 339-341.

CHAPTER 6. THE VULNERABILITY OF OIL REFINERIES AND POWER PLANTS TO STORM SURGE ALONG THE U.S. GULF COAST

6.1 Introduction

The energy industry along the U.S. Gulf Coast plays a central role in the regional and national economy. This industry powers the nation through the development of oil and gas reserves, the creation of electric power, and, more recently, the development of renewable energy. This region also has the capacity to refine and process large quantities of raw materials from both domestic and international sources.

The oil and gas industry is especially established offshore and along the coastline of Texas and Louisiana. As of 2011, the 27 petroleum refineries in Texas accounted for approximately 27% of the refining capacity in the U.S., and Texas comprised approximately 28% of marketed gas production in the nation (U.S. Energy Information Administration 2012). Considering other energy sources, Texas provides approximately 16% of U.S. energy (U.S. Energy Information Administration 2010). Louisiana accounts for approximately 17% of the national refining capacity (U.S. Energy Information Administration 2010) and ranked second only to Texas in refinery capacity in 2010 (U.S. Energy Information Administration 2012). The Louisiana Offshore Oil Port (LOOP) provides the only U.S. port where deep draft tankers can offload crude oil. Regionally, the Gulf Coast provides approximately 45% of the nation's refining capacity and 31% of natural gas processing plant capacity (U.S. Energy Information Administration 2013).

Although the energy industry accounts for a lower proportion of the economy in Alabama and Mississippi, these states still contain critical energy infrastructure. For example, Chevron's largest U.S. refinery is located in Pascagoula, Mississippi, and is setup to process heavier, sour crude oil (Chevron Corporation 2010). Alabama produces a

considerable amount of hydroelectric power, accounting for 5% of the nation's capacity, whereas Louisiana and Texas produce less than 1% (U.S. Energy Information Administration 2010).

The robust energy industry in this region requires the development and maintenance of extensive industrial infrastructure. Gulf Coast states collectively contain 52 refineries (U.S. Energy Information Administration 2013b), as well as more than 42,000 km of onshore pipelines and 3,800 production platforms (Paskal 2010). The \$800 billion in energy assets make up approximately 90% of industrial assets in the region (Entergy 2010).

Three major environmental factors threaten energy production in this region: hurricanes, storm surges and subsidence/sea-level rise. These natural hazards have inflicted large economic losses, which are estimated to be \$14 billion/year (Entergy 2012). These hazards work together, as strong hurricane winds generate high waves and storm surges, which are exacerbated by subsidence and sea-level rise.

Hurricanes that form in the Gulf of Mexico, or track into the Gulf from the Atlantic Ocean or Caribbean Sea, are a threat from June – November every year. These storms frequently threaten the entire region, from Texas to Florida. For example, 12 of 18 cities along the Gulf Coast observe hurricane strikes every 10 years or less (Keim et al. 2007), and each of the five Gulf Coast states contain at least one of these 12 cities with active hurricane-strike climatologies. These storms have produced some of the strongest winds on Earth observed at a coastline. For example, Hurricane Camille produced maximum sustained winds of 85 m s^{-1} at landfall, which was only exceeded by Super Typhoon Haiyan in the Philippines in 2013 (Masters 2013). Hurricanes have caused

approximately \$3.7 trillion (2010 dollars) in asset damage over past century in Alabama, Mississippi, Louisiana and Texas (Pielke et al. 2008; Entergy 2012). In 2005, hurricanes Katrina and Rita caused a record breaking \$15 billion in losses to energy markets, two-thirds of which were associated with physical damage to energy infrastructure (Kaiser et al. 2009).

The combination of an active hurricane climatology and shallow bathymetry provides the ingredients for devastating storm surges in this region. This region observes an average of 18 storm surges ≥ 1 m and one storm surge ≥ 5 m every decade, which is the second highest frequency of storm surges in the world exceeding these thresholds, ranking the region behind the Bay of Bengal of high-magnitude storm surges and East Asia for low-magnitude storm surges (see Chapter 2). Hurricane Katrina generated an 8.53-m storm tide in Mississippi (Knabb et al. 2011), which was the highest storm tide ever observed in the Western Hemisphere (see Chapter 2). Hurricane Camille produced a 7.5-m storm tide in the same area in 1969 (Simpson et al. 1970). In 1900, the Galveston Hurricane generated a 6.1-m storm tide at Galveston, Texas (Garriott 1900), and killed at least 8,000 people (Blake et al. 2011), in the deadliest natural disaster in U.S. history (Emanuel 2005).

In addition to damaging infrastructure and rendering facilities inoperable for a period of time, high storm surges in the region have also triggered hazardous material releases. As Hurricane Camille's storm surge inundated Venice, Louisiana, hazardous materials, including oil, were released from loading and petroleum storage facilities (U.S. Army Corps of Engineers 1970). A large amount of oil was released from a floating storage tank at a refinery in coastal Mississippi (Chevron 1998) when a 2.93-m storm

surge inundated Pascagoula during Hurricane Georges in 1998 (Guiney 1999). A tank containing hazardous gasoline additives at this same facility floated from its foundations (Chevron 1998). More recently, almost 50 oil spills were reported near the coastline during Hurricane Katrina (Pine 2006). The Murphy Oil Spill released 819,000 gallons of oil into a densely populated region of St. Bernard Parish, and was one of five releases that exceeded 800,000 gallons (Pine 2006). This spill occurred as surging waters dislodged and lifted an above-ground storage tank. During the same event, approximately 10,500 gallons of oil from the Shell Oil Spill reached the coastline and polluted coastal marshes (Pine 2006).

Rising sea levels threaten to exacerbate coastal flooding events in the region, as the central and western Gulf Coast states are experiencing the fastest rates of sea-level rise in the nation. A combination of localized subsidence, or sinking ground levels, and global sea-level rise, have produced high relative sea-level rise (RSLR) rates in the region, particularly in South Louisiana and Southeast Texas. Analysis of long-term water level trends at 128 tide gauges in the United States reveals that the three highest rates of RSLR in the nation are occurring at Eugene Island and Grand Isle, Louisiana, as well as Galveston, Texas (National Oceanic and Atmospheric Administration 2014). RSLR rates at these locations are 0.965 cm yr^{-1} , 0.924 cm yr^{-1} , and 0.684 cm yr^{-1} , respectively. These rates mean that in South Louisiana, sea-levels will rise nearly 1 m per century relative to land, which is five times higher than the global average observed over the past century (Doyle et al. 2010). These rapid RSLR rates in South Louisiana have produced the fastest rates of coastal erosion in the United States (Gosselink et al. 1998; Stone et al. 2003).

The rapid rate of RSLR rise in this region places ports and energy infrastructure at risk to inundation. For example, a 61-cm increase in RSLR may impact 64% of the port facilities in this region, while a rise of 1.22 m would impact nearly 75% of these facilities (Climate Change Science Program 2008; Burkett 2011). Such impacts may be most severe in South Louisiana, which contains more than half of the energy facilities in the nation located ≤ 1.22 m above sea level (Carraway 2013). Looking into the future, the combination of subsidence/sea-level rise and asset growth may increase asset loss by as much as 30% from 2010-2030 (Entergy 2010).

Climatological data on hurricane strikes and rising sea levels have been made widely available, making it possible to assess the vulnerability of coastal infrastructure to these hazards through statistical analysis. For example, The Atlantic Oceanographic and Meteorological Laboratory Hurricane Research Division (HRD) of the National Oceanic and Atmospheric Administration (NOAA) has developed The Hurricane Database (HURDAT), which provides data on the track and intensity of Atlantic hurricanes and tropical storms since 1851 (Atlantic Oceanographic and Meteorological Laboratory 2014). This robust dataset has been used to analyze the vulnerability of energy infrastructure to hurricanes, or to validate modeling studies that conduct such analyses (Reed et al. 2010; Rose et al. 2013). The U.S. Army Corps of Engineers (USACE) and the National Ocean Service (NOS) have operated long-term tide gauges in the region, which provide extensive sea-level datasets. The USACE established its first tide gauge in Louisiana in 1933, and has expanded coverage to more than 80 sites in the state (Penland and Ramsey 1990). The NOS established eight tide gauges in the region by 1947, and a gauge at Galveston, Texas, has been operational since 1908 (Penland and Ramsey 1990).

Long-term sea-level trend data have been used to analyze the vulnerability of energy infrastructure in the region (Climate Change Science Program 2008; Burkett 2011).

However, an analysis that investigates the vulnerability of Gulf Coast energy infrastructure to storm surges using observed data has not yet been conducted, as a comprehensive archive of observed storm surge events has only recently become available. Needham and Keim (2012) developed The Storm Surge Database (SURGEDAT), which began as a peak storm surge database for the U.S. Gulf Coast. Needham et al. (2013) expanded on this work by developing a global peak storm surge database, and expanding the U.S. dataset to include all storm surge observations from tropical cyclones, not just peak observations. SURGEDAT now archives more than 8,000 high watermarks created by more than 350 tropical cyclones along the U.S. Gulf and Atlantic Coasts since 1880.

This chapter addresses a critical gap in the literature by providing the first empirical analysis of energy infrastructure vulnerability to storm surge inundations in the region. Although storm surges threaten a wide range of infrastructure, this study focuses on the vulnerability of oil refineries and power plants. Such facilities are widespread throughout the region's coastal zone and are crucial to the regional and national economy. Although other infrastructure, like pipelines and offshore platforms, are also critical to the energy industry, analyzing the vulnerability of these structures would add considerable complication and uncertainty to this study. Pipelines run great distances and are located above ground, below ground, and below water, making it difficult to assess their vulnerability even if extensive storm surge data are available for a location. Limited offshore storm surge data make it difficult to analyze the vulnerability of offshore

platforms using observed surge data, and modeling efforts may produce better results for this topic.

This chapter addresses three primary research questions: 1) What proportion of refineries and power plants in the U.S. Gulf Coast region are vulnerable to various storm surge return levels, like the 100-year flood; 2) What sub-regions contain the highest and lowest quantities of vulnerable facilities; and 3) How can this analysis be applied for future energy development and planning. Such questions should help us better understand the risk of storm surge inundations to critical energy facilities along the U.S. Gulf Coast, and improve future industrial planning.

6.2 Data

6.2.1 Storm Surge Data

Storm surge data are provided by SURGEDAT, a global storm surge database that provides more than 8,000 high watermarks produced by more than 350 tropical cyclones along the U.S. Gulf and Atlantic Coasts since 1880 (Needham and Keim 2012; Needham et al. 2013). This dataset provides a comprehensive archive of storm surge observations, as it was constructed through an exhaustive literature search from government and academic sources, as well as extensive newspaper archives.

In Chapter 5, I utilized SURGEDAT to create historical storm surge climatology at 26 locations along the U.S. Gulf Coast. This climatology is based on storm surge and storm tide observations taken over the 114-year period from 1900-2013. I used the observations at each site to estimate return levels for 10-, 25-, 50-, 100-, 200-, and 500-yr storm surge return periods, using Point Process and Logarithmic Plotting methods. The Logarithmic Plotting method provided a better fit to observed data, as the Point Process

method underestimated storm surge heights. Although the Logarithmic Plotting method is designed to analyze extreme values for time periods at the length of the observed dataset or shorter, it is possible that this method also provides the best prediction of 200- and 500-yr return levels, as it outperformed the Point Process method in the Kolmogorov-Smirnov goodness-of-fit test for all storm surge quantiles.

Storm surge return levels developed in Chapter 5 depict considerable geographic variability in this region (Table 6.1, Figure 6.1). For example, 100-year return levels at Bay St. Louis/Pass Christian, and Gulfport/Biloxi, Mississippi, as well as Baytown, Texas, all exceed 7 m, whereas return levels at Cedar Key and Tampa, Florida, as well as Morgan City, Louisiana, are less than 3 m. Such variability is caused by a variety of factors, including differences in hurricane tracking patterns, bathymetry, and the shape, geometry and aspect of the coastline.

Table 6.1. Storm surge return levels (m) for 26 locations along the U.S. Gulf Coast, using Logarithmic Plotting.

| Location | 10-Yr | 25-Yr | 50-Yr | 100-Yr | 200-Yr | 500-Yr |
|---------------------|-------|-------|-------|--------|--------|--------|
| South Padre Island | 1.13 | 2.27 | 3.14 | 4 | 4.86 | 6 |
| Corpus Christi | 1 | 2.28 | 3.26 | 4.23 | 5.21 | 6.49 |
| Port Lavaca | 0.6 | 2.71 | 4.3 | 5.9 | 7.49 | 9.6 |
| Freeport | 1.86 | 3.04 | 3.94 | 4.83 | 5.73 | 6.91 |
| Galveston | 2 | 3.34 | 4.35 | 5.36 | 6.38 | 7.71 |
| Baytown | 1.71 | 4.03 | 5.78 | 7.54 | 9.29 | 11.61 |
| Sabine Pass | 1.56 | 2.68 | 3.54 | 4.39 | 5.24 | 6.36 |
| Cameron | 1.14 | 2.58 | 3.67 | 4.76 | 5.85 | 7.29 |
| Morgan City | 1.21 | 1.83 | 2.31 | 2.78 | 3.25 | 3.88 |
| Grand Isle | 1.44 | 2.27 | 2.91 | 3.54 | 4.17 | 5.01 |
| Shell Beach | 2.09 | 3.29 | 4.19 | 5.1 | 6 | 7.2 |
| New Orleans Lakefro | 1.85 | 2.56 | 3.1 | 3.65 | 4.19 | 4.9 |
| Frenier | 1.49 | 2.43 | 3.14 | 3.84 | 4.55 | 5.49 |

Table 6.1 (continued). Storm surge return levels (m) for 26 locations along the U.S. Gulf Coast, using Logarithmic Plotting.

| | | | | | | |
|-------------------------------|------|------|------|------|------|-------|
| Mandeville | 1.79 | 2.36 | 2.79 | 3.22 | 3.65 | 4.22 |
| Slidell | 1.68 | 2.85 | 3.74 | 4.63 | 5.51 | 6.68 |
| Bay St. Louis/ Pass Christian | 2.15 | 4.46 | 6.2 | 7.95 | 9.69 | 12 |
| Gulfport/ Biloxi | 2.13 | 4.12 | 5.63 | 7.13 | 8.64 | 10.63 |
| Dauphin Island | 1.22 | 2.44 | 3.37 | 4.3 | 5.23 | 6.45 |
| Mobile | 1.76 | 2.64 | 3.3 | 3.97 | 4.64 | 5.52 |
| Pensacola | 1.34 | 2.46 | 3.3 | 4.14 | 4.98 | 6.09 |
| Panama City | 0.99 | 2.17 | 3.07 | 3.97 | 4.87 | 6.05 |
| Apalachicola | 1.44 | 2.08 | 2.56 | 3.04 | 3.52 | 4.16 |
| Cedar Key | 1.15 | 1.7 | 2.12 | 2.53 | 2.95 | 3.49 |
| Tampa | 1.18 | 1.77 | 2.21 | 2.65 | 3.1 | 3.68 |
| Fort Myers/ Cape Coral | 0.88 | 1.76 | 2.43 | 3.09 | 3.76 | 4.64 |
| Key West | 1.03 | 2.31 | 3.28 | 4.25 | 5.22 | 6.5 |

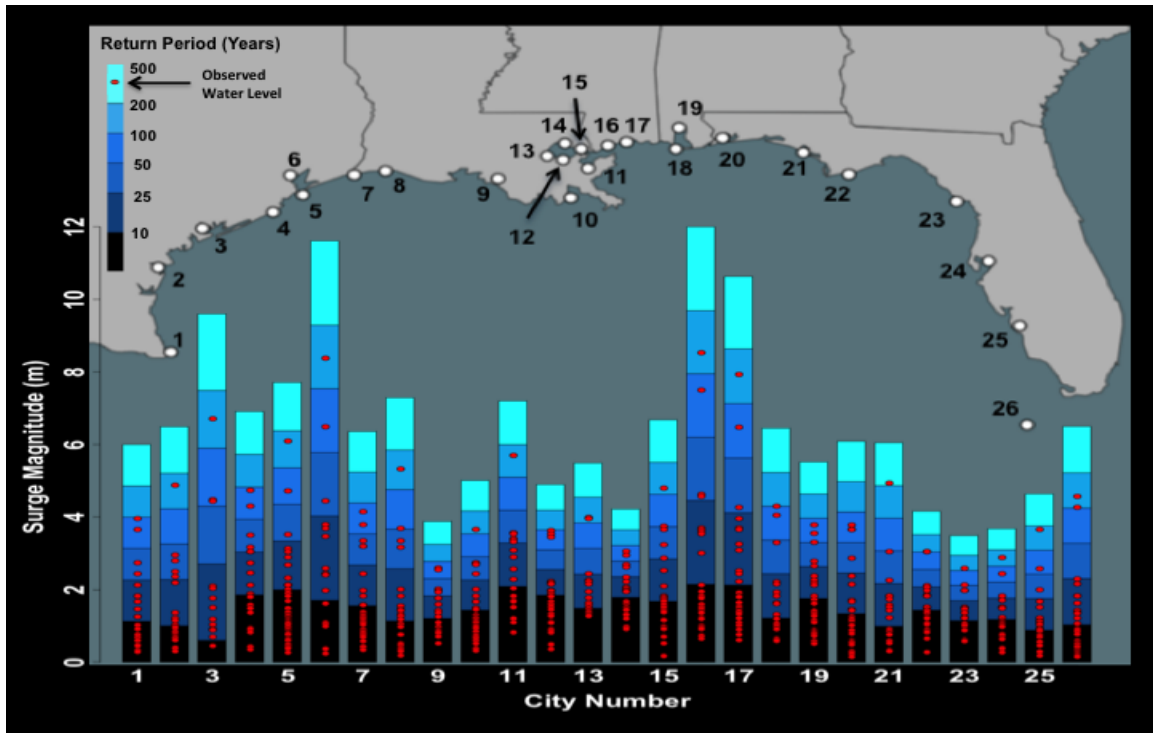


Figure 6.1. Storm surge return levels and observed surge events for 26 cities along the U.S. Gulf Coast. This graphic was produced in Chapter 5.

6.2.2 Energy Facility Data

Locations of energy facilities in a 10-state U.S. Southeast region were identified through a geospatial database comprised of thermoelectric power plants, hydropower facilities, renewable energy facilities, and oil refineries. The dataset was provided by Oak Ridge National Laboratory and represents the results of a collaboration involving Oak Ridge National Laboratory (ORNL), Idaho National Laboratory (INL), and Argonne National Laboratory (ANL) to develop an energy infrastructure database. This dataset is part of the Homeland Security Infrastructure Protection (HSIP) Freedom database, accessible through the Homeland Security Information Network. The HSIP Freedom database is analogous to the HSIP Gold database, but with increased data sharing within the Federal, State, and Local emergency response communities. The database was developed using open source information including digitized published open source, unrestricted reports; Federal Energy Regulatory Commission (FERC) filings - openly published with unlimited distribution; remote sensing imagery; and datasets contributed by the various collaborating national laboratories.

This dataset indicates that 1,711 electricity generation facilities are located in the 10-state southeast region, with the three most common fuel types comprised of natural gas, hydropower, and other renewables. Net operating capacity among these facilities was largely attributed to natural gas, coal, or nuclear plants. Electricity generation facilities included those operated by electrical utilities engaged in the generation, transmission, and distribution of electricity as well as industrial generators. The database also contained 54 oil refineries, which were concentrated in Texas and Louisiana, as well as the refining capacity of those facilities. As fossil fuels are the predominant fuel source for electricity

generation facilities in the region, those facilities representing renewable energy (hydropower, solar, geothermal) were excluded from the study.

The database includes facilities that have been decommissioned, as well as those that have been planned but are not yet generating. Both were included in the case study, as former facilities have potential to be used in the future through redevelopment and repowering of the existing site, while the latter may be exposed to future climate change once operations commence. The majority of these facilities were adjacent to the Gulf of Mexico, which has been described as the ‘Energy Coast’ (AWF et al. 2008), and which has been the focus of prior energy infrastructure vulnerability assessments (Needham et al. 2012; Strauss and Ziemiński 2012).

6.3 Methods

The first step in this study involved selecting a subset of energy facilities that are located in the Gulf of Mexico coastal zone, and potentially exposed to tropical cyclone-generated storm surges. Exposed facilities were identified by comparing facility locations with land areas at risk of inundation from hurricane storm surge events. Land areas at risk of inundation were derived from Maloney and Preston (2014), based on analyses of archived composite simulations with the Sea, Lake and Overland Surges from Hurricanes (SLOSH) model from the National Hurricane Center (NHC), of the National Oceanic and Atmospheric Association (NOAA) (NWS 2011).

The SLOSH model estimates storm surge heights associated with hurricanes by simulating the effects of storm size, forward speed, track, wind speed and atmospheric pressure on water heights in the coastal zone. Data products from the SLOSH model are available for 37 basins along the coasts of the Atlantic Ocean, Gulf of Mexico, Caribbean

Sea, and Hawaii that are exposed to hurricanes, including population centers, ports, and low-lying topography where the effects of storm surge are greatest (NWS 2011; Burkett and Davidson 2012). Composite simulations are based on several thousand simulations using varying forward speeds, landfall directions, and landfall locations for each basin (Frazier et al. 2010). Model simulations generate values for the maximum storm surge surface water elevation obtained in each grid cell, called Maximum Envelopes of Water (MEOWs) (Rygel et al. 2006; Kleinosky et al. 2007; Frazier et al. 2010). The MEOWs for each basin form a composite dataset called Maximum of MEOWS (MOMs) (Rygel et al. 2006; Kleinosky et al. 2006; Frazier et al. 2010). The MOMs represent the spatial distribution of potential storm surge elevation for a particular category of tropical cyclone at a particular tide (NWS 2011). For storm surge heights of individual hurricanes, this model is accurate to within +/- 20% (NWS 2011).

To estimate inundation from MOMs, storm surge elevations at high tide for the 16 SLOSH basins along the Gulf Coast were compared with the underlying land elevation, which was represented by a composite grid of USGS 1 arc-second (~30 m horizontal resolution) National Elevation Dataset (NED) tiles (Gesch et al. 2002; Gesch 2007), corresponding with the spatial extent of the MOM (Maloney and Preston 2014). Areas where the land surface elevation for each basin was less than the storm surge surface water elevation were labeled as being at risk of inundation, and these areas were extracted as a set of five GIS data layers corresponding to different hurricane intensities (i.e., categories 1–5) on the Saffir-Simpson scale. As the entire Gulf Coast is potentially exposed to landfalling category 5 hurricanes, energy facilities in the Southeast intersecting the category 5 storm surge inundation layers for each of the Gulf Coast

basins were selected for inclusion in the current study. This process selected 207 electricity generation facilities and 33 oil refineries, however, the number was reduced to 152 and 32, after facilities along the U.S. Atlantic Coast were eliminated from the study.

After these sites were selected, elevation data were assigned to each facility to analyze its vulnerability to storm surge inundation. Estimates of facility elevations were calculated by comparing latitude and longitude coordinates for facility locations with the NED 30 m resolution elevation data. This process provided one elevation value per facility, which is an estimate of the average facility elevation. In practice, many facilities sprawl across large areas and may contain structures with different elevations. However, it was necessary to obtain an average elevation and estimated center point for each facility, to assess the vulnerability of each site to storm surge inundation.

It was necessary to assign each energy facility to a coastal location with adequate storm surge data, to analyze the vulnerability of oil refineries and electric power plants to storm surge inundation. Figure 6.2 provides a map of oil refineries, power plants and cities with storm surge data. I utilized the R Program for Statistical Software (R Development Core Team 2010) to run spatial queries that measured the distance from each facility to each of the 26 coastal cities for which I estimated storm surge return levels in Chapter 5. Facilities were assigned with the closest coastal city with storm surge data.

Energy infrastructure data provided by Oak Ridge National Lab and storm surge data provided by SURGEDAT. However, these assignments were modified for two special cases. A facility and a city were not matched if the Mississippi River or New Orleans' Industrial Canal traversed a line connecting the city and facility. In other words,

I did not want to match facilities with surge data from the other side of these waterways. High levees along the Mississippi River typically inhibit storm surges from crossing the river, although Hurricane Katrina's massive storm surge was high enough to cross the river in Plaquemine's Parish, Louisiana, south of New Orleans (Interagency Performance Evaluation Taskforce Report 2006; Keim and Muller 2009).



Figure 6.2. The location of oil refineries, power plants, and cities with surge data.

The Industrial Canal also provides a boundary in the eastern portion of New Orleans; areas to the west of this feature are vulnerable to storm surge inundation from Lake Pontchartrain, while areas to the southeast of this feature, near Arabi and Chalmette, are vulnerable to storm surge flowing from the east and passing near Shell Beach. New Orleans East is a relatively small area to the northeast of the Industrial Canal that can actually be flooded from both Lake Pontchartrain and from water pushed up the Mississippi River Gulf Outlet (MRGO), and passing near Shell Beach. The one facility in this region is adjacent to a levee that is vulnerable to surge from the east, so this facility was assigned to Shell Beach.

For cases in which the city closest to a facility was on the other side of the Mississippi River or Industrial Canal, facilities were re-assigned the closest city on the same side of these waterways. These adjustments changed the matching of four refineries and 18 power plants in Louisiana. Several distinct patterns emerged from these adjustments. The city of New Orleans had the most facilities reassigned, as New Orleans had three refineries and seven power plants before the adjustments, but zero refineries and only one power plant after the adjustments. Two of the three refineries were re-assigned to Shell Beach, and the other to Grand Isle. Of the seven power plants originally assigned to New Orleans, four were re-assigned to Shell Beach and two to Grand Isle. Morgan City and Frenier swapped many power plants that had to be re-assigned because the closest city to these plants was on the other side of the Mississippi River. Five power plants from the Morgan City zone were re-assigned to Frenier, and six power plants that were originally assigned to Frenier were re-assigned to Morgan City.

Table 6.2 provides the number of refineries and power plants assigned to each city. The majority of these facilities were concentrated in Texas and Louisiana. For example, approximately 85% of the power plants were located in Texas and Louisiana, while around 15% of these facilities were located in Mississippi, Alabama and Florida. Texas and Louisiana also contained approximately 91% of oil refineries, while Mississippi, Alabama and Florida contained only 9% of these facilities. Baytown, Texas, contained more power plants than any other location, as 25 facilities were assigned to this city. Baytown and Sabine Pass both were assigned five refineries, which were the highest numbers of any region. The Gulf Coast of Florida contained no refineries and only 7% of the power plants.

After each facility was assigned to a coastal city, I compared the return levels for 10-, 25-, 50-, 100-, 200-, and 500-year storm surge return periods with the elevation of facilities at each location. Following this methodology, I was able to quantify the number of facilities that would be inundated by the various storm surge return levels, and thereby generate a customized facility inundation profile for each coastal region.

Table 6.2. The number of oil refineries and electric power plants assigned to each of the 26 cities with adequate storm surge data.

| Location | Refineries | Power Plants |
|-------------------------------|------------|--------------|
| South Padre Island | 0 | 0 |
| Corpus Christi | 2 | 8 |
| Port Lavaca | 0 | 7 |
| Freeport | 0 | 9 |
| Galveston | 3 | 8 |
| Baytown | 5 | 25 |
| Sabine Pass | 5 | 16 |
| Cameron | 4 | 14 |
| Morgan City | 3 | 18 |
| Grand Isle | 1 | 3 |
| Shell Beach | 2 | 5 |
| New Orleans Lakefront | 0 | 1 |
| Frenier | 4 | 15 |
| Mandeville | 0 | 0 |
| Slidell | 0 | 0 |
| Bay St. Louis/ Pass Christian | 0 | 1 |
| Gulfport/ Biloxi | 0 | 2 |
| Dauphin Island | 1 | 4 |
| Mobile | 2 | 5 |
| Pensacola | 0 | 1 |
| Panama City | 0 | 0 |
| Apalachicola | 0 | 2 |
| Cedar Key | 0 | 1 |

Table 6.2 (continued). The number of oil refineries and electric power plants assigned to each of the 26 cities with adequate storm surge data.

| | | |
|------------------------|---|---|
| Tampa | 0 | 6 |
| Fort Myers/ Cape Coral | 0 | 1 |
| Key West | 0 | 0 |

6.4 Results

I calculated the quantity and proportion of power plants and refineries that would be inundated by the 10-, 25-, 50-, 100-, 200-, and 500-year storm surge (Table 6.3). Although storm surge return levels are estimated locally, this table provides basin-wide counts. These results indicate that storm surges threaten a higher quantity of power plants, but a higher proportion of refineries. This is a logical outcome, as the quantity of power plants in the coastal zone is nearly five times the quantity of refineries. However, refineries are especially concentrated in the Central and Western Gulf Coast, where surge heights are highest, which explains the high proportion of flooded refineries. Despite these differences, both power plants and refineries in the region are vulnerable to storm surge inundation. For example, the 100-year storm surge would flood approximately 72% (23 of 32) of the coastal refineries and 63% (95 of 152) of the coastal power plants.

Table 6.3. Number of facilities and proportion of facilities flooded by each storm surge return level along U.S. Gulf Coast. Return levels are localized but these data are compiled from a basin-wide count.

| Return Period | Power Plants | Power Plants Flooded | Pct. Power Plants Flooded | Refineries | Refineries Flooded | Pct. Refineries Flooded |
|---------------|--------------|----------------------|---------------------------|------------|--------------------|-------------------------|
| 10-year | 152 | 21 | 13.8 | 32 | 5 | 15.6 |
| 25-year | 152 | 45 | 29.6 | 32 | 12 | 37.5 |
| 50-year | 152 | 66 | 43.4 | 32 | 18 | 56.3 |
| 100-year | 152 | 95 | 62.5 | 32 | 23 | 71.9 |
| 200-year | 152 | 116 | 76.3 | 32 | 27 | 84.4 |
| 500-year | 152 | 129 | 84.9 | 32 | 29 | 90.6 |

Figures 6.3 and 6.4 depict the elevation of power plants and refineries near each city, superimposed on top of the storm surge return levels provided in Figure 6.1. These images provide a visualization of the numbers of facilities that would be flooded by various storm surge return levels near each city.

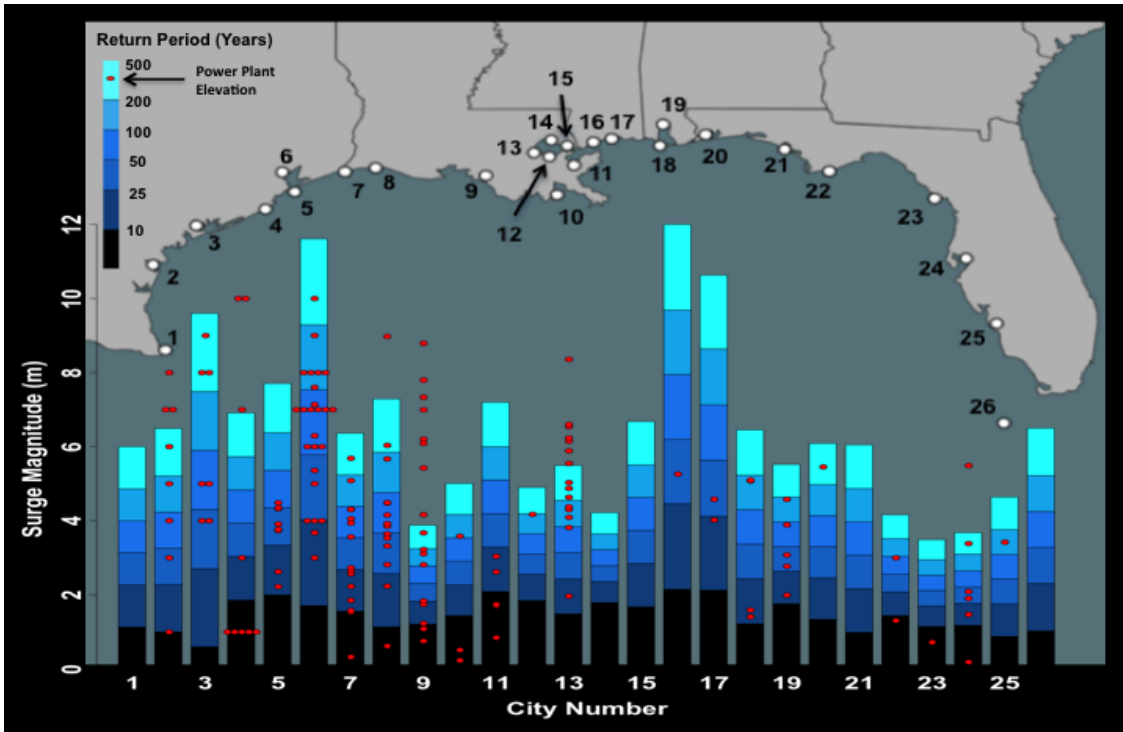


Figure 6.3. Surge return levels and power plant elevations for the U.S. Gulf Coast

I also compiled numeric counts of the number of facilities flooded at each location by each of the storm surge return levels (Tables 6.4 and 6.5). Storm surge threatens a high quantity and high proportion of power plants in Eastern Texas and Southwest Louisiana. For example, the 100-year storm surge would flood more than eight power plants near Galveston, Baytown, Sabine Pass, and Cameron, with 18 flooded power plants near Baytown providing the highest quantity (Figure 6.5). This flood level would inundate 100% of the plants near Galveston, 75% near Baytown, 88% near Sabine Pass, and 79% near Cameron.

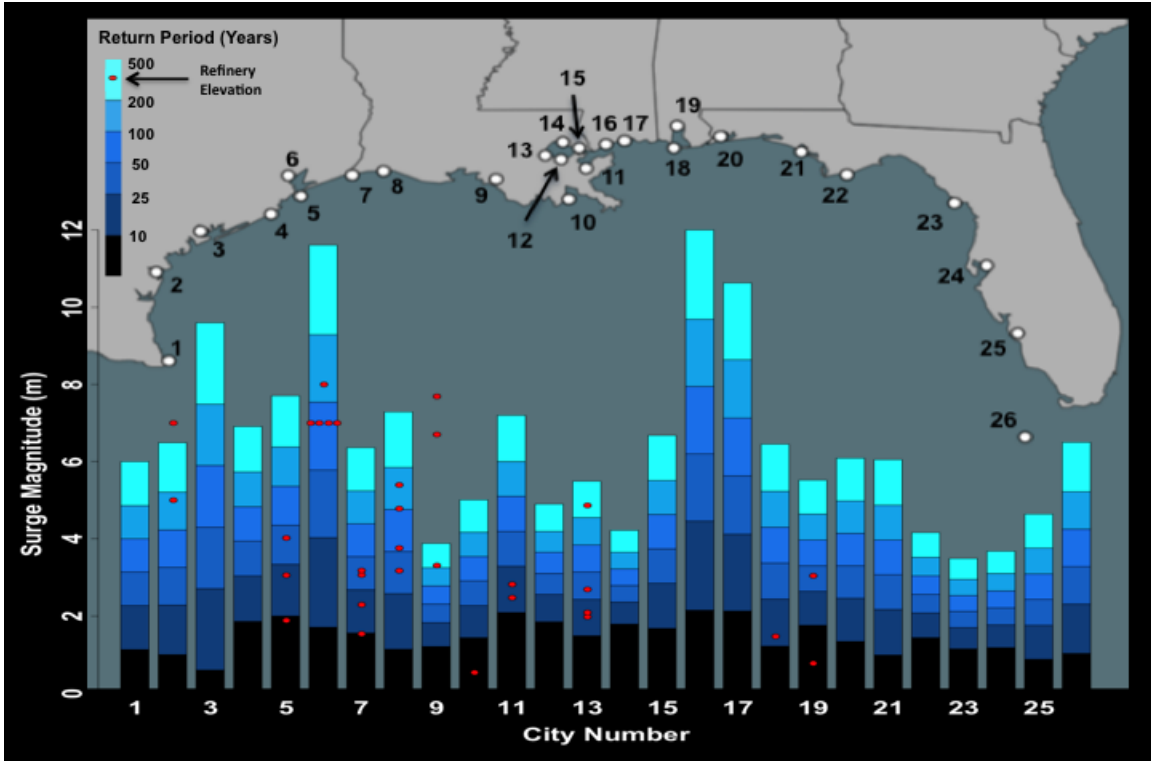


Figure 6.4. Surge return levels and refinery elevations for the U.S. Gulf Coast

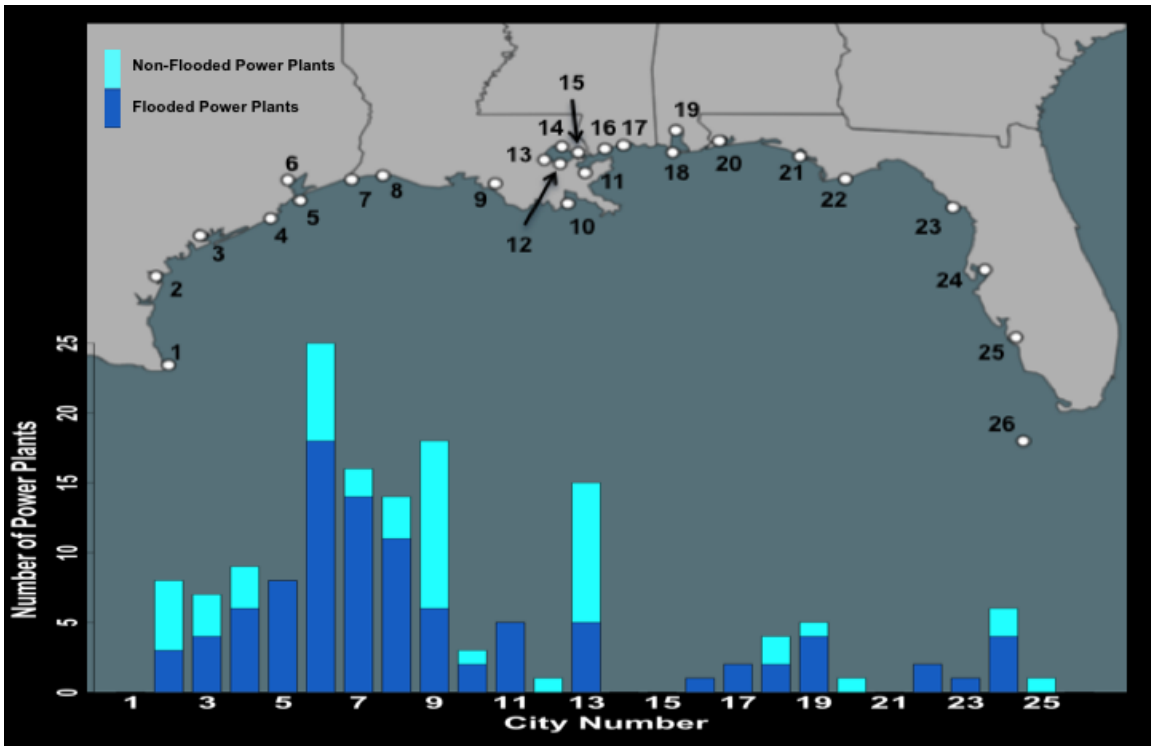


Figure 6.5. Number of flooded and non-flooded power plants in the 100-yr surge.

Table 6.4. The number of power plants flooded by various storm surge return levels at 26 locations along the U.S. Gulf Coast. 100-yr refers to the height of the 100-year storm surge level.

| Location | No. of Power Plants | 10-Yr | 25-Yr | 50-Yr | 100-Yr | 200-Yr | 500-Yr |
|-------------------------------|---------------------|-------|-------|-------|--------|--------|--------|
| South Padre Island | 0 | 0 | 0 | 0 | 0 | 0 | 0 |
| Corpus Christi | 8 | 1 | 1 | 2 | 3 | 4 | 5 |
| Port Lavaca | 7 | 0 | 0 | 2 | 4 | 4 | 7 |
| Freeport | 9 | 5 | 6 | 6 | 6 | 6 | 6 |
| Galveston | 8 | 0 | 2 | 6 | 8 | 8 | 8 |
| Baytown | 25 | 0 | 5 | 7 | 18 | 24 | 25 |
| Sabine Pass | 16 | 3 | 8 | 9 | 14 | 15 | 16 |
| Cameron | 14 | 1 | 2 | 6 | 11 | 12 | 13 |
| Morgan City | 18 | 3 | 5 | 6 | 6 | 9 | 10 |
| Grand Isle | 3 | 2 | 2 | 2 | 2 | 3 | 3 |
| Shell Beach | 5 | 3 | 5 | 5 | 5 | 5 | 5 |
| New Orleans Lakefront | 1 | 0 | 0 | 0 | 0 | 1 | 1 |
| Frenier | 15 | 0 | 1 | 1 | 2 | 5 | 8 |
| Mandeville | 0 | 0 | 0 | 0 | 0 | 0 | 0 |
| Slidell | 0 | 0 | 0 | 0 | 0 | 0 | 0 |
| Bay St. Louis/ Pass Christian | 1 | 0 | 0 | 1 | 1 | 1 | 1 |
| Gulfport/ Biloxi | 2 | 0 | 1 | 2 | 2 | 2 | 2 |
| Dauphin Island | 4 | 0 | 2 | 2 | 2 | 4 | 4 |
| Mobile | 5 | 0 | 1 | 3 | 4 | 5 | 5 |
| Pensacola | 1 | 0 | 0 | 0 | 0 | 0 | 1 |
| Panama City | 0 | 0 | 0 | 0 | 0 | 0 | 0 |
| Apalachicola | 2 | 1 | 1 | 1 | 2 | 2 | 2 |
| Cedar Key | 1 | 1 | 1 | 1 | 1 | 1 | 1 |
| Tampa | 6 | 1 | 2 | 4 | 4 | 4 | 5 |
| Fort Myers/ Cape Coral | 1 | 0 | 0 | 0 | 0 | 1 | 1 |
| Key West | 0 | 0 | 0 | 0 | 0 | 0 | 0 |

Table 6.5. The number of refineries flooded by various storm surge return levels at 26 locations along the U.S. Gulf Coast. 100-yr refers to the height of the 100-year storm surge level.

| Location | No. of Refineries | 10-Yr | 25-Yr | 50-Yr | 100-Yr | 200-Yr | 500-Yr |
|-------------------------------|-------------------|-------|-------|-------|--------|--------|--------|
| South Padre Island | 0 | 0 | 0 | 0 | 0 | 0 | 0 |
| Corpus Christi | 2 | 0 | 0 | 0 | 0 | 1 | 1 |
| Port Lavaca | 0 | 0 | 0 | 0 | 0 | 0 | 0 |
| Freeport | 0 | 0 | 0 | 0 | 0 | 0 | 0 |
| Galveston | 3 | 1 | 2 | 3 | 3 | 3 | 3 |
| Baytown | 5 | 0 | 0 | 0 | 4 | 5 | 5 |
| Sabine Pass | 5 | 2 | 3 | 5 | 5 | 5 | 5 |
| Cameron | 4 | 0 | 0 | 1 | 2 | 4 | 4 |
| Morgan City | 3 | 0 | 0 | 0 | 0 | 0 | 1 |
| Grand Isle | 1 | 1 | 1 | 1 | 1 | 1 | 1 |
| Shell Beach | 2 | 0 | 2 | 2 | 2 | 2 | 2 |
| New Orleans Lakefront | 0 | 0 | 0 | 0 | 0 | 0 | 0 |
| Frenier | 4 | 0 | 2 | 3 | 3 | 3 | 4 |
| Mandeville | 0 | 0 | 0 | 0 | 0 | 0 | 0 |
| Slidell | 0 | 0 | 0 | 0 | 0 | 0 | 0 |
| Bay St. Louis/ Pass Christian | 0 | 0 | 0 | 0 | 0 | 0 | 0 |
| Gulfport/ Biloxi | 0 | 0 | 0 | 0 | 0 | 0 | 0 |
| Dauphin Island | 1 | 0 | 1 | 1 | 1 | 1 | 1 |
| Mobile | 2 | 1 | 1 | 2 | 2 | 2 | 2 |
| Pensacola | 0 | 0 | 0 | 0 | 0 | 0 | 0 |
| Panama City | 0 | 0 | 0 | 0 | 0 | 0 | 0 |
| Apalachicola | 0 | 0 | 0 | 0 | 0 | 0 | 0 |
| Cedar Key | 0 | 0 | 0 | 0 | 0 | 0 | 0 |
| Tampa | 0 | 0 | 0 | 0 | 0 | 0 | 0 |
| Fort Myers/ Cape Coral | 0 | 0 | 0 | 0 | 0 | 0 | 0 |
| Key West | 0 | 0 | 0 | 0 | 0 | 0 | 0 |

Further east, storm surge is less of a threat to power plants because most locations either have fewer facilities or observe lower storm surge heights. For example, storm surges reach the highest levels along the Mississippi Coast, however, the two Mississippi locations included in this study only contain a combination of three power plants. The entire Gulf Coast of Florida, from Pensacola to Key West, only contains 11 coastal power plants, which is less than half of the number of plants near Baytown, Texas. However, storm surge does threaten a large proportion of plants along Florida's Gulf Coast, as the 100-year storm surge would inundate approximately 64% (7 of 11) of these facilities, and 67% (4 of 6) of the plants near Tampa. Morgan City, Louisiana, was assigned 18 power plants, which is the second highest quantity for any location, however, relatively low storm surge heights at that location pose only modest risk to facilities. The 100-year storm surge at Morgan City would flood 33% of the power plants (6 of 18).

Refineries are particularly vulnerable to storm surge in East Texas. The 100-year storm surge would inundate 100% of the refineries near Galveston (3 of 3) and Sabine Pass (5 of 5), and 80% of the refineries near Baytown (4 of 5). From another perspective, the 100-year storm surge threatens to inundate 92% (12 of 13) of the refineries in the Galveston-Baytown-Sabine Pass region. These 12 inundated facilities represent more than half of the refineries along the U.S. Gulf Coast that would be flooded by the 100-year storm surge (Figure 6.6). Inundation rates decrease east of the Texas/Louisiana border, where 50% of the refineries near Cameron (2 of 4) and none of the refineries near Morgan City (0 of 3) would flood in the 100-year surge. The proportion of facilities increases in the western portion of Lake Pontchartrain, where 75% of the refineries near Frenier (3 of 4) would flood in the 100-year storm surge. Storm surge is less of a threat to

refineries in Mississippi, Alabama and Florida, as only three of the 32 Gulf Coast refineries are located in these states. Nonetheless, the 100-year storm surge would inundate 100% (3 of 3) of the refineries closest to Dauphin Island and Mobile, Alabama.

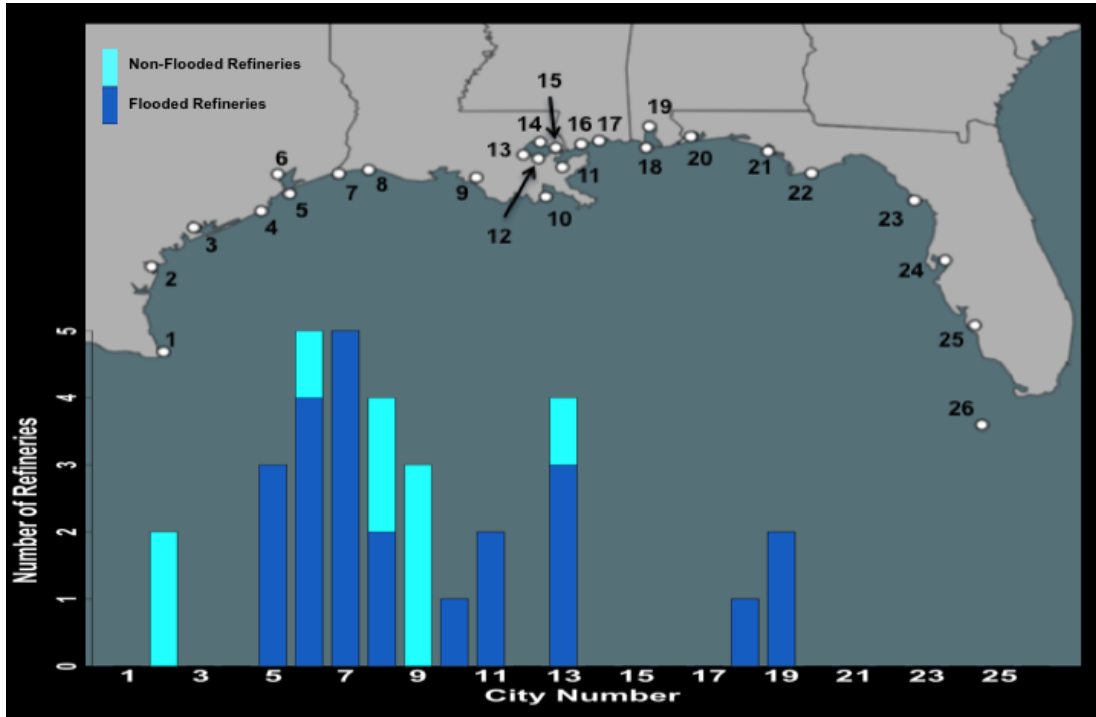


Figure 6.6. Number of flooded and non-flooded refineries in the 100-yr surge.

6.5 Discussion

These results indicate that storm surge is a considerable threat to energy facilities along the U.S. Gulf Coast. The 200- and 500-year storm surges threaten the most infrastructure, however, storm surge return levels used in this study were estimated through logarithmic plotting methods employed in Chapter 5, which were not designed to predict storm surge return levels beyond the length of the observed data, which was a 114-year period. As such, 100-year storm surge levels are the highest credible water levels provided in this study. Caution should be taken when considering the 200- and 500- year levels, nonetheless, I included these time periods in this analysis, as they may provide the best available estimates of surge levels at these return periods.

Although I usually assigned refineries and power plants to the closest city for which storm surge data were available, the matching of facilities and cities sometimes covers relatively long distances and crosses state boundaries. Therefore, we should take caution to consider that facilities are located *near* cities with storm surge data, not *at* these cities. For example, the one refinery assigned to Dauphin Island, Alabama, is actually located in the state of Mississippi, but was closer to Dauphin Island than Biloxi/Gulfport.

The greatest distances between facilities and cities usually occur when refineries or power plants are located well inland, but storm surge models suggest the location could be inundated by an extreme storm surge. Data for Morgan City provide the best example of this pattern. Only one of the 18 electric plants assigned to Morgan City actually has a physical address in that location. The other facilities were located in Broadmoor, Baldwin, Centerville, Garden City, Hahnville, Houma, Norco, Plaquemine, Port Allen, Saint Gabriel, Seymourville, and Thibodaux, Louisiana. The three plants in Plaquemine are located more than 50 km north of Morgan City, and the distance between the Port Allen plant and Morgan City is approximately 85 km.

These distances are considerable, and these locations have not previously observed storm surge flooding in recent memory. However, models suggest that these facilities may be vulnerable to the most extreme storm surges, as the elevation of all of these plants is less than 8 m, and elevations just west of these areas, near the Atchafalaya floodplain and Intracoastal Waterway, are only several meters above sea level. Also, all of these plants are located along or to the south of the I-10 corridor, which has been vulnerable to past storm surges. Hurricanes Rita in 2005 and Ike in 2008 pushed storm

surge inland considerable distances in South Louisiana, inundating locations as far north as I-10. In southwest Louisiana, Hurricane Rita's surge washed inland more than 60 km (McGee et al. 2013), and Ike's surge washed inland at least 55 km (Federal Emergency Management Agency 2008). Extensive inland storm surge flooding has also been observed in low-lying deltas of other ocean basins. For example, in the Irrawaddy Delta of Myanmar, a storm surge event in 1975 pushed sea water at least 100 km inland (Dube et al. 2008), while Cyclone Nargis in 2008 pushed a storm surge inland more than 50 km in the same region (Fritz et al. 2009).

Numerous power plants in Ascension Parish, Louisiana, were assigned to Frenier, a small community on the western shore of Lake Pontchartrain. The distance between Frenier and these plants exceeds 50 km, though surge affecting these locations would most certainly pass near Frenier to get there. Although models indicate that storm surge could potentially reach these facilities, this study suggests that these plants are beyond the reach of the 100-year surge. Due to the large distance between Frenier and many of its assigned plants, I estimate that the 100-year surge would inundate only 13% (2 of 15) of the plants in the Frenier group. On the contrary, the 100-year storm surge would inundate 75% (3 of 4) of the refineries near Frenier.

Although storm surge heights can be localized and vary considerably between two nearby locations, errors in this study are minimized by the fact that long distances between facilities and cities typically occur when facilities are located inland. In most cases, the closest city with surge data accurately represents the storm surge climatology near the location where storm surge would hit the coast and begin working inland. As

such, long distances between facilities and cities do not typically extend along the coastline, where storm surge heights could vary greatly between two distant locations.

Although I accounted for levees along the Mississippi River and Industrial Canal of New Orleans, another limitation of this study is that I did not consider the influence of any other levees or flood control structures. Such features may reduce the vulnerability to both fresh-water and coastal flooding, and likely decrease the risk of storm surge inundation provided by this analysis.

The United States contains vast public and private levee networks, which may extend for more than 160,000 km across the landscape (American Society of Civil Engineers 2010). The most high-profile of these levee systems are extensive public projects that are maintained by the U.S. Army Corps of Engineers, or other state or federal agencies. For example, the U.S. Army Corps of Engineers maintains a network of levees around the New Orleans metropolitan area that is constructed to protect against the 100-year flood (U.S. Army Corps of Engineers 2011). This network is extensive, as more than 5,700 km of levees protect this metropolitan area (Van Heerden 2007).

However, more than 85% of the levees in the United States are locally owned (American Society of Civil Engineers 2010), and are maintained by local and regional levee districts, or private enterprises, like corporations that have constructed levees to protect industrial infrastructure. As many organizations maintain levees in different parts of the country, the full extent of levee protection in the United States is unclear (American Society of Civil Engineers 2010). Unfortunately, at this time there is no central database of levee locations and heights. Therefore, it is not practicle to account for the impact of levees on storm surge inundation in this study.

Even if facilities are protected by a levee, it is important to remember that no levee is flood-proof, and levees may provide a false sense of security. In some cases, levees may actually attract more development to flood-prone areas, in a pattern known as the “levee effect” (Kates et al. 2006; U.S. Global Change Research Program 2009). However, high-magnitude floods sometimes cause the widespread failure of flood defense systems, causing widespread economic losses. For example, Hurricane Katrina’s massive storm surge destroyed, breached or damaged more than half of New Orleans’ levees (Van Heerden 2007), which led to the flooding of 80% of the metropolitan area (Kates et al. 2006). In the previous decade, a rain-induced flood in the Upper Midwest in 1993 caused approximately 70% of the levees in this region to fail (Tobin 1995). In both of these cases, catastrophic flooding occurred behind levee systems. Nonetheless, levees usually protect communities from floods and areas inside a levee system are less vulnerable to flooding than areas outside. As such, it is important to note that not every facility will flood when a local storm surge height exceeds a facility elevation.

The limitations imposed by both scaling problems and the presence of levees is perhaps best demonstrated by considering the vulnerability of refineries near Galveston, Texas. At a first glance, it may appear that Galveston is in grave danger, because the 50-year storm surge is higher than 100% (3 of 3) of its refineries. Upon closer examination, however, the energy facility database indicates that all of these facilities are located in Texas City, not Galveston, but following my methodology, they were assigned to Galveston as the closest city with storm surge data. Fortunately, the U.S. Army Corps of Engineers constructed a ring levee around Texas City, which proved valuable in 2008, when Hurricane Ike’s storm surge rose within 0.61 m of the top of the levee (U.S. Army

Corps of Engineers 2012). In this case, this study provides assurance that the ring levee around Texas City was a wise investment, as multiple refineries would be vulnerable to frequent flooding without protection.

By comparison, the refineries near Baytown all have higher elevations than the Texas City refineries, which place all of these facilities higher than the 50-year storm surge. However, the 100-year surge level is high enough to inundate 80% (4 of 5) of these refineries, and, unlike Texas City, the inner portion of Galveston Bay has limited public flood protection. This realization is sobering when one considers that area near Baytown contains the largest petroleum and petrochemical complex in the United States (ExxonMobil 2014), and local citizens are relying on private companies to maintain adequate levees to prevent a widespread chemical release during a major surge event.

Another limitation of this study is that the coastal flooding data are derived completely from historic storm surge observations, and do not account for future changes in climate or coastal geography. I assume stationarity in my long-term storm surge climatology, however, the coastal environment is changing, as sea levels rise and land is subsiding in much of the region. Changes in climate and coastal geography will likely increase future losses in the energy industry. For example, climate events presently cost the industry approximately \$14 billion/year, but these losses may increase to \$18 billion/year even with no climate change, or \$23 billion/year with extreme climate change by the year 2030. These losses may further increase to \$26 - \$40 billion/year by the year 2050, depending on the extent of climate change (Entergy 2012). From another perspective, the cumulative impact of climate hazards from the years 2010-2030 may

reach \$370 billion, which is enough capital to reconstruct the city of New Orleans six times or to construct 700 stadiums like New Orleans' Superdome (Entergy 2010).

Although there is some uncertainty regarding climate change impacts on hurricane frequency and intensity (Needham et al. 2012), rapid sea-level rise has been clearly observed along the Gulf Coast over a period of many decades, particularly in South Louisiana and East Texas. The rate of Relative Sea-Level Rise (RSLR) near Morgan City averages 1.52 cm/yr (Penland and Ramsey 1990), which means we would expect more than 1.5 m of RSLR over the next century if rates remain constant. This water rise accounts for > 50% of the 100-year storm surge level, which is 2.78 m (Table 6.1). Therefore, although storm surge levels at Morgan City are the lowest of any city from South Padre Island, Texas, to Apalachicola, Florida, rapidly rising sea levels near this location will exacerbate coastal flooding in the future. Grand Isle, Louisiana, also observes lower storm surge heights than some nearby locations, but is experiencing rapid rates of sea-level rise. On the other hand, the Mississippi Coast observes the highest storm surge levels in the region, but the stable coastline in that area will reduce the impacts of sea-level rise compared to nearby Louisiana.

This study provides new insights that industry professionals can use for site selection of new energy infrastructure. This may be especially applicable for cities that are near each other geographically but have dramatic differences in storm surge risk. For example, although Mandeville, Louisiana, and Bay St. Louis, Mississippi, are separated by only 70 km, the 100-year storm surge at Bay St. Louis is more than 4.7 m higher than Mandeville. The distance between Freeport and Baytown, Texas, is 90 km, but the difference in the 100-year storm surge at these locations exceeds 2.7 m. If possible, it

may be beneficial to establish future energy infrastructure, like power plants, in areas with lower risk.

This analysis may also provide helpful insights for protecting existing facilities. This is especially important for refineries, as local opposition and environmental regulations have prevented any new refineries from opening in the United States since the late 1970s (Kesicki 2010). Therefore, it is crucial that existing refineries are protected from floods or any other hazards that may threaten their operation.

While it is important to protect existing and proposed infrastructure from flooding, it is also important to assess flood risk to prepare for inevitable inundations. From an insurance perspective, the problem of storm surge inundation for large energy facilities relates to weather derivatives, an emerging concept that enables stakeholders to insure against losses caused by extreme weather (Zeng 2000; Campbell and Diebold 2004). Weather derivatives enable policyholders to insure against a weather event that exceeds some damaging threshold. For example, a retailer could insure against a snowfall in New York on Black Friday, which would drastically reduce profits. In this case, the derivative policy would clearly state a time (Black Friday), magnitude (5 cm of snow), and precise location of the severe weather event (Central Park), and policyholders would receive a payout if the event surpassed the predetermined threshold, regardless of actual monetary losses. Derivative policies based on temperature, precipitation and wind velocities have been relatively easy to develop because of the massive amounts of historical climate data for these variables, however, absence of credible storm surge data has prevented the development of such products for storm surge. This study may provide beneficial information to guide the development of storm surge derivative policies in the

region, as insurance and energy professionals need to understand potential risks to infrastructure before they could agree on a storm surge threshold that would trigger a payout.

This analysis may also help coastal cities prepare for the impacts of future disasters, as impacts vary considerably from one city to the next, and do not necessarily depend on the severity of the severe weather event. For example, Pensacola and Cedar Key, Florida, each have one power plant near the city. The plant in Cedar Key is located at a low elevation and would be flooded by the 10-year storm surge. The plant near Pensacola, however, is less prone to inundation, as it is located at an elevation above the 200-year storm surge. This means that electric power may be less impacted by storm surge at Pensacola than Cedar Key, even though surge heights at Pensacola are higher. Assessing the vulnerability of such infrastructure could help communities plan for future disasters, and assess potential impacts from storm surge events.

6.6 Summary and Conclusion

The energy industry along the U.S. Gulf Coast provides critical resources that help drive the regional and national economy. The oil and gas industry is especially well-developed along the Texas and Louisiana Coast, as these two states combine to provide more than 40% of the refining capacity in the U.S. (U.S. Energy Information Administration 2010; U.S. Energy Information Administration 2012), and a large portion of natural gas processing. This robust industry has developed more than 90% of the industrial assets in the region (Entergy 2010).

Hurricanes, storm surges and sea-level rise are three natural hazards that impact the energy industry in this region. Much of the region has an active hurricane

climatology, as 12 of 18 cities along the Gulf Coast observe a hurricane strike every 10 years or less (Keim et al. 2007). Massive storm surges often accompany hurricanes in this region, as the U.S. Gulf Coast observes the second highest frequency of large and small storm surges in the world (see Chapter 2). These surges are deadly and destructive, and can induce complicated industrial problems, like hazardous materials releases. Sea-level rise is a long-term hazard in this region that particularly threatens Southeast Texas and South Louisiana. The combination of rising seas and sinking land, known as relative sea-level rise, is occurring at a rate of at least 1 m/ century in portions of South Louisiana.

Climatological data on hurricane strikes and sea-level rise have been well established along the U.S. Gulf Coast, however, storm surge climatology for the region has only recently been established through the SURGEDAT project. The present study utilized observed data to analyze the vulnerability of energy infrastructure to storm surge inundations in the region.

Storm surge data were obtained from analysis in Chapter 5, where estimates are provided for the 10-, 25-, 50-, 100-, 200-, and 500-year storm surge return levels at 26 cities along the U.S. Gulf Coast, using a logarithmic plotting method on observed data from SURGEDAT. Oak Ridge National Laboratory (ORNL) provided energy facility data that represent collaborative work between ORNL, Idaho National Laboratory (INL), and Argonne National Laboratory (ANL). This dataset provided 1,711 power plants and 54 refineries in a 10-state region of the southeast United States. The Sea, Lake and Overland Surges from Hurricanes (SLOSH) model from the National Hurricane Center (NHC), was used to determine how many of these facilities could potentially be inundated from storm surge. This analysis reduced the number of facilities to 152 power

plants and 32 refineries near the U.S. Gulf Coast that could potentially be inundated by surge.

I assigned each facility to one of the 26 cities with storm surge return levels developed in Chapter 5. Facilities were typically matched with the closest cities, however, facilities were not matched with cities that were located on opposite sides of the Mississippi River or New Orleans' Industrial Canal, because high levees along those features typically contain storm surge to one side of these features.

The majority of refineries and power plants were assigned to cities in Texas and Louisiana. These states contained 91% of the refineries and 85% of the power plants in the region. Baytown, Texas, provides an example of the massive amount of energy infrastructure in that state, as this city was assigned 25 power plants, which is more than the combined total of all the Gulf Coast plants in Mississippi, Alabama and Florida.

Results of this study show that energy facilities along the U.S. Gulf Coast are considerably vulnerable to storm surge inundation. The 100-year storm surge would inundate approximately 72% (23 of 32) of the coastal refineries and 63% (95 of 152) of the coastal power plants. The 25-year storm surge would flood approximately 38% (12 of 32) of the refineries and 30% (45 of 152) of the power plants.

The highest quantity and proportion of flooded power plants are found in Southeast Texas and Southwest Louisiana. The 100-year storm surge would inundate 100% of the plants near Galveston, 75% near Baytown, 88% near Sabine Pass and 79% near Cameron. Numerically, this flood level would inundate at least eight power plants near each of these locations, and as many as 18 plants near Baytown.

Southeast Texas experiences the greatest storm surge threat to refineries. The 100-year storm surge would flood 100% of the refineries near Galveston (3 of 3) and Sabine Pass (5 of 5), and 80% of the refineries near Baytown (4 of 5). This concentrated area of refinery flood risk is remarkable, when considering that these 12 inundated refineries account for more than half of the flooded refineries along the entire U.S. Gulf Coast. Refinery risk is also high near the western shores of Lake Pontchartrain, where the 100-year storm surge would inundate 75% (3 of 4) of the refineries near Frenier.

Inundation risks are relatively low along the Eastern Gulf Coast, as the Gulf Coast of Mississippi, Alabama and Florida only contain three refineries and 23 power plants. Also, storm surge heights in Western Florida are relatively low at Cedar Key and Tampa, Florida, where the 100-year surge level is less than 3 m. Nonetheless, infrastructure near Tampa is vulnerable to surge, as the 100-year storm surge would inundate 67% (4 of 6) of the power plants near the city.

Morgan City is potentially an attractive location to place energy infrastructure, as it is located in the heart of the Gulf Coast Energy Belt, but observes lower surge heights than all locations west of Apalachicola, Florida. The relatively low 100-year surge height at this location (2.78 m), threatens to inundate no refineries (0 of 3), and only 33% (6 of 18) of the power plants in this region. However, the rate of relative sea-level rise near Morgan City exceeds 1.5 m/ century, placing infrastructure at risk to long-term inundation. Nearby Grand Isle also observes lower surge heights than many other cities along the Northern Gulf Coast, but the rate of sea-level rise near this city is also high.

A limitation of this study is that it does not account for environmental changes, like sea-level rise or coastal erosion. Another limitation includes the fact that relatively

large distances, in excess of 50 km, sometimes separate energy facilities and the cities with surge data. However, these long distances typically occur when refineries or power plants are located well inland, and the city to which they are assigned accurately represents storm surge climatology near the closest point on the coast. I also did not account for localized levees and other flood control devices, as the majority of such structures are privately owned and information about them is not readily available. As such, we cannot assume that facilities will actually flood if storm surge return levels exceed facility elevations. Nonetheless, vulnerable facilities require the construction and maintenance of flood control structures, and such infrastructure sometimes fails, causing widespread flooding.

These results will likely provide a wide range of applications, as this is the first regional assessment of storm surge risk to energy infrastructure based on observed data. Industry professionals may find this study useful for siting new facility locations or improving the protection of existing facilities. This analysis may also help coastal communities assess the impact of potential surge events on energy services, or to assess the risk of hazardous materials releases from a high-magnitude storm surge. Professionals in both the insurance and energy sectors may consult this analysis to establish storm surge thresholds that would trigger payouts on derivative policies. In summary, stakeholders in many professions that relate to the development and success of the energy industry along the U.S. Gulf Coast may find this study beneficial.

6.7 References

American Society of Civil Engineers, 2010: *So, You Live Behind a Levee!* 28 pp. Report available on the Web at: <http://content.asce.org/files/pdf/SoYouLiveBehindLevee.pdf>.

Atlantic Oceanographic and Meteorological Laboratory, 2014: HURDAT Re-Analysis Project. Data and metadata available on the Web at: http://www.aoml.noaa.gov/hrd/hurdat/Data_Storm.html.

AWF (America's Wetland Foundation), America's Energy Coast, Entergy Corporation, 2008: Building a Resilient Energy Gulf Coast: Executive Report America's Energy Coast, America's Wetlands Foundation, Entergy Corporation [online] Available at <http://entergy.com/gulfcoastadaptation/>.

Blake, E.S., C.W. Landsea, and E.J. Gibney, 2011: The Deadliest, Costliest, and Most Intense United States Tropical Cyclones from 1851 to 2010 (And Other Frequently Requested Hurricane Facts). *NOAA Technical Memorandum NWS NHC-6*. This publication is available on the Web at: <http://www.nhc.noaa.gov/pdf/nws-nhc-6.pdf>.

Burkett, V., 2011: Global climate change implications for coastal and offshore oil and gas development. *Energy Policy*, 39, 7719-7725.

Campbell, S.D., and F.X. Diebold, 2004: Weather forecasting for weather derivatives, CFS Working Paper, No. 2004/10, <http://nbn-resolving.de/urn:nbn:de:hebis:30-10621>

Carraway, T.M., 2013: An Analysis of the Influences on Household-Level Adaptations to Environmental Hazards. Thesis submitted to the Department of Environmental Sciences, Louisiana State University, December, 2013. Available on the Web at: http://etd.lsu.edu/docs/available/etd-08272013-162913/unrestricted/TiiaCarraway_Thesis2013.pdf.

Chevron, 1998: Hurricane George. *Spotlight*, 11, 10.

Chevron Corporation, 2010: Chevron Pascagoula Refinery, Types of Crude Oil. Available on the Web at: <http://pascagoula.chevron.com/home/abouttherefinery/whatwedo/typesofcrudeoil.aspx>.

Climate Change Science Program, 2008: Impacts of climate change and variability on transportation systems and infrastructure: Gulf Coast Study, Phase I. In: Savonis, M.J., Burkett, V.R., Potter, J.R. (Eds.), *Synthesis and Assessment Product 4.7*, U.S. Department of Transportation, Washington, DC, pp. 445.

Doyle, T.W., K.W. Krauss, W. H. Conner, A.S. From, 2010: Predicting the retreat and migration of tidal forests along the northern Gulf of Mexico under sea-level rise. *Forest Ecology and Management*, 259, 770-777.

Dube, S.K., A.D. Rao, P.C. Sinha and P. Chittibabu, 2008: Storm Surges: Worst Coastal Marine Hazard. Chapter 9, pp. 125-140, in: Murthy, C.R., P.C. Sinha, and Y.R. Rao, *Modelling and Monitoring of Coastal Marine Processes*. Co-published by Springer and Capital Publishing Company, 246 pp.

Emanuel, K., 2005: *Divine Wind-The History and Science of Hurricanes*. Oxford University Press, 296 pp. ISBN-10: 0195149416. ISBN-13: 9780195149418.

Entergy, 2010: Effectively addressing climate risk through adaptation for the Energy Gulf Coast. Report written October, 2010. Available on the Web at: http://www.entergy.com/content/our_community/environment/GulfCoastAdaptation/report.pdf.

Entergy, 2012: Building a Resilient Energy Gulf Coast. Executive Report. Available on the Web at: [http://usbcso.org/documents/Building_a_Resilient_Gulf_Coast%20\(Executive%20Summary\).pdf](http://usbcso.org/documents/Building_a_Resilient_Gulf_Coast%20(Executive%20Summary).pdf).

ExxonMobil, 2014: About Our Facilities: Facts about the ExxonMobil facilities at Baytown, Texas. Available on the Web at: <http://corporate.exxonmobil.com/en/company/worldwide-operations/locations/united-states/baytown/about?parentId=da547204-0aaa-4776-850a-83fd38e3fc21>.

Federal Emergency Management Agency, 2008: Hurricane Ike in Texas and Louisiana. Mitigation Assessment Team Report. Available on the web at: http://www.fema.gov/library/file?type=publishedFile&file=757_ape_final.pdf&fileid=71147ed0-b6a2-11df-97ce-001cc4568fb6.

Frazier, T.G., N. Wood, B. Yarnal, and D.H. Bauer, 2010: Influence of potential sea level rise on societal vulnerability to hurricane storm-surge hazards, Sarasota County, Florida. *Applied Geography*, 30, 490-505.

Fritz, H.M., C.D. Blount, S. Thwin, M.K. Thu, and N. Chan, 2009 : Cyclone Nargis storm surge in Myanmar. *Nature Geoscience*, 2, 448-449.

Garriott, E.B., 1900: West Indian hurricane of September 1-12, 1900. *Monthly Weather Review*, 28, 371-378.

Gesch D., M. Oimoen, S. Greenlee, C. Nelson, M. Steuck, and D. Tyler, 2002: The national elevation dataset. *PE & RS- Photogrammetric Engineering & Remote Sensing* 68, 5-11.

Gesch, D.B., 2007: The National Elevation Dataset. in Maune D (ed.) *Digital Elevation Model Technologies and Applications: The DEM Users Manual*, 2nd Edition. American Society for Photogrammetry and Remote Sensing, Bethesda, Maryland, 99–118.

Gosselink, J. G., J. M. Coleman, and R. E. Stewart, Jr., 1998: Coastal Louisiana. pp. 385–436. In M. J. Mac, P. A. Opler, C. E. Puckett Haecker, and P. D. Doran 1998. *Status and Trends of the Nation's Biological Resources*, 2 Vols. Reston: U.S. Department of the Interior, U.S. Geological Survey.

Guiney, 1999: Preliminary Report, Hurricane Georges, 15 September – 01 October 1998. National Hurricane Center, Miami, Florida, USA. Report completed January 5, 1999. Available on the Web at: <http://www.nhc.noaa.gov/1998georges.html>.

Interagency Performance Evaluation Taskforce Report (IPET), 2006: Performance Evaluation of the New Orleans and Southeast Louisiana Hurricane Protection System, Draft Final Report of the Interagency Performance Evaluation Task Force. U.S. Army Corps of Engineers, Volume 1- Executive Summary and Overview, June 1, 2006.

Kaiser, M.J., Y. Yu, and C.J. Jablonowski, 2009: Modeling lost production from destroyed platforms in the 2004-2005 Gulf of Mexico hurricane seasons. *Energy*, 34, 1156-1171.

Kates, R.W., C.E. Colten, S. Laska, and S.P. Leatherman, 2006: Reconstruction of New Orleans after Hurricane Katrina: A research perspective. *Proceedings of the National Academy of Sciences of the United States of America*, 103, 14653-14660.

Keim, B.D., R. Muller, and G. Stone, 2007: Spatiotemporal Patterns and Return Periods of Tropical Storm and Hurricane Strikes from Texas to Maine. *Journal of Climate*, 20, 3498-3509.

Keim, B.D., and R.A. Muller, 2009: *Hurricanes of the Gulf of Mexico*. Louisiana State University Press, 216 pp.

Kesicki, F., 2010: The third oil price surge – What’s different this time? *Energy Policy*, 38, 1596-1606.

Kleinosky, L.R., B. Yarnal, A. Fisher, 2007: Vulnerability of Hampton Roads, Virginia to storm-surge flooding and sea-level rise. *Natural Hazards*, 40, 43-70.

Knabb, R.D., J.R. Rhome, D.P. Brown, 2011: National Hurricane Center Tropical Cyclone Report on Hurricane Katrina. Published on the Web at: http://www.nhc.noaa.gov/pdf/TCR-AL122005_Katrina.pdf.

Maloney, M.C., and B.L. Preston, 2014: A Geospatial Dataset for U.S. Hurricane Storm Surge and Sea-Level Rise Vulnerability: Development and Case Study Applications. *Climate Risk Management*, in press.

Masters, J., 2013: Super Typhoon Haiyan: Strongest Landfalling Tropical Cyclone on Record. *Dr. Jeff Masters' Wunderblog*, November 7, 2013. Available on the Web at: <http://www.wunderground.com/blog/JeffMasters/super-typhoon-haiyan--strongest-landfalling-tropical-cyclone-on-recor>.

McGee, B.D., B. B. Goree, R. W. Tollett, B.K. Woodward, and W.H. Kress, 2013: Hurricane Rita Surge Data, Southwestern Louisiana and Southeastern Texas, September to November 2005. U.S. Geological Survey. Data Series 220. Page last modified January 13, 2013. Available on the Web at: pubs.usgs.gov/ds/2006/220/index.htm#desc.

National Oceanic and Atmospheric Administration, 2014: NOAA Tides and Currents. Sea Level Trends global map available on the Web at: <http://tidesandcurrents.noaa.gov/sltrends/sltrends.shtml>.

Needham, H., D. Brown, and L. Carter, 2012: *Impacts and Adaptation Options in the Gulf Coast*. Center for Climate and Energy Solutions, Arlington, VA.

Needham, H.F., and B.D. Keim, 2012: A Storm Surge Database for the U.S. Gulf Coast. *International Journal of Climatology*, 32, 14, 2108-2123. DOI: 10.1002/joc.2425.

Needham, H.F., B.D. Keim, D. Sathiaraj, and M. Shafer, 2013: A Global Database of Tropical Storm Surges. *EOS, Transactions American Geophysical Union*, 94, 24, 213-214.

NWS, 2011: SLOSH Pages: Sea, Lake, and Overland Surge from Hurricanes. National Hurricane Center, NOAA, Washington DC.

Paskal, C., 2010: The Vulnerability of Energy Infrastructure to Environmental Change. *China and Eurasia Forum Quarterly*, 8, 2, 149-163.

Penland, S., and K.E. Ramsey, 1990: Relative Sea-Level Rise in Louisiana and the Gulf of Mexico: 1908-1988. *Journal of Coastal Research*, 6, 323-342.

Pielke, Jr., R.A., J. Gratz, C.W. Landsea, D. Collins, M.A. Saunders, and R. Musulin, 2008: Normalized Hurricane Damage in the United States: 1900-2005. *Natural Hazards Review*, 9, 29-42.

Pine, J., 2006: Hurricane Katrina and Oil Spills: Impact on Coastal and Ocean Environments. *Oceanography*, 19, 37-39.

R Development Core Team, 2010: *R: A Language and Environment for Statistical Computing*. Vienna, Austria: R Foundation for Statistical Computing. ISBN 3-900051-07-0.

Reed, D.A., M.D. Powell, and J.M. Westerman, 2010: Energy Infrastructure Damage Analysis for Hurricane Rita. *Natural Hazards Review*, 11, 3, 102-109.

Rose, S., P. Jaramillo, M.J. Small, and J. Apt, 2013: Quantifying the Hurricane Catastrophe Risk to Offshore Wind Power. *Risk Analysis*, 33, 12, 2126-2141.

Rygel, L., D. O'Sullivan, and B. Yarnal, 2006: A Method for Constructing a Social Vulnerability Index: An Application to Hurricane Storm Surges in a Developed Country. *Mitigation and Adaptation Strategies for Global Change*, 11, 741-764.

Simpson, R. H., A.L. Sugg, and Staff at National Hurricane Center, 1970: The Atlantic hurricane season of 1969. *Monthly Weather Review*, 98, 293-306.

Stone, G.W., A. Sheremet, X. Zhang, and D. Braud, 2003: Coastal Land Loss and Wave-Surge Predictions During Hurricanes in Coastal Louisiana: Implications for the Oil and Gas Industry. Final report prepared for Louisiana Department of Natural Resources, U.S. Geological Survey, and U.S. Minerals Management Service. Available on the Web at: <http://dnrucm.dnr.state.la.us/ucm/groups/coastalprotectionrestoration/documents/ocpr/3891297.pdf>.

Strauss B, and R. Ziemiński, 2012: Sea Level Rise Threats to Energy Infrastructure. Climate Central, Washington, DC.

Tobin, 1995: The Levee Love Affair: A Stormy Relationship? *JAWRA Journal of the American Water Resources Association*, 31, 3, 359-367.

U.S. Army Corps of Engineers, 1970: *Report on Hurricane Camille*. New Orleans District Office.

U.S. Army Corps of Engineers, 2011: 100-Year Level of Protection. Website explains 100-year flood protection project for New Orleans, available on the Web at: www2.mvn.usace.army.mil/hps2/hps_100_year.asp.

U.S. Army Corps of Engineers, 2012: Texas City Hurricane Flood Protection, TX. Fact sheet updated on February 6, 2012. Available on the Web at: <http://www.swd.usace.army.mil/Portals/42/docs/civilworks/Fact%20Sheets/Galveston/FY13%20Texas%20City%20Hurricane%20Flood%20Protection,%20TX.pdf>.

U.S. Energy Information Administration, 2010: Independent Statistics and Analysis. National maps of energy distribution, refineries, power plants, coal mines and renewable energy, available on the Web at: <http://www.eia.doe.gov/state/>.

U.S. Energy Information Administration, 2012: U.S. State Profiles and Energy Estimates. Quick Fact Sheets Last Updated July, 2012. Available on the Web at: <http://www.eia.gov/state/>.

U.S. Energy Information Administration, 2013: Gulf of Mexico Fact Sheet. Release date: July 1, 2013. Available on the Web at: http://www.eia.gov/special/gulf_of_mexico/data.cfm.

U.S. Energy Information Administration, 2013b: Refinery Capacity Report. Data updated January 1, 2013. Available on the Web at: <http://www.eia.gov/petroleum/refinerycapacity/>.

U.S. Global Change Research Program, 2009: Global Climate Change Impacts in the United States. Available on the Web at: <http://nca2009.globalchange.gov/>.

Van Heerden, I.L., 2007: The Failure of the New Orleans Levee System Following Hurricane Katrina and the Pathway Forward. *Public Administration Review*, 67, 24-25.

Yergin, D., 2006: Ensuring Energy Security. *Foreign Affairs*, 85, 2, 69-82.

Zeng, L., 2000: Weather derivatives and weather insurance: concept, application and analysis. *Bulletin of the American Meteorological Society*, 81, 9, 2075-2082.

CHAPTER 7. CONCLUSION

7.1 Justification for Research

In the past decade, tropical cyclone-generated storm surges have emerged as a major natural hazard that are not well understood. In 2005, Hurricane Katrina inflicted one of the most severe natural hazards in U.S. history, as this storm killed more than 1,800 people (McTaggart-Cowan et al. 2008) and inflicted more than \$100 billion in damage (Blake et al. 2011). Katrina's catastrophic storm surge reached the highest level of any surge in the Western Hemisphere (see Chapter 2), which was surprising, as this hurricane made landfall as a category-3 hurricane in the same region where Hurricane Camille made landfall as a category-5 hurricane in 1969 (Simpson et al. 1970; Knabb et al. 2011). Katrina was the first of several large hurricanes in recent years that generated devastating storm surges in the United States.

In the years following Katrina, storm surge modeling efforts have attempted to better understand the processes by which tropical cyclones generate storm surges. Modern research now indicates that in addition to maximum sustained winds, a hurricane's size (Irish et al. 2008; Nielsen 2009; Dietrich et al. 2011), forward speed (Rego and Li 2009), as well as the coastal shape and bathymetry (Weisberg and Zheng 2006; Resio and Westerink 2008; Westerink et al. 2008; Chen et al. 2008) all influence storm surge heights. Research has also investigated the vulnerability of specific locations to storm surges, after losses from Katrina caused instability in the insurance industry. For example, the Federal Emergency Management Agency (FEMA) has collaborated closely with the National Hurricane Center to investigate the maximum potential for storm surge along the U.S. Gulf and Atlantic Coasts, in order to update Flood Insurance Rate Maps

(FIRM). This effort has relied upon the Sea, Lake and Overland Surges from Hurricanes (SLOSH) model that is run at the National Hurricane Center (Jennings 2013).

All of these efforts relied upon modeling, as empirical storm surge research was not yet possible without a credible storm surge database for the United States. However, in my master's thesis, I developed the first storm surge database for the U.S. Gulf Coast, which was later developed into a peer-reviewed journal article (Needham and Keim 2012). This database, called SURGEDAT, started as a peak storm surge database for the U.S. Gulf Coast, but has expanded to include all high water marks from all tropical cyclones for the U.S. Gulf and Atlantic Coasts (Needham et al. 2013).

This dissertation has continued the momentum of the SURGEDAT project. The coverage of storm surge data was expanded to a global scale, while U.S. Gulf Coast data were used to analyze how tropical cyclones generate storm surges, and to understand the storm surge vulnerability of specific locations in this region. These analyses pioneered new territory, as they provided the first data-driven approach for researching storm surge along the U.S. Gulf Coast.

7.2 Summary of Results

The first analysis chapter (Chapter 2) provided a global literature review of storm surge data. I reviewed data sources, observations and impacts in six ocean basins that frequently observe tropical cyclone-generated storm surges. Available literature provided more than 700 unique storm surge events since 1880, the majority of which were found in the Western North Atlantic Basin. The Bay of Bengal in the Northern Indian Ocean consistently observes the world's highest storm surges, as this sub-basin averages five surges ≥ 5 m per decade, and has observed credible storm tide levels reaching 13.7 m

(Dube et al. 1997). This sub-basin also observes the deadliest surges, as six tropical cyclones in this region have killed at least 138,000 people (Dube et al. 1997; Fritz et al. 2009). The Western North Pacific observes the highest rate of low-magnitude storm surges, as the coast of China averages 54 surges ≥ 1 m per decade (Tang et al. 2011), and rates are likely even higher in the Philippines. Analysis in Chapter 1 has found that the U.S. Gulf Coast observes an average of one storm surge ≥ 5 m and 18 storm surges ≥ 1 m per decade, which ranks this region in second place for high- and low-magnitude storm surge counts in a global context.

Chapter 3 provided an analysis of the correlation between storm surge heights and tropical cyclone wind speeds at and before landfall. A landfall/ surge classification system was developed to provide a consistent landfall classification among all storms. This methodology yielded 117 wind/ surge events from 1880-2011 with useable data. Storm surge heights in this study correlated best with pre-landfall wind speeds, with wind speeds 18 hours before landfall producing the optimal correlation. Higher wind-surge correlations were found when testing a more recent sample of data that contained 63 wind-surge events since 1960. The highest correlation for these data were found when wind speeds 18 hours before landfall were raised to a power of 2.2, which provided R-squared values that approached 0.70. R-squared values at landfall for these same data were only 0.44.

Chapter 4 also provided an analysis on the relationship between storm surge heights and tropical cyclone characteristics, however, in this chapter tropical cyclone size was correlated with surge heights. For this analysis, I constructed a unique hurricane size dataset from nine different data sources, which provided the radius of maximum winds

(Rmax) and radii of 34-kt, 50-kt and 64-kt winds. Statistical analysis revealed an inverse correlation between storm surge magnitudes and Rmax sizes, while positive correlations existed between storm surge heights and the radius of 34-kt, 50-kt and 64-kt winds. Storm surge heights correlated best with the pre-landfall radius of 50-kt winds, with a Spearman Correlation Coefficient value of 0.8158, significant at the 99.9% confidence level. The 1900 Galveston Hurricane, the 1935 Labor Day Hurricane and Hurricane Camille in 1969 support these results, as they all had small Rmax sizes, but generated catastrophic surges (Garriott 1900; U.S. Army Corps of Engineers 1935; Simpson et al. 1970) Hurricane Katrina demonstrated the importance of large wind fields, as hurricane-force winds extending 90 nmi from the center of circulation (Demuth et al. 2006) enabled this large storm to generate a higher storm surge level than Hurricane Camille along the same stretch of coast, even though Camille's pre-landfall winds were slightly stronger than Katrina's (see Chapter 3).

In Chapter 5, I conducted the first empirical analysis of storm surge return levels along the U.S. Gulf Coast. This analysis used a web-tool that provided a comprehensive list of historical water levels for any location in the region from 1900-2013. This tool returned an average of 26 observations for 26 coastal locations. These data included historic storm surge and storm tide observations. Geodetic and tidal datum adjustments removed errors in the dataset and provided storm tide heights above mean sea level for the year of the flood event. Statistical analysis utilized the Point Process (PP) model of Extreme Value Theory as well as a Logarithmic Plotting (LP) method to estimate 10-, 25, 50-, 100-, 200, and 500-yr return levels in the region. A two-tailed Kolmogorov-Smirnov statistic indicated the LP method provided a better fit to observed data, as the PP method

underestimated water levels at most sites. Although the LP method is not designed to estimate return levels beyond the length of the data record, the results are still useful for predicting out to the 100-yr level. This method showed considerable geographic variability in return levels, as the highest 100-yr level was 7.95 m at Bay St. Louis/ Pass Christian, Mississippi, and the lowest level was 2.53 m at Cedar Key, Florida. Relatively low return levels were also found at Morgan City, Louisiana, where strong easterly winds in advance of a hurricane tend to blow offshore and moderate storm surge levels.

Chapter 6 provided a regional vulnerability analysis that considered the risk of oil refineries and power plants to surge inundations. Storm surge return levels estimated in Chapter 5 provided water level data, while a unique dataset provided by Oak Ridge National Laboratory contained 152 power plants and 32 refineries that could potentially be inundated by Gulf Coast storm surges. Texas and Louisiana contained most of this infrastructure, as 91% of refineries and 85% of power plants in the region were located in these states. Results indicate that storm surge is a serious threat in this region, as the 100-year surge would inundate 72% of the oil refineries and 63% of the power plants in the coastal zone. East Texas stands out as the most vulnerable sub-region, as the 100-year storm surge would inundate 92% (12 of 13) refineries in the Galveston-Baytown-Sabine Pass region, and 18 power plants near Baytown. Lower surge heights near Morgan City make this location attractive for infrastructure, however, high rates of sea-level rise induce long-term threats in this area.

7.3 Benefits of this Research

The analyses conducted in these chapters sufficiently answered the six research questions posed in the introduction. The global literature review revealed that the U.S.

Gulf Coast is one of the most vulnerable regions of the world to storm surge inundations, while providing an estimate of the number of low- and high-magnitude storm surges that occur per decade in this and other tropically active basins. The two chapters on the physical processes that generate storm surges revealed that storm surge heights correlate better with pre-landfall tropical cyclone conditions, including maximum sustained winds and cyclonic size, than they correlate with those storm conditions at landfall. The two chapters on vulnerability of the Gulf Coast suggest that while storm surge presents a great threat to this region, the risk of storm surge is highly localized. Storm surge return levels are highest in coastal Mississippi and the inner portion of Galveston Bay, while the greatest risk of inundation for energy infrastructure occurs in Southeast Texas.

These results will hopefully contribute to the improvement of storm surge models. A thorough literature review revealed that only Jordan and Clayson (2008) had conducted research on the importance of pre-landfall winds for generating storm surge, and their paper had not yet been cited as of 2013, which indicates that models are not likely using this important discovery, which was developed in greater detail in this dissertation. No papers have yet been published on the importance of pre-landfall size for generating storm surge.

The data-driven storm surge return levels and vulnerability assessment for Gulf Coast energy infrastructure will provide crucial information on the risk of storm surge at specific locations in the region. As the results provided by this study are noticeably higher than previous statistical and modeling efforts, this research will hopefully help communities prepare for storm surges that are higher than previously thought.

7.4 Limitations

This research also encountered several limitations, the most severe of which is the fact that the results of these analyses are restricted by the availability and quality of the data. Although SURGEDAT provides the most comprehensive storm surge dataset available, several gaps still exist in this dataset. Internationally, most storm surge data were missing for large regions, including the Caribbean Sea and Central America, most of East Asia, the West Coast of Mexico, as well as portions of Oceania and the Southwest Indian Ocean. Along the U.S. Gulf Coast, where surge data are best developed, SURGEDAT is still missing approximately 9% of possible storm surges since 1900 (see Chapter 6), and for some massive surge events, like the 1900 Galveston Hurricane, few data are available. Also, SURGEDAT only provides data since 1880, which is a short time period in Earth's history. This means that we may not realize the potential magnitude of storm surges in areas that have not observed a high-magnitude storm surge since 1880, like the West Coast of Florida. In other words, just because a massive surge hasn't been observed in a given location in the past 135 years, doesn't mean that location is immune to large surges.

Another limitation of this research has been the inability to successfully employ extreme value modeling to observed surge data. I attempted to utilize the Point Process representation of extreme value behavior, which is a peaks-over-threshold approach that uses observed data to predict return levels beyond the length of the dataset. Unfortunately, this methodology did not work well in this study, as it underestimated storm surge return levels. Inadequate data quantity may explain the poor performance of this method, as an average of only 19 observations remained for each location after

applying the truncation level, and some components of this method, like the Maximum Likelihood approach, do not perform well with small sample sizes (Katz et al. 2002).

A limitation of the energy infrastructure analysis was that it did not account for local levees and flood control devices, with the exception of levees along the Mississippi River and infrastructure along New Orleans' Industrial Canal. This limitation reduces the usefulness of this study, as infrastructure risk to storm surge may be overestimated in areas with privately-owned or locally-maintained levees. However, it is important to remember that levees sometimes fail, and they may require maintenance and repairs, adding cost to facilities in flood-prone areas.

7.5 Suggestions for Future Research

This analysis confirmed that storm surge data are useful for empirical analysis on the relationship between surge heights and tropical cyclone characteristics. Future research could investigate the relationship between surge heights and additional variables, such as tropical cyclone forward speed and the angle of approach to the coastline, as well as coastal shape and bathymetry. Also, an investigation of the relationship between storm surge heights and Integrated Kinetic Energy (IKE) of tropical cyclones may prove insightful, because IKE considers wind speeds over a gridded domain, essentially combining storm intensity and size into a useful index for understanding a hurricane's destructive potential (Powell and Reinhold 2007). Data mining, an emerging field within computer science, may be useful for conducting multivariate analysis on this topic, in an effort to uncover the complex processes by which tropical cyclones generate storm surges.

The analysis of energy infrastructure vulnerability provided unique insights into the risk of storm surge damage on billions of dollars of assets. This study proved that such analysis is feasible given localized storm surge return levels and an infrastructure database that contains the latitude, longitude and elevation of facilities. As the data-driven storm surge climatology for the region has now been established, it would take limited effort to analyze data from additional economic sectors, provided that facility data were available. Potential avenues for such research might investigate the vulnerability of healthcare infrastructure, like medical clinics and hospitals, or high-security facilities that require additional time to evacuate, such as prisons.

Scholars should investigate the climatological pattern that led to the hyperactive number of high-magnitude storm surges in the Bay of Bengal during the 1960s and 1970s. Various studies have found relationships between El Nino Southern Oscillation (ENSO) phases and tropical cyclone activity in this region using data starting in 1983 (Ng and Chan 2012) and 1993 (Girishkumar and Ravichandran 2012). Tropical cyclogenesis also relates to phases in the Indian Ocean Dipole, according to data starting in 1981 (JunPeng and Jie 2013), and 1993 (Girishkumar and Ravichandran 2012). Although these findings are important, it should be possible for researchers to look back farther and acquire synoptic climatology data from the 1960s and 1970s to determine what atmospheric patterns correlated with the period of extreme storm surge activity in the region.

Future research should also investigate statistical methods that may better predict storm surge return levels using limited empirical datasets. Although the logarithmic plotting method provided a good fit to observed data, this method was not designed to

predict extreme levels beyond the length of a dataset. Extreme value theory provides various methodologies to predict rare events, however, in this study, the Point Process model underestimated surge levels. Better results may be provided by different methodologies, or perhaps the same methodologies after many more surges are observed in the region.

7.6 References

Blake, E.S., C.W. Landsea, and E.J. Gibney, 2011: The Deadliest, Costliest, and Most Intense United States Tropical Cyclones from 1851 to 2010 (And Other Frequently Requested Hurricane Facts). *NOAA Technical Memorandum NWS NHC-6*. This publication is available on the Web at: <http://www.nhc.noaa.gov/pdf/nws-nhc-6.pdf>.

Chen, Q., L. Wang, and R. Tawes, 2008: Hydrodynamic response of northeastern Gulf of Mexico to hurricanes. *Estuaries and Coasts*, 31, 1098-1116.

Demuth, J., M. Demaria, and J.A. Knaff, 2006: Improvement of advanced microwave sounder unit tropical cyclone intensity and size estimation algorithms. *Journal of Applied Meteorology*, 45, 1573-1581.

Dietrich, J.C., M. Zijlema, J.J. Westerink, L.H. Holthuijsen, C. Dawson, R. A. Luettich, Jr., R. Jensen, J.M. Smith, G.S. Stelling, and G.W. Stone, 2011: Modeling Hurricane Waves and Storm Surge using Integrally-Coupled, Scalable Computations. *Coastal Engineering*, 58, 45-65.

Dube, S.K., A.D. Rao, P.C. Sinha, T.S. Murty, N. Bahulayan, 1997: Storm surge in the Bay of Bengal and Arabian Sea: The problem and its prediction. *Mausam*, 48, 283-304.

Fritz, H.M., C.D. Blount, S. Thwin, M.K. Thu, and N. Chan, 2009 : Cyclone Nargis storm surge in Myanmar. *Nature Geoscience*, 2, 448-449.

Garriott, E.B., 1900: West Indian hurricane of September 1-12, 1900. *Monthly Weather Review*, 28, 371-378.

Girishkumar, M.S., and M. Ravichandran, 2012: The influences of ENSO on tropical cyclone activity in the Bay of Bengal during October-December. *Journal of Geophysical Research-Oceans*, 117, article number C02033.

Irish, J.L., D.T. Resio, and J.J. Ratcliff, 2008: The Influence of Storm Size on Hurricane Surge. *Journal of Physical Oceanography*, 38, 2003-2013.

Jennings, R., 2013: Personal correspondence with R. Jennings, Hurricane Program Specialist with FEMA Region 4. Communication through e-mail, November 2013.

Jordan II, M.R., and C.A. Clayson, 2008: Evaluating the usefulness of a new set of hurricane classification indices. *Monthly Weather Review*, 136, 5234-5238.

JunPeng, Y., and C. Jie, 2013: North Indian Ocean tropical cyclone activities influenced by the Indian Ocean Dipole mode. *Science China-Earth Sciences*, 56, 5, 855-865.

Katz, R.W., M.B. Parlange, P. Naveau, 2002: Statistics of Extremes in Hydrology. *Advances in Water Resources*, 25, 1287-1304.

Knabb, R.D. J.R. Rhome, and D.P. Brown, 2011: Tropical Cyclone Report, Hurricane Katrina, 23-30 August 2005. Report produced by the National Hurricane Center, Miami, Florida, and published on the Web at: http://www.nhc.noaa.gov/pdf/TCR-AL122005_Katrina.pdf.

McTaggart-Cowan R., G.D. Deane, L.F. Bosart, C.A. Davis, T.J. Galarneau, Jr., 2008: Climatology of tropical cyclogenesis in the North Atlantic (1948-2004). *Monthly Weather Review*, 136, 1284-1304.

Needham, H.F., and B.D. Keim, 2012: A Storm Surge Database for the U.S. Gulf Coast. *International Journal of Climatology*, 32, 14, 2108-2123. DOI: 10.1002/joc.2425.

Needham, H.F., B.D. Keim, D. Sathiaraj, and M. Shafer, 2013: A Global Database of Tropical Storm Surges. *EOS, Transactions American Geophysical Union*, 94, 24, 213-214.

Ng, E.K.W., and J.C.L. Chan, 2012: Interannual variations of tropical cyclone activity over the north Indian Ocean. *International Journal of Climatology*, 32, 6, 819-830.

Nielsen, P., 2009: How storm size matters for surge height. *Coastal Engineering*, 56, 1002-1004.

Powell, M.D., and T.A. Reinhold, 2007: Tropical Cyclone Destructive Potential by Integrated Kinetic Energy. *Bulletin of the American Meteorological Society*, April 2007, 513-526.

Rego, J.L., and C. Li, 2009: On the importance of the forward speed of hurricanes in storm surge forecasting: A numerical study. *Geophysical Research Letters*, 36, 7.

Resio, D.T., and J.J. Westerink, 2008: Modeling the physics of storm surges. *Physics Today*, 61, 33-38.

Simpson, R.H., A.L. Sugg and Staff, 1970: The Atlantic Hurricane Season of 1969. *Monthly Weather Review*, 98, 4, 293-306. The National Hurricane Center, Weather Bureau, ESSA, Miami, Florida, United States. Report available on the Web at: <http://www.aoml.noaa.gov/general/lib/lib1/nhclib/mwreviews/1969.pdf>.

Tang, L., J.M. Zhan, and Y.Z. Chen, 2011: Typhoon Process and Its Impact on the Surface Circulation in the Northern South China Sea. *Journal of Hydrodynamics*, 23, 1, 95-104.

U.S. Corps of Engineers, 1935: 1935 Labor Day Hurricane, Limits of Destruction and Storm Surge Heights. Chart File No. 3-16-10,409 produced on October 21, 1935. Published in Knowles, T.N., 2009: Category 5: The 1935 Labor Day Hurricane. University Press of Florida, 350 pp.

Weisberg, R.H., and L. Zheng, 2006: Hurricane storm surge simulations for Tampa Bay. *Estuaries and Coasts*, 29, 899-913.

Westerink, J.J., R.A. Luetich, J.C. Feyen, J.H. Atkinson, C. Dawson, H.J. Roberts, M.D. Powell, J.P. Dunion, E.J. Kubatko, and H. Pourtaheri, 2008: A Basin- to Channel-Scale Unstructured Grid Hurricane Storm Surge Model Applied to Southern Louisiana. *Monthly Weather Review*, 136, 833-864.

VITA

Hal Needham was born as Harold Francis Needham, III, in Allentown, Pennsylvania, on October 6, 1974. He grew up in Whitehall, where he graduated from high school in 1993. He then attended Penn State University, where he graduated in 1997 with a B.S. in Geography.

After graduating from Penn State, Hal lived in various regions of the world, working on cross-cultural and science projects. He worked on cross-cultural projects in North Africa and the Middle East from 1997-2001, living in Casablanca, Morocco, and Cairo, Egypt for much of that time. From 2005-2007, Hal lived in Alaska, working on science projects with a cross-cultural emphasis for Native Alaskans.

In 2008, Hal moved to Baton Rouge, Louisiana, to pursue a master's degree in geography/ climatology. After completing this degree in 2010, he began working full-time for LSU and pursuing a doctorate degree. Hal's graduate research has mostly focused on data-driven storm surge analysis. He lives in Brusly, Louisiana, with his wife, Kari, and two-year-old twins, Luke and Della.